DEVELOPMENT OF A LABORATORY SCALE PROCEDURE FOR PREDICTING THROUGHPUT OF HIGH PRESSURE GRINDING ROLLS

by

Stefan Nadolski

BE (Mechanical), The University of Sydney, 2005

A THESIS SUBMITTED IN PARTIAL FULFILLMENT OF THE REQUIREMENTS FOR THE DEGREE OF

MASTER OF APPLIED SCIENCE

in

The Faculty of Graduate Studies

(Mining Engineering)

THE UNIVERSITY OF BRITISH COLUMBIA

(Vancouver)

APRIL 2012

Abstract

The throughput capability of a high pressure grinding roll (HPGR), a critical process parameter, has been found to heavily depend on the sample type being processed. Existing HPGR test methods require the use of pilot machines and large sample quantities to assess the throughput characteristics of a certain ore type. Addressing the need for a laboratory scale HPGR test, a laboratory procedure was proposed to assess the throughput capability of mineral samples. Existing procedures were adopted from the fields of terramechanics and soil mechanics, and used as a basis for predictive HPGR throughput models. The applicability of the proposed tests was assessed through the comparison of predicted throughput with observed values from pilot HPGR testing. Results showed that outcomes of the proposed laboratory scale tests were statistically significant when used for the prediction of HPGR throughput. Primarily, the frictional properties of feed samples, as characterized by a direct shear box test, were found to be of particular significance. An approach to modelling the pressure profile which occurs on the HPGR roller surface was also proposed for potential use in a force-based model. Based on the results, an approach to HPGR testing requiring a reduced amount of sample was presented. Further work on characterizing the frictional properties of mineral samples was recommended. Analysis of HPGR outcomes indicated that strong relationships exist between power, throughput and roll gap, hence holistic approaches to HPGR modelling may be most appropriate for future predictive models.

Preface

The results of this study were published in abbreviated form in the proceedings of the SAG2011 conference:

Nadolski, S, Bamber, A. S., Klein, B., Drozdiak, J. (2011) Investigation into Laboratory Tests for High Pressure Grinding Rolls. Paper presented at SAG Conference 2011, Vancouver, B.C., Canada.

I was responsible for developing the test approach, conducting test work and interpreting the results. I consulted with my supervising committee who provided feedback. Jeff Drozdiak assisted with pilot HPGR testing. Wayde Bosman assisted with direct shear testing. Section A of the appendix is based on the results of size distribution tests conducted by Ahsan Chaudhary.

TABLE OF CONTENTS

LIST OF TABLES

LIST OF FIGURES

List of Symbols

Symbol	Description
a	Pressure – displacement parameter
b	Pressure – displacement exponent
c	Cohesion
D	Roll diameter
e	Extrusion angle
E_{sp}	Net specific energy consumption
F	Hydraulic pressing Force
F_{SP}	Specific pressing Force
HPi	High pressure index
H20	Moisture
I	Position along roller width
j	Horizontal soil deformation
K_3	Circuit parameter
k	Shear deformation modulus
M	Throughput
m	Gaudin-Schuhmann slope parameter
M_{ih}	HPGR ore work index
$\dot{m}$	Specific throughput constant m-dot
n	Void ratio
P	Total roll motor power
p	Piston pressure
S_h	Coarse ore hardness parameter
s	Roll gap
r	Radius
T	Torque
V_s	Volume of voids
V_v	Volume of solids
$\dot{V}_p$	The product or roll velocity, roll width and diameter
W_h	HPGR work index
w	Roll width

x_c	Critical gap
x_g	Roll gap at the nip (zero angle), equivalent to s
Z(p)	Displacement at piston pressure p
α	Compression angle
α_n	Nip angle
ß	Force reaction angle
$ß_n$	n^{th} Regression variable
Θ	Internal angle of friction
λ	Position along roll width divided by overall roll width
μ	Circumferential roll speed
ρ_c	Material density at the compression angle
ρ_b	Feed bulk density
ρ_g	Material density at nip (zero angle)
σ	Normal stress
τ	Shear stress
ϕ	Porosity

ACKNOWLEDGEMENTS

This thesis was conducted as part of the UBC HPGR research program which is centered at the University of British Columbia and supported by the metallurgical processing division of the Canadian Mining Industry Research Organization (CAMIRO). Support from sponsors of the research program was instrumental in providing the equipment and funds necessary to carry out the study.

Dr. Bern Klein and Dr. Andrew Bamber provided supervision and guidance throughout the course of the study. Pilot HPGR results, made available by Koeppern Machinery Australia, were fundamental to the research. BC Mining Research contributed significantly to the thesis through their involvement with UBC and the CAMIRO research program.

The assistance of Jeff Drozdiak, Wayde Bosman and Aaron Wright with the carrying out of test work was greatly appreciated. Discussion with Dr. Peter Radziszewski (McGill University) provided insight into the field of terramechanics, which proved to be an important component of the research.

Overall the work would not have been possible without input from the many mineral processors, scientists and engineers which I have been fortunate to come across.

I am indebted to my wife, Yuri, for her continuous support and encouragement provided throughout the course of the study.

1 INTRODUCTION

1.1 Background

Industry accepted laboratory scale tests are well established for comminution equipment such as cone crushers, Semi-Autogenous Grinding mills (SAG) and ball mills. However, there is an obvious absence of proven laboratory scale High Pressure Grinding Roll (HPGR) tests resulting in reduced uptake of the technology (Bamber et al, 2009). For this reason the assessment of an HPGR comminution flowsheet is typically attempted only once a sizeable amount of sample is available. A proven laboratory scale approach to HPGR testing is required to bridge the gap between scale-up capabilities of the competing comminution technologies, in order to provide engineers with the ability to practically consider HPGR during early stages of project development.

To date a majority of attempts at establishing laboratory scale HPGR tests have focused on the relationships between compression breakage and energy consumption of sample types, principally through piston and die type tests. In comparison, the work presented in this thesis determines the characteristics of sample types in terms of terra-mechanic principles and relates them to pilot HPGR test results. The initial approach to laboratory testing drew upon existing methods of evaluating the trafficability of a soil for ground transport vehicles. Further refinement of these laboratory tests was carried out based on the degree of correlation to pilot HPGR data. The determined relationships between the investigated tests and HPGR performance not only widens the available resources to address the outlined objective, but also helps define the interactions between ore and rollers. Overall, an improved definition of the critical ore parameters in terms of HPGR processing was achieved.

1.2 Thesis objectives

The aim of the thesis was to develop laboratory scale tests which would provide results that are applicable to the prediction of HPGR performance, particularly throughput and operating gap. In order to work towards fulfilling the stated objective of the thesis, the following intermediate objectives were set and form the structure of the document:

- Identify shortcomings in current test methodologies and formulate alternate approaches
- Develop an understanding of the interactions occurring between rollers and granular material through the review of published work from a variety of areas of research, particularly those which examine geometrically similar conditions

- Carry out and analyze pilot HPGR test results to determine the error associated with pilot testing, investigate machine and material responses and create a reference database of pilot test results
- Carry out material analyses, which are typically associated with mineral processing, on HPGR feed samples for material characterization purposes
- Propose, develop and carry out laboratory scale tests for comparison to pilot HPGR test results
- Determine equations for the prediction of HPGR roll gap and throughput using available input variables, including those from developed laboratory scale tests
- Analyze and discuss the source of input variables selected for use in predictive equations
- Suggest further work based on a newly developed understanding of the critical material properties in terms of HPGR processing

1.3 Thesis outline

The research presented in this thesis addresses an industry need for a laboratory scale test which is used to evaluate the suitability of a sample to processing with HPGR rolls. Prediction of HPGR roll gap and throughput were identified as important performance indicators that had received comparatively little attention in literature. This thesis is a documentation of the path taken from defining deficiencies in previous HPGR laboratory scale test developments to evaluating the applicability of newly developed laboratory scale tests.

A review of HPGR based literature, primarily the history of the comminution technology and scale up methodologies, is presented in Chapter 2. Publications from other fields of research such as soil mechanics and terra-mechanics, which were identified as bearing potentially applicable test methodologies, were also reviewed and formed the basis of proposed laboratory scale tests.

An outline of the overall experimental program is discussed in Chapter 3. Samples used for the program as well as the relation of experimental procedures to the main scope of the thesis are presented.

Chapter 4 describes the approach to pilot HPGR testing, including the type of equipment used and parameters measured. Results of pilot HPGR testing, such as throughput rates, were input into a database for later comparison to predictive models.

The analysis of inter-relationships between HPGR input and response variables, such as specific throughput and roll gap, are shown in Chapter 5. Results of pilot HPGR tests were used to define the target outcomes of predictive throughput models.

Proposed laboratory tests are described in Chapter 6. Methodologies for direct shear testing, a soil mechanics based laboratory test, and piston press testing are outlined in detail. The influence of material parameters, such as moisture, on test outcomes is also presented.

Comparisons of predicted HPGR throughput and results from proposed HPGR models are shown in Chapter 7. Three main modelling approaches were used: linear stepwise regression, nonlinear models and a force based method.

Results and conclusions of HPGR throughput test development and modelling are presented in Chapter 8.

Recommendations for further work towards HPGR throughput modelling and test development are outlined in Chapter 9.

2 LITERATURE REVIEW

2.1 Introduction

The extraction of valuable minerals from ores inevitably involves a process of comminution, carried out by a collection of equipment which is selected for its cost effectiveness. Assessment of the potential profitability of a mineral deposit is broken down into stages of engineering design, increasing in level of detail addressed while at the same time reviewing the selection of comminution equipment based on the value they provide to the overall project. Metallurgical testing procedures for individual pieces of comminution equipment have been developed which differ significantly in terms of the sample quantity they require, confidence in scale up and their applicability across variations in ore type and process conditions. In this context the assessment of ore applicability to HPGR lags behind that of competing comminution technologies. Industry acceptance of a laboratory scale HPGR test would provide engineers with the ability to design HPGR based flowsheets at earlier stages of engineering.

In order to provide a basis of knowledge for addressing the development of a laboratory scale HPGR test, particularly one for the prediction of throughput, literature from various fields of study have been reviewed and presented in this section, as shown in Figure 1.

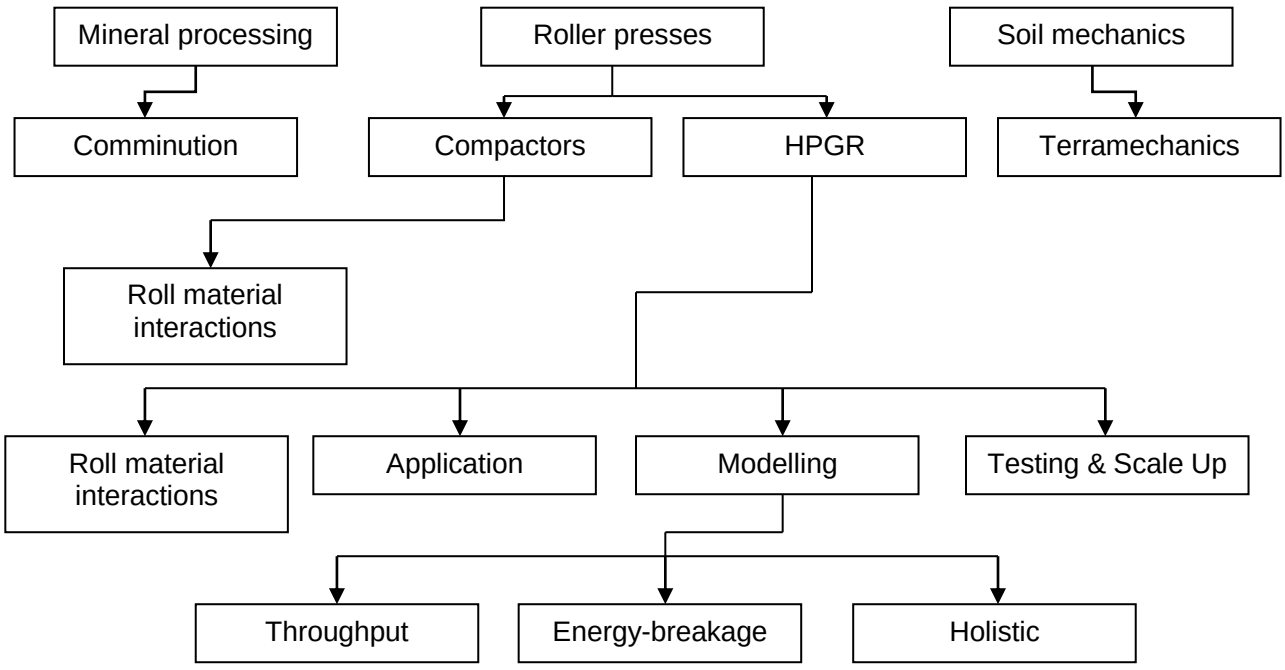

Figure 1 - Breakdown of literature review

2.2 HPGRs in mineral comminution

The unique introduction of HPGR technology to the mineral processing industry emphasizes the fact that it is a fundamentally different machine to other comminution equipment such as ball mills, SAG mills and cone crushers, which are considered to be well established within the industry. A review of the historical adaptation of the roller press to different applications, including mineral comminution, provided insight into other fields of research which may be relevant to the development of a laboratory scale test for the prediction of HPGR throughput.

The high pressure grinding roller press originates from similar equipment used for compacting fines, such as coal into briquettes which was carried out since the mid-19th century (Lynch et al, 2005). From the 1870s to the 1940s Germany was one of the biggest producers of coal briquettes. As such, a variety of machines associated with the industry were invented in Germany, including variations of the roller press. The gradual decline of briquetted coal in Europe, as an industrial and domestic fuel, pushed roll press manufacturers into investigating new applications for their technology (Mukherjee, 1940). Research and development of roller press technology, including improvements in press design, hydraulic systems, feed mechanisms and wear linings, allowed consideration to be given to further expand the application of roller presses into new areas of compaction and conversely, comminution.

The method of breakage carried out by HPGRs, rather than the equipment itself, was initially developed and patented in 1979 by Professor Klaus Schönert. The patent provided exclusivity to the patent holders for a method of comminution, by way of subjecting a bed of particles to a pressure of at least 500 kN/cm^2. The patent claims also included, among other claimed methods, the use of a roller mill with cylindrical rollers to carry out this form of comminution (Schönert, 1979). Hence, it is important to note that the claimed invention was the method of comminution itself and the existing roller press was modified to practically implement the invention and consequently referred to as a high pressure grinding roll.

The first commercial application of HPGR was in the cement industry in 1985 at the Dortmund CEMEX cement plant (CEMEX Deutschland AG, 2005). Compared to standard comminution methods of the time, the high pressure grinding roll was found to be substantially more energy efficient. Energy savings of 10 to 30% are typically outlined in literature, some claiming up to 50% reduction in energy due to the inclusion of HPGR in comminution circuits (Casteel, 2005; Günter et al, 1996). Subsequently more than 500 HPGR units have been installed in the comminution industry (Morley, 2010).

The first use of HPGR for comminution outside of the cement industry was an installation at the Premier Diamond Mine (currently named the Cullinan Mine) in 1987-1988 (Casteel, 2005). Another application to diamond processing followed in 1990 at the Argyle Diamond Mine in Australia (Dunne et al, 2004). Through these installations a new role was found for HPGRs: the liberation of diamonds from kimberlitic host rock and the reduction of gangue to a small size so that it can be removed by downstream classification equipment. The damage to diamonds was found to be able to be minimized through control of the roll pressing force and mechanical adjustment of the minimum gap setting to be greater than the largest expected diamond size (Daniel, 2007). The entry of high pressure grinding into diamond processing brought to light a new HPGR associated process benefit, breakage along grain boundaries of constituent minerals leading to improved liberation.

During the 1990s HPGR was successfully introduced to base metal process plants in a fine grinding role. The main application was to grind iron ore concentrate to generate pellet plant feed (Casteel, 2005). The use of HPGR in a duty similar to that of a tertiary crusher also came about in the 1990s. One of the first applications of the technology to hard rock ore was an 18 month trial at Cyprus Sierrita in 1995. The trial was considered to be unsuccessful due to high wear of the roller surfaces (Morley, 2010). A similar result was found in 1990 at the previously mentioned Argyle diamond mine, where HPGR was introduced to treat a hard lamproite ore (Dunne et al, 2004). Experiences from both mentioned installations prompted manufacturers to improve wear lining designs and mineral processors to review the role of HPGRs in comminution flowsheets.

The primary hindrance to further uptake of HPGR technology in minerals comminution was the high wear rate of roller wear linings at sites such as Cyprus Sierrita and Argyle. Manufacturers addressed this through further research and development of tire linings and in-house tests aimed at characterizing ore in terms of the roll wear inflicted during HPGR operation. Mineral process engineers were also forced to understand the causes for roll wear and design comminution flowsheets accordingly (Burchardt et al, 2011).

Uptake of the technology has since improved and now two base metal operations which treat tonnages in excess of 100,000 tonnes per day, Cerro Verde and Boddington, include HPGRs in their mineral processing plants. Both ores have high work indices and are frequently referenced when consideration is given to using HPGR for large base metal applications. Various sources indicate that the trend of increasing HPGR applications in hard rock ore will continue into the near future. However, a significant barrier to increased adoption of the technology that has been identified is the lack of appropriate laboratory scale tests (Bamber et al, 2009).

2.3 Description of high pressure grinding roll design

At the time of writing, five major manufacturers are active in marketing HPGRs for mineral and cement applications. Although the detailed design of components does vary, the design of functional components which allow for the continual compression of a flow of material is essentially the same. The principal components of the HPGR are shown in Figure 2.

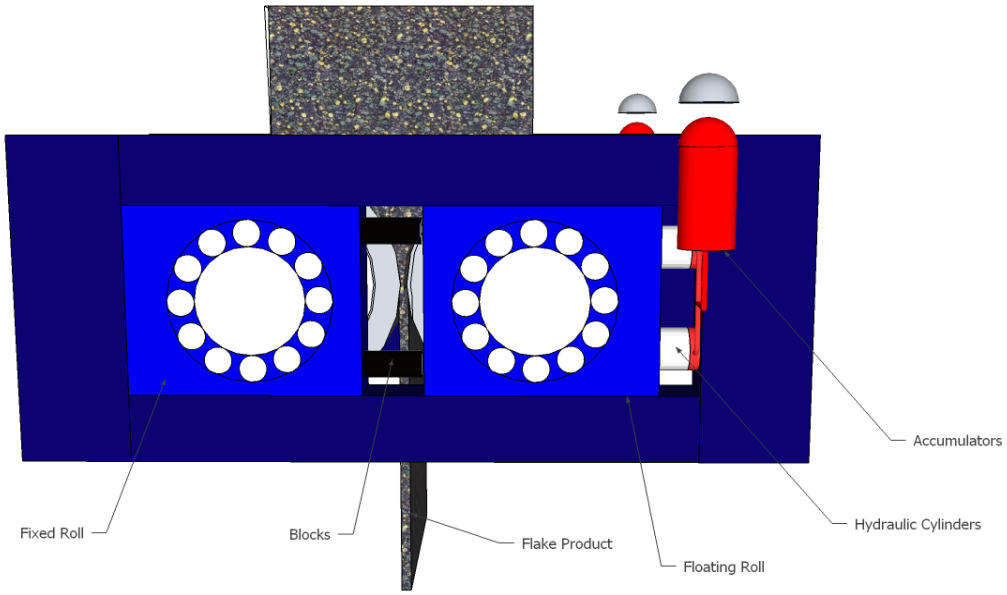

Figure 2 - Depiction of an HPGR

The HPGR machine is described by two parallel counter rotating rollers mounted on bearings and contained by a frame (Schönert, 1988). One of the rolls, referred to as the floating roll, is movable in the lateral position within the press frame. Hydraulic pistons mounted between the floating roll bearings and frame-ends exert a compressive force towards the opposite roll, referred to as the fixed roll. Nitrogen accumulators are connected to the hydraulic cylinders and function as hydro-pneumatic springs to reduce hydraulic pressure peaks. Blocks located between the roll bearings prevent the rollers from colliding. Material is usually gravity fed to the press through the use of a frame mounted hopper, which directs feed to an area above and between the rollers. During operation a constant level of material is maintained in the hopper to ensure that choke feeding takes place (Günter, 1996). Acting as an extension of the feed hopper walls, cheek plates serve to contain pressurized material located between the rolls. Comminution performance suffers when cheek plates are worn or are not located close to the roller edge, exacerbating the poorer comminution effect known as ‘edge effect’, where material undergoes single particle crushing rather than inter-particle crushing (Rule et al, 2008).

Typically the rolls are driven by individual drive trains through the use of planetary gearboxes and electric motors (Klymowsky et al, 2002). In most installations variable frequency drives are used to regulate the roll speed to achieve the desired throughput. The rolls are typically solid, but may contain water cooling channels for circulation of water to prevent overheating of drive train components.

During the 1990s, wear linings were provided in the form of segments, which would bolt onto the roll, or in the form of tires. Trials showed that segments were not suitable for hard rock applications and further lining evolutions were focused on tire based wear surfaces. Welded linings are still used in the cement industry, but are not applied to hard rock ore.

Tire designs rely on the adhesion of feed material, referred to as an autogenous protection layer, to critical areas of the tire surface. Studded lining is used in the majority of hard rock mineral applications and a picture of the surface is shown in Figure 3. The tire wear life is the main factor affecting the availability of the HPGR in operation (Morley, 2010).

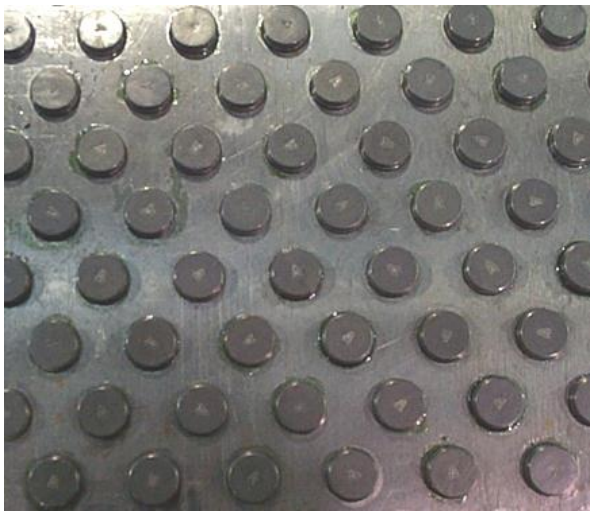

Figure 3 - Studded wear lining

The largest HPGR advertised in manufacturer catalogues has a roll diameter of 2.6 m and a roll width of 1.75 m (Thyssenkrupp 2007; Maschinenfabrik Köppern, 2010; KHD Humboldt Wedag, 2007; Citic, 2012). However, at the time of writing, industry word of mouth has suggested that orders have been awarded for larger HPGRs than those catalogued. It is apparent that the size of the rollers, directly impacting capacity, and the wear resilience of the linings are design areas which when improved will significantly increase the applicability of the technology to comminution.

2.4 HPGR sizing and performance parameters

Studies in the field of HPGR have led to the establishment of HPGR specific parameters which have become accepted by industry and academia and are described in this section. These definitions were also used to convey the significance of the results generated in this thesis.

Specific throughput constant $\dot{m}$

The specific throughput constant $\dot{m}$ represents the throughput for a particular material, operating with a roll of a certain geometry and peripheral speed. It is presented by von Seebach (1987) as the key parameter for roll sizing and is described by the following equation:

$$\dot{m} = \frac{M}{(D.w.\mu)} \qquad (1)$$

where M is the throughput in tonnes per hour, μ is the circumferential velocity of the roll, D is the roll diameter and w is the roll width. The resulting units are expressed as ts/hm^3. The ṁ value is used extensively in literature as a representation of throughput for certain machine parameters and feed conditions.

Based on the presented equation, knowledge of the ṁ value for a material and set of machine parameters allows a diameter, roll width and roll speed to be chosen for a throughput requirement. Application of the formula is based on the assumption that roll diameter, roll width and speed are linearly related to throughput. Von Seebach et al (1987) attribute first order changes in $\dot{m}$ to variations in feed size distribution, top size, particle shape, specific gravity, bulk density, internal friction and roll surface type as well as the friction between feed and the roll surface. The influence of roll geometry and roll speed is considered by von Seebach et al (1987) to be of second order. Further work by Schönert et al (1992) reported an inverse relationship between $\dot{m}$ and roll speed, i.e. a reduction in $\dot{m}$ occurs when roll speed is increased, and considered the degree of non-linearity to be of significance. Klymowsky et al (2002) also state that $\dot{m}$ is greater for rollers with larger diameters, as a result of improved material intake characteristics. The experiences of two HPGR operations, PT Freeport Indonesia Grasberg and Boddington Gold, support this suggestion. For both operations extensive pilot HPGR test work was carried out during the design phase to determine sizing factors such as $\dot{m}$. According to Banini et al (2011), the HPGR ṁ recorded at PT Freeport Indonesia was found to be 30% higher than evaluated during pilot HPGR testing. This led to the operator having to investigate methods of reducing the effective capacity of the machine in order to increase the specific energy applied to material being processed. Similarly, at the Boddington operation it was found that the design ṁ determined from HPGR pilot test work was approximately

30% higher during actual plant operation (Hart et al, 2011). The HPGR roll diameter at both sites is approximately 2 to 3 times larger than that of the pilot machines used for testing.

Discrepancies regarding the sensitivity of $\dot{m}$ to roll speed and the lack of published validations strongly suggest that the relationship of the parameters to throughput is more complex than presented by the formula.

Operating gap

The operating gap is defined as the smallest distance between the fixed and floating roller surfaces and is a dynamic parameter, the size of which depends on feed material properties, roll surface structure, specific pressing forces and roll speed (Schönert et al, 2002). The parameter is of particular significance to this thesis as it is used widely in literature for the derivation of throughput, albeit generally in these cases the derivation of operating gap itself is based on simple linear relationships which are not completely justified.

An example of such a generalization is the assumption that the ratio of diameter to operating gap is constant for otherwise equivalent operating conditions, as used by JKSimMet simulation software (Daniel, 2004). The reason for a relation between diameter and roll gap is addressed in detail by other fields, such as terramechanics, and is discussed later in this literature review. The apparent lack of detailed studies based on deriving a value for HPGR operating gap shows that a lot of work remains to be done in order to establish a valid method for its prediction.

Specific pressing force

Specific pressing force is used to compare the pressing force of rollers which are of different geometry (Schönert, 1985). It is a machine setpoint which is used to control energy input and shown by Austin et al (1993) and Lim et al (1997) to be inversely related to throughput.

Specific pressing force is expressed by the following equation:

$$F_{SP} = \frac{F}{D.w} \qquad (2)$$

where F is the hydraulic pressing force. The units for specific pressing force are normally presented as N/mm^2. Some publications present units of specific pressing force as megapascals. Although it can be said that the units are equivalent to that of pressure, it is apparent from the definition that the purpose of specific pressing force is to normalize the hydraulic pressing force according to roll geometry. The stress fields occurring between the rolls form a subject which is treated separately and discussed further in this document.

Net specific energy consumption

Net specific energy consumption is used to represent the net energy input of the HPGR per tonne of ore processed. More specifically it is defined as the total energy consumed through turning of the rolls during high pressure grinding minus the energy used during idle operation per unit mass and expressed in relation to the throughput, having units of kWh/t (Daniel, 2002).

Compression and nip angles

Many attempts at modelling the throughput of high pressure grinding rolls incorporate either the nip or compression angle, which define critical regions of the interface between the roller surface and feed material. The terms have been introduced into the field of HPGR from earlier work such as that of Johanson (1965), which addresses the prediction of briquetter performance.

The compression angle, α, is defined as the angle at which a pressure increase occurs between the rolls and material stressing begins. Figure 4 shows the general location of the compression angle in relation to the HPGR rolls. Similar to the operating gap, it is a fluctuating dimension and a function of machine parameters and feed properties (Schönert et al, 1992). References to the compression angle typically state values in the range of 7 to 12 degrees. Often throughout literature the terms nip angle and compression angle are interchanged, however they are distinct. The nip angle refers to the region of the roll where no slip occurs between the material bed and roll surfaces (Johanson, 1965). Whereas Schönert et al's (1992) definition of the compression zone does not define a slip-less region. Therefore, the nip angle is less than or equal to the compression angle.

Force reaction angle

The angle of force reaction β, shown in Figure 4, was introduced as a sizing parameter by a few authors including Schönert et al (1985) and Klymowsky et al (2002). The horizontal grinding force vector occurs at a certain distance from the roll nip. The roll angle at which the force vector occurs is referred to as the force reaction angle. It is related to torque, T, total pressing force and roll diameter by the following (Schönert, 1988):

$$T = DFsin\beta = \beta DF = \beta D^2 wF_{SP} \qquad (3)$$

Due to the small size of the reaction angle in HPGR operation, $sin\beta\ is$ replaced with β in equation (3).

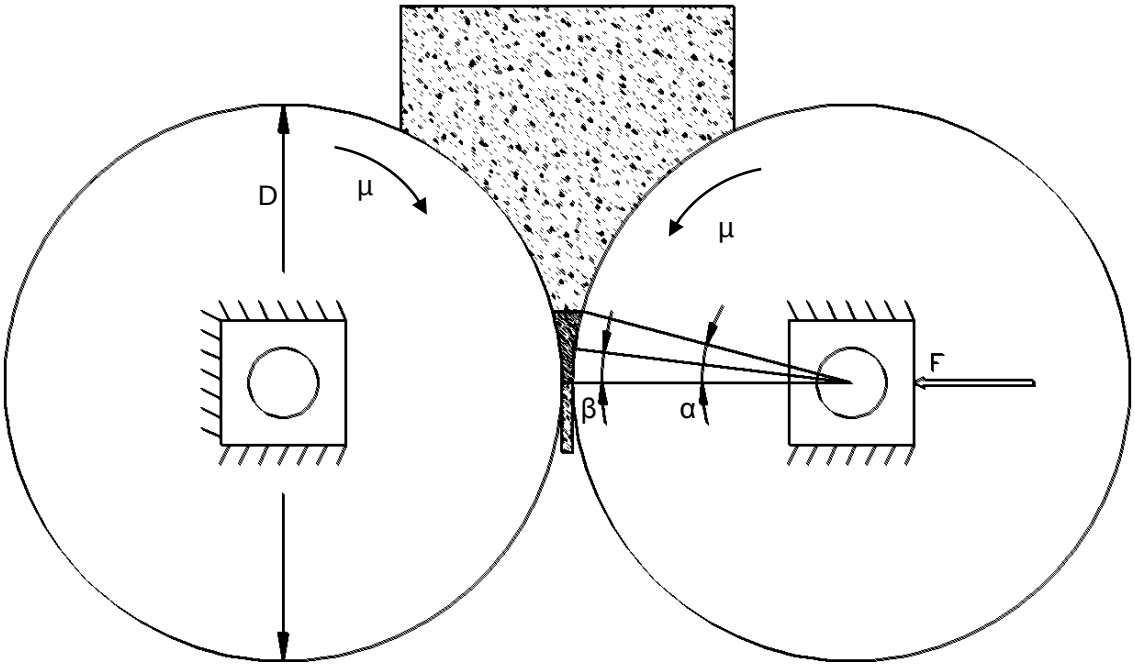

Figure 4 - Force reaction angle β and compression angle α (based on Schönert, 1985)

2.5 Scale up of HPGR units and motors

The results of a laboratory scale HPGR test are ultimately intended to be applied practically for engineering calculations such as the sizing of HPGRs. The main motors and rollers are the principle HPGR components which require sizing for a specific throughput duty, after which the size of the press frame, bearings and drive train components are specified. Different scale-up methodologies have been shown through literature and are summarized in this section.

Sizing of HPGR motors

The sizing of HPGR motors is based on application of either the force reaction angle or the net specific energy consumption, both of which are considered to remain constant within the range of scale-up. In the case where the force reaction angle is applied, its value is substituted into the following equation, as outlined by Schönert (1988), to derive the total specific motor power:

$$P = 2\beta \dot{V}_p F_{sp} \quad (4)$$

$$where\, \dot{V}_p = \mu w D \quad (5)$$

Alternatively, the total specific motor power can be derived through multiplying the net specific energy consumption value by the predicted machine throughput, as shown by equation (6).

$$P = E_{sp} M \quad (6)$$

where E_{sp} is the net specific energy consumption.

To determine rated motor power an application factor, f, is applied, which is stated by Klymowsky et al (2002) to generally be 10 to 15% higher than the specific motor power, thus the rated power of each individual motor becomes:

$$P_{motor} = \left(\frac{fP}{2}\right) \quad (7)$$

Critical evaluation of both methods is present in literature, such as that of Schönert (1988) who mentions that there is no indication of the force reaction angle being impervious to changes in geometry and machine parameters. The accuracy of both motor sizing methodologies is directly dependent on the precision of predicted throughput. As a result the development of an accurate method for throughput prediction will also improve the ability to size HPGR motors for an application.

Sizing of roll geometry

The sizing of roll geometry is directly related to the required machine throughput. Two primary approaches are discussed in literature, the first being the use of the previously introduced specific throughput constant $\dot{m}$ formula, which is used to size a roll for a desired throughput based on a known $\dot{m}$ value.

Another method for the sizing of HPGR rollers is based on the material flow geometry, as defined by the roller geometry, and material density. This particular relation of throughput and roll geometry is presented by Austin et al (1993) as:

$$M = \mu . w . x_g . \rho_g \quad (8)$$

where x_g and ρ_g are the roll gap and the density of material at the nip respectively. The above equation is based on the assumption that the material travels at the same speed as the roll surface and for this reason does not contain a variable for material slip. This is a reasonable assumption and is discussed later in this thesis. The continuity formula, also referred to as plug flow formula, is used in the comminution flowsheet package JKSimMet as a method to size rollers. The methodology requires knowledge of the density and gap for a certain roll diameter and roll angle.

2.6 Bearing of feed and press parameters

The influences of feed conditions and machine parameters on HPGR performance have been discussed since the implementation of HPGR technology. Known effects of feed and machine parameters on the HPGR process, primarily throughput, have been outlined in this section.

Critical feed parameters which have been identified by literature are: feed moisture content, mineralogy and size distribution. Roll parameters such as speed, surface type and geometry as well as specific pressing force have also been known to significantly affect HPGR performance.

Feed moisture content in HPGR operations typically ranges from 1 to 5 %, where variations within this range have been found to have a considerable influence on operational parameters. Fuerstenau et al (2007) reported a reduction in roll gap and throughput when higher feed moisture levels were processed, which is consistent with results of other publications. The influence of moisture on throughput has been reported to depend on the type of lining used; studded rolls being less affected than smooth rollers. In the case of studded lining, small amounts of moisture are known to assist in the development of an autogenous layer on the wear surface, thus reducing the roll wear rate, while higher levels of moisture generally result in greater roll wear (Klymowsky, 2002). Conversely, increases in feed moisture have been shown to result in higher specific power draws at the PT Freeport Indonesian process plant (Banini et al, 2011) and also at an HPGR operation treating copper porphyry ore (Herbst et al, 2011).

Roll wear rates have been shown to increase when the HPGR feed top size has been increased, especially where single particle breakage occurs. In the case of single particle breakage, substantially higher local peak loads are claimed to occur on the roll surface in comparison to those occurring during the grinding of feeds finer than the operating gap (Klymowsky, 2002).

Truncation of HPGR feed, where certain fractions of fines are not present in feed material, has been found to generally reduce machine throughput capacities (Morley, 2010) and significantly increase studded lining wear rates (Lane et al, 2009). However, fines are removed from HPGR feed using wet screens at the Khumani Iron Ore operation, where high roll wear rates were not experienced (Burchardt, 2011). It is evident that more work needs to be done to understand the effects of feed size distribution on HPGR performance and is a topic which is particularly relevant to the aims of this thesis.

To date little work has been carried out on narrowing down the effects of mineralogy on HPGR comminution. HPGR results for a wide range of ore types have been published; however there is little evidence of detailed analyses on the effects of mineral grain size or texture on HPGR performance. Assessments of rock mineralogy and its influence on HPGR operation has been mostly focused on the aspect of roll wear rate.

Abouzeid et al (2009) investigated the HPGR grinding of mineral mixtures consisting of soft and hard minerals, limestone and quartz respectively. The specific energy consumption was found to be independent of the ratio of limestone to quartz. However, larger operating gaps and throughputs

were recorded when greater proportions of limestone were included in feed mixtures. The increase in gap and throughput due to a greater proportion of 'soft' material, represented by limestone, is of particular interest with regards to the objectives of this thesis. The normalized comminution energy utilized for breakage of the quartz, represented by an energy split factor, decreased as greater amounts of limestone were added to the feed mixture. Overall, greater size reduction was found with limestone for the tested range of mixtures and it was posited that the quartz was considered to have the effect of a grinding aid. Similar comminution effects were found by Benzer et al (2011) for grinding mixtures of clinker and soft materials. Further work incorporating petrographic analysis is required to determine the role of mineral content and texture within the field of high pressure comminution. Such a study would certainly be able to be carried out on a laboratory scale and would potentially be relevant to not only HPGR throughput prediction, but overall HPGR performance.

Specific pressing force is used to control the fineness of HPGR product and subsequently affects the motor power drawn (Banini et al, 2011). Other effects of increasing specific pressing force are known to be the reduction in operating gap and HPGR throughput as described by Austin et al (1993). Similarly, the operating gap of an HPGR operating at the Tarkwa gold mine was found to decrease when a higher specific pressing force was applied (Dundar et al, 2011). These findings are consistent with those of other literature and indicate that specific pressing force is a parameter which needs to be carefully considered during development of a laboratory test targeting HPGR throughput.

Aside from being directly related to throughput, roll speed has been known to affect the wear rate of roll surfaces, where higher speeds lead to increased wear rates (Klymowsky, 2002). For this reason the roll speeds of four HPGRs operating at the Boddington process plant are controlled individually by a DCS according to the specific throughput recorded for each individual HPGR. In order to increase the overall roll wear life, the roll speeds of HPGRs operating at Boddington with higher specific throughputs are automatically increased while roll speeds of HPGRs operating with low specific throughputs are decreased (Hart et al, 2011). Although it is unclear as to why different specific throughput values would be experienced at the same mining operation for equally sized machines. Lubjuhn et al (1993) reported that for otherwise equivalent operating conditions, changes in roll speed were found to have no significant influence on comminution.

As previously discussed, studded lining rollers have become the norm in comminution of minerals with HPGR. The influence of various types of roll liner on HPGR performance was a focus of earlier HPGR based papers, which were published at a time when various roll liner designs were being considered. The relevance of the roll surface is of particular interest when trying to derive key parameters affecting throughput, such as the friction between feed and roll surface. In this context higher throughputs have been associated with studded and profiled roll liners in comparison to that of smooth roll linings (Morley, 2003; Schönert et al, 2002). The work of Lim et al (1997) also showed

that larger operating gaps were measured when studded lining was used, in comparison to that of smooth lining. The increase in roll gap was attributed to be due to a larger frictional coefficient existing between the feed material and the autogenous layer on the studded roll surface. Supporting this point, Lubjuhn et al (1993) stated that in order to achieve higher throughputs the friction on the roller surface should be maximized. It has been reported that roll surface type has only a minor influence on the degree of comminution (Lubjuhn et al, 1993). Other studies have found that comminution efficiency is lower with studded rolls when compared to smooth rollers, possibly due to differences in operating gap size (Lim, 1999). In retrospect, previous investigations into the effect of roll liners on HPGR performance have suggested that the frictional coefficient between feed material and the roll surface has a significant relation to throughput and gap. This leads one to posit that for one type of roll surface, the coefficient of friction will vary according to the material being processed. Therefore, the frictional properties of feed material are a parameter which has a proven relevance to throughput, operating gap and consequently the work of this thesis.

Roll geometry, as defined by the width and diameter, are machine design variables which are referenced in the previously presented throughput capacity and pressing force equations. The aspect ratio of the roller, width to diameter, is a design parameter which has an influence on the product size and throughput characteristics. Coarser products have been associated with low aspect ratio rolls, due to the fact that a larger proportion of material is crushed in the edge zone, where a smaller degree of comminution is known to occur. Overall, roll diameter is typically considered throughout literature to have a greater influence on HPGR performance then roll width; examples being higher $\dot{m}$ values attributed to larger roll diameters as stated by Klymowsky et al (2002) and the relation of gap to roll diameter as mentioned by Ntsele et al (2007). The influence of diameter on throughput and gap prediction necessitates more fundamental work to explain the observances and for its adequate incorporation into predictive models.

2.7 Analysis of roll surface and material interactions

The geometry of the HPGR effective area, aside from variations in feeding mechanisms, is equivalent to that of roller presses used in compaction applications. The role of the roller press as a comminution device is a relatively new one and for this reason a greater amount of research has been published on the science of roll compaction rather than HPGR. It can be argued that certain analyses of forces, material flow and geometry occurring in roll compactors can be applied to the study of HPGR. Hence, texts from both applications are referenced in this section.

The geometrical variables which are generally referenced in studies of roller presses are shown in Figure 5.

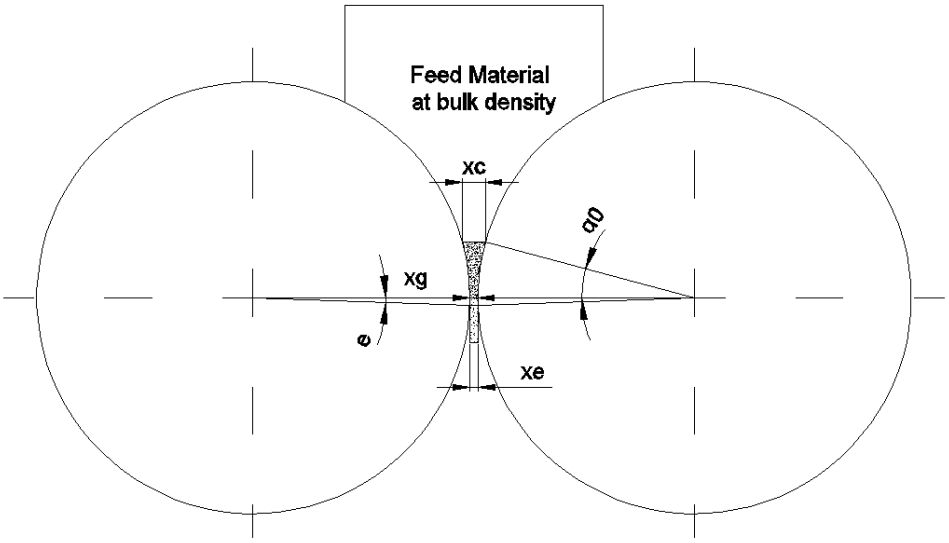

Figure 5 - Geometry of rollers and material

2.7.1 Geometrical description of rolls and material

The horizontal distance between the surfaces at the compression angle, α, is referred to as the critical gap, x_c, and is shown in Figure 5. The critical gap can be determined from knowledge of the roll diameter, operating gap and material densities at the beginning of the compression zone and at the roll nip (Morrell et al, 1997):

$$x_c = 0.5\left\{\left(D + x_g\right) - \left[\left(D + x_g\right)^2 - \frac{4\rho_g x_g}{D\rho_c}\right]^{0.5}\right\} \qquad (9)$$

where x_g is the operating gap, ρ_c and ρ_g are material densities at the beginning of the compression zone and at the roll nip respectively. The formula is based on the assumption that material is transported within the compression angle at the same speed as the roll surface, viz. it is equivalent to the nip angle. Schönert et al (2002) found through roll stress distribution analyses that this assumption is appropriate in application to HPGR. Lubjuhn (1992) stated that in cases where feed particles are smaller than the operating gap, the size of the compression angle is determined only by the internal and external angles of friction of the feed, assuming the material supply and friction angles are not affected by the feed particle size. Studies in soil mechanics show that material particle size generally has an influence on the internal angle of friction, but the significance given to frictional properties is still noteworthy for the purposes of HPGR laboratory test design.

The entry and extrusion angles (also referred to as exit angle and release angle), have received surprisingly little attention in geometrical analyses of HPGR roll–material interaction zones. Cunningham (2005) found that the size of the entry angle, the angle at which the surface of the roll makes initial contact with feed material, had an influence on the density of sample at the roll nip of a

compactor. Lubjuhn (1992) found that the exit angle, the angle at which HPGR product makes final contact with the roll surface, varies from 3 to 9 degrees through testing with a laboratory scale HPGR.

It is acknowledged in both powder compaction and comminution literature that acceleration of material may occur in the extrusion zone, also known as the relaxation zone and defined in Figure 5 by angle e. The reduction of compressive forces in the extrusion zone allows compacted material to expand volumetrically. Geometrical definitions of the interface between rolls and material are useful tools that could potentially be applied for a mechanistic approach to throughput modelling.

2.7.2 Pressure distribution on roll surface

Hydraulic force applied to the bearings of an HPGR roll eventuates in a distributed pressure profile being present on the roll surface. It is reported to depend on the material type and machine operating conditions. The pressure profile occurring in the HPGR is one that could be potentially repeated in a controlled fashion using laboratory test equipment providing results for inclusion in predictive equations. Hence, within the work of this thesis the roll pressure profile is considered to be a fundamental aspect of HPGR, which necessitates careful consideration during test development.

The roll pressure distribution is typically discussed in literature according to 2 dimensional visualisations. This subject has found to be comprehensively addressed by the work of Johanson (1965), Lubjuhn (1992) and Schönert et al (2002). A depiction of the published 2D profiles is presented in Figure 6 as a 3D image.

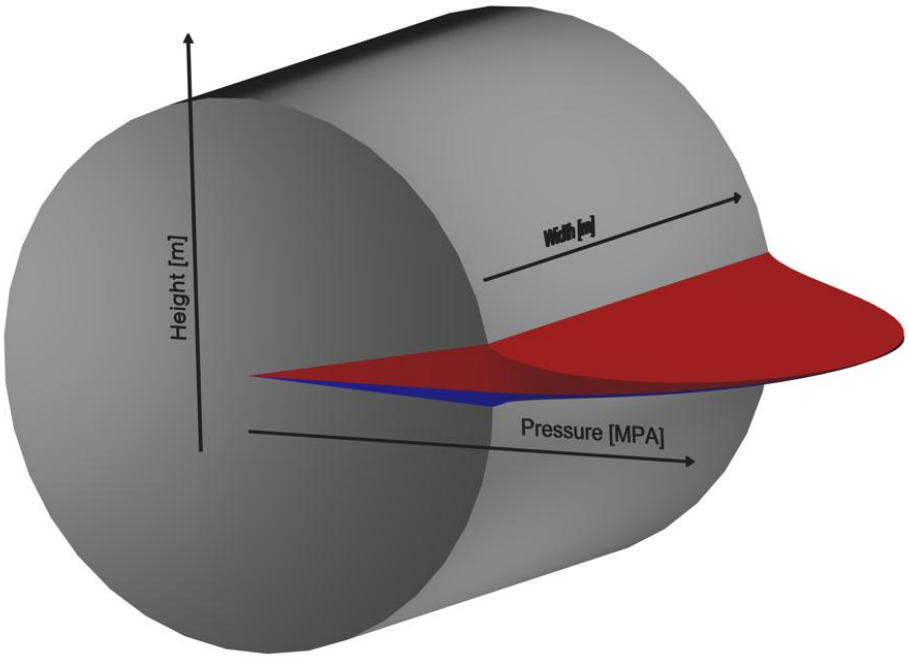

Figure 6 - Depiction of roll pressure distribution (drawn with Autocad 2012)

Lower pressures occurring at the extremities of the HPGR roll, referred to as edge effect, have been attributed to the presence of static walls, also called cheek plates, which inhibit the rate of flow at the edges of the rolls and thereby the roller gap is depleted of material in these areas (Kleeberg, 2007). The edge effect is considered to be substantial in that the method of comminution within this area is reported to be due to single particle crushing rather than interparticle comminution.

Based on detailed analysis of the axial pressure distribution, Lubjuhn (1992) suggested that the profile is independent of feed material properties and described it by a function of the following form:

$$\frac{p(\lambda)}{p(\lambda=0)} = 1 - (2|\lambda|)^n \qquad (10)$$

where λ = I/w, I is equal to the axial location on the roll (at the centre of the roll I=0) and n is slightly dependent on the specific pressing force setpoint, but having an approximate value of 1.6 (Lubjuhn, 1992). Conversely, Cunningham (2005) found that a greater frictional coefficient between cheek plates and material corresponded to a greater reduction in pressure at the centre of a compactor roll. These conflicting findings indicate that more work on the behavior of the axial pressure distribution is required.

A radial pressure profile as measured with a roll mounted pressure sensor is shown in Figure 7, where it can be seen that the peak pressure value occurs just prior to the zero roll angle. Shear stress measurements also found that initially shear works against the direction of rotation and changes direction at a point above the zero angle.

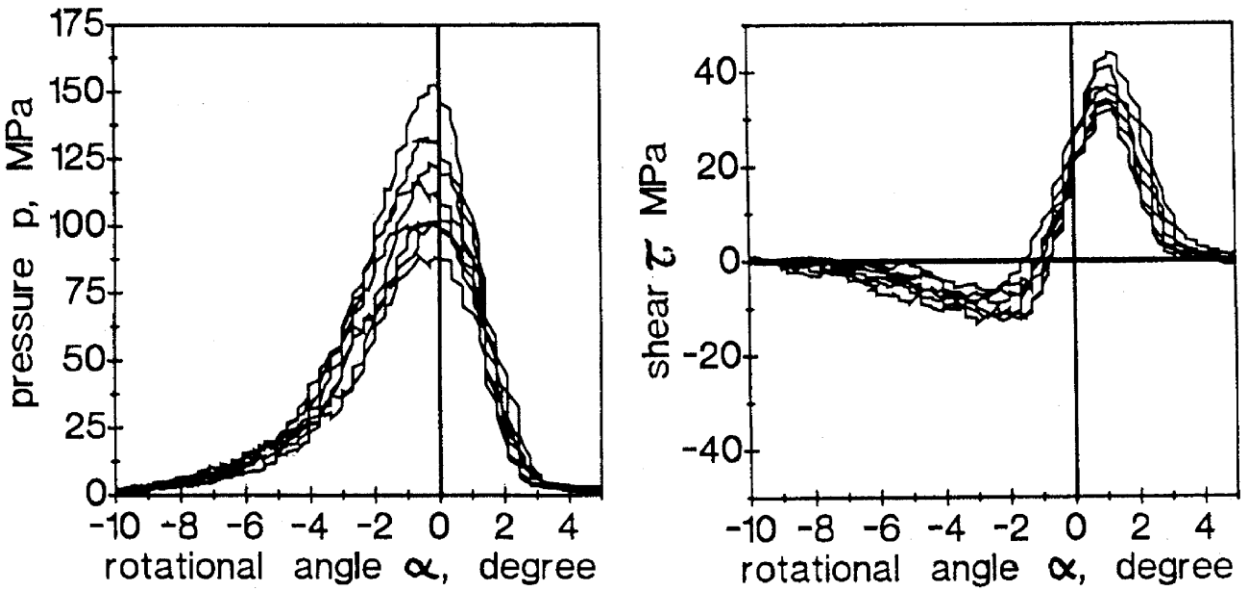

Figure 7 - Measured pressure distribution in the compression zone (Schönert et al, 2002)

Further work by Schönert et al (2002) showed that the ratio of shear stress to normal stress on the roll surface was smaller than the measured external friction angle of the material throughout the entire compression zone. From this it was posited that as a general rule no slip occurs at the roll nip, where α = 0 degrees, however slip exists near the outlet where material relaxation occurs. These findings are consistent with that of Johanson (1965), whose rolling theory for granular solids also concluded that slip cannot occur at the zero angle. This finding has great implications on a potential throughput model incorporating the results of a laboratory scale test.

Schönert et al (2002) and Unland et al (1998) attempted to determine the overall dissipation of hydraulic pressing forces through application of known or theoretical radial pressure distributions. Both of the mentioned modelling attempts included the use of material parameters which represent the compressibility and frictional properties of feed. The derivation of either model is beyond the scope of this literature review, however they do provide a solid basis for the comparison of material friction and compressibility to measured HPGR throughput, a focus of this dissertation.

2.7.3 Influence of fluid entrainment in the material bed

The pressurization of air in the compression bed has been brought up in literature with varying views on the associated effects on the HPGR process. A comparison carried out by Mütze et al (2008) of stress velocities in application to confined beds, showed that the capability of air to escape the particle bed was a factor that affected specific energy consumption. Less efficient comminution was said to have resulted with higher compression velocities, due to the additional energy expense of compressing air (Mütze et al, 2008). Similarly, Unland et al (2008) attributed greater specific energy

consumption at higher roll velocities to energy consumed at the expense of de-aeration of the material bed. Water entrainment and its effects on high pressure grinding has not been widely discussed and may be of particular relevance to the work outlined in this document.

2.8 Inter-particle breakage

Inter-particle breakage is a comminution method where a particle bed is subjected to a level of compression which is sufficient to induce breakage of individual particles located in the bed. This method of breakage, which occurs in high pressure grinding rolls, is quite distinct when compared to that of other crushing and grinding machinery. Proper reference to the breakage characteristics occurring in confined material particle beds is required in order to help develop an approach to HPGR laboratory test development.

Analysis of energy utilization in stressed particle beds has outlined how energy is dissipated through this method of comminution. Sub-processes in batch type compression have been shown as being the following (Mütze et al, 2008):

- Energy absorption till breakage occurs (breakage energy);
- Friction between particles (friction losses);
- Inelastic deformation of particles (plastic deformation work);
- Frictional losses by displacing the fluid in the pores (flow losses);
- Compression of entrained fluids in the particle bed

The breakage which takes place during high pressure comminution is described by Gutsche et al (1999) as the fracture of particles occurring from high inter-particle stresses generated locally at the contact points of neighboring particles. Taking into consideration that the stress experienced by a certain particle is dependent on: the intensity of the stress field, location of the particle in the confined bed and number of contacting particles, it is apparent that the granular composition of a material has a bearing on the facture kinetics. Conversely, the presence of a large amount of fines in the compaction bed will retard the breakage of coarse particles. A large number of contact points between a coarse particle and surrounding fine particles results in isostatic pressure being transmitted, also referred to as retardation (Gutsche et al, 1999; Schönert, 1979).

Diminishing benefits in breakage for incremental increases in pressing forces are typically seen during operation of high pressure grinding rolls. Discrete Element Modelling (DEM) has been used to analyze the asymptotic relation between compression and size reduction. The ultimate size distribution of compacted material is said to be fractal in nature and thus self-similarity has been used in attempts at modelling inter-particle breakage (Ben-nun et al, 2010).

2.9 Comminution equipment and testing

The paths taken by other researchers to successfully implement metallurgical tests for comminution equipment are obvious benchmarks for the development of a laboratory scale test for HPGR throughput. Examples of industry accepted laboratory scale grinding tests as offered by major commercial testing facilities are:

- Bond Ball Mill Work Index Test
- Bond Rod Mill Index Test
- Bond Low-Energy Impact Crushing Work Index Test
- JK Drop Weight Tests

The Bond ball mill work index test was developed through the correlation of energy and comminution results from a 1 foot diameter ball mill to that of an 8 foot ball mill (Gupta et al, 2006) and is currently the industry standard for predicting the specific energy of ball mills. Bond's empirical approach differs considerably to the JK Drop Weight Test where single particular impact breakage is carried out at controlled energy levels and the results of which are principally applied to specific energy prediction of Autogenous (AG) and Semi-Autogenous (SAG) mills (Shi et al, 2009). The applicability of the JK Drop Weight Test to tumbling mills is based on the observation that impact breakage, as carried out in a controlled manner in the JK Drop Weight Test, occurs during mill operation. Comminution through abrasion is also identified as occurring in AG and SAG mills, for which reason JK Drop Weight Tests are carried out in parallel with abrasion tests and the results of both are combined mathematically for a single power prediction. Thereby two proven approaches to comminution test development are apparent from comparison of the Bond and Drop Weight Test methodologies: one where the results of a scaled down piece of equipment are correlated with that of its full scale equivalent as exemplified by Bond's ball mill test; the identification of individual breakage mechanisms which are consequently the focus of individual sub-tests and combined as a test suite. Both of the two historically proven approaches are potentially applicable to the development of a test for the prediction of HPGR throughput.

2.9.1 HPGR testing development

The assessment of ore amenability to HPGR is currently carried out with laboratory and pilot scale HPGRs. Most testing facilities are operated with involvement from HPGR manufacturers. Procedures for pilot testing have not been standardized across the mining industry, but typically involve a series of batch tests with each test varying in machine and/or feed parameters.

HPGR laboratory and pilot testing

Attempts at standardizing laboratory HPGR tests have been made by the Julius Kruttschnitt Minerals Research Centre (JKMRC). The tests are conducted on a 0.25 meter diameter Labwal machine and require 25 kg of sample per test. Scale up from the JK test is based on the assumption that the relationship between the feed size distribution, feed bulk density, working gap and roll diameter for the laboratory scale test will be the same as that found in full scale operation. However, measurement of the Labwal operating gap is deemed to be difficult and thus a significant variation in machine sizing may potentially result (Daniel et al, 2009).

Klymowsky et al (2002) suggested that laboratory sized machines may be used for preliminary conceptual testing. Laboratory and pilot HPGR test programs would subsequently be used to investigate the influence in variation of grinding pressure, moisture (if applicable) and feed size distribution.

The fact that laboratory scale HPGR units, such as the Labwal, have not replaced pilot HPGR testing is due to the discussed inaccuracies in scale-up of results. Due to wall effects, a practical limit in scale-down of machines from an industrial scale to a miniaturized version must exist. Thus, the Labwal sized unit may well be considered to be outside of this practical limit.

Piston press testing

Through review of literature, it can be seen that HPGR has been developed as a result of the study of inter-particle comminution primarily through confined bed pressure testing. After development of the HPGR, the piston press was revisited in order to attempt the prediction of HPGR operation. To some extent the piston press test approach has been standardized by Schönert (1996), where geometrical guidelines for researching inter-particle breakage were established through a systematic series of piston press tests. However, wall effects in this test are significant and geometry must be carefully specified. The appropriate geometry of the material bed in the die was defined as having a height more than six times the particle size and a diameter of more than three times the height. Many piston press studies including that of Daniel, (2002), Oettel et al, (2004), and Hawkins, (2007) used this guideline as a basis for piston press testing.

Stressing material with a piston press allows the operator to directly specify the pressure applied to the material bed. However, as previously discussed, no clear method for estimating the pressure being applied at a specific point on the roll surface of an HPGR has been developed to date. A popular approach has been to translate the specific energy consumed during a piston press to an

HPGR specific energy value. The energy consumed during a piston press cycle can be determined through integration of the force versus displacement curve resulting in units of work (or power if units of time are observed). This approach has shown to be the principal method of comparing specific energy of the piston press and HPGR, and was included in studies such as that of Fuerstenau et al (1996), Oettel et al (2001), Daniel (2002), Hawkins (2007) and Bulled et al (2009).

Examples of using piston press testing as a direct method for predicting HPGR performance are studies carried out by Hawkins (2007), Bulled et al (2009) and Kalala et al (2011). Hawkins (2009) compared piston press results to lab scale HPGR results through force and displacement energy methods as well as geometrical methods where distances between solid working surfaces of both pieces of equipment were adjusted to be equivalent. Due to difficulties in measuring initial and final piston positions as well as the greater number of variables associated with the geometrical method, the energy method was primarily used. It was found that the piston and die test could be used to predict the product of an HPGR, which is operating primarily through inter-particle breakage (where feed is finer than the operating gap), and also the specific energy consumption at which retardation in breakage occurs. However, due to lack of knowledge of the HPGR bed pressure, the piston press needed to be complemented by HPGR laboratory scale test results.

Piston press equipment has also been used to attempt the derivation of a High Pressure grindability index (HPi) (Bulled et al, 2009). The test, referred to as the Static Pressure Test (SPT) utilizes 100 and 70 mm diameter dies and a modified workshop press rated at 50 tonnes of compressive force. The procedure involves preparing 2 to 3 kg of piston press feed to a top size of 19 mm and a minimum size of 3.35 mm and is carried out as a locked cycle test. The feed is compressed in the piston press at a constant displacement rate until it reaches a setpoint pressure of 55 or 110 MPa. Material smaller than 3.35 mm is screened out of the piston press product and fresh -19 mm material , including material smaller than 3.35 mm, is added to make up for the weight of removed material. The compression tests are repeated using this batch methodology until the value of particles smaller than 3.35 mm is consistently achieved. The specific energy consumed during a test is derived from the force, displacement and time recorded. A representative specific energy for the series is determined from the average of the final three batch cycles, where typically five tests are sufficient to achieve stabilization of the test series. The measured specific energy consumption, feed and product sizes are combined to determine the HPi index through the following equation, which is similar to that of Bond's third rule:

$$E = 10 * HPi * (\sqrt{(1/P_{80})} - \sqrt{(1/F_{80})}) \qquad (11)$$

where F80 and P80 are the aperture sizes of a screen through which 80% of the respective feed and product masses pass through. SPT results were calibrated to Labwal HPGR test results to support

the predictive equation (Bulled, 2009). It must be noted that the 55 MPa application pressure used by the SPT test only barely exceeds the pressure stipulated in Schönert's (1979) patented method of inter-particle comminution, where compression is specified as being 50 MPa or greater, and the relationship of feed top size, initial bed height and die geometry is considerably different to the guidelines established by Schönert (1996). Further alignment of the test with these parameters is perhaps required.

Kalala et al (2011) were able to achieve similar product size distributions to that of high pressure grinding rolls. However, the energy input into both devices for equivalent product sizes was shown to be considerably different when higher HPGR specific pressing forces were used. To date, developments in piston press test and interpretation methodologies have not shown direct applicability to the prediction of HPGR performance and suggests that sole use of such equipment is not adequate for the prediction of HPGR performance. This is especially apparent when the complex pressure distribution occurring along HPGR roll surfaces is taken into account.

Application of comminution index tests

Review of literature shows that there has been no successful application of comminution tests, originally developed and applied to other comminution equipment, to the estimation of HPGR performance. This fact is most likely due to the uniqueness of the breakage mechanism, inter-particle breakage, associated with HPGR.

The SMC Test ® is marketed by SMC Testing and test license holders as a comminution test which provides a means for estimation of specific energy consumption of comminution circuits using various combinations of comminution equipment such as: autogenous and semi-autogenous mills, ball mills, rod mills crushers and HPGRs. The test uses pieces of core or rock having a median size of approximately 30 mm or smaller (Morrell, 2009). The test was originally developed to predict the specific energy of AG and SAG mills using pieces of small diameter core. The pieces of rock or core are separated according to certain size specifications and broken in an impact device where the impact energy can be closely controlled. Feed and product sizes, and impact energy are used to characterize the breakage of samples (Morrell, 2004). One outcome of the SMC Test ® is an HPGR work index, M_{ih}, which is applied to an empirical equation based on the results of 19 different HPGR circuits. The following is the equation used to determine the HPGR specific energy, W_h, for a certain feed and product size, circuit configuration and an ore specific HPGR work index M_{ih} value:

$$W_h = S_h K_3 M_{ih} 4 \left(x_2^{f(x_2)} - x_2^{f(x_1)} \right) \qquad (12)$$

where x_2 and x_1 are the HPGR circuit product and feed P80 particle sizes in microns respectively, S_h is a coarse ore hardness parameter and K_3 is a circuit parameter which is dependent on whether the HPGR operates in open or closed circuit configuration.
The values of $f(x_1)$ and $f(x_2)$ are determined from the following equation (Morrell, 2009):

$$f(x_j) = -(0.295 + \frac{x_j}{1000000}) \quad (13)$$

From literature and marketing documentation related to the SMC Test ®, it is unclear how the HPGR work index, $W_{h,}$ is derived. Little clarification has been provided regarding the applicability of an impact breakage test to a process characterized by compression breakage and furthermore the methodology does not incorporate feed moisture which is known to affect HPGR energy consumption. Overall, more empirical data and perhaps test development is necessitated to confirm the validity of using the SMC Test® method for HPGR energy prediction.

2.10 HPGR models

The results of an HPGR laboratory scale test will inevitably be applied through the use of a predictive model and for this reason previous attempts at HPGR modelling are presented in this section. Performance indicators of HPGR operation have been typically divided between energy-comminution models and throughput models, with considerable emphasis on the former. Throughput and energy-comminution models are covered separately in this section.

2.10.1 HPGR energy-comminution models

The popularity of energy-comminution modelling in application to HPGR stems from the origins of the technology: studies focusing on static compression breakage and its relation to energy consumption. Through review of literature it is apparent that an important modelling tool is the phenomenon of HPGR product size distributions being self-similar as described in the review of inter-particle breakage literature.

Pre-existing crushing and grinding models have been applied to HPGR, one example being that of Fuerstenau et al (1995). The following is a batch grinding time dependant model originally extended to continuous grinding systems to describe the product size distribution (Reid, 1965) :

$$Z_i(t) = \sum_{j=1}^{i} w_j(t) = \sum_{n=1}^{i} c_{n,i} exp(-k_n t) \quad (14)$$

where $z_i(t)$ is the % weight greater than size $x_{i,}$ w_j is the weight on a screen j, and the breakage rate k_n and constants $c_{n,i}$ are derived experimentally. As grinding time is not the governing factor in HPGR comminution, Fuerstenau et al (1995) replaced time t with a rescaled energy E', normalized

the energy breakage rate function and introduced an energy dissipation component y in the following way:

$$E' = \frac{E^{(1-y)}}{(1-y)} \qquad (15)$$

where E is the specific energy. Substituting into Reid's (1965) equation it becomes:

$$Z_i(E') = \sum_{j=1}^{i} w_j(E') = \sum_{n=1}^{i} c_{n,i} exp(-k_i^0 E') \qquad (16)$$

In order to apply the above equation, the parameters y, k_i^0 and constants $c_{n,I}$ need to be derived from an experimental set of data. Thereafter a size distribution can be estimated for a specific energy input. Although this form of population balance equation was shown to fit well to a few sets of actual HPGR data (Fuerstenau et al, 1995), it does not address the retardation of breakage rates which occurs when a large amount of fines are present, the influence of specific energy on transport inefficiencies nor the effect of the gap on limiting the top size of the product.

Many energy input based empirical models have been proposed for the estimation of HPGR comminution, examples being the work of Lim et al (1996), Liu et al (1996), Morrell (2010) and Hinde et al, (2009). Interestingly the aforementioned models do not account for the influence of the gap on product size. Austin et al (1993) applied and critically reviewed HPGR models which were modified forms of the batch grinding equation as well as one based on a roll crusher model. The resulting claim was that the tested models were not suitable for predicting HPGR product and that accurate simulation of the HPGR requires knowledge of the effects of specific grinding pressure, roll speed on throughput, power draw and product size distribution as the roll speed and pressure are the two control variables available to an operator. It is important to note that the previously discussed pressure distribution and associated maximum pressure have not yet been successfully integrated into an HPGR comminution model.

2.10.2 HPGR throughput models

A few attempts at establishing a model to describe the rate at which material is being transferred by the rolls have been carried out in the past. Approaches to developing a throughput model and the desired outcomes have varied greatly. Generally, study of the throughput of the high pressure grinding roll has been quite minimal in comparison to that of inter-particle breakage and energy relationships. Specifically little attention has been given to the effect of feed properties on the roll transportability of material.

The throughput calculations outlined earlier in this review can be considered to be forms of throughput models. A majority of these calculations and their applicability relies on the constancy of either of the following:

- gap to diameter ratio
- compression angle
- throughput as a function of roll dimensions and roll speed

Austin et al (1993) developed an empirical throughput model based on flow continuity and grinding pressure. The model assumes that material located at the beginning of the compression zone has a density equal to that of the bulk density and the following equation was derived:

$$1 - \theta_g = (1 - \theta_c)\left[(1 + \frac{1-cos\alpha_c}{x_g/D}\right] cos\alpha_c \qquad (17)$$

where $\theta_g$is the porosity of material in the gap nip and θ_c is the porosity of material at the nip angle.

Based on this derivation, an empirical form was developed which accounted for pressing force:

$$\left(1 - \theta_g\right) - (1 - \theta_0) = aP^b \qquad (18)$$

where θ_0 is the porosity for zero pressing force, a and b are empirically derived values and P is the specific pressing force. Constants a and b were found to vary with material type and size distributions (Austin et al, 1993). Further critical review of the model through application to lab and pilot sized HPGRs determined that the model is inadequate. Derived values of material porosity were negative in some instances as well as theoretically impossible angles of compression were calculated. Inaccuracy of the model was explained as being primarily due to the assumption of slip-less transport in the compression zone. Additional development of a throughput model was carried out on the basis that the throughput constant $\dot{m}$ varies as a linear function of the logarithm of specific pressing force (Lim et al, 1997):

$$\dot{m} = F_r F_s F_w F_T F_u (1 + slog F_{sp}) \qquad (19)$$

where variables Fi are factors for surface roughness, machine scale-up, feed moisture content, feed top size and roll size. The constant s represents the sensitivity of throughput to changes in specific pressing force. The factors and constant s were derived from laboratory and pilot test work (Lim et al, 1997). The potential for slip in the compression zone is accounted for in the mentioned empirical model; however it is dealt with using an empirical formula. Later experiments of Schönert et al (2002) showed that recorded roll shear and normal pressure ratios were lower in the compression zone than the material surface friction coefficient. Thus slip was not included in theoretical modelling approaches.

2.10.3 Holistic HPGR models

Attempts at developing holistic models which simultaneously address aspects of throughput, power and comminution have been published and are reviewed in this section. Morrel et al (1997) proposed an approach referred to as the Morrell-Tondo-Shi model which incorporated throughput, energy and comminution outcomes. Input parameters were derived from laboratory scale HPGR tests. The throughput model is based on the continuity formula while the energy consumption is directly measured from the test HPGR unit. The roll gap determined through test work is scaled and used as an input parameter for a roll crusher function known as the pre-crusher zone. Further comminution in the compression zone is defined by two breakage functions: a compressive breakage function which models comminution occurring at the centre of the roll, and another roll crusher function which predicts single particle breakage taking place at the edge of the roll. A material split function determines the degree of influence of either compressive or roll crusher function. This model has also been incorporated in similar form in the JKSimMet mineral processing software (Daniel et al, 2004). Similarly, Torres et al (2009) used separate comminution models to estimate initial breakage through relating particle size to material bed width and subsequent inter-particle compression. The difference between breakage in centre and edge zones was also addressed. The throughput model is similar to that of Morrell-Tondo-Shi, however energy is derived from a known force reaction angle which is assumed to be constant for different roll geometries (Torres et al, 2009).

The described models clearly go beyond the many empirical energy based derivations which have been used primarily for estimation of the degree of breakage. A comminution model which incorporates crushing of coarse particles as a result of geometrical roll boundaries can be considered to be semi-mechanistic. Furthermore, the incorporation of pressure distribution functions into a holistic HPGR model is an opportunity to reduce the reliance on specific energy based empirical breakage functions and justifiably extend predictions beyond the empirical database.

Shortcomings in holistic HPGR models raise questions about the approaches and input parameters used by researchers to date. The majority of holistic HPGR models treat energy-breakage and throughput as individual components of a modelling methodology. Energy losses due to the transportation of material via the roll surface have been typically assumed to be non-existent, which has shown to be untrue based on the degree of shear measured on the surface of HPGR rolls. Furthermore, the complex interrelation of compression and shear has been rarely addressed in the field of HPGR unlike other fields, such as terramechanics, which deal with similar geometries. A review of HPGR models has shown that a greater understanding of material parameters and the 3 dimensional roll pressure profile is required to improve the chance of developing a laboratory scale test for HPGR throughput, prompting to look outside the field of mineral comminution.

2.11 Terramechanics

The physical mechanics of land locomotion, primarily with respect to ground vehicles, is a field of study which is covered by terramechanics and is outlined in this literature review, as it forms the basis of experimental methodologies used towards the aim of developing HPGR laboratory tests targeting throughput. The introduction of the field of terramechanics to a study on a piece of mineral processing equipment, is in-line with the aim of identifying and applying knowledge from fields of study which deal with the geometrically similar problem of predicting roll and material interactions.

The connection between HPGR and terramechanics is most apparent when looking at the geometry analyzed in studies of a rigid wheel traversing a soft soil, as shown in Figure 8. Aside from an obvious difference of 90 degrees in orientation, the two principal embodiments from each field of study are very similar and support the analogy.

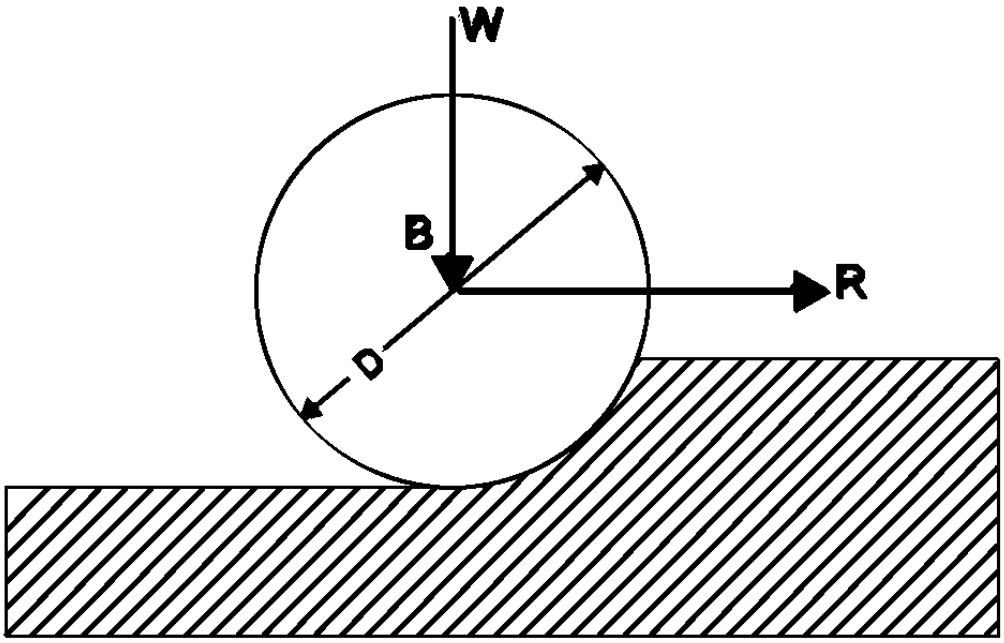

Figure 8 - Geometry of wheel-soil interaction (based on Bekker, 1956)

Previously discussed areas of HPGR research such as modelling of pressure profiles and prediction of energy utilization are also subject areas in terramechanics which have been covered extensively. Other parameters of terramechanics can be considered to be analogous to those covered by HPGR researchers, an example being the analogy of HPGR specific pressing force to the weight exerted onto a wheel. Differences between mineral comminution and terramechanics testing methodologies were embraced in this thesis, as they were considered to be a resource of tools which could potentially be transformed and applied for the development of a laboratory scale HPGR throughput test.

2.11.1 Background to terramechanics

The ability for a ground vehicle to traverse a particular terrain pertains to a variety of applications including construction, agriculture, forestry and military with increasing emphasis on space exploration. As academic study of terrain and vehicle parameters extends from the early 20th century, coupled with the range of industries which deal with land locomotion, material published on the subject matter is extensive when compared to that of HPGR focused studies.

The degree to which a vehicle can traverse a terrain is primarily defined by the ability of soil to provide sufficient resistance to the vehicle weight and to produce the necessary thrust, also referred to as tractive effort. To approach this problem the weight and thrust of a vehicle needs to be related to certain material properties of soil (Bekker, 1957). Thus, terramechanics also draws heavily upon the subject matter of soil mechanics and consequently another field of study is introduced into this HPGR focused research and discussed later in this thesis.

Terramechanics is a wide field which is selectively drawn upon in this section based on the author's interpretation of its applicability to the problem of predicting HPGR operation. In this respect, the characterization of soils and mathematical modelling of wheel and soft terrain interactions, particularly the case of a rigid wheel traversing a soft terrain, has been identified as being potentially analogous to the study of HPGR roll and ore interactions.

2.11.2 Parameters and terms referenced in terramechanics

This section aims to introduce the parameters referenced in terramechanics, in particular studies of rigid wheel and soft terrain interactions for a vehicle in a driving state, and conveys their potential application to HPGR.

Wheel sinkage

Sinkage is the vertical displacement of a wheel due to soil deformation and is similar to the notion of 'floatability', which is an indication of the ability of a vehicle to overcome sinkage. These terramechanics based parameters, can be considered to be analogous to the operating gap of an HPGR. It is interesting to note that predictive sinkage equations are usually of exponential form, such as the initial empirical equations brought forward by Russian agricultural engineers in the early 20th century:

$$P = kz^n \qquad (20)$$

where P is the pressure exerted by the loading surface, k is the coefficient of proportionality and n is an exponent whose value is dependent on the soil type. k is described as being a function of soil properties, and the form and dimension of the loading surface.

It has been found that floatability is improved for vehicles when the traversed material has a higher density as well as greater frictional and cohesive properties (Bekker, 1956). Based on this relation, an advocate of the HPGR-terramechanics analogy would expect a larger HPGR operating gap to be achieved when processing feed material having a higher density, angle of friction and cohesive properties.

Slip sinkage is described as the vertical wheel displacement due to horizontal soil deformation and has usually been omitted from predictive sinkage equations or treated as a vertical displacement component independent of static sinkage. Lyasko (2009) measured a significant increase in overall sinkage when shear deformation of soils was induced. This is supported by the assertion of Muro et al (2004) that slip sinkage will occur due to the existence of soil dilatancy phenomena associated with the shearing of soils at a peripheral interface. The influence of shear deformation on HPGR operating gap has been rarely discussed in HPGR based literature and its introduction to the study of roller and material interactions should improve methodologies for HPGR throughput prediction.

Thrust

Also referred to as gross tractive effort, thrust is typically related to the wheel dimensions, vehicle weight and the frictional and cohesive properties of a soil. Early attempts at determining the available thrust for a particular soil started with Coulomb's equation:

$$\tau_{max} = c + ptan\theta \qquad (21)$$

where τ_{max} is the maximum shear stress, c is the cohesion of the soil, θ is the internal angle of friction of the soil and p is the pressure normal to the shear plane.

Through multiplication of the wheel-soil contact area an equation for thrust became the following:

$$T = lbc + Wtan\,\theta \qquad (22)$$

where T is soil thrust (Newtons), l and b are the wheel-ground contact length and width respectively and W is the load borne by the wheel (Bekker, 1957; Janosi et al, 1961). Thrust can be simply described as the gross horizontal force which can be exerted onto a wheel for specific wheel load and geometry, set of operating conditions and soil parameters. In the context of HPGR processing, Schönert et al (2002) showed that a significant amount of shear, approximately a quarter of the normal stress, can be measured at the HPGR roll surface. A form of the terramechanics based thrust equation is potentially an indicator of HPGR throughput as improved intake of material may be achieved with a feed material which can bear large shear forces.

Rolling resistance

Rolling resistance is the net opposing force to the horizontal motion of a wheel, denoted by the integral of the horizontal component of radial soil forces. The rolling resistance depends on the physical soil properties, wheel dimensions and operating conditions (driven or in a braking state) (Onafeko, 1969). Typically, rolling resistance is included as a component of the total resistance to vehicle motion. Opportunity exists for exploring the relation of rolling resistance of an HPGR roller to the motor torque.

Compaction resistance

The magnitude of the motion resistance due to terrain compaction is defined as compaction resistance, R_c (Wong, 1993). Various empirical formulas have been established to predict the degree of motion resistance due to compaction, mainly based on Bekker's definition:

$$R_c = b\int_0^{\theta} \sigma r sin\theta d\theta \qquad (23)$$

where σ is the normal stress, r is the wheel radius and θ is the angle from the entry point of the wheel into the soil bed to the bottom of the wheel (Meirion-Griffith et al, 2010). A modified form of this approach is regularly applied in HPGR based studies, where recorded rotational energy is generally attributed solely to the degree of crushing carried out on feed sample.

2.11.3 Experimental procedures for characterizing the trafficability of soils

Experimental procedures have been developed to assess the trafficability of soils through prediction of some of the aforementioned terramechanics based parameters. Procedures and methodologies which are unique to terramechanics are presented and their potential applicability to predicting HPGR throughput is discussed in this section.

Direct shear test

The direct shear test box is used to measure the frictional and cohesive properties of granular samples. Results from the test are interpreted using terramechanics based methodologies and used as inputs for predictive models. The importance of frictional properties of feed material is often suggested in HPGR studies, particularly where throughput and gap prediction is being carried out. However, detailed methods for determining the frictional and cohesive properties of HPGR feed has rarely, if ever, been put forward. Hence, the direct shear box test presents itself as a proven test methodology in the field of terramechanics, which can be adopted and potentially modified for the purposes of HPGR throughput prediction.

As shown in Figure 9, the direct shear box is comprised of two individual upper and lower sections which are filled with test sample. A normal load is applied to the top of the specimen and one section is moved laterally in a controlled manner, while the second section is held stationary by a fixed load cell. Thereby, the horizontal load recorded by the load cell is a measure of the shear force being transferred by the specimen (Craig, 2004). Three or more normal loads are tested on a soil so that a plot of the horizontal and normal forces can be made.

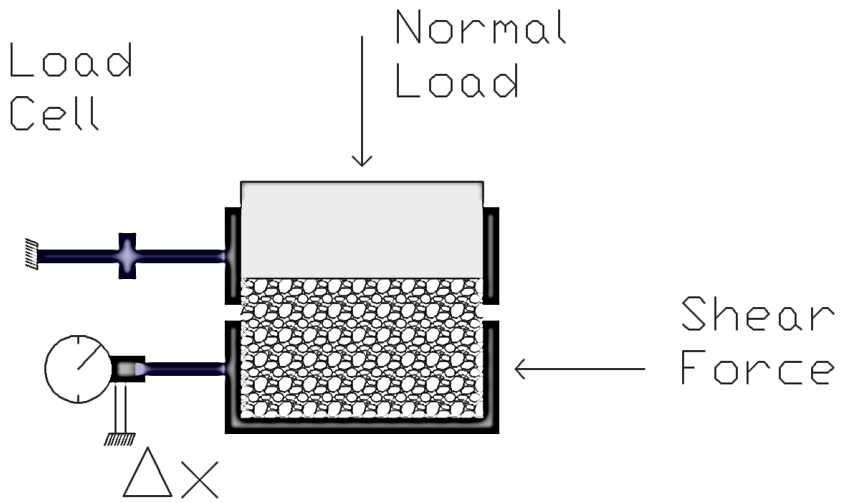

Figure 9 - Depiction of a direct shear test box

Typical results are shown in Figure 10, from which the peak and critical state shear forces can be derived. The constant shear force observed for a large displacement is defined as the critical state shear force, τ_{cs}. The peak and critical state angles, Φ'p and Φ'cs respectively, are derived from the plot of horizontal and vertical force (Budhu, 2006). Depending on the characteristics of the sample tested, a value for cohesion may or may not be recorded, which is defined by the y-intercept of the shear stress versus normal stress graph.

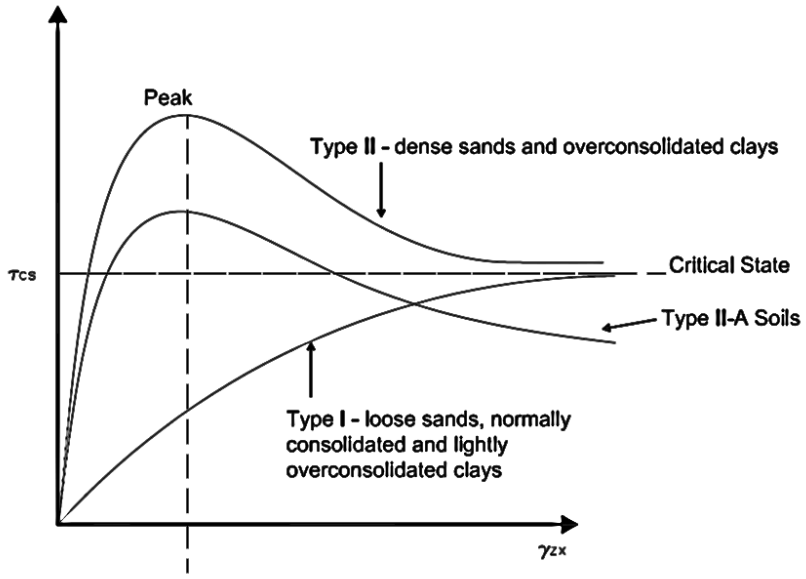

Figure 10 - Example of direct shear box test outcomes (based on Budhu, 2006)

Studies published in literature have pointed to the existence of general relationships between direct shear test parameters and the outcomes of the test:

- A coarser sample top size, or a smaller box geometry typically results in higher friction angles being determined (Cerato et al, 2006; Nakao et al, 2008)
- Higher shear rates generally result in lower friction angles being measured (Nakao et al, 2008)
- Larger quantities of coarse gravel in sandy mixtures were attributed to increases in peak friction angle due to higher dilatancy (increase in sample volume) and the measurement of larger critical state angles (Simoni et al, 2004)
- A larger gap between top and bottom halves, in relation to the feed particle size, reduces the determined peak angle of friction up until a limiting point. Material loss and the influence of stress release at boundary edges were considered to eventually significantly affect the determined friction values should very large separation gap sizes be used. A gap size of approximately 10 to 20 times the 50% percent passing size was suggested as being appropriate (Shibuya et al, 1997)

From comparison of shear strength results to field data, the early thrust equation (22) was modified to the following:

$$T = (c + p\tan\theta)(1 - e^{\frac{-j}{k}}) \qquad (24)$$

where j is the soil deformation in the horizontal direction and k is a deformation modulus of a soil shear stress-strain curve. Figure 11 shows how the value of k can be interpreted from a shear stress-strain curve (Janosi et al, 1961). Not all soil shear stress-strain curves follow the characteristic shown in Figure 11, which was used as a basis for the formula. In the case where shear exhibits a peak followed by a constant residual shear stress, more complicated derivations of thrust have been proposed such as that of Wong (1993).

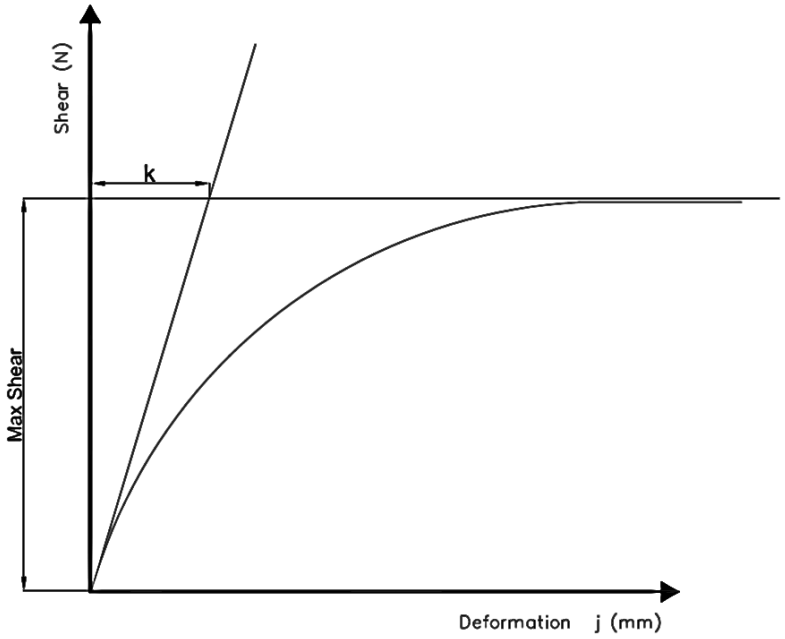

Figure 11 - Evaluation of 'k' from a soil shear stress-strain curve (based on Janosi et al, 1961)

The derivation of a parameter k, which represents the shear displacement where the maximum or critical state shear stress occurs, is unique to terramechanics. A distinct difference between the maximum normal stresses applied by the shear test and that occurring on the HPGR roll needs to be taken note of when considering this test as a candidate for HPGR throughput predictions. Based on the previously discussed pressure profile occurring on the HPGR roller surface, it is safely assumed that a certain proportion of the HPGR roll surface experiences a normal stress which is at the same order of magnitude as that applied to sample in a shear test box. At some point between the compression and zero angles of HPGR rollers, the normal stress is an order of magnitude higher than that achievable with typical shear test box equipment. Comparisons of direct shear test results and HPGR performance can ultimately confirm applicability of the standard direct shear box test to predicting the response of samples to the HPGR process. The direct shear box test has clear potential in offering new valuable shear based characterizations of HPGR feed sample. The popular method of Janosi et al (1961) presents a foundation for relating shear test results to HPGR parameters such as throughput or roll gap.

Bevameter test

The bevameter is a test apparatus that is designed to measure the horizontal and vertical stress-strain relationships of soils. Effectively it combines three individual tests into one test suite. Originally developed by the U.S. Army Tank Automotive Command, the depiction of the test, shown in Figure 12, illustrates the approach and form of recorded data.

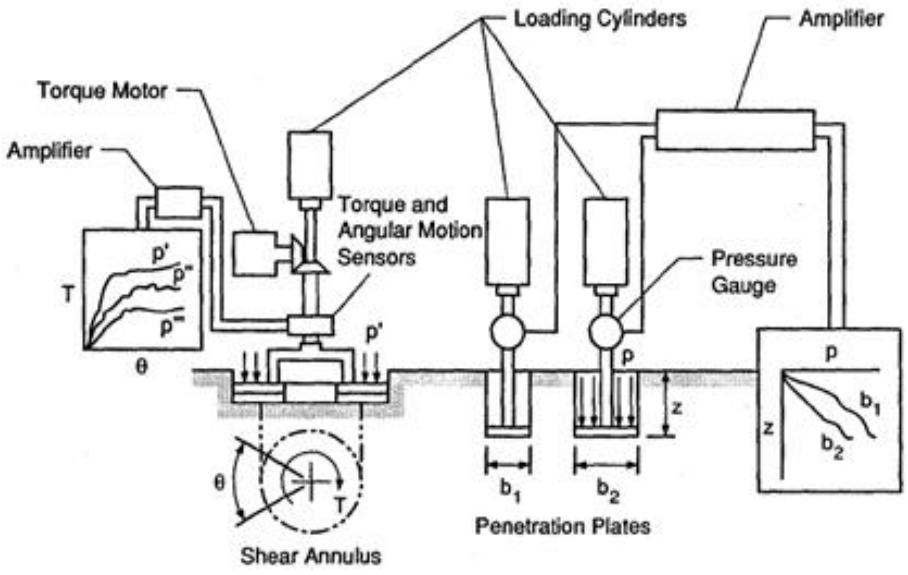

Figure 12 - Components of a bevameter (Bekker, 1969)

The horizontal stress-strain relationship is derived from an annular shear ring and interpreted similarly to the results of the previously discussed direct shear box test. Sinkage tests are carried out using two or more plates having a different diameter to determine the vertical stress-strain relationship. The following equations of Onafeko et al (1967) can be used to fit the empirical data of pressure, p, for any sinkage value:

$$p = (k_1 + k_2 b)(\frac{z}{bn}) \qquad (25)$$

where k_1, k_2 and n are defined as soil parameters and can be determined through application of the least squares fitting method. The data recorded by the bevameter can be achieved with separate pieces of equipment. In the case of characterizing terrain, the integration of separate tests into one piece of mobile equipment served as a convenient solution.

Plate sinkage testing can be considered to be similar to piston press testing used in application to HPGR, however the scale up procedures between the two fields are shown to be considerably different. The use of a series of plate sizes for the purposes of wheel scale up is an interesting

testing method which can be easily adopted for the purposes of developing a laboratory scale HPGR test.

2.12 Soil mechanics

The characterization of the shear strength of soils is a subject covered under the broad area of soil mechanics. The previously discussed study of terramechanics addresses normal loads which are an order of magnitude smaller than the pressing forces exerted by HPGRs. For this reason, the potential of successfully extending methodologies of terramechanics to HPGR can be clearly improved by giving consideration to the fundamentals of soil mechanics. In addition, the analysis of civil engineering based characterization methods further expands the tools available for developing a laboratory scale HPGR test.

2.12.1 Shear strength of soils

The peak shear strength of a soil is a result of shearing resistance due to sliding, dilatancy effects, crushing and the rearrangement of particles. The shearing resistance due to crushing is significant for high normal effective stresses (Budhu, 2006), which is particularly relevant to the HPGR process. Critical state shear strength is defined by a constant shearing resistance where the material density is constant for an increasing shear strain (Craig, 2004).

It has been well documented that the difference between peak and critical state shear strength reduces with increasing normal stress, as shown in Figure 13. This is primarily due to the corresponding decrease in ultimate void ratio, which lowers the degree of dilation. The effect of crushing of particles due to high effective normal stresses reduces the effect of particle interlocking, contributing to the reduction in discrepancy between peak and critical state shear strengths (Craig, 2004).

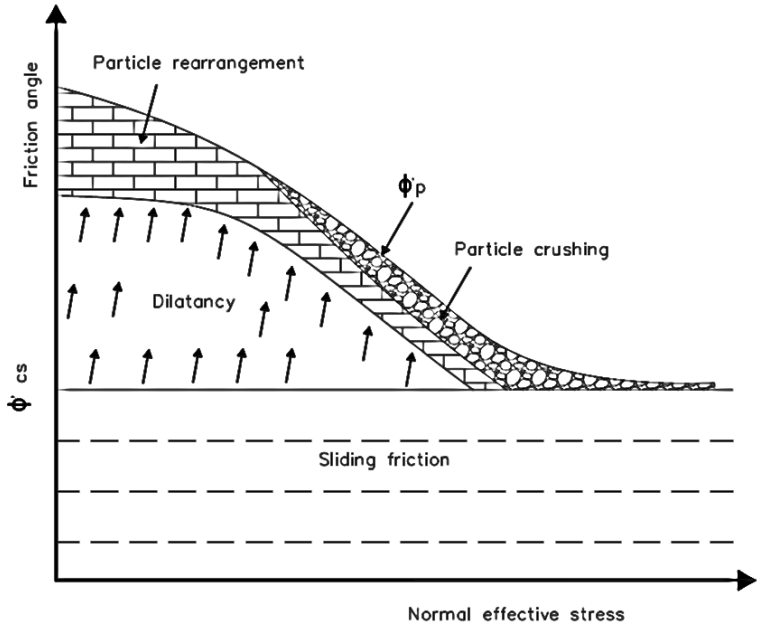

Figure 13 - Effect of normal stress on the shear strength of soils (based on Budhu, 2006)

Referring back to the pressure profiles occurring on the HPGR roller surface, it is apparent that the peak and critical state shear strengths will converge at a point close to the zero angle, where normal stresses approach the maximum. From knowledge of soil mechanics based shear strength, it can be inferred that dilatancy, particle rearrangement, particle crushing and sliding friction will have varying effects on the friction angle of feed material as it is drawn in between two HPGR rollers and released as a crushed and compacted product. As previously discussed, a few HPGR based studies identified the frictional properties of feed material as a parameter which has influence on HPGR throughput and gap size. This would indicate that the dilatancy, particle arrangement and sliding friction of feed material as a response to normal stress have a bearing on HPGR throughput and operating gap. Further work is required to quantify these material specific effects in the form of a laboratory scale test for relation to HPGR throughput.

2.12.2 Soil mechanics terms and associated tests

Parameters and tests used for the characterization of soils, which have been identified as potentially beneficial to this HPGR focused study, are briefly outlined in this section of the literature review.

Void ratio and porosity

The void ratio, e, is the ratio of the volume of voids to the volume of solids. It is expressed by the following equation:

$$e = \frac{V_v}{V_s} \qquad (26)$$

where, V_v is the volume of voids and V_s is the volume of solids.

Porosity, n, is related to the void ratio and is defined by the ratio of the volume of voids to the total volume (Budhu, 2006):

$$n = \frac{V_v}{V} \qquad (27)$$

Parameters describing the degree of packing of a sample viz., porosity, void ratio, and packing density, can be used to describe the various states of material during HPGR processing and are candidate inputs for a new throughput model.

Proctor density

HPGR comminution typically involves the processing of feed material which varies in moisture content. Water content is known to have an effect on HPGR throughput and operating gap, however detailed analysis of the underlying effects of water content on material properties is rarely carried out.

The Proctor density test, which is used to determine the relationship between soil water content and degree of compaction, is a potential laboratory scale method for the prediction of the effects of water on HPGR operation. The test involves a rammer which is dropped from a specified height onto a layer of sample contained in a die of certain geometry. The number of blows, sample layers and the die geometry has been standardized for certain sample gradations (ASTM Standard D698, 2007). The procedure is typically carried out for a range of sample moisture values so that the water content at which the maximum dry unit weight occurs can be determined. This is referred to as the optimum water content. The role of moisture in compacted soils differs according to its relation to the optimum water content. When the water content is less than or equal to the optimum water content, the water effectively facilitates the arrangement of soil grains, causing a denser packing of soil grains per unit volume. Conversely, water displaces particles when the sample moisture content is in excess of the optimum moisture level and a lower density of solids is achieved (Budhu, 2006).
The modified proctor test which is used for coarse gravels and requires approximately 5 kg of sample, has been identified as being particularly applicable to measuring the effects of water on HPGR feed material density. Furthermore, the test provides a standardized method for applying repeatable compactive energy to samples which most certainly improves the accuracy of material density measurements.

2.12.3 Soil mechanics tests used in terramechanics

Terramechanics can in some ways be seen as an extension of the fundamentals of soil mechanics for the purpose of describing dynamic wheel-soil interactions. For this reason, characterization of

soft soils in terms of trafficability is also carried out using the analysis techniques of civil and geotechnical engineers.

The following tests, which are used within soil mechanics and terramechanics, have also been identified as having potential value for the prediction of HPGR performance:

- Triaxial compression Tests
- Unconfined Compressive Strength (UCS)

ASTM standardized test procedures have been published for the above listed tests and interpretations of test results are similarly addressed in terramechanics. The applicability of UCS to HPGR operation has been mentioned in some literature, however this is considered to be putative as no real analysis has been published in support of this relation. Further work is required to investigate for correlation between the compressive strength of individual feed particles and their response to the HPGR process.

2.13 Summary of literature review

The reviewed literature provided not only a background to the field of HPGR, but also emphasized that the uptake of a comminution technology, which has been proven to offer a range of benefits such as improvements in energy efficiency, has been held back due to the lack of a suitable laboratory scale method for predicting HPGR performance. Attempts at developing laboratory scale tests for HPGR have included the pragmatic mineral processing approach of using a miniaturized version of the equipment being studied, in this case a laboratory sized HPGR, with little regard to identifying key feed material parameters or the magnified influence of wall boundaries. Such an approach is in contrast with the industry accepted JK Drop Weight Test in application to AG/SAG milling, where crushing and grinding mechanisms are regarded as key functions of overall mill performance and as such are assessed separately. Other attempts at HPGR laboratory scale test development have been primarily based on compression breakage and energy relationships, and have rarely addressed the energy efficiency associated with the transfer of material via the HPGR rollers. This imbalance necessitates further work towards establishing a laboratory test for predicting HPGR throughput.

The presented literature review has also shown that frictional properties of feed material have been referred to as having an impact on HPGR performance, primarily throughput and roll gap. The role of material friction is described more fundamentally in other fields such as terramechanics, where it is used to predict the performance of a solid wheel traversing soil; potentially analogous to HPGR processing. Overall, the established testing methods used in terramechanics and soil mechanics have been found to offer great potential as a foundation for HPGR throughput test development.

In retrospect, it is envisaged that a successful laboratory scale HPGR test will take into account the inter-relation of pressure, gap and roll geometry as shown to exist through analyses of roll pressure profiles. Initial steps towards such a holistic model require further work towards identifying the key material and machine parameters which can be used to predict HPGR throughput. Hence, the primary objective of this thesis has been proposed as the development of a laboratory scale throughput test.

3 EXPERIMENTAL PROGRAM

3.1 Introduction

In order to approach the development of a laboratory scale HPGR test for throughput, an experimental program was designed to generate potentially scalable HPGR laboratory data as well as data representing industrial scale HPGR operation.

The experimental program was broken down into sets of sub-programs, comprising pilot HPGR tests and investigative laboratory scale tests. Other fields of research such as terramechanics and soil mechanics were referenced during laboratory scale test development.

3.2 Sample set description

The applicability of any developed methodologies across ore types is particularly dependent on the sample set used for the investigation. The study focused particularly on mineral applications, thus a reference sample set of various mineral types was established. Table 1 shows the range of ore types used for the study. Approximately 1 to 5 tons of each sample type was handled to ensure that sufficient material was available for exploratory HPGR pilot testing.

Table 1 - Sample types used in the experimental program

Sample Type
Copper Nickel Sulphide
Mafic / Ultramafic
Copper Porphyry
Volcanogenic Gold
Taconite
Quartz
Dolomite
Limestone
Kimberlite

3.3 Broad approach to the experimental program

The major components of the experimental program are shown in Figure 14. Further detail is provided in sections dedicated to the individual elements of the flowsheet.

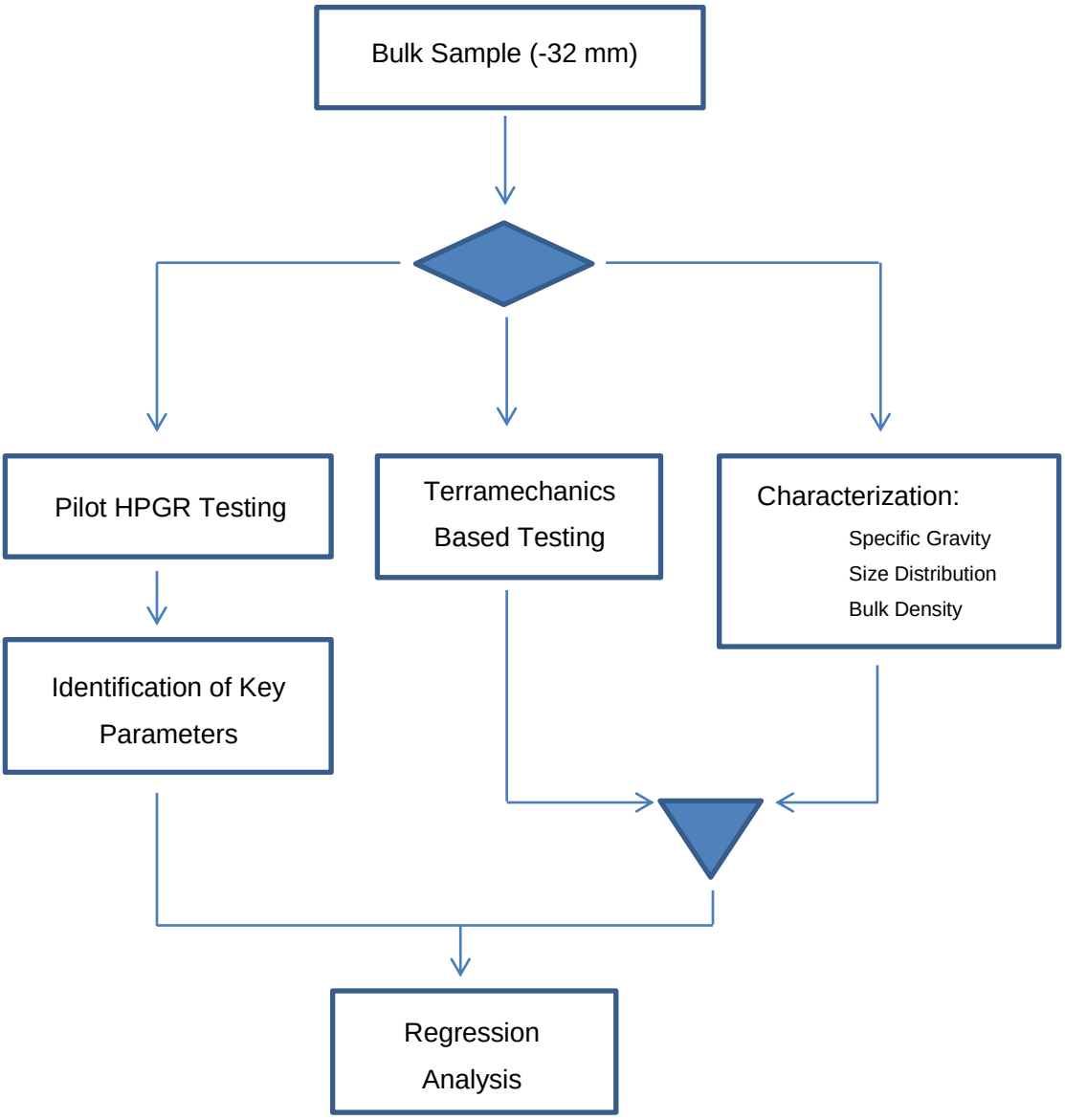

Figure 14 - Outline of experimental program

4 HPGR PILOT TESTING

4.1 Introduction

Testing procedures developed by Köppern and as used in commercial testing at the University of British Columbia, were followed while carrying out pilot HPGR test work. Equivalent procedures and equipment were used to successfully size and install HPGR rollers and motors for two Australian industrial applications. For both installations, the industrial HPGRs underwent performance testing to ensure that the machines were able to provide specific throughput and size reduction performance. In both cases performance testing showed that the motor and roll sizes, determined from pilot HPGR test work, met the requirements of the application. For this reason the results of the pilot HPGR test work were considered to be suitably representative of industrial results. Thereby, verification of scalability from new laboratory testing procedures to pilot HPGR test results was considered to also verify scalability of the designed laboratory methods to full scale HPGR machines.

4.2 Equipment

4.2.1 Pilot HPGR

A Köppern pilot HPGR, as shown in Figure 15, located at the University of British Columbia was used for the HPGR testing component. The machine is an industrial unit which was built specifically for the purpose of pilot HPGR testing. In comparison to typical industrial HPGR units, the pilot machine is designed with particular attention to instrumentation, data-logging capacity and material handling layout. The small aspect ratio of the rollers allows smaller amounts of sample to be used with a large diameter roll, where a large diameter increases the scalability of the results to larger industrial sized machines.

Figure 15 - Pilot HPGR at the University of British Columbia

The design specifications of the pilot test HPGR are outlined in Table 2.

Table 2 - Pilot HPGR specifications

Parameter	Units	Value
Roll Diameter	[mm]	750
Roll Width	[mm]	220
Installed Main Motor Power	[kW]	200
Maximum Specific Pressing Force	[N/mm^2]	8.5
Maximum Roll Speed	[ms^{-1}]	1.57
Wear Lining	[-]	Profiled Hexadur®
Feed System	[-]	Gravity

Aside from material analyses of pilot HPGR feed and products, logged instrument data from individual tests formed a substantial component of the analyzed test outcomes. Data logs were analyzed upon the completion of pilot HPGR tests, summarized and used with data from material analyses to calculate parameters describing the operational performance. A list of logged machine parameters is shown in Table 3.

Table 3 - Logged machine parameters

Description	Units
Motor Power Drawn	[kW]
Roll Gap – Motor Side	[mm]
Roll Gap – Non-Motor Side	[mm]
Hydraulic Pressure – Motor Side	[bar]
Hydraulic Pressure – Non-Motor Side	[bar]
Product Splitter Gate Position	Open / Closed
Roll Speed	[ms^{-1}]

For each sample type, a systematic series of pilot HPGR tests was carried out to determine the influence of feed or machine parameters on operating performance. Through use of the PLC interface, machine setpoints could be adjusted between test runs. Table 4 shows the machine setpoints which were under direct control of the operator.

Table 4 - Pilot HPGR setpoint parameters

Description	Units
Roll Speed	[ms^{-1}]
Hydraulic Pressure – Motor Side	[bar]
Hydraulic Pressure – Non-Motor Side	[bar]
Minimum Roll Gap – Motor Side	[mm]
Minimum Roll Gap – Non-Motor Side	[mm]

4.2.2 Material handling equipment

The key pieces of equipment used for the phase of HPGR pilot testing are described in this section.

HPGR product conveyor splitter and gate

Material located at the edges and center of the conveyor was separated with a material splitter located at the end of the HPGR product conveyor. Ore which was processed at either the center or edge areas of the roll could be collected separately, due to the trans-axial orientation of the conveyor to the rollers. An adjustable gate mounted onto the splitter assembly allowed an entire belt width of product material to be diverted to an individual drum. In summary, the splitter-gate assembly was used to separate product material into four separate containers.

Rotary sample splitter

A rotary splitter having a capacity of approximately 8 x 30 litres was used to homogenize and split large samples.

Figure 16 - Rotary splitter

Crushers and screening equipment

In cases where material needed to be reduced in size prior to HPGR testing, a 7 HP jaw crusher and a 48 inch Sweco vibratory screen were used.

4.3 HPGR pilot testing procedure

Pilot testing was carried out in a systematic way using a similar approach irrespective of the sample type. The amount of parameters tested per sample was dependant on the quantity of sample available. Sample preparation and analysis was significantly more time consuming than actual HPGR operation.

4.3.1 Feed material preparation

The initial step of ore preparation was dependent on the particle size and quantity of sample received from mines. The top size of feed material for the pilot HPGR was designated as 32 mm, and material was either supplied at this size or crushed and screened in the laboratory. Following

crushing and screening procedures, samples were homogenized with a rotary splitter and split into individual drums, each drum containing approximately 300kg of sample and representing feed for one individual HPGR test. During final homogenization and sample splitting, representative sub-samples were removed for feed characterization and laboratory scale test development.

4.3.2 Pilot testing procedure

Depending on the amount of sample available and the potential grinding role of HPGR in application to the sample, a range of process and machine parameters were tested for each ore type. Prior to HPGR testing an outline of intended test parameters was created. Typically explored input process parameters for an ore type were the following:

- Specific pressing force
- Feed moisture
- Roll speed
- Feed top size
- Closed circuit testing (batch recycle series of three to four tests)

Taking into account the listed variables, a change in only one input variable was carried out per test. Typically three sets of results were created for each variable listed. Investigation into the influence of specific pressing force was carried out at the initiation of each program to nominate the most suitable specific pressing force for the sample type. The nominated specific pressing force was then constantly applied to remaining tests which explored the HPGR response to other input variables.

The setpoints used during pilot HPGR testing were chosen based on practical machine capabilities in industrial settings. Hence, the experimental approach is not balanced in the multi-variable space and produced data which was concentrated for a narrower range of settings. An effect of this was the generation of a dataset benefiting the study of HPGR parameters within the confines of practical machine application rather than an investigation into fundamental inter-relationships.

The variation in tested HPGR parameters allowed relationships between HPGR parameters themselves, as well as the applicability of laboratory scale tests, to be investigated in this study. One 200 liter drum of material, approximately 300 kg, was used per test. HPGR product was split at the end of the product conveyor discharge using a splitter gate.

From each test the following three products resulted:

- Waste material
- Center product
- Edge products – motor side and non-motor side

During testing, a period of stabilization was noticed to occur due to the sudden release of feed material from the feed hopper onto the HPGR rolls. Stable operation was verified to occur approximately 5 seconds after the introduction of feed and continued for a period of approximately 20 seconds, after which the lack of material in the feed hopper affected process stability. For this reason, products collected during the initial and final periods of operation were diverted to a waste drum. Product which was collected during stable operation was separated into center and edge streams, so that the differences in roll pressure could be distinguished through size analysis of the individual streams. During each test product flake was collected and bagged separately.

4.3.3 Material analyses

Sub-samples of center and edge HPGR product streams were taken for product analysis. Primarily the size distribution of center and edge material was determined. The thickness and density of collected flake samples was also measured.

4.3.4 Pilot HPGR test outcomes

Logged instrumentation data was used in combination with material test results for calculation of HPGR operational parameters. The position of the waste gate was logged and used in combination with the datalog to calculate the average machine response during stable machine operation. Primary test outcomes are shown in Table 5.

Table 5 - Pilot HPGR primary test outcomes

Parameter	Units
Specific Pressing Force	[N/mm^2]
Specific Throughput Constant $\dot{m}$	[ts/hm^3]
Machine Throughput	[t/h]
Specific Energy Consumption	[kWh/t]
Main Motor Power	[kW]
Roll Gap	[mm]
Roll Speed	[ms^{-1}]
Feed Size Distribution	[-]
Product Size Distribution - Centre	[-]
Product Size Distribution - Edge	[-]
Flake Product Density	[t/m^3]

The primary test outcomes from each test were input into a database and used as a reference for determining relationships between parameters.

5 INVESTIGATION INTO HPGR PARAMETERS

5.1 Introduction

Prior to addressing the development of a laboratory scale test, the interrelations between HPGR test parameters were analyzed. The interrelationships of easily measurable feed properties, HPGR setpoint parameters and HPGR operation have been covered in literature to some extent. Further verification of these interrelationships was achieved through analysis of the pilot test database. The investigated parameters were screened based on the strength of their relation to HPGR throughput and roll gap. A goal of analyzing and describing the interrelationship of HPGR parameters was to justifiably reduce the number of descriptive parameters used in the development of a model predicting HPGR throughput.

5.2 Experimental approach

The analyzed input variables and response parameters are outlined in this section. The influence of input variables on response parameters was analyzed to help answer which input variables are important for use in a potential throughput model. Response parameters were investigated to assist in understanding why the response parameters occur as observed.

5.2.1 Analyzed input variables

The designated set of input parameters included: specific pressing force, roll speed setpoints as well as feed moisture and feed size. To characterize the HPGR feed size distributions, the Gaudin-Schuhmann equation was found to provide a generally better fit than the Rosin-Rammler method. The slope parameter, m, of the Gaudin-Schuhmann equation was used as a feed describing input variable (Gaudin, 1962):

$$\frac{M(x)}{M_0} = (\frac{x}{K})^m \qquad (28)$$

where x is the particle size, M(x) is the weight of undersize and K is the size modulus. A value of K equal to the feed material top size was used for all approximations, assigning the slope parameter, m, a unique value for each size distribution.

Neither qualitative nor quantitative values representing feed mineralogy were included in this stage of the study. Specific gravity reflects aspects of sample mineralogy and was included in later analyses. Datasets were grouped according to sample type to remove the influence of mineralogy on the investigation of parameter inter-relationships. Table 6 shows the input variables which were analyzed in this section of the study.

Table 6 - Analyzed HPGR input variables

Input Variable	Units
Specific Pressing Force	[N/mm^2]
Roll Speed	[ms^{-1}]
Feed Distribution Slope m	[-]
Feed Moisture	[%]

5.2.2 Response measurement

Response parameters included the previously discussed HPGR primary test results. The outcome of size reduction was represented in terms of reduction ratio of critical percentage particle sizes. F80/P80 and F50/P50 reduction ratios were calculated for each test, where P80 and P50 are the respective 80 and 50 percent passing particle sizes of HPGR center product.

The observed response parameters are shown in Table 7. The operating gap was presented in relation to the pilot HPGR roll diameter, and referred to as relative roll gap. Net motor power was used in combination with the mass of material processed during a test to determine the net specific energy consumption. Through this method the power used to rotate the drive train alone was removed from logged power values.

Table 7 - Analyzed HPGR response parameters

Response Parameter	Units
Specific Throughput Constant $\dot{m}$	[ts/hm^3]
Relative Roll Gap	[-]
Net Specific Energy Consumption	[kWh/t]
Reduction Ratio F80/P80	[-]

5.3 HPGR testing results

The results of approximately 80 individual HPGR tests were used to investigate relationships between input variables and response parameters, primarily specific throughput and roll gap.

Test data was grouped into sub-sets according to sample type used as well as feed and process parameters. Scatter plots were initially used to visually check for inter-relationships after which adequacy measures of linear function estimation were used to determine their significance.

5.3.1 Specific throughput constant and input variables

The influence of four separate input variables on specific throughput and roll gap was investigated for a range of sample types and operating conditions.

Specific pressing force

A total of nine datasets was used to investigate the influence of specific pressing force on specific throughput. The specific pressing force was the only variation within datasets, each dataset contained three to four data points. Figure 17 shows the results for four sample types, all of which show an inverse relationship between specific throughput and specific pressing force. This relationship was found to hold for all nine datasets and is consistent with results shown in literature (cf. Austin et al, 1993;, Schneider et al, 2008).

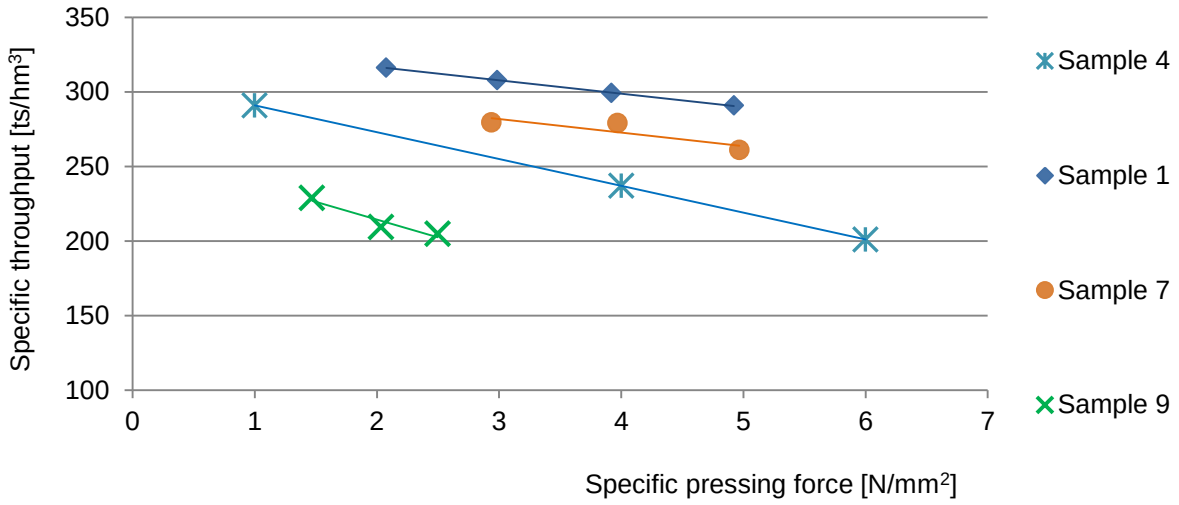

Figure 17 - Specific throughput constant and specific pressing force

Roll speed

Datasets generated from five sample types were analyzed for roll speeds ranging from 0.6 to 0.92 ms^{-1}. All sample types were processed at equivalent pressing force settings of 4 N/mm^2 and a feed moisture content of approximately 2%. Generally a slight decrease in specific throughput was observed as roll speed was increased; however this was not consistent for all datasets. Schönert (1992) observed a similar relationship between roll speed and specific throughput.

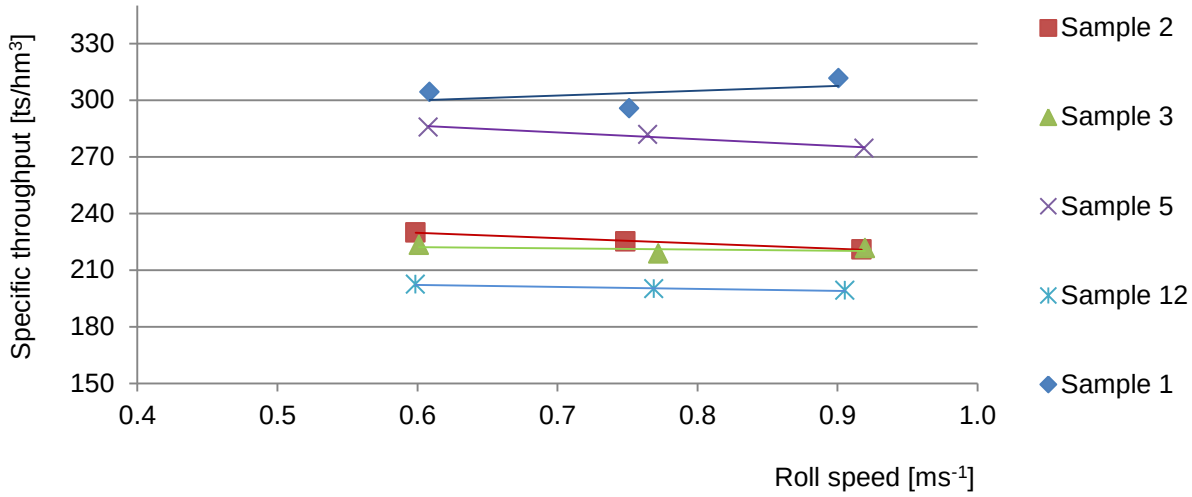

Figure 18 - Specific throughput constant and roll speed

Feed size distribution slope

As previously introduced, the Gaudin-Schuhmann slope parameter, m, was used to characterize the slope of the size distribution, where a higher m value represents a wider distribution. To attribute throughput response exclusively to the influence of this input variable, the results of batch re-circulating load tests were grouped into datasets. Each series of closed circuit tests was carried out on the same sample type at equivalent moisture content, top size and machine set-point parameters. The product of an initial HPGR test was screened and a new feed sample was prepared containing screen oversize and fresh feed. This process was repeated for three cycles. A different slope parameter was measured for each test in the batch series, which was compared to the associated specific throughput constant and formed the basis of this investigation. It was assumed that preferential breakage of softer and harder materials did not occur throughout the course of the batch recycle series. This assumption was supported by the quick stabilization of response parameters, as typically seen when carrying out HPGR closed circuit tests.

The observed values of specific throughput constant for different samples varying in size distribution slope are shown in Figure 19, where no consistent relationship between the input variable and response parameter is apparent. Based on literature it was expected that a lower feed m value, i.e. a wider feed size distribution, would result in a higher throughput. More work is required to determine the effect of feed size distribution on throughput.

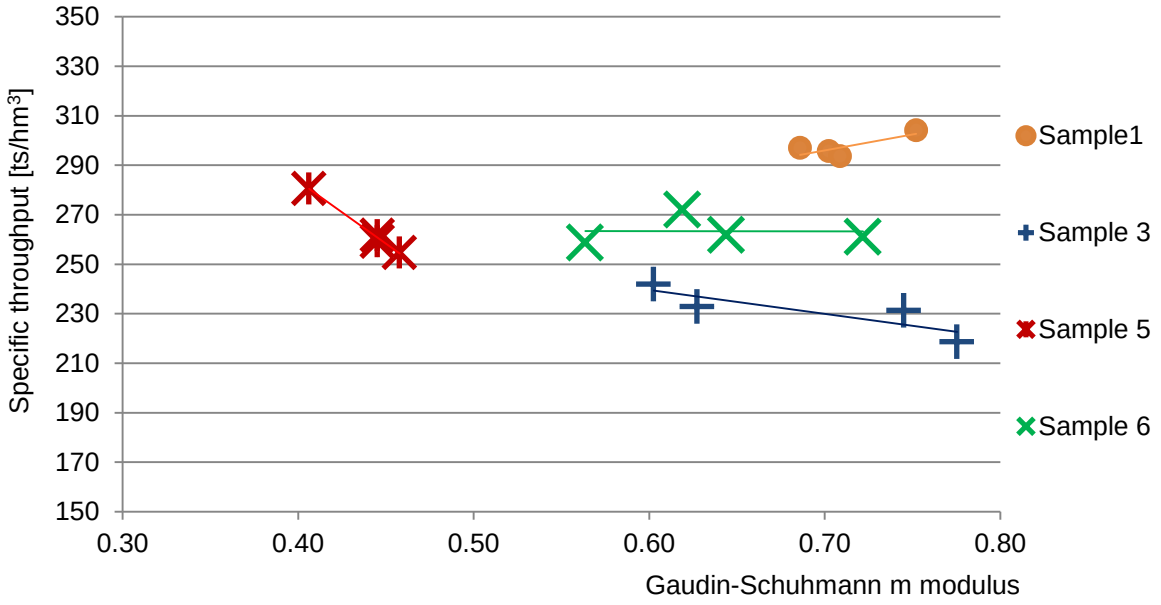

Figure 19 - Specific throughput constant and Gaudin-Schuhmann modulus m

Feed moisture

A consistent reduction in specific throughput was found when feed moisture content was increased for a range of sample types. As previously reviewed, data presented by Fuerstenau et al (2007) showed a reduction in throughput and gap for elevated feed moisture. Figure 20 shows the resulting relationship for four sample types, where an inverse relationship between moisture and specific throughput was consistently found for the six investigated datasets. Thereby the results showed that a lower throughput is achieved when a higher level of moisture is present in feed material, which is consistent with that of literature.

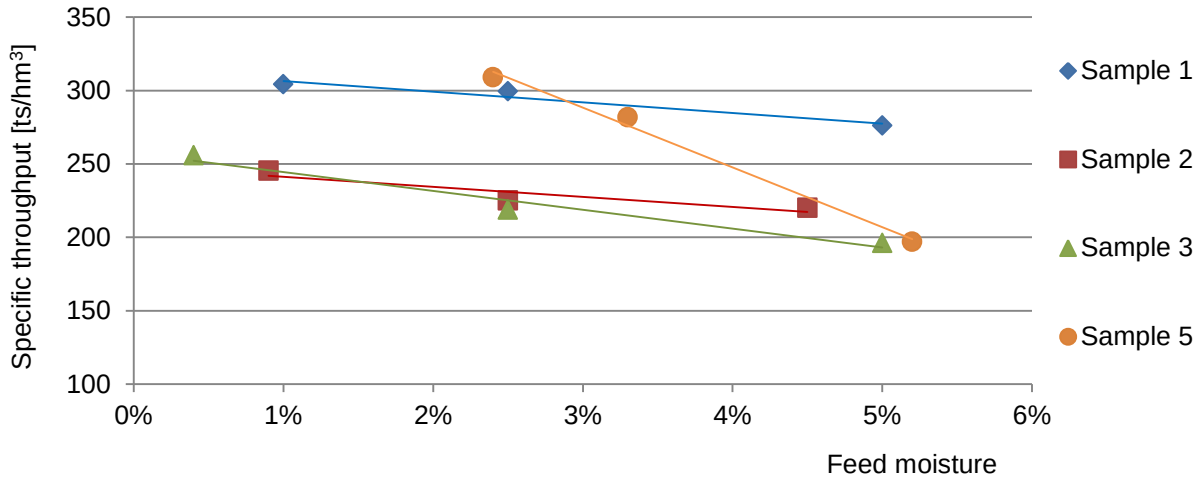

Figure 20 - Specific throughput constant and feed moisture

Summary of input variables and response of specific throughput

The investigations showed that the influence of roll speed and slope of feed size distribution was not consistent across sample types. Results for larger ranges of both roll speed and size distribution slopes may be required to clarify the general influence of either input variable on specific throughput. The reduction of specific throughput due to increases in specific pressing force and feed moisture was found to be consistent across datasets. These findings confirm those mentioned previously in literature.

In order to compare the strength of interrelationships, linear stepwise regression was applied to the results of three equivalent test programs each carried out on unique sample types. Eleven tests were included in each test program: consisting of four pressing force tests, two roll speed tests, three closed circuit tests and two moisture tests. Input parameters were scaled to unitless values having a range of -1 to 1 for each dataset and included in linear regression models fitted to specific throughput and roll gap. A stepwise regression algorithm available in Matlab was applied, which initially uses forward selection of input variables followed by backwards elimination based on their respective p-values. Terms having a p-value less than 0.05 were introduced into the model during the forward selection step, subsequent backwards elimination removed terms which had a p-value greater than 0.1. The p-value thresholds were not modified for the remainder of the study. Coefficients were fitted to parameters which were deemed to be statistically significant by the algorithm and resulted in a predictive model of the following form:

$$Y_i = ß_0 + ß_1 X_{i1} + ß_2 X_{i2} \ldots + ß_p X_{ip} \qquad (29)$$

where Y_i is the response variable for test number i, $ß_{0 \text{ to }} ß_p$ are fitted coefficients and X_i are the predictor variables.

The fitted coefficients and degree of fit achieved for each sample types are shown in Table 8 and 9. From the application of stepwise regression it was found that generally feed moisture and specific pressing force had the greatest predictive significance for both specific throughput and roll gap. Roll speed was found to be statistically insignificant in relation to the target response variables for all three sample types. The reduction of throughput due to the application of a higher pressing force and feed moisture content was in line with expectations.

Table 8 - Linear regression, $\dot{m}$

Description	Specific Pressing Force	Roll Speed	Feed Moisture	Feed Size Modulus m	R^2
Sample No.	B_1	B_2	B_3	B_4	
Sample 1	-12.5	-	-15.3	-	0.75
Sample 2	-10.9	-	-29.4	-6.3	0.94
Sample 3	-36.4	-	-59.0	-	0.97

Table 9 - Linear regression, roll gap

Description	Specific Pressing Force	Roll Speed	Feed Moisture	Feed Size Modulus m	R^2
Sample No.	B_1	B_2	B_3	B_4	
Sample 1	-2.0	-	-1.5	0	0.86
Sample 2	-1.3	-	-3.1	0	0.94
Sample 3	-3.2	-	-4.9	-0.5	0.98

5.3.2 Specific throughput constant and response parameters

The association between three response parameters and the specific throughput constant was analyzed to determine the existence of any inter-relationships and their extent.

Relative roll gap

A clear relationship between the relative roll gap and specific throughput was found for a set of 80 tests. Although the dataset consists of experimental conditions varying in feed type and machine parameters, a distinct relationship is apparent. Box and Draper et al (1987) suggest that the adequacy of estimation of a function be judged by the ratio of the sum of squares of regression to the sum of squares of residuals, represented by F, where an F value greater than 10 represents an adequate level of fit. A linear function was fitted to the operating gap and specific throughput data and resulted in an F value of 10.19, shown in Figure 21, thus implying that the relationship is significant even though variations in sample type were not accounted for.

The results showing an increase in specific throughput coinciding with an increase in flow area were in line with expectations. However, the high degree of statistical significance found for a large data set representing samples of varying material density and operating conditions was considered to be an important finding.

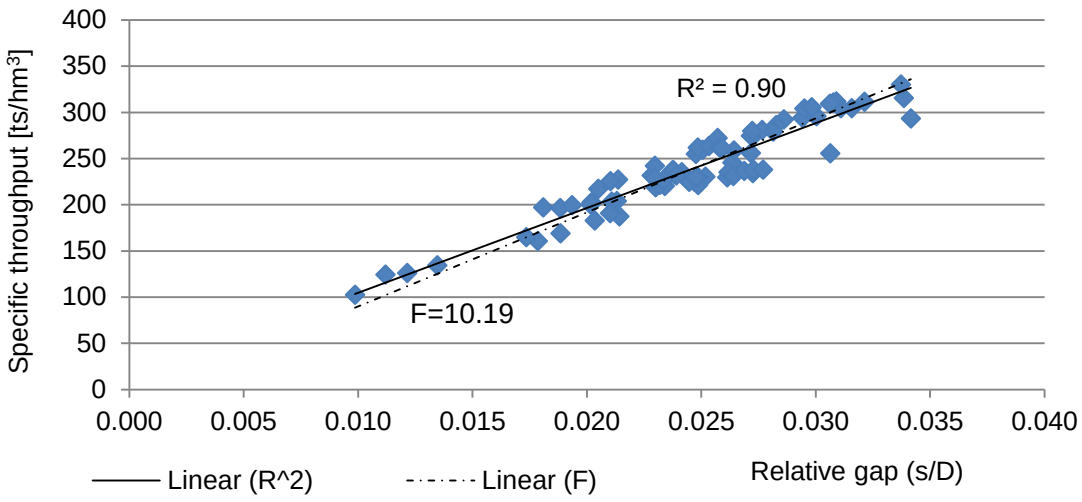

Figure 21 - Specific throughput and relative gap

Net specific energy consumption

The same dataset, as used for the relative roll gap analysis, was used to investigate the relationship between specific throughput and net specific energy consumption. An inverse relationship between specific throughput and net specific energy consumption is shown in Figure 22; although the scatter in the data suggests that the inter-relationship is quite sensitive to the variation in multiple parameter values within the dataset. An F fitting value of only 1.43 could be attained with linear approximation.

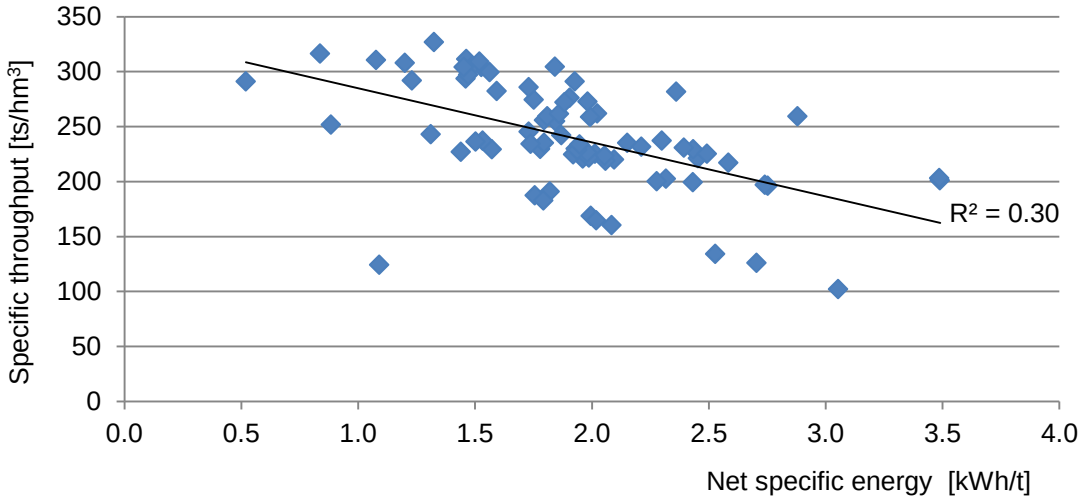

Figure 22 - Specific throughput and net specific energy

Separation of test data according to feed properties confirmed that the two response parameters, specific throughput and net specific energy consumption, are inversely related. The inverse relationship was similar for nine of the observed datasets. The findings were consistent with earlier

graphs showing that a higher specific pressing force setting resulted in greater energy input and a reduction in specific throughput.

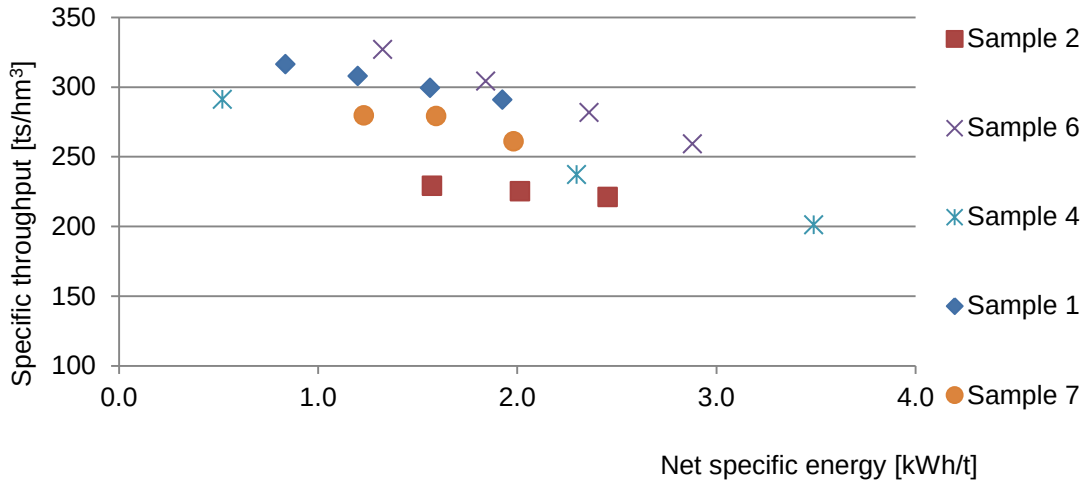

Figure 23 - Specific throughput and net specific energy

Size reduction

An inverse relationship between specific throughput and F80/P80 size reduction ratios was found for all tested sample types, shown in Figure 24. As discussed later in this thesis, reductions in throughput occurred due to the higher pressing force set points which contributed to lower throughput rates.

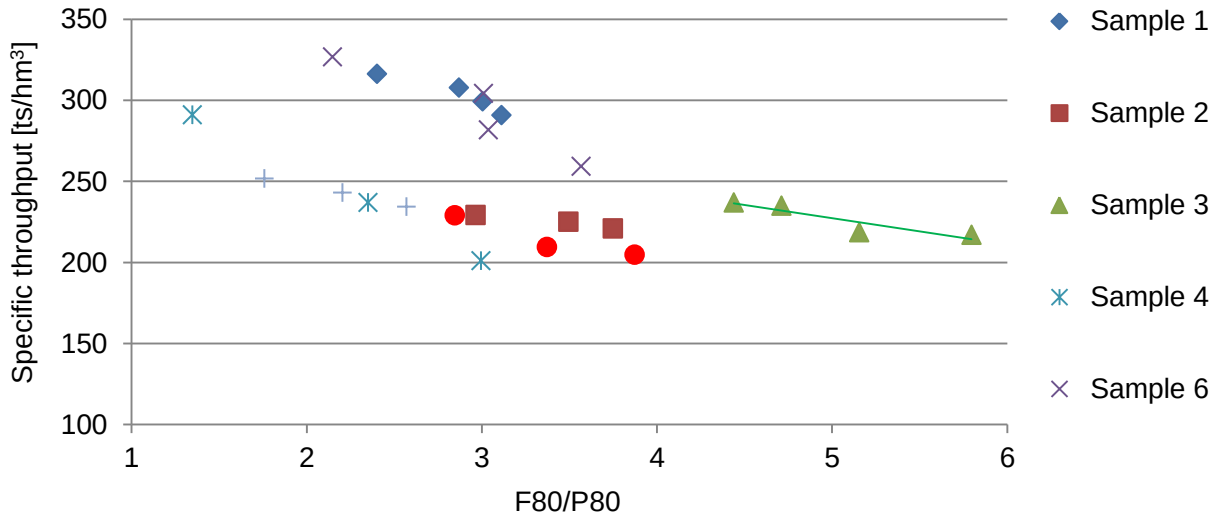

Figure 24 - Specific throughput and reduction ratio F80/P80

Summary of response parameters and specific throughput

A comparison of response parameters showed that specific throughput and relative roll gap are strongly related. To a lesser extent, relationships between both net specific energy consumption and size reduction were also found. As previously discussed, the observed response parameters were found to be related to the specific pressing force setting. Hence, the reason for the observed inter-relationships was primarily attributed to the fact that a variation of specific pressing force set points was used for each sample type.

5.3.3 Modelling of specific throughput and relative roll gap

Specific throughput and relative roll gap were the target response parameters to be predicted through modelling. A strong direct relationship between the two parameters was found to exist as shown in the previous section. Further improvement in the prediction of specific throughput was carried out through consideration of additional input parameters using programmatic step-wise regression. A list of considered parameters and their respective p-values is shown in Table 10.

Table 10 - Investigated parameters for specific throughput

Input Parameter	Symbol	p-value
Roll gap	s	9.0×10^{-43}
Feed Bulk Density	ρ_b	3.3×10^{-18}
Feed Size Slope m	m	1.1×10^{-4}
Specific Pressing Force	F_{SP}	0.07
Feed Moisture	H_20	0.19

The determined model for predicting specific throughput from knowledge of roll gap was of the following form:

$$\dot{m} = ß_0 + ß_1 s + ß_2 \rho_b + ß_3 m \qquad (30)$$

Figure 25 shows a comparison of the predicted and observed specific throughput values. The results indicate that a very good prediction of specific throughput can be made through knowledge of the operating roll gap, bulk density and feed slope parameter.

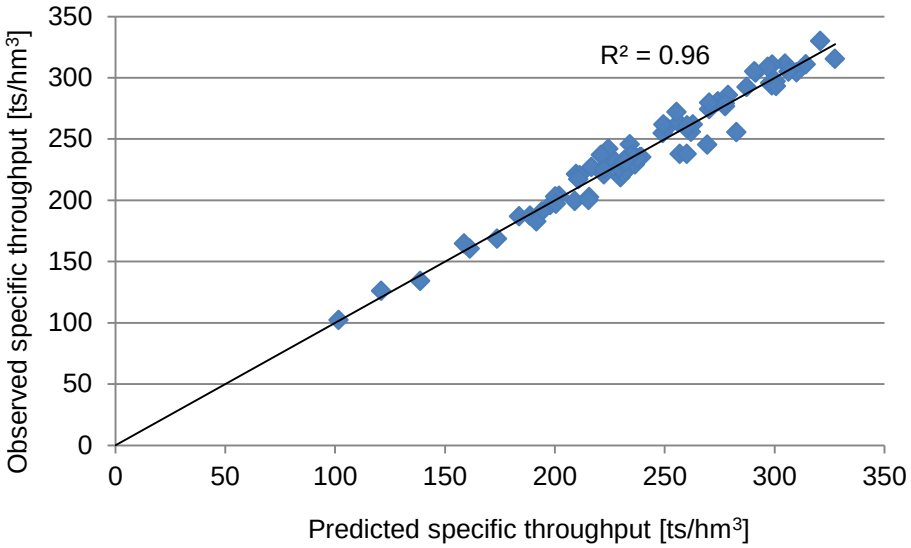

Figure 25 - Observed and predicted specific throughput

The following equation was fitted using stepwise regression with consideration for pairwise interaction between variables:

$$\dot{m} = ß_0 + ß_1 s.\rho_b + ß_2 s.m + ß_3 FSP \qquad (31)$$

The above equation provided only a slight improvement in fitting accuracy and involves an additional input variable, specific pressing force. The statistical significance of interaction variables, gap-density and gap-feed slope parameter, confirmed that the actual interrelation of parameters is complex.

5.4 Discussion and conclusions - HPGR testing

A significant finding of the inter-response parameter relations is the clear association between gap and specific throughput for a large data set representing results from various sample types and experimental conditions. This relation was further improved through inclusion of the feed bulk density and size distribution slope. More refined measurements of feed density, such as the use of standardized Proctor density measurements, should further improve the predictive strength of a model relating roll gap to specific throughput.

Specific pressing force was found to strongly influence specific throughput, viz. increases in pressing force resulted in a reduction in throughput. Examples of the response of roll gap to changes in specific pressing force are shown in Figure 26.

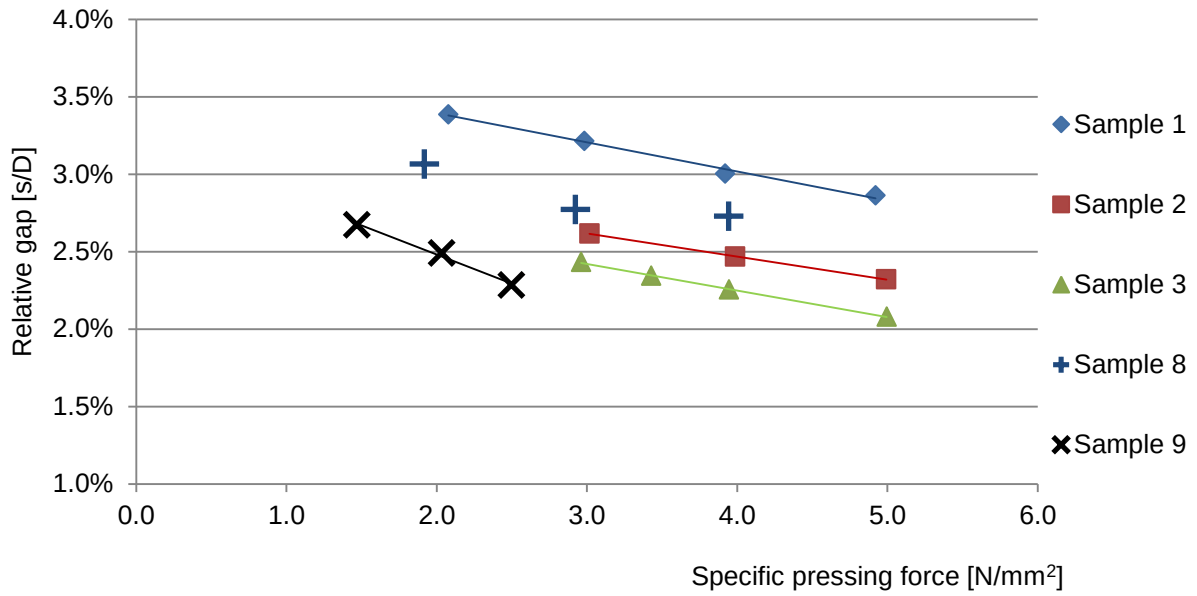

Figure 26 - Relative gap and specific pressing force

The inverse relation between pressing force and roll gap is of interest when considering that a higher pressing force will inevitably increase the density of the pressed material. According to the throughput continuity formula, material density and gap size have an equivalent influence on the throughput outcome. The findings therefore suggest that an increase in pressing force brings about a relative change in roll gap which is greater than the relative change in material density. For this reason, the relation between material density at the roller nip and specific pressing force was looked at in further detail.

The range of possible values for material density within the physical HPGR envelope is bound by the bulk density and specific gravity of the ore. The apparent specific gravity of feed samples was tested through the use of the water displacement method. A range of particle sizes was measured for each sample type and a final averaged value determined. Back calculation of the material density at the roll nip for a range of tests showed that the apparent specific gravity value was exceeded at high specific pressing forces, shown in Figure 27. It was acknowledged that the actual specific gravity of tested material could not have been exceeded, and this pointed to deficiencies in the method used to determine specific gravity; such as the immersion of coarse whole particles rather than pulverized samples. Impermeable voids located within individual particles most probably reduced the determined specific gravity. Knowledge of the volume of voids within individual particles may be valuable for future comparisons of material properties and HPGR operational response. Overall, results showed that the calculated density in the nip region varied depending on the sample type

processed. The density of material at the roll zero angle most likely approached the specific gravity of HPGR feed sample.

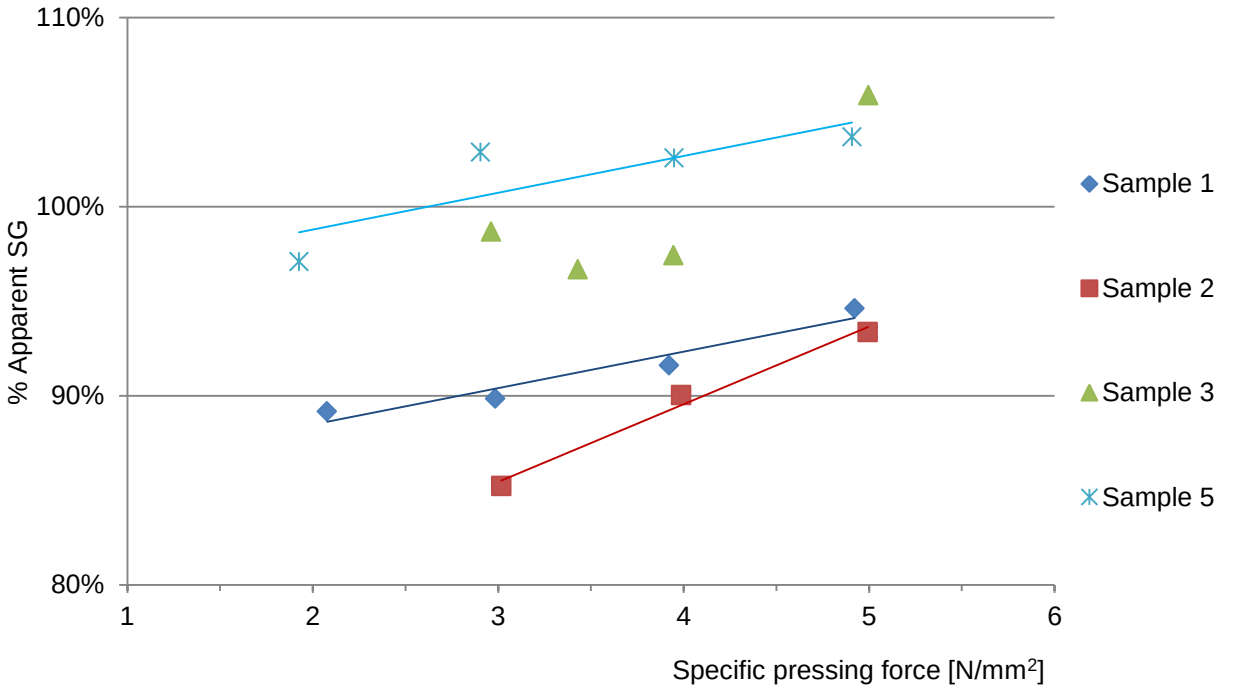

Figure 27 - Material density in the roll nip region and specific pressing force

On the premise of the HPGR testing results, the following was posited:

- Specific throughput constant $\dot{m}$ and roll gap are interrelated to such a degree that the value of either outcome can be estimated from knowledge of the other. The prediction of either response parameter can be significantly improved with inclusion of feed bulk density and size distribution modulus in a linear equation
- The degree of inter-relation between specific throughput and relative gap, net specific energy consumption and size reduction varied depending on sample type
- A satisfactory quantity and spread of data was not available to properly evaluate the sole influence of size distribution slope or roll speed on specific throughput behavior
- Specific pressing force and feed moisture both showed an inverse relation to specific throughput for all tested sample types, similar to results published in literature
- Higher pressing forces resulted in a reduction in gap size, thus increasing material density to a value which approaches its specific gravity. This relation was different for each tested sample type

6 LABORATORY SCALE TEST DEVELOPMENT

As previously discussed, a clear need for an industry accepted laboratory scale procedure for characterizing samples in terms of HPGR throughput potential is apparent. The majority of attempts to date have focused on determining the HPGR motor power requirement for a certain degree of breakage. The goal of this section was to identify tests which provide information on the throughput capability of a sample type, an area which has received little attention in studies on HPGR operation. From the results of the previous section it was made apparent that throughput can be determined from knowledge of the roll gap, feed size and bulk density. The size of the roll gap is carefully referenced during HPGR application design, as it suggests the suitable feed size as well as the top size of the HPGR product (Morrell, 1997; Morley, 2009). Therefore, a suite of tests providing a means to predict the HPGR roll gap will provide a mineral processor with a considerable amount of machine sizing data.

Working towards the initial goal of developing a test for prediction of HPGR throughput, it was decided to adopt terramechanics test methodologies and compare them primarily to measured HPGR roll gap. This was done for the following reasons:

- An accurate prediction of HPGR throughput could be achieved from knowledge of roll gap
- Vehicle wheel sinkage, as presented by terramechanics, and HPGR roll gap were identified as being distinctly analogous
- Knowledge of roll gap provides significant value for sizing of HPGRs

6.1 Direct shear box test

Direct shear box testing equipment was used to measure frictional properties of ores. Terramechanics methodologies were referenced when interpreting the direct shear box test results and applying them to predictions of roll gap.

Pilot HPGR results were available for these ore types so that the statistical significance value of the test outcomes as model input variables could be determined.

6.1.1 Experimental equipment

Direct shear box equipment, as shown in Figure 28, was used to measure the frictional properties of samples. The standard soil mechanics testing unit was modified to accept a larger volume of material, as the original design was intended for containing finer soils. An electric motor was installed onto the unit to ensure that a constant shear rate was applied during testing. Load cell and analog depth gauges were used to measure the shear load and shear displacement. Vertical loads

were applied onto the top shear section through a hanging weight assembly. All surfaces of the container, which were in contact with the sample, were made of smooth steel.

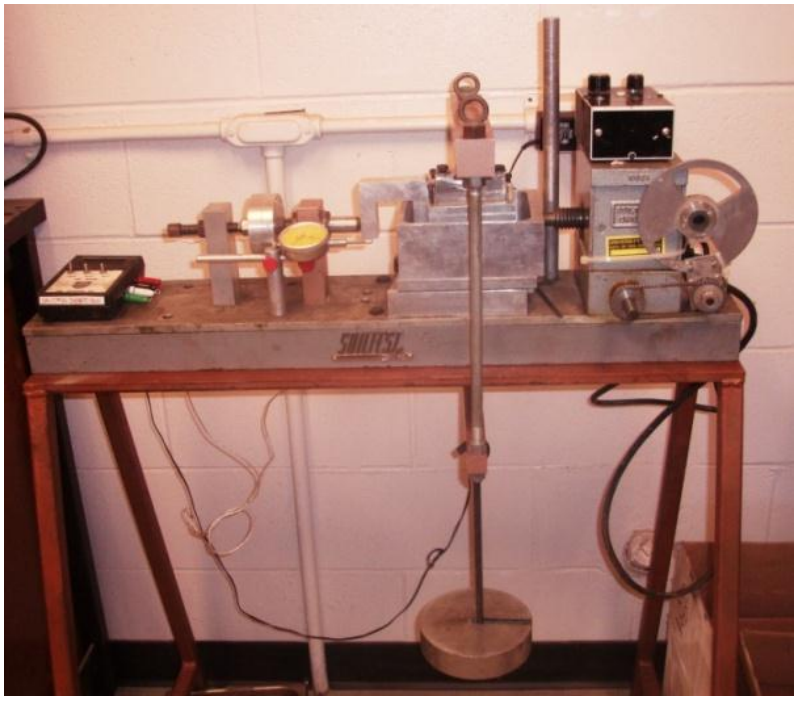

Figure 28 - Direct shear box equipment

A cross-section of the testing equipment is shown in Figure 29, where it can be seen that the full depth of the bottom portion of the container was filled with sample.

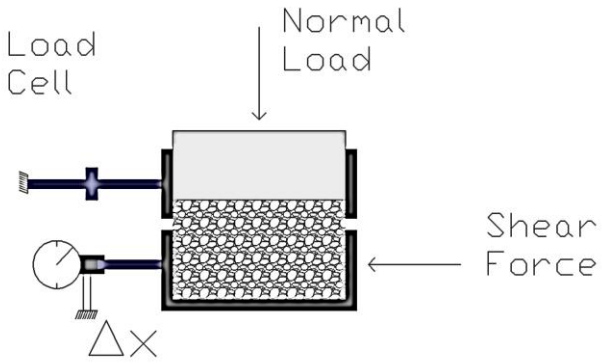

Figure 29 - Cross-section of shear box

The length and width of the container was 75 mm. A total horizontal displacement of 18 mm could be achieved with the testing rig, due to the length of the shear load applying rod.

6.1.2 Experimental procedure

Standard ASTM procedures exist for measuring the friction angle of soils. However, it was intended to use the equipment to measure HPGR feed sample, which in the case of pilot testing had a top size of 32 mm. It was apparent that a shear box feed size would need to be nominated such that the relation of box geometry to individual particle size was suitable for determining the frictional properties of the granular samples. From investigations of top size scale effects, Cerato et al (2006) advised that the box width to particle diameter ratio should be greater than 6 when testing for shear angle. Based on this recommendation, a feed top size of 4 mm was nominated.

At the beginning of each test the gap between lower and upper halves was set to a height of 6 mm using jacking screws. The gap was suggested by Shibuya et al (1997) to be approximately 10 to 20 times the 50^{th} percentage passing particle size, P50, of the tested sample. For the range of tested samples, the ratio of gap to sample P50 size was approximately 4 to 7. Based on investigations into gap effects published by Shibuya et al (1997), the slightly smaller ratio of P50 particle size to gap opening was not considered to have a significant effect on the peak friction angle. Gaps larger than 6 mm were not set, due to concerns that material loss and stress release at the boundary edges would affect the results.

A shearing rate of 1 mm per minute was used for all tests, due to the use of analogue gauges faster shearing speeds would not allow sufficient time for manual recording of displacement data to be carried out.

Approximately 500g was used for each shear test. In order to reduce errors due to variation in initial packing of sample into the shear box, a standardized compaction procedure was established. Sample was filled to a height above the boundary between lower and upper box halves. A hammer head weighing 0.8 kg was dropped ten times from a height of 40 cm onto a lid covering the sample. A second hammer weighing 4.5 kg was dropped three times from a height of 20 cm. Standard soil shear testing procedures typically require a minimum of three different normal loads to be applied for three individual shear runs (Budhu, 2006). To increase confidence in results, five normal loads ranging from 10 to approximately 50 kg were used for each sample investigation. Pilot HPGR feed samples were screened at 4 mm and tested at their original gradation. In order to account for the effects of moisture on measured friction, the samples were adjusted to the same moisture as used for HPGR pilot testing.

Typical test results are shown in Figure 30 and Figure 31 for a quartz sample. The critical state angle was determined from each test as well as the k shear deformation modulus which is specific to terramechanics. k values were fitted using the equation of Janosi et al (1961):

$$T = (c + p\tan\theta)(1 - e^{\frac{-j}{k}}) \qquad (32)$$

where measured shear force was substituted for thrust T.

Two values of k could be fitted depending on whether the peak or critical state angle was included. The k value shown in Figure 30 represents the distance between the y-axis and the intercept of: the tangent to the shear force-displacement curve drawn through the origin, and a horizontal line extending from the maximum shear force. In the case where a peak angle was determined, a value for cohesion was used as measured with the shear box test. Overall five quantitative test outcomes were determined from each test run: peak angle, critical state angle, cohesion and parameter k fitted to either peak or critical state conditions.

Table 11 - Samples tested with the direct shear box

Ore type	**Sample Types**	**Moisture Range Tested**
Quartz	1	0 – 2%
Limestone	1	0 – 10%
Dolomite	1	0 – 3.6%
Kimberlite	1	0 – 8 %
Copper Nickel	1	0 – 5%
Copper Porphyry	3	0 – 5%
Taconite	1	0 – 3%
Volcanogenic Gold Ore	1	0 – 2%
Mafic / Ultra Mafic	1	0 – 5%

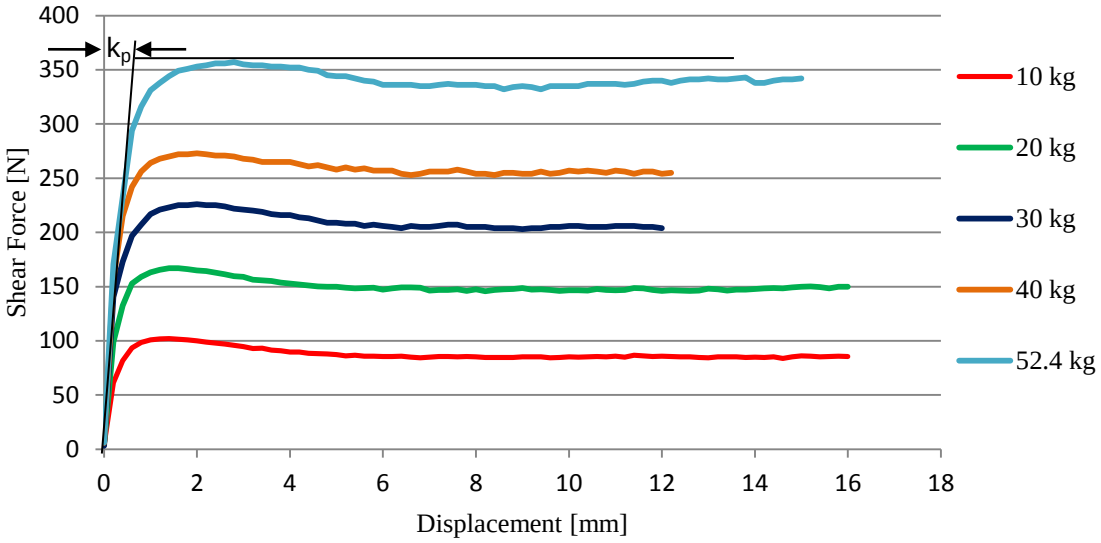

Figure 30 - Shear force and displacement

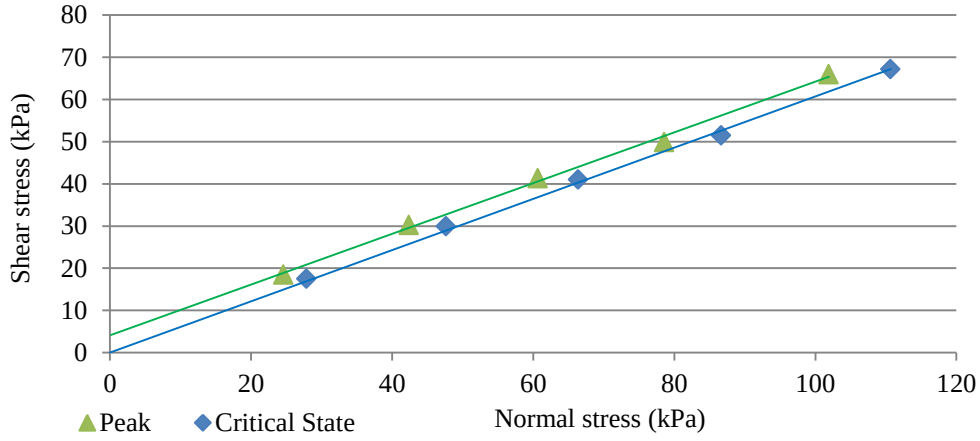

Figure 31 - Shear stress and normal stress

6.1.3 Direct shear test result analysis

Approximately 30 tests were carried out on a range of feed types and moisture levels. Various characteristic shear force and lateral displacement curves were recorded depending on the sample type and moisture.

In the field of soil mechanics, the shear response of a soil to normal load is indicative of the group of soils to which it belongs. Two main soil groups and respective characteristic curves are referred to as, type I and type II soils (Budhu, 2006). This classification system has been adopted for the purposes of this study; characteristic features of these responses as found with the tested ores are shown in Figure 32.

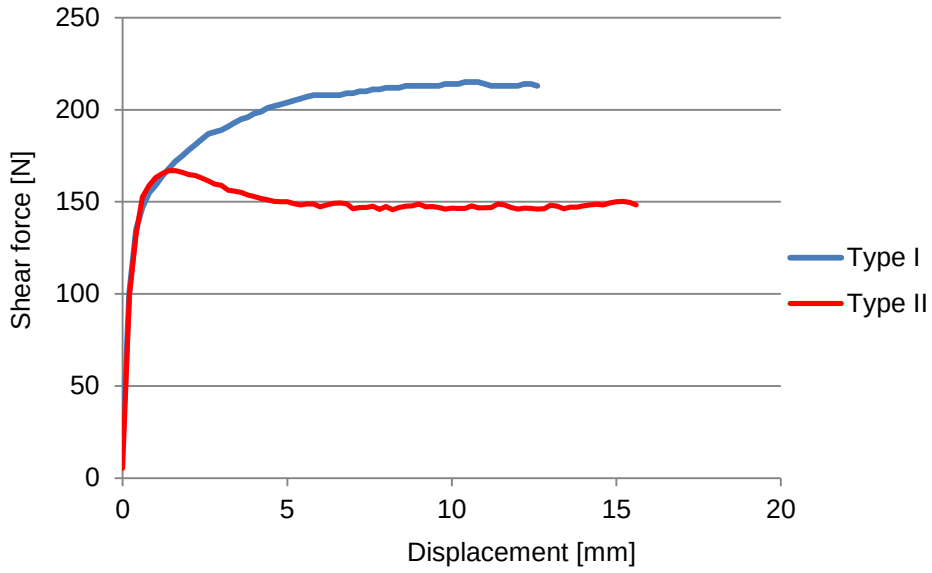

Figure 32 - Type I and type II shear response curves

A general summary of shear test results found for the tested ores is shown in Table 12.

Table 12 - Summary of shear test results

Description	Peak Friction Angle	Critical State Angle	Cohesion	k – Peak	k- Critical State
Units	[deg.]	[deg.]	[N/m^2]	[mm]	[mm]
Average	38.5	37.8	865	1.02	0.89
Max	42.6	42.3	6030	2.05	1.99
Min	32.3	31.3	0	0.28	0.21

Influence of feed parameters on direct shear test outcomes

Knowledge of the effect of feed properties on shear test outcomes is necessary in order to understand the information which the shear test results present. Due to the popularity of the direct shear box test in soil applications, information regarding the general influence of soil properties on the friction angle and cohesion is relatively well known and was discussed in the literature review. Less information is available on the sensitivity of the terramechanics based shear deformation modulus, k, to variation in feed parameters.

The influence of moisture, within a range of 0 to 5%, on shear test results was measured for seven different sample types. For almost all tested samples, a type II characteristic curve would result

when tested dry. Most samples would transition to a type I characteristic curve when adjusted to a moisture content of 2% or more. No consistent association between moisture and critical state angle was found at the moistures tested. Increasing sample moisture content did increase the shear deformation modulus k value for almost all samples tested, viz., the shear displacement required to attain the maximum shear force generally increased as moisture content increased. The effect of size distribution slope on shear test results was not investigated as the focus of the study was to test for potential application to HPGR throughput prediction. Shear test results for each sample tested are shown in the appendix.

6.1.4 Application of terramechanics to direct shear test and HPGR results

The direct shear test is used in the field of terramechanics to assess the thrust which can be achieved from a terrain for certain wheel conditions. This can be considered to be analogous to the throughput performance of an ore when being processed with an HPGR.

Through analysis of the shear test outcomes with respect to equation (32), of Janosi et al (1961), three potential methods of determining a final shear value became apparent. Different values of k or internal friction angle Ɵ could be substituted into the thrust equation, depending on whether all ores were treated as being in a critical state, resulting in equation (33) or whether peak angles were taken into account, represented by equation (34). The inclusion of cohesion produced a third approach, equation (35), to applying the thrust equation to HPGR roll gap. To compare the applicability of each approach to HPGR, attempts at correlating to measured HPGR $\dot{m}$ and gap were made using three different modified forms of the thrust equation. Similar to the previous step-wise regression attempt, HPGR pilot test results were grouped according to specific pressing force and roll speed parameters. The following modified forms of the soil thrust equation, (32), of Janosi et al (1961) were related to HPGR roll gap, s,:

$$s = (ß_1 tan\theta_{CS})(1 - e^{\frac{-j}{k(cs)}}) + ß_2 \quad (33)$$

$$s = (ß_1 tan\theta)(1 - e^{\frac{-j}{k}}) + ß_2 \quad (34)$$

$$s = (c + ß_1 tan\theta)(1 - e^{\frac{-j}{k}}) + ß_2 \quad (35)$$

where j is the wheel specific slip value, $ß_1$, represents normal stress, and $ß_2$ is a constant. The constants j, $ß_1$, and $ß_2$ were fitted for each dataset.

The first fitting trial, as denoted by equation (33), incorporated the shear deformation modulus parameter k(cs), as measured for a critical state, and the critical state angle.

For the second fitting attempt, represented by equation (34), the magnitude of the friction angle Ɵ and deformation modulus k was used according to the type of characteristic curve, I or II, measured

for a particular sample, i.e. in the case of a type II curve, the peak friction angle was input for Θ, while for a type I curve the critical state friction angle was used. In this case the shear results were assumed to be cohesionless, meaning the line of best fit for the shear stress-normal stress data was forced through the origin.

The final fitting trial, equation (35), was similar to that of attempt two, equation (34), with the exception of measured cohesion being included.

As all three fitting attempts made use of three fitted variables, viz. j, $ß_1$, and $ß_2$, the degrees of freedom were equivalent and the coefficient of determination, R^2, was used as a comparative indicator of the degree of fit achieved.

The results presented in Table 13 show that a higher degree of fit could be achieved when using equation (34), which does not take cohesion into account. It was also found that overall a considerably lower degree of fit was achieved for the larger datasets, such as dataset #1 and #3. This was attributed to the variation in sample within those datasets, indicating that further parameters for sample characterization are required to improve predictability.

Table 13 - Application of the thrust equation to HPGR roll gap

		HPGR Setpoints		Roll Gap: Fitted R^2		
Data Set. #	No. of Tests	Roll Speed (m/s)	F_{SP} (N/mm^2)	Attempt One	Attempt Two	Attempt Three
1	8	0.75	5	0.46	0.62	0.45
2	5	0.9	4	0.49	0.76	0.53
3	16	0.75	4	0.53	0.58	0.36
4	4	0.6	4	0.55	0.95	0.60
5	6	0.75	3	0.59	0.75	0.22

6.1.5 Discussion of direct shear test results

The application of terramechanics based interpretations to a soil mechanics test provided results which showed potential applicability to predicting HPGR gap, from which throughput would subsequently be derived. This investigation made available additional input variables for HPGR throughput modelling purposes. It is important to note that the normal loads applied with the shear test during the study were less than 1% of the maximum normal load applied by HPGR rollers during operation. The study of the shear response of materials to higher normal loads, similar to the pressure within the HPGR roll nip, could potentially improve the degree of correlation. Also, a shear rate of 1 mm/s was applied using the direct shear box. The retention time in the compression zone of

the pilot HPGR was approximately 0.06 seconds, meaning that shear rates were most probably much greater than that tested with the shear box.

The following are main outcomes of the shear test investigation:

- Three different shear test interpretation methods were compared based on gap predictability. A proposed method which takes into account the initial shape of the shear-displacement curve and disregards cohesion was found to provide the most accurate roll gap predictions
- The shear test provided additional input variables for consideration in further regression attempts at modelling roll gap, which would be subsequently used to derive throughput

6.2 Piston press test work

A substantial amount of work has been carried out by researchers on the applicability of piston press test results to predicting HPGR performance, primarily aimed at describing the comminution effect. Similar pressure sinkage tests are used in the field of terramechanics to assess the trafficability of terrain. In the aim of designing laboratory scale tests which can be used for the prediction of HPGR throughput, this previous work is drawn upon and applied to available hydraulic piston press equipment at the University of British Columbia. As with the previously outlined shear tests, the piston press tests were carried out on sub-samples of HPGR feed and applicability was assessed.

6.2.1 Experimental equipment

An instrumented hydraulic piston press, shown in Figure 33, was used to apply compression to samples contained in a die. A maximum load of 165 tonnes could be applied in a controlled fashion to piston and die assemblies. Axially located load cells were used to measure the load applied. Two piston and die assemblies were manufactured from hardened steel and had effective diameters of 100 and 45 mm. Two load cells with different load ratings were used for the study and had the following effective working ranges:

- Heavy duty load cell: 10 to 160 tonnes
- Light duty load cell: 0.01 to 50 tonnes

The mechanical strain of the hydraulic piston press and die assemblies was measured for the full range of hydraulic load application.

Figure 33 - Hydraulic piston press

6.2.2 Experimental procedure

The piston press testing program was carried out with regard to load cell specifications and die geometries, resulting in four distinct test parameters which are described in Table 14.

Table 14 - Description of piston and die test setpoints

Description	Setup #1	Setup #2	Setup #3	Setup #4
Die Diameter (mm)	100	45	100	45
Sample Top Size (mm)	4	4	4	4
Tested Pressure Range (MPa)	17 - 185 MPa	17 - 185 MPa	0.03 - 15 MPa	0.03 - 15 MPa
Loading / Displacement Rate	13.8 MPa/min	13.8 MPa/min	2 mm/min	2 mm/min

Initial compression tests were carried out using the 100 mm diameter piston and die assembly. A sample top size of 4 mm and sample volume of 300 ml provided test geometries which were similar to the testing guidelines established by Schönert et al (1996). This equated to approximately 500 g of sample being required for each test. Pressurization of the hydraulic cylinder was controlled by a PLC based on a setpoint pressure rate or piston displacement rate. A range of load application rates and maximum loads was applied to pilot HPGR feed samples. Piston press and HPGR tests were

carried out at equivalent sample moisture levels. Testing was also carried out using a 45 mm diameter piston and die assembly using a feed top size of 4 mm. In this case the relation of sample size to piston diameter did not conform to the die geometry guidelines, but did provide a means for measuring the influence of piston diameter on compressibility of samples. Initially 60 ml of sample (approximately 100 grams) was used with the 45 mm diameter die, which resulted in an initial sample bed height of 40 mm at bulk density, equal to that used with the 100 mm diameter piston press tests. The focus of the testing was to determine the strain of samples with respect to applied load. Pressures of up to 185 MPa were applied to samples, which is in the range of maximum nip pressures occurring in the HPGR (cf. Lubjuhn, 1992 and Schönert et al, 2002). The strain of mechanical equipment was subtracted from the strain measured with sample present. Sample types tested are described in Table 15.

Table 15 - Samples tested by the piston press

Ore type	# of Sample Types	Moisture Range Tested
Quartz	1	0 – 2%
Limestone	1	0 – 10%
Dolomite	1	0 – 3.6%
Copper Nickel	2	0 – 5%
Copper Porphyry	3	0 – 5%
Taconite	1	0 – 3%
Volcanogenic Gold Ore	1	0 – 2%
Mafic / Ultra Mafic	1	0 – 5%

Overall, approximately 70 tests were carried out using the 100 and 45 mm die assemblies. Test outcomes were directly related to the form of load versus displacement curve, which could be described by exponential or power equations. At the beginning of each test a nominated packing pressure was applied and the corresponding sample volume recorded. The specimen would then be subjected to a controlled load or displacement rate until a specified pressure would be reached.

6.2.3 Piston press results

An example of applied load and sample strain measured for different piston diameters using the heavy duty load cell is presented in Figure 34. In the example shown, piston displacement was zeroed at a pressure of 17 MPa, due to use of the heavy duty load cell. The relation between applied pressure and measured sample strain could be fitted suitably well by an exponential equation of the form:

$$P = ae^{bx} \quad (36)$$

where P is pressure, x is sample strain, and a and b are fitted coefficients.

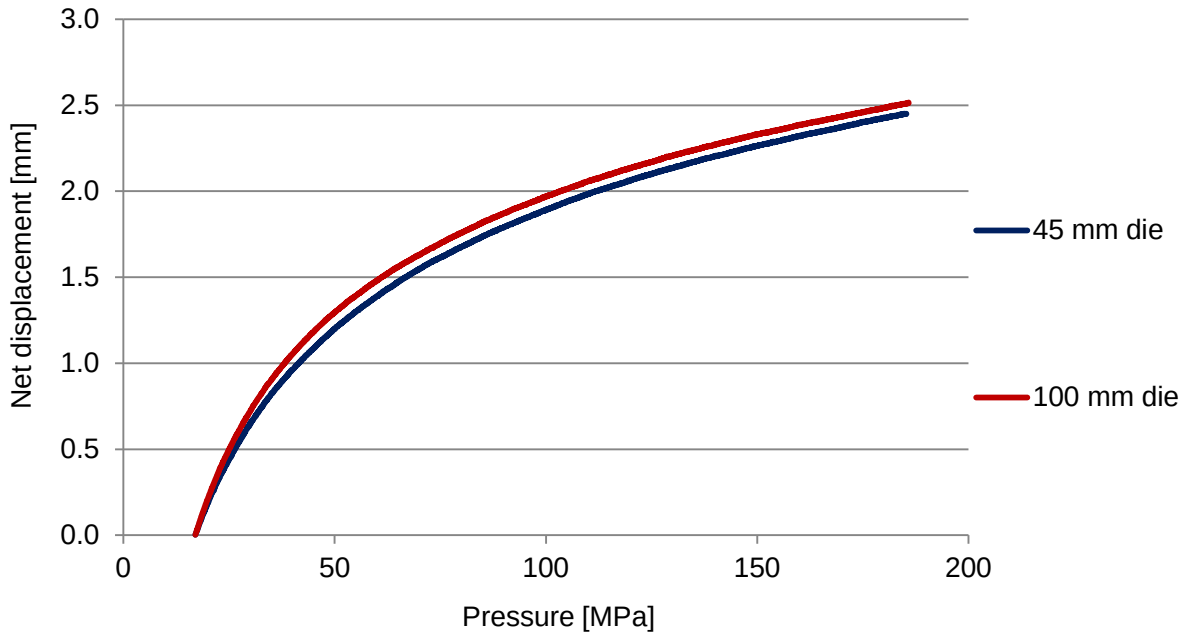

Figure 34 - Applied pressure and sample strain

Due to the use of uncompacted samples in the piston press and low sensitivity of the load cell, the initial volume of the sample at the beginning of pressure application was difficult to measure for each individual test. Ideally, a reliable outcome of the test would be the percent change in volume and its relation to piston pressure.

Influence of moisture on piston press results

Variations in sample moisture on piston sinkage were found to be dependent on the sample type and the applied range of pressures. From Figure 35 it can be seen that for applied piston pressures of 0.03 to 5 MPa, vertical displacement generally increased for the three tested sample types when higher levels of moisture were present.

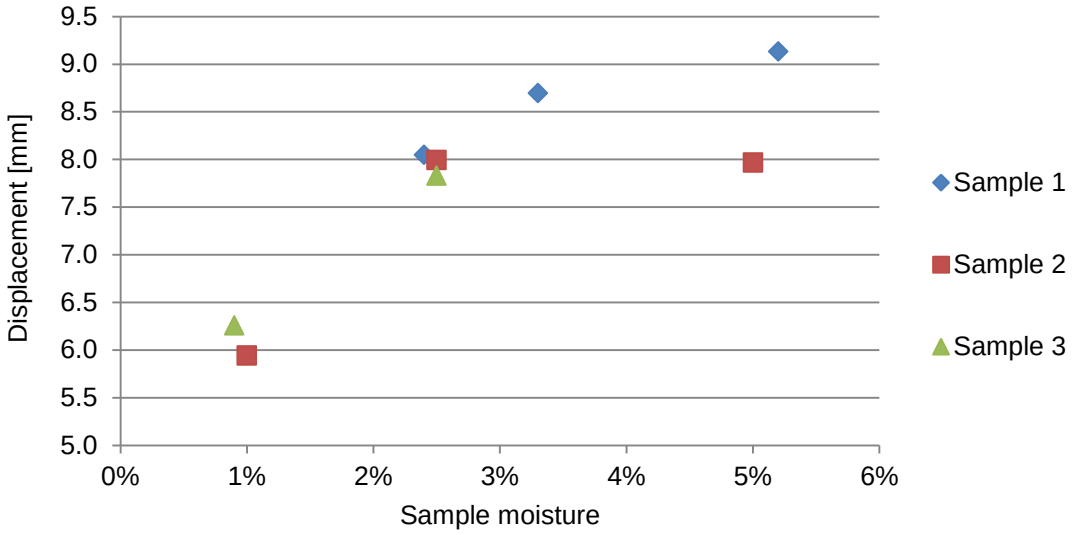

Figure 35 – 100 mm Piston and moisture, 0.03 - 5 MPa

When the displacement of samples at pressures above 5 MPa were observed, moisture was generally found to inhibit piston displacement, as presented in Figure 36.

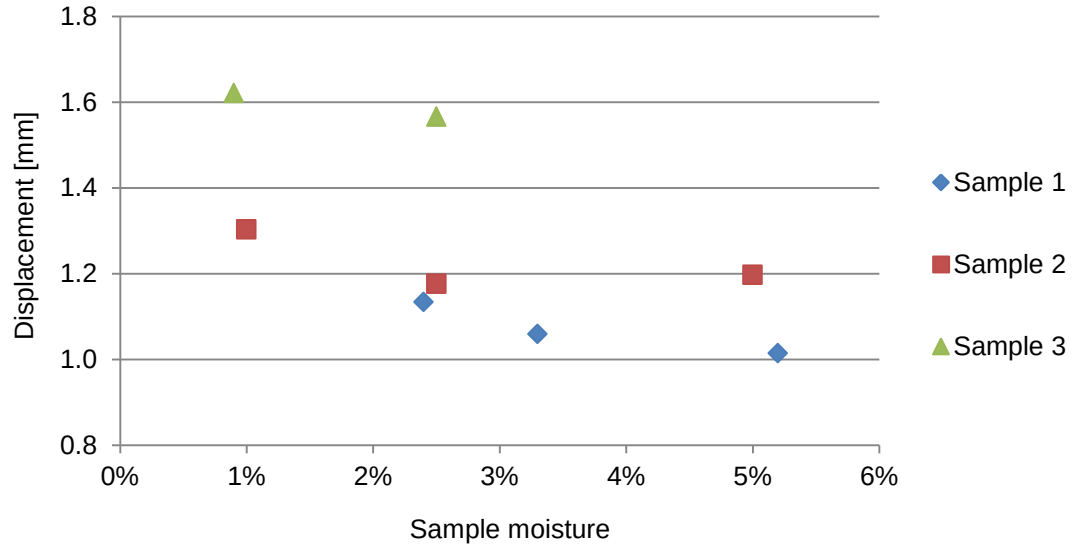

Figure 36 - 100 mm Piston and moisture, 5 - 10 MPa

As pressure was increased to the maximum test set point of 185 MPa, the influence of moisture on piston displacement was found to be inversely related to displacement. This is supported by Figure 37.

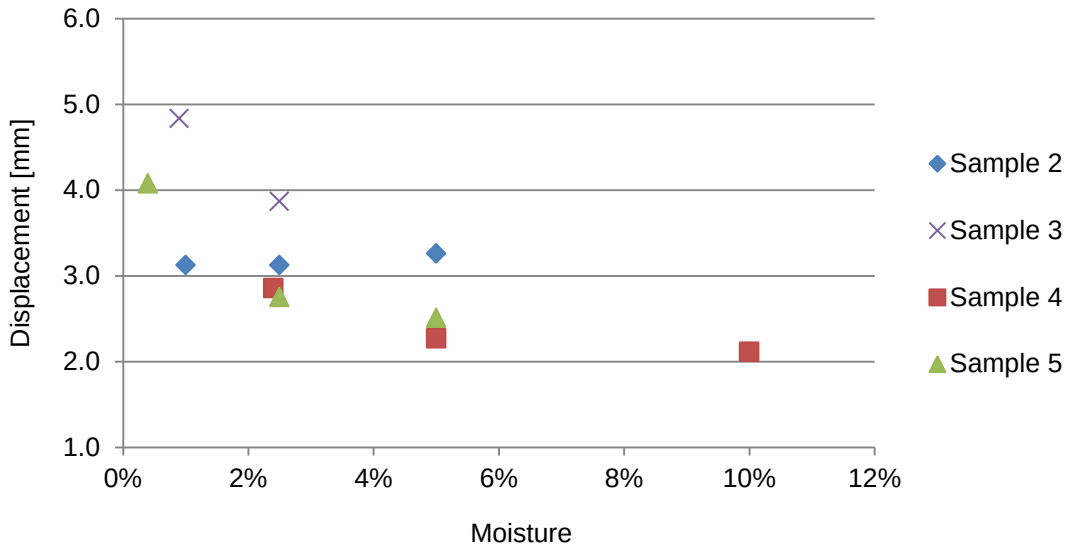

Figure 37 - 100 mm Piston and moisture, 17 - 185 MPa

The results suggest that the effect of moisture experiences a transition between pressures of 0.03 to 10 MPa. This may also imply that at lower applied pressures, higher piston displacements are achieved due to moisture facilitating the packing of particles.

During testing it was noted that for samples with a moisture content of 5 % or more, a layer of water was present at the top of the compressed sample after removal of the piston. This was especially apparent for high pressure tests which reached a maximum pressure of 185 MPa. In rare cases, water escaped the die through a gap between the piston and die walls during pressure application.

6.2.4 Discussion of piston press test results

Piston press test results provided an indication of the pressure-displacement characteristics of HPGR feed materials.

The following are main outcomes of the piston press test investigation:

- The role of moisture on pressure-displacement was found to undergo a transition at pressures of 0 – 10 MPa
- The testing methodology suffered from variation in initial sample height and porosity, due to the use of uncompacted sample at the beginning of each test
- Challenges in accurate splitting of -4 mm sample were experienced when attempting investigations using piston press die equipment having a diameter of 45 mm

The combination of pressure-displacement parameters, derived from piston press testing, with other parameters determined from shear tests and material characterization was tested and presented in the modelling stage of this document.

7 THROUGHPUT AND GAP MODELLING

The outcomes of HPGR pilot tests and proposed laboratory scale tests were combined in an attempt at establishing a model for prediction of specific throughput and roll gap. The results of three different laboratory tests were compiled into three separate datasets and used for comparison of measured and predicted HPGR roll gap results. Successful development of a roll gap model would allow the throughput constant to also be predicted using the previously described gap-throughput relations.

7.1 Linear stepwise regression

Linear stepwise regression was carried out to determine the statistical relevance of the input variables determined from new laboratory scale tests. Shear test outcomes, which in previous sections had shown the highest applicability to predicting gap and throughput, were used in this stage of linear stepwise regression. The piston displacement measured at piston pressures ranging from 5 to 185 MPA was used as piston press related input variables and referred to as z(5) to z(185) respectively. Additionally, material parameters such as moisture, porosity and bulk density were included in the list of input variables. Interaction effects of variables were also considered, which substantially increased the size of the input variable matrix. All input variables were coded to a range of -1 to 1 using the following expression:

$$coded\ x(i) = \frac{2x(i)-(max(x)+min(x))}{max(x)-min(x)} \qquad (37)$$

The coded variables were used with interactive Matlab stepwise regression in relation to recorded HPGR gap. The selection and rejection of variables was carried out with reference to p-values and the author's judgment based on knowledge of the variable source. Due to the large amount of variables available for selection, user input was found to be necessary to avoid the formulation of overly complex models containing combinations of variables which were considered to be illogical.

During the modelling phase it was noted that the results from both direct shear and piston press tests were described using non-linear equations. The shear deformation modulus was derived from the direct shear test using an equation of exponential form. The relation of pressure to displacement found in piston press testing was also of exponential form. With respect to the source of the laboratory scale test results, non-linear models need to be considered when assessing the predictive value of these tests. Exponential equations were not transformed into linear models through substitution as new errors would be created which would be dependent on the value of the input terms. Therefore, the parameters derived from each test were used independently as input variables in linear stepwise regression. Table 16 shows the input variables which were used for linear regression modelling.

Table 16 - Input variables for modelling

Description	Symbol	Source
Feed bulk density	ρ_b	Material analysis
Gaudin-Schuhmann m parameter	M	
Moisture	H20	
Porosity	ϕ	
Roll speed	μ	HPGR pilot testing
Specific pressing force	F_{SP}	
Shear deformation modulus	k	Direct shear box testing
Shear angle	Θ	
Displacement at 5 MPa	Z(5)	Low pressure piston press
Displacement at 10 MPa	Z(10)	
Displacement at 15 MPa	Z(15)	
Displacement at 17 MPa	Z(17)	High pressure piston press
Displacement at 25 MPa	Z(25)	
Displacement at 30 MPa	Z(30)	
Displacement at 50 MPa	Z(50)	
Displacement from 17 to 25 MPa	Z(17-25)	
Displacement from 17 to 100 MPa	Z(17-100)	
Displacement from 17 to 150 MPa	Z(17-150)	
Displacement from 17 to 185 MPa	Z(17-185)	
Displacement at 20 MPa	Z(20)	Low & high pressure piston press tests
Displacement at 50 MPa	Z(50)	
Displacement at 100 MPa	Z(100)	
Displacement at 150 MPa	Z(150)	
Displacement at 185 MPa	Z(185)	

7.1.1 Linear modelling with shear test results

Shear tests results were available for 51 sets of experimental conditions, the largest dataset used in the linear modelling exercise. When analyzing first-order effects of input variables, only feed bulk density, moisture and specific pressing force were found to be statistically significant in predicting roll

gap. The achieved predictive accuracy was poor, represented by an R^2 value of 0.50. The following equation resulted from the analysis:

$$\hat{y} = \beta_0 + \beta_1.H20 + \beta_2.\rho_b + \beta_3.F_{SP} + \beta_4.k \qquad (38)$$

Variables in the above and subsequent predictive equations shown in this section, are presented in the order of their statistical significance. i.e. the p-value of input variable H20 was the lowest of the four input variables shown in equation (38), hence it had the highest statistical significance.

For the same dataset, linear stepwise regression was carried out with consideration to interaction effects and resulted in the following predictive equation:

$$\hat{y} = \beta_0 + \beta_1.H20 + \beta_2.F_{SP}.k + \beta_3.\rho_b \qquad (39)$$

Predictive accuracy was slightly improved to an R^2 value of 0.52 for a greater number of degrees of freedom, as shown in Figure 38, when compared to that achieved with the first order equation. The improvement was due to introducing the interaction effect of specific pressing force and shear deformation modulus.

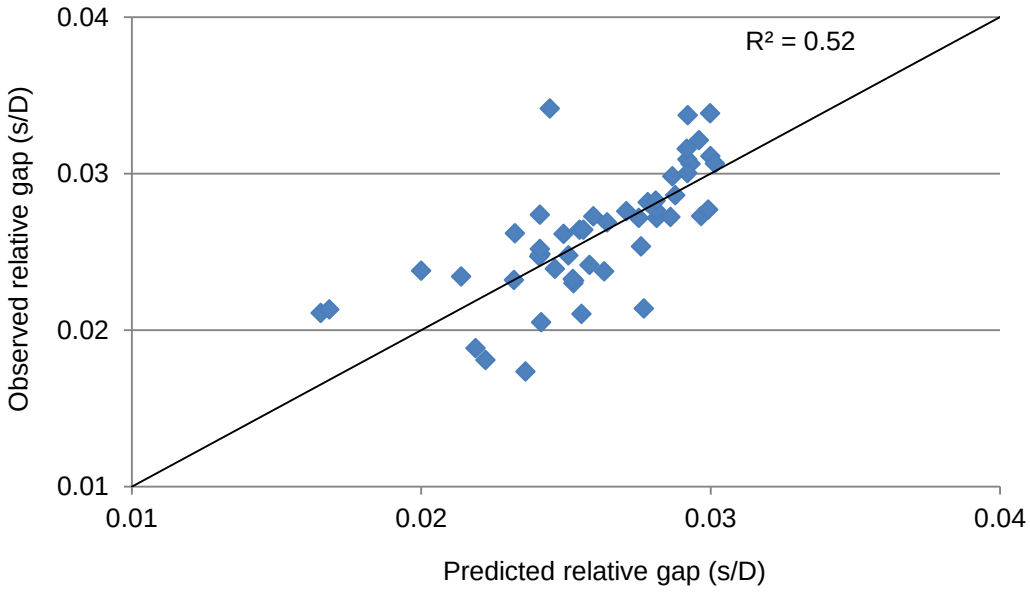

Figure 38 - Shear test results and relative gap prediction

7.1.2 Linear modelling with shear test and low pressure test results

Shear and low pressure test results were available for forty sets of experimental conditions. As carried out previously, the statistical significance of first order relationships was initially considered. The resulting first order predictive equation included five input variables, neither of which was sourced from low pressure piston press testing. The following predictive equation resulted:

$$\hat{y} = \beta_0 + \beta_1.H20 + \beta_2.\rho_b + \beta_3.k + \beta_4.m + \beta_5.F_{SP} \quad (40)$$

The equation was able to be fit to an R^2 value of 0.80, and a comparison to observed results is shown in Figure 39.

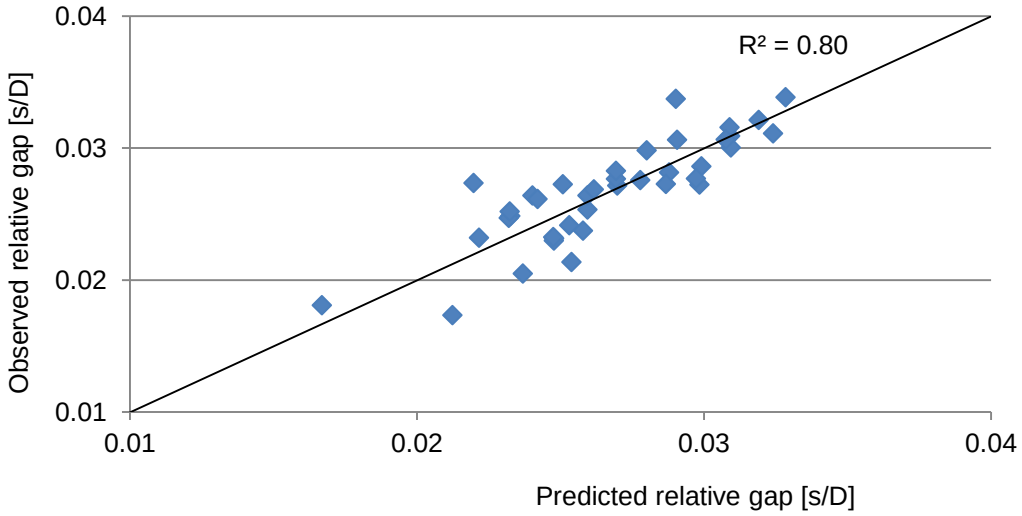

Figure 39 - 1st order low pressure piston and shear test modelling

A second modelling attempt which accounted for interaction effects did not result in an improved degree of fit.

7.1.3 Linear modelling with shear test and high pressure test results

Forty six sets of results were available for high pressure piston press, shear and pilot HPGR tests. Stepwise linear regression was carried out to determine the predictive equation (41), which provided an R^2 value of 0.60.

$$\hat{y} = \beta_0 + \beta_1.F_{SP} + \beta_2.k + \beta_3.\theta + \beta_4.Z(17-25) + \beta_5.H20 \quad (41)$$

A plot of measured and predicted relative gap values is shown in Figure 40.

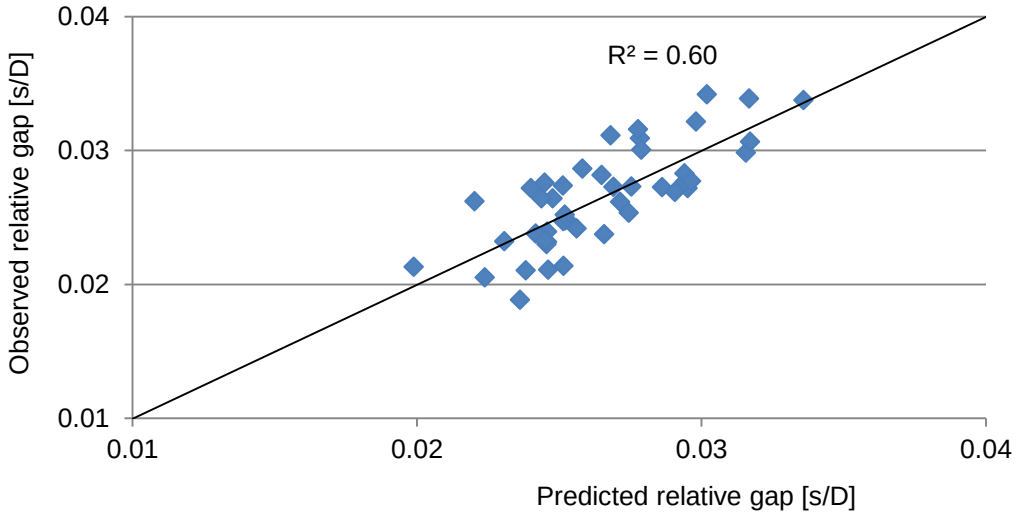

Figure 40 - 1st order high compression piston and shear test modelling

A predictive equation with four input variables was formulated when modelling with consideration to interaction effects. The following equation was determined:

$$\hat{y} = \beta_0 + \beta_1 . F_{SP} . k + \beta_2 . \theta + \beta_3 . Z(17 - 25) + \beta_4 . H20 \qquad (42)$$

As can be seen in Figure 41, an improved degree of fit was achieved when interaction effects were included. The improvement was represented by a higher R^2 of 0.67 for greater degrees of freedom.

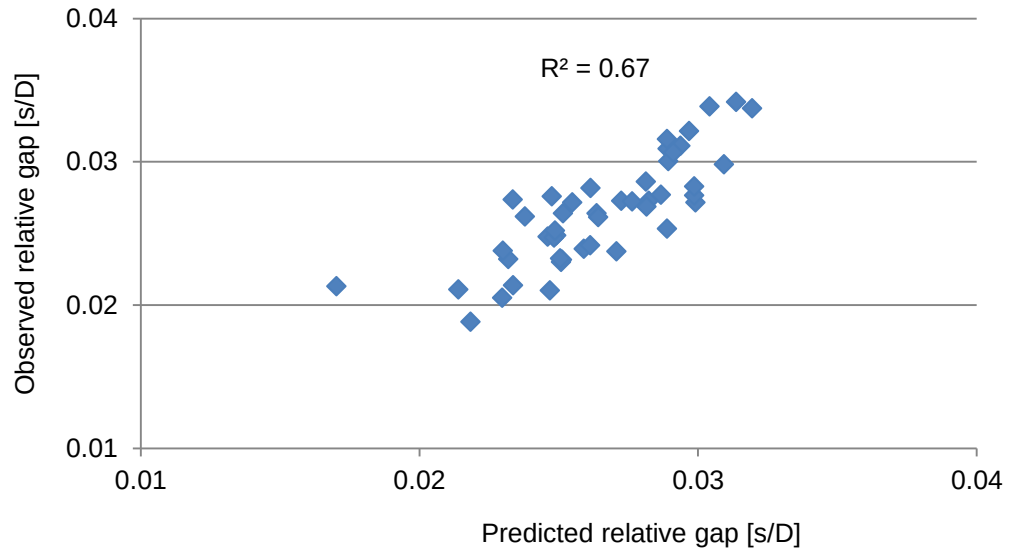

Figure 41 - High pressure piston and shear test modelling with interaction effects

7.1.4 Linear modelling with shear test and complete pressure test results

Both low and high pressure piston press results were available for a smaller dataset of 36 data points. The results of the piston press results were combined to create variables which represent sinkage from applied piston pressures of 0 to 185 MPa. The sinkage measured for a pressure range of 0 to 150 MPa was considered to be statistically significant for a first order predictive equation:

$$\hat{y} = \beta_0 + \beta_1.k + \beta_2.m + \beta_3.F_{SP} + \beta_4.\rho_b + \beta_5.\theta + \beta_6.Z(0-150) \qquad (43)$$

The shear deformation modulus, k, was found to have the highest statistical significance, and an R^2 value of 0.90 was achieved as shown in Figure 42.

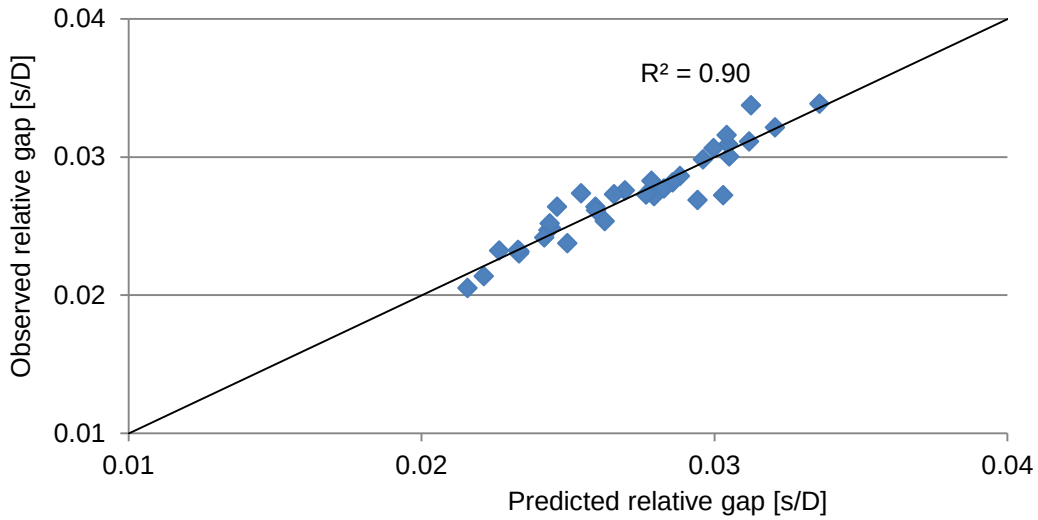

Figure 42 - 1st order piston and shear test modelling - gap

An improved predictive model could not be achieved through the inclusion of interaction effects.

Earlier comparisons of gap and throughput showed that throughput could be derived from knowledge of gap, material slope parameter m and bulk density. Since these input variables are already present in equation (43), the same equation was used to predict specific throughput as shown in Figure 43. The constants β of equation (43) were adjusted to minimize the residual sum of squares with regards to specific throughput. The achieved degree of fit, an R^2 value of 0.91, verified that a model targeting gap could be used to predict specific throughput.

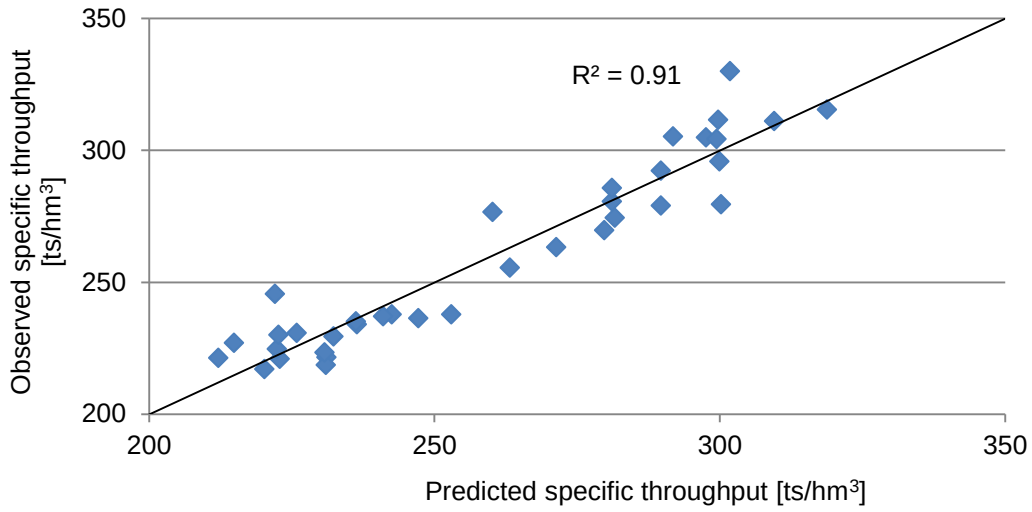

Figure 43 - 1st order piston and shear test modelling - throughput

The outlined regression attempts are summarized in Table 17. The coefficient of determination achieved when fitting with respect to specific throughput is also shown. Overall, the degree of fit was similar for both relative gap and specific throughput when applying the same predictive equations.

Table 17 – Summary of throughput and gap modelling

# of Data points	Linear Regression Model	Relative Gap R^2	Specific Throughput R^2
51	$\hat{y} = \beta_0 + \beta_1.H20 + \beta_2.\rho_b + \beta_3.F_{SP} + \beta_4.k$	0.50	0.60
51	$\hat{y} = \beta_0 + \beta_1.H20 + \beta_2.F_{SP}.k + \beta_3.\rho_b$	0.52	0.62
40	$\hat{y} = \beta_0 + \beta_1.H20 + \beta_2.\rho_b + \beta_3.k + \beta_4.m + \beta_5.F_{SP}$	0.80	0.73
46	$\hat{y} = \beta_0 + \beta_1.F_{SP} + \beta_2.k + \beta_3.\theta + \beta_4.Z(17-25) + \beta_5.H20$	0.60	0.57
46	$\hat{y} = \beta_0 + \beta_1.F_{SP}.k + \beta_2.\theta + \beta_3.Z(17-25) + \beta_4.H20$	0.67	0.64
36	$\hat{y} = \beta_0 + \beta_1.k + \beta_2.m + \beta_3.F_{SP} + \beta_4.\rho_b + \beta_5.\theta + \beta_6.Z(0-150)$	0.90	0.91

7.2 Non-linear modelling

Non-linear gap models were attempted using exponential regression and also terramechanics based empirical equations as a reference for an initial form of model. However, the degree of fit achieved with investigated non-linear models was considerably lower than attained with linear models.

The following empirical equation for wheel sinkage is an example of a terra-mechanics based equation used as a reference for a form of model (Wong, 1993):

$$z = \left[\frac{3W}{b(3-n)(\frac{k_c}{b}+k_\phi)\sqrt{D}}\right]^{(2/(2n+1))} \quad (44)$$

where k_c and k_ϕ are compression factors determined from plate sinkage test results.

Compression factors were derived from the piston press tests and used with equations of similar form to that of the terramechanics based sinkage equation. Constants were adjusted to minimize the error in gap prediction, however the predictive accuracy of the model was still less than that achieved with linear stepwise regression. Similarly, gap predictions were attempted using the original form of the terramechanics thrust equation. All of the mentioned non-linear variables were combined with statistically significant linear variables and adjusted according to the degree of fit. The attempted non-linear models were considerably poorer in predictive accuracy when compared to the degree of fit achieved by the previously suggested linear models.

7.3 Force-based model

As discussed previously in the literature review section, during HPGR operation roll pressing force is applied entirely to the material present between the rolls. Knowledge of the pressure profiles in relation to rotational angle of the roll and roll width allows a volume to be calculated which has resulting units of force. With knowledge of the material specific pressure-displacement curve generated from piston press tests, a compression angle was derived and compared to that observed during HPGR pilot testing. The compression angle can be used to determine throughput by use of the continuity formula, equation (8), presented earlier in the literature review.

Knowledge of the pressure displacement curve from 0 to 185 MPa was required, as this full range of pressure was expected to occur at the roller surface. For this reason, the results of low and high pressure piston press tests were combined and expressed in exponential form:

$$P = ae^{bx} \quad (45)$$

where P is pressure, a and b are fitted parameters and x is displacement. An example of a pressure-displacement curve for a quartz sample is shown in Figure 44. Parameters a and b were fitted for each individual pressure-displacement curve.

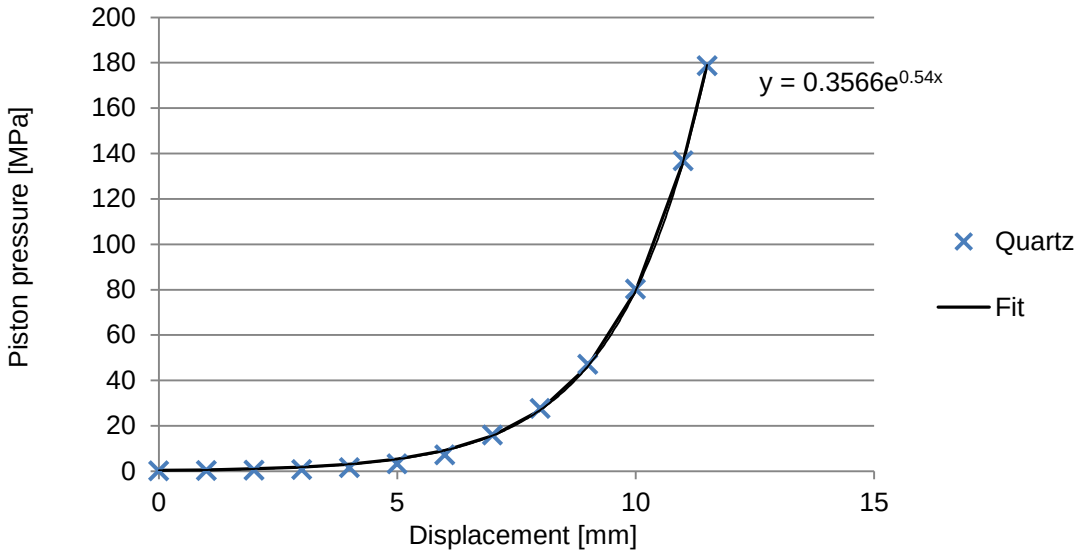

Figure 44 - Pressure-displacement curve

Ideally, the change in pressure to the percent change in piston die volume would be derived from the piston press test. However, due to the use of uncompacted samples in the piston press and low sensitivity of the piston press load cell, the initial volume of the sample at the beginning of pressure application was difficult to measure for each individual test.

The approach used to translate results of the piston press to the HPGR roll is best shown by Figure 45. Distance x represents the horizontal displacement carried out at the surface of the roll, from the beginning of the compression angle to the zero angle, directly analogous to the vertical displacement observed in a piston press test. As discussed earlier, the compression angle, defines the point on the roll surface where pressure application onto feed material begins.

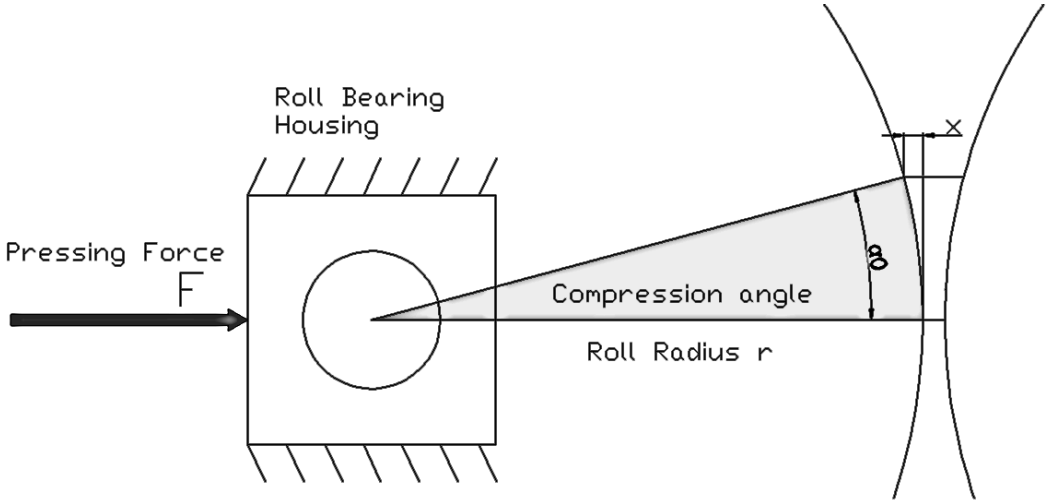

Figure 45 – Application of pressure-displacement curve

For the purposes of modelling compression angle, α, and roll pressure profile, it was assumed that the hydraulic pressing force is completely applied onto material which is in contact with the roller surface at the compression angle. The extrusion zone, located below the zero angle of the roller, was not taken into account as published results showed that it was comparatively small in terms of force application. Therefore, the known pressing force from HPGR tests could be related to the piston pressure-displacement curve in order to model the compression angle and roll pressure profile.

Figure 46 shows that the horizontal displacement of the roller surface, x, can be related to compression angle, α and roller radius, r, by the following:

$$cos\alpha = \frac{(r-x)}{r} \qquad (46)$$

And,

$$x = r(1 - cos\alpha) \qquad (47)$$

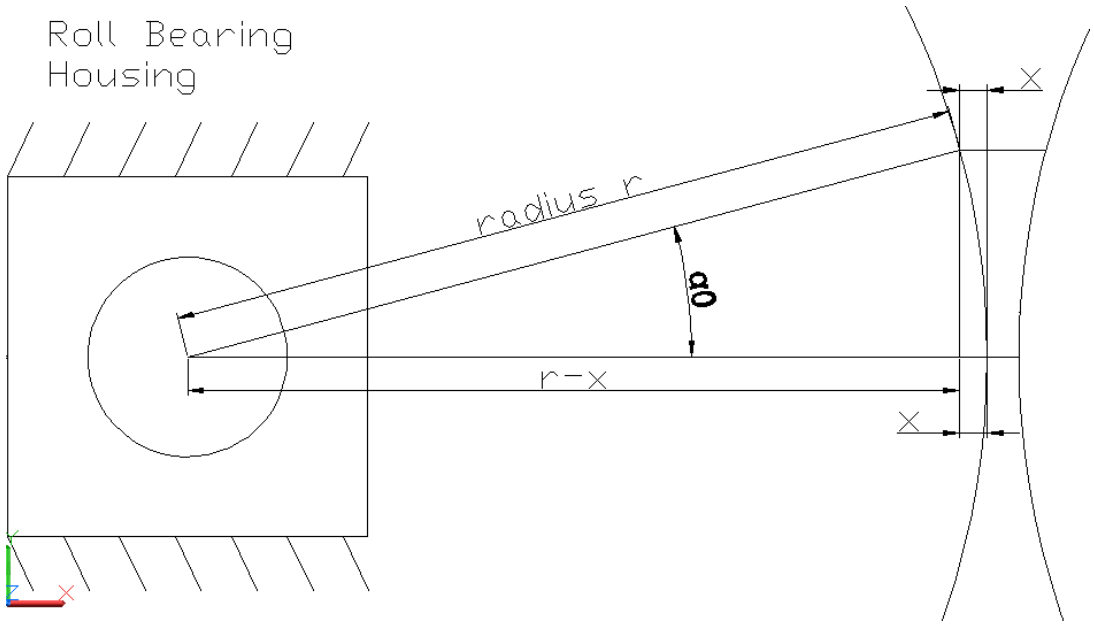

Figure 46 – Compression angle and displacement geometry

In order to account for lower pressures at the roller edge, the edge profile equation of Lubjuhn (1992) was used. For clarity it is presented again.

$$\frac{p(\lambda)}{p(\lambda=0)} = 1 - (2|\lambda|)^n \qquad (48)$$

where λ = l/w, l is equal to the axial location on the roll (at the centre of the roll l=0) and n is slightly dependent on the specific pressing force setpoint, but having an approximate value of 1.6 (Lubjuhn, 1992). For this thesis it was assumed that n=1.6.

From equation (48) it can be seen that the roll pressure at any point in the horizontal plane, P(λ), can be derived from knowledge of the pressure at the center of the roll (within the same plane) and the width of the roll, w. Since the pressure at a specified coordinate was of interest, equation (48) was presented as:

$$p(\lambda) = p(\lambda = 0).(1 - (2|\lambda|)^n \qquad (49)$$

Based on a roll width of 220 mm, as used with the pilot HPGR at UBC, the resulting pressure profile along the roll width is shown in in relation to the pressure at the center of the roll, p(centre) by Figure 47.

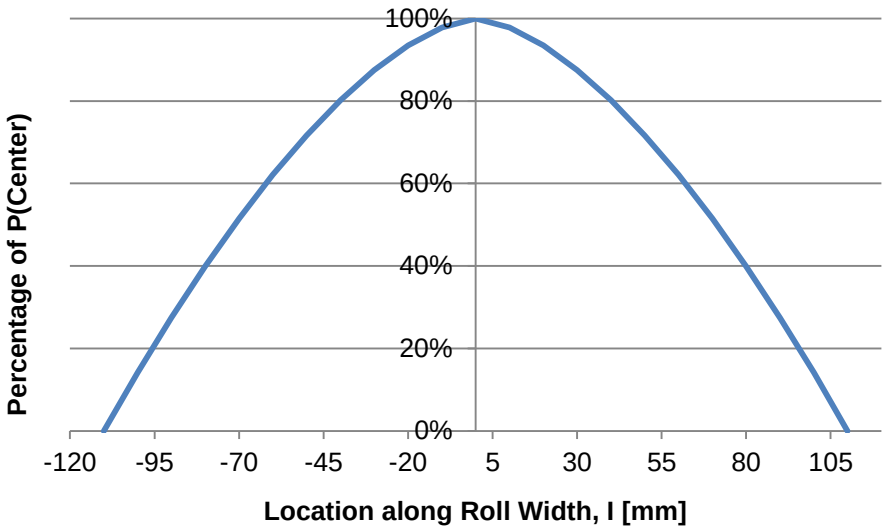

Figure 47 - Plot of roll pressure in horizontal plane

For simplicity, the term specifying the location along the roll width, λ, was expanded into full form and the absolute value was removed, as shown in equation (50).

$$p(I) = p(centre).\left[1 - \left(\frac{2.I}{width}\right)^{1.6}\right] \tag{50}$$

Equation (50) represents one equal half of the pressure profile, however, the pressure profile is symmetrical about the y-axis, as shown in Figure 47, and the total area can be determined by the following:

$$Area = 2.\int p(I)\,dI = 2.\int p(centre).\left[1 - \left(\frac{2I}{width}\right)^{1.6}\right] dI \tag{51}$$

$$= 2p(centre).\int_0^{width/2} 1 - \left(\frac{2.I}{width}\right)^{1.6} dI \tag{52}$$

$$= 2p(centre).\left[\left(\frac{width}{2}\right) - \left(\left(\frac{2}{width}\right)^{1.6}.\frac{\left(\frac{width}{2}\right)^{2.6}}{2.6}\right)\right] \tag{53}$$

The pressure profile area of the horizontal plane was used as shown by equation (53). The pressure-displacement curve, as presented by equation (45), was introduced for P (centre), thus relating the area of the pressure profile to a certain displacement, x, as labeled in Figure 46.

$$Area(x) = ae^{bx}.2.\left[\left(\frac{width}{2}\right) - \left(\left(\frac{2}{width}\right)^{1.6}.\frac{\left(\frac{width}{2}\right)^{2.6}}{2.6}\right)\right] \tag{54}$$

where a and b are determined from the pressure-displacement curve of a piston press test.

The volume of the pressure profile, represents pressing force, which can related to displacement, x, by carrying out the following integration:

$$F(Newtons) = Volume(x) = 2a.\left[\left(\frac{width}{2}\right) - \left(\left(\frac{2}{width}\right)^{1.6}.\frac{\left(\frac{width}{2}\right)^{2.6}}{2.6}\right)\right].\int e^{bx}dx \qquad (55)$$

The integration was carried out through expressing the limits of the integration in terms of compression angle. This was done with the use of equation (47), which relates displacement, x, to compression angle, α. Since there are two rollers, the total change in horizontal displacement was equal to x multiplied by 2.

$$F(Newtons) = Volume(x) = 2a.\left[\left(\frac{width}{2}\right) - \left(\left(\frac{2}{width}\right)^{1.6}.\frac{\left(\frac{width}{2}\right)^{2.6}}{2.6}\right)\right].\int_0^{2r(1-cos\alpha)} e^{bx}dx \qquad (56)$$

$$F(Newtons) = 2a.\left[\left(\frac{width}{2}\right) - \left(\left(\frac{2}{width}\right)^{1.6}.\frac{\left(\frac{width}{2}\right)^{2.6}}{2.6}\right)\right].(e^{2br(1-cos\alpha)} - 1) \qquad (57)$$

Therefore, the total pressing force in Newtons, as applied by the hydraulic system, is expressed as a function of compression angle. Alternatively, the compression angle could be determined from the pressing force:

$$\alpha = a.cos.\left\{1 - \frac{1}{2br}ln\left[\frac{F}{2a.\left(\frac{width}{2} - \left(\frac{2}{width}\right)^{1.6}.\frac{\left(\frac{width}{2}\right)^{2.6}}{2.6}\right)} + 1\right]\right\} \qquad (58)$$

Using equation (58), the compression angle, α, could be determined through knowledge of

- Pressing force setpoint in Newtons, F
- The radius of the HPGR roll, r (mm)
- Width of the HPGR roll, width (mm)
- The pressure-displacement curve from a piston press test, from which a, and b, could be determined

A surface plot of a calculated HPGR roll pressure profile was generated in Matlab using the form of equation (50) and is shown for a copper porphyry ore in Figure 48.

Table 18 – Pressure profile parameters

Description	Units	Value
Pilot HPGR Roll Radius	mm	375
HPGR Roll Width	mm	220
Pressing Force	kN	660 kN
Specific Pressing Force	N/mm^2	4
Piston press, parameter a	-	0.0063
Piston press, exponent b	-	0.778

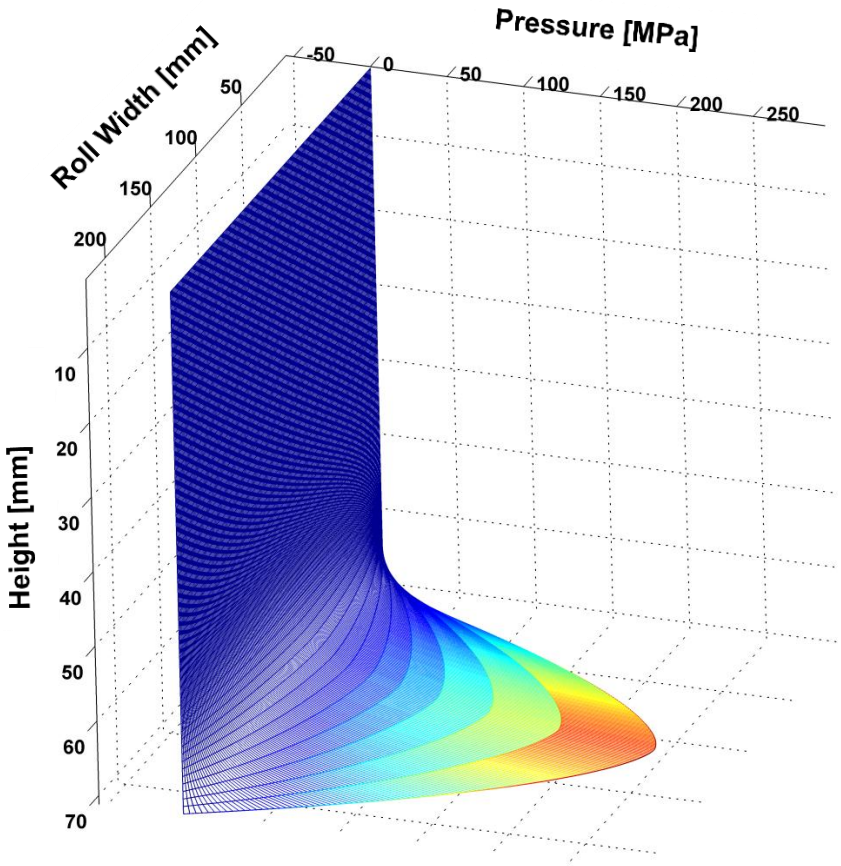

Figure 48 - Modelled stress field for a copper porphyry sample

The above figure also shows that the highest pressure, also referred to as Pmax, was determined to be approximately 240 MPa at the zero angle. A compression angle of approximately 11 degrees was used to generate the profile, whereas the derived compression angle, using equation (58), was 12.4 degrees. Use of the derived angle resulted in Pmax values of close to 4500 MPa, a value which is

much higher than the expected range of 200 – 300 MPa referenced in literature, and most likely an impossibility.

The piston press methodology was used to predict compression angles for 10 test conditions. These results were then compared to compression angles from pilot HPGR testing, which were calculated using the following equation:

$$x_c = 0.5\left\{\left(D + x_g\right) - \left[\left(D + x_g\right)^2 - \frac{4\rho_g x_g}{D\rho_c}\right]^{0.5}\right\} \quad \textit{(Morrell et al, 1997) (59)}$$

where D is the roll diameter, x_g is the operating gap, ρ_c and ρ_g are material densities at the beginning of the compression zone and at the zero angle respectively. x_c is called the critical gap and is the distance between the roller surfaces at the compression angle. Therefore it could be related to the previously referred to displacement, x, the horizontal displacement between the roller surface from the compression angle to the zero angle, shown earlier in Figure 46.

$$x_c = x_g + 2x \quad \textit{(60)}$$

Through use of the relation between compression angle and displacement, x, shown earlier in equation (47), the compression angle, α, could be found from the following:

$$\alpha = acos\left(1 - \frac{x_c - x_g}{2r}\right) \quad \textit{(61)}$$

For equation (59), the material bulk density was used for ρ_c, and the measured flake density was input for ρ_g. Compression angles which were predicted using the piston press methodology were compared to the compression angles that were calculated using equations, (59) and (61), as shown in Table 19. Direct correlation between the two datasets was fair, represented by an R^2 value of approximately 0.53. It needs to be noted that the use of equations (59) and (61) assumes that slipless transport occurs throughout the compression angle. Whereas the piston press methodology does not.

Table 19 – Comparison of compression angles

Test No.	Pilot HPGR Test Observed	Piston Press Methodology (Predicted)
	Compression angle, α	**Compression angle, α**
Test #1	6.2	12.4
Test #2	6.1	11.7
Test #3	5.2	12.5
Test #4	7.8	13.1
Test #5	8.4	13.4
Test #6	5.3	12.3
Test #7	4.5	12.5
Test #8	8.3	13.6
Test #9	6.6	12.3

Compression angles are generally referred to as being in the range of 7 to 9 degrees. As seen from Table 19, compression angles predicted by the piston press methodology were approximately double those calculated from pilot HPGR test results. For this reason it was not further applied to calculation of the roll gap. The following are possible reasons for the discrepancy between observed and predicted compression angles:

- Force dissipation in the extrusion zone is not taken into account with the piston press methodology. Lower compression angles would be calculated if this were accounted for
- Application of the pressure-displacement curve from piston press tests effectively assumed that the volume of the piston die was the same as the volume of material between the HPGR rolls
- The axial force, applied by the material bed onto cheek plates, was not taken into account
- The piston press test characterized the pressure-displacement curve of a static sample, whereas material between the HPGR rollers undergoes compressed and shear simultaneously.
- The observed compression angle is based on the flake density being equivalent to the density at the zero angle. However, flake material is most definitely less dense than material at the roll nip, as it undergoes extrusion prior to exiting the roll mill, meaning the observed compression angle is most likely larger than presented

Accurate prediction of the compression angle would provide a means to predict operating gap and throughput using the continuity formula, equation (8), which was introduced earlier.

Direct comparison of HPGR compression angles derived from pressing force and pressure-displacement curves showed a small degree of correlation. Further work is required to improve the accuracy of the methodology for eventual use in an HPGR throughput model.

7.4 Summary of modelling

Linear regression modelling showed that the investigated laboratory tests provided new variables which are statistically significant in terms of improving the accuracy of predictive gap models. The shear deformation modulus was found to be the most statistically significant of the laboratory test sourced variables, followed by variables derived from piston press testing.

The moisture of feed material and bulk density were found to be statistically significant input variables for the majority of analyzed datasets. This suggested that more work needs to be done on understanding the effects of moisture on ore. Also, a more accurate method for determining bulk density, such as the Proctor density method, would improve the statistical significance of this parameter.

Improvements in non-linear modelling should be achieved once more information, in the form of machine and material variables, is made available for input into proposed mechanistic models. The previously discussed HPGR holistic model is an example of a potential basis for a mechanistic model.

Force based modelling showed that the HPGR compression angle, a parameter used in throughput equations, could be derived from application of piston press testing. Although prediction of comminution effects is not a focus of this thesis, it can be seen that a derived roll pressure profile is a potentially valuable input for an HPGR comminution model.

In retrospect, the linear stepwise regression stage of the study supported the applicability of laboratory scale shear and compression testing to the prediction of HPGR throughput performance.

8 DISCUSSION AND CONCLUSIONS

A principal outcome of the study was the statistical justification of proposed laboratory testing methods to the prediction of HPGR throughput performance. The shear properties of a feed sample, assessed using terramechanics based methodologies, were determined to be the most valuable predictors of HPGR roll gap size. To a lesser extent, piston press results were also found to improve the accuracy of roll gap predictions when used in linear predictive equations. The results prompt further investigation into the scalability of laboratory scale shear and compression based tests to HPGR performance.

Linear regression showed that the results of laboratory tests could be used to predict HPGR throughput performance to a considerably high level of accuracy. As an intermediate step towards removing the need for pilot HPGR testing, the proposed laboratory scale tests could be used for the assessment of how ore variability impacts HPGR throughput and gap. The approach shown in Figure 49 has been proposed.

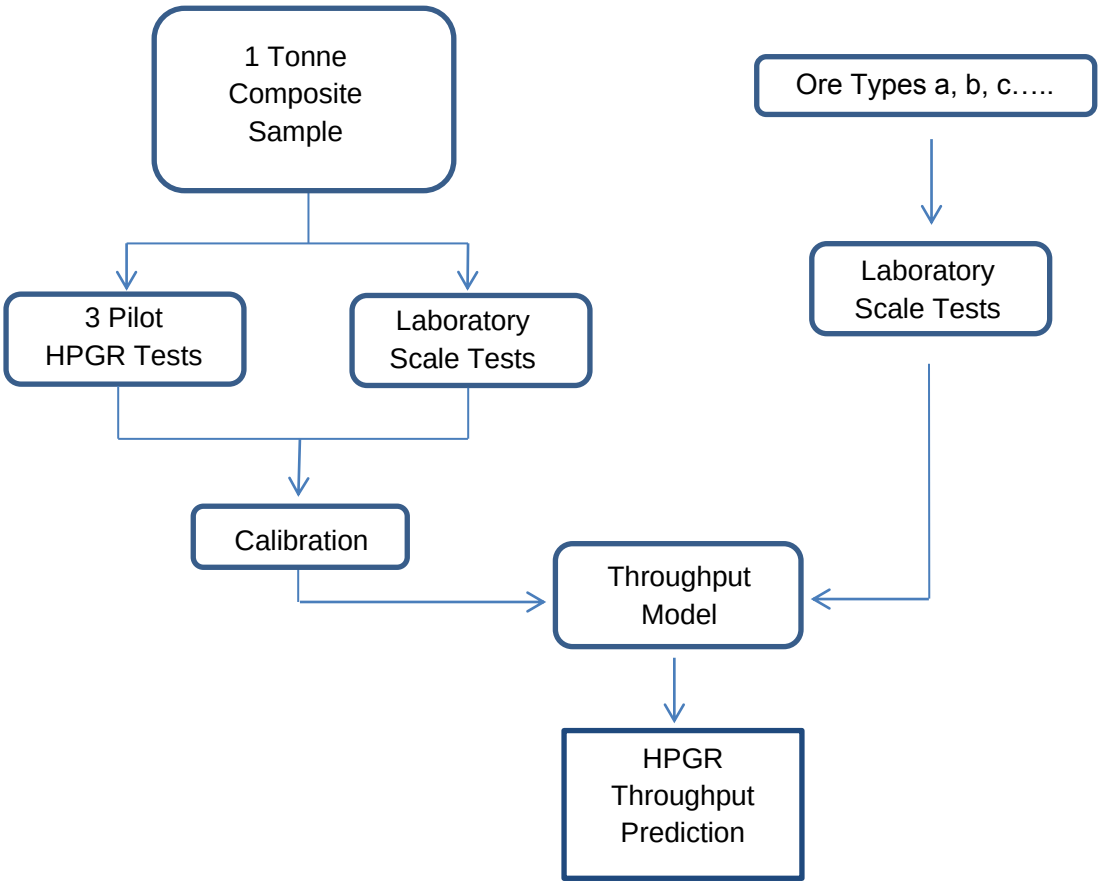

Figure 49 - Application of laboratory scale tests

As shown in Figure 49, pilot HPGR and laboratory scale testing would be carried out in parallel so that calibration of the model to a reference ore type could be conducted. Approximately three HPGR tests, each varying in pressure set-point, would be required for the calibration stage. Following calibration, variations of the reference ore type would be tested using the laboratory suite of tests and their associated HPGR throughput performance would be predicted. Ultimately HPGR parameters such as comminution and energy would also be outcomes of laboratory scale tests, providing a complete HPGR based characterization of the various sample types. The described approach provides a means to not only assess HPGR applicability using a smaller amount of composite sample, but also to evaluate ores taken from different areas of a deposit based on their predicted HPGR process performance. Further test development would allow for the complete assessment of HPGR solely through laboratory scale testing.

Material properties which are typically observed by mineral processors such as moisture content and bulk density were confirmed to be important in terms of predicting throughput. Due to lack of data at the time of writing, the applicability of Proctor density as an alternative to bulk density could not be assessed. One HPGR input parameter, specific pressing force, was consistently included in determined linear models.

A mechanistic approach to deriving the roll compression angle, a parameter used in throughput equations, was investigated. This methodology also brought to light the ability to model the roll pressure profile, which has great potential for the prediction of HPGR comminution. Thus, this mechanistic approach provides a means for establishing a holistic HPGR model and necessitates further work.

Throughout the study the primary limitations of considered laboratory equipment was the relation between the top size of tested particles and the boundary walls of the test equipment. The considerable difference in top size between pilot HPGR and laboratory test feed materials may be a limiting factor in the application of these tests. An understanding of frictional properties and compressive strength of individual particles may complement the results of the multi-particle analyses presented in this study.

The interaction of rollers with a bed of granular material is indeed a complex problem which has been studied to a large extent in fields outside of mineral comminution. As evidenced by the patent for high pressure comminution, the application of rollers conveying high normal loads to particle beds is relatively new to the field of mineral processing. The application of terramechanics based methodologies provided an inroad into further development of laboratory tests for the prediction of HPGR performance.

9 RECOMMENDATIONS

Further areas of research which are potentially relevant to the development of laboratory scale HPGR tests have become apparent through work completed in this study. Primarily, additional methods for characterization of samples as well as computer based methods for roll and particulate interaction have been suggested.

The additional measurement of material parameters through simple laboratory based methods is suggested to increase the number of available input variables for HPGR modelling. An example of such a parameter is the modified Proctor density test, the results of which were not used for modelling in this study due to the lack of available data. The Proctor density test is carried out with wet sample, thereby also capturing the effect of moisture on sample compactibility. Specific gravity measurements using pulverized samples are also suggested to account for the presence of impermeable voids in individual particles. The combination of Proctor density with an accurate measure of specific gravity would potentially allow for the determination of an improved, in terms of applicability to HPGR, calculated value of material porosity.

In order to improve the force based modelling methodology, controlled compaction of samples prior to piston press testing is recommended. This would allow for the initial sample height and degree of packing to be consistent at the beginning of each test. Furthermore, the piston press test could be modified to capture the effect of pressure in the extrusion zone. This would require controlled removal of the piston from the die after pressure application has been completed.

Information reflecting the strength of tested samples, as defined by existing testing methodologies within mineral processing, was not applied for modelling of roll gap and throughput. The strength of particles as characterized by drop weight or compressive strength tests could provide additional input variables of statistical significance.

The work carried out in this study has shown that the internal frictional properties of samples and compressibility are statistically significant when used for the prediction of HPGR throughput and roll gap. In contrast to the individual shear and compression tests presented in this work, shear and compression are simultaneously applied to feed materials during high pressure roll grinding. Testing methodologies where shear and compression are applied and measured simultaneously to samples are more representative of the process occurring in HPGR material beds. The results of such a test would potentially provide an improved prediction of throughput and relative gap.

Discrete element modelling (DEM) using software which allows the roll and material interaction to be simulated in three dimensions is strongly recommended. HPGR analyses are already being supplemented with piston press results, such as the work of Herbst et al (2011). Similarly, DEM

analyses could be coupled with ring-shear test results to provide a better understanding of the behavior of materials between HPGR rollers as well as potentially improve modelling capabilities.

The final recommendation resulting from the presented study relates to the general approach to developing laboratory scale tests and methodologies for the prediction of HPGR performance. Previously published work and also the results of testing shown in this document indicate that material transportability and energy-size reduction are interrelated outcomes of HPGR processing. Hence, a holistic approach which accounts for the inter-relationships between roll gap, compression angle, material strength and resulting particle breaking pressures within the compression bed is strongly recommended.

REFERENCES

Abouzeid, A. M., Fuerstenau, D. W., 2009. Grinding of mineral mixtures in high pressure grinding rolls. International Journal of Mineral Processing 93, pp. 59-65.

ASTM Standard D698. 2007. ASTM D698 - 07e1 Standard test methods for laboratory compaction characteristics of soil using standard effort (12 400 ft-lbf/ft^3 (600 kN-m/m^3)).

Austin, L. G., Weller, K. R., Lim, W. I. L., 1993. Phenomenological modelling of the high pressure grinding rolls. XVIII International Mineral Processing Congress, Sydney, Australia, pp. 87-95.

Bamber, A., Klein, B., Nadolski, S., Drozdiak, J., 2009. HPGR NSERC Proposal Location: Vancouver, BC, Canada.

Banini, G., Villanueva, A., Hollow, J., Mosher, J., 2011. Evaluation of scale up effect on high pressure grinding roll (HPGR) implementation at PT Freeport Indonesia. SAG Conference 2011, Vancouver, B.C., Canada.

Bekker, M. G., 1956. Theory of land locomotion. USA: The University of Michigan Press.

Bekker, M. G., 1957. Latest developments in off-the-road locomotion. Journal of the Franklin Institute (May, 1957), pp. 411 - 423.

Bekker, M. G., 1969. Introduction to terrain-vehicle systems. USA: The University of Michigan Press.

Ben-nun, O., Einav, I., 2010. The role of self-organization during confined comminuton of granular materials. Philosophical Transactions of the Royal Society A-Mathematical Physical and Engineering Sciences 368, pp. 231-47.

Benzer, H., Aydogan, N. A., Dündar, H., 2011. Investigation of the breakage of hard and soft components under high compression: HPGR application. Minerals Engineering 24 , pp. 303-307.

Box, G. E. P., Draper, N. R., 1987. Empirical model-building and response surfaces. USA: John Wiley & Sons, Inc.

Budhu, M., 2006. Soil mechanics and foundations. 2nd ed. Hoboken, N.J.: John Wiley & Sons Canada.

Bulled, D., Husain, K., Lozano, C., 2009. A small scale test to determine a work index for high pressure grinding rolls. Proceedings of the 41st Annual Canadian Mineral Processors Conference, Ottawa, Canada.

Burchardt, E., Patzelt, N., Knecht, J., Klymowsky, R., 2011. HPGR's in minerals: What do existing operations tell us for the future? Paper presented at SAG Conference 2011, Vancouver, BC. Canada.

Casteel, Kyran. 2005. High-pressure grinding -- playing a wider role. Mining & Quarry World 2 (3) (09): 12-7.

CEMEX Deutschland AG. Unsere Zementwerke - CEMEX Deutschland. 2005 [cited 03/08 2011]. Available from http://www.cemex.de/zementwerke.htm.

Cerato, A. B., Lutenegger, A. J., 2006. Specimen size and scale effects of direct shear box tests of sands. Geotechnical Testing Journal 29 (6).

CITIC Homepage. Accessed March, 2012 http://www.citic-hic.com.

Craig, R. F., 2004. Craig's soil mechanics. Seventh ed. London, UK: Spon Press.

Cunningham, J. C. 2005. Experimental studies and modelling of the roller comapaction of pharmaceutical powders. Phd., Drexel University.

Daniel, M. J., 2002. HPGR verification and scale-up. Master of Engineering Science (research). University of Queensland.

Daniel, M. J., Morrell, S., 2004. HPGR model verification and scale-up. Minerals Engineering 17 (11-12) (12), pp. 1149-61.

Daniel, M. J., 2007. Energy efficient liberation using HPGR technology. PHD., University of Queensland.

Daniel, M. J., Bailey, C., 2009. Uses and benefits of laboratory scale HPGR tests. Proceedings of the VI International Mineral Processing Seminar, pp. 147-156.

Dundar, H., Benzer, H., Mainza, A. N., Dzomeku, C., 2011. Effects of the rolls' speed and pressure on the HPGR performance during gold ore grinding. Paper presented at SAG Conference 2011, Vancouver, BC. Canada.

Dunne, R., Maxton, D., Morrell, S., Lane, G., 2004. HPGR - the Australian experience. Paper presented at Plant Operators' Forum 2004.

Fuerstenau, D. W., Kapur, P. C., 1995. Newer energy-efficient approach to particle production by comminution. Powder Technology 82, pp. 51-57.

Fuerstenau, D. W., Gutsche, O., Kapur, P. C., 1996. Confined particle bed comminution under compressive loads. International Journal of Mineral Processing 44-45, pp. 521-537.

Fuerstenau, D. W., Abouzeid, A. M., 2007. Role of feed moisture in high-pressure roll mill comminution. International Journal of Mineral Processing 82, pp. 203-210.

Gaudin, A. M., Meloy, T. P., 1962. Model and a comminution distribution equation for single fracture. Society of Mining Engineers of AIME 223 (March 1962): 40.

Günter, H., Müller, M., Sonntag, P., 1996. The application of roller presses for high pressure comminution.

Gupta, A., Yan, D. S., 2006 Mineral Processing Design and Operation: An Introduction. Elsevier Science.

Gutsche, O., Fuerstenau, D. W., 1999. Fracture kinetics of particle bed comminution — ramifications for fines production and mill optimization. Powder Technology 105, pp. 113-118.

Hart, S., Parker, B., Rees, T., Manesh, A., Mcgaffin I., 2011. Commissioning and ramp up of the HPGR circuit at Newmont Boddington Gold. Paper presented at SAG Conference 2011, Vancouver, B.C., Canada.

Hawkins, R. 2007. A piston and die test to predict laboratory-scale HPGR performance. Master of Philosophy (Engineering and Related Technology). Julius Kruttschnitt Mineral Research Centre, Dept. of Mining, Minerals and Materials Engineering, University of Queensland.

Herbst, J. A., Mular, M. A., Pate, W. T., Qiu, X., 2011. Detailed modelling of an HPGR/HRC for prediction of plant scale unit performance. Paper presented at SAG Conference 2011, Vancouver, B.C., Canada.

Hinde, A. L., Kalala, J. T., 2009. The application of a simplified approach to modelling tumbling mills, stirred media mills and HPGR's. Minerals Engineering 22 (7-8), pp. 633-641.

Janosi, Z., Hanamoto, B., 1961. An analysis of the drawbar pull vs slip relationship for track laying vehicles. Detroit, Michigan, USA: Land Locomotion Laboratory Research Division.

Johanson, J. R., 1965. A rolling theory for granular solids. Journal of Applied Mechanics Series E 32 (4): 842.

Kalala, J. T., Dong, H., Hinde, A. L., 2011. Using piston-die press to predict the breakage behavior of HPGR. Paper presented at SAG Conference 2011, Vancouver, BC, Canada.

KHD Humboldt Wedag. 2007. High pressure grinding roller presses. Brochure.

Kleeberg, J., 2007. Untersuchungen zur Oberflächenbelastung der Walzen von Guttbett-walzenmühlen. PhD., Technischen Universität Bergakademie Freiberg.

Klymowsky, R., Patzelt, N., Knecht, J., Burchardt, E., 2002. Selection and sizing of high pressure grinding rolls. Mineral Processing Plant Design, Practice, and Control Proceedings, pp. 636-668.

Lane, G., Daniel, M., Dunne, R., Morrell, S., Maxton, D., 2009. HPGR application in Australia: Status and future directions. Procemin 2009, Proceedings of the VI International Mineral Processing Seminar, Ed Amelunxen, Kracht and Kuyvenhoven, Santiago, Chile, November 2009, pp. 179.

Lim, W. I. L., Voigt, W., Weller, K. R., 1996. Product size distribution and energy expenditure in grinding minerals and ores in high pressure rolls. International Journal of Mineral Processing 44-45 (3), pp. 539-59.

Lim, W. I. L., Weller, K. R., 1997. Modelling of throughput in the high pressure grinding rolls. Proceedings of the XX International Mineral Processing Congress, Aachen, Germany, pp. 173-184.

Lim, W. I. L., Campbell, J. J., Tondo, L. A., 1997. The effect of rolls speed and rolls surface pattern on high pressure grinding rolls performance. Minerals Engineering 10 (4), pp. 401-419.

Lim, W. I. L., 1999. Some benefits of using studded surfaces in high pressure grinding rolls. Minerals Engineering 12 (2), pp. 187-203.

Liu, J., Schönert, K., 1996. Modelling of interparticle breakage. International Journal of Mineral Processing 44, pp. 101-115.

Lubjuhn, U. 1992. Materialtransport und Druckverteilung im Spalt der Gutbettwalzenmühle. Fortschrittberichte. Vol. 3 Verfahrenstechnik. Düsseldorf, Germany.

Lubjuhn, U., Schönert, K., 1993. Material flow in the acceleration zone and throughput of high pressure roller mills. XVIII International Mineral Processing Congress, pp. 161-168.

Lyasko, M., 2009. Slip sinkage effect in soil-vehicle mechanics. Journal of Terramechanics 47, pp. 21-31.

Lynch, A. J., Rowland, C. A., 2005. The history of grinding. Society for Mining, Metallurgy, and Exploration. Colorado, USA.

Maschinenfabrik Köppern. 2010. High-pressure grinding. Brochure.

Meirion-Griffith, G., Spenko, M., 2010. An empirical study of the terramechanics of small unmanned ground vehicles. Big Sky, MT, USA.

Morley, C., 2003. HPGR in hard rock applications. Mining Magazine, September, 2003.

Morley, C., Daniel, M. J., 2009. HPGR flowsheets - the next generation. Proceedings of the VI International Mineral Processing Seminar, Ed Amelunxen, Kracht and Kuyvenhoven, Santiago, Chile, November 2009, pp. 157-168.

Morley, C., 2010. HPGR -FAQ. The Journal of the Southern African Institute of Mining and Metallurgy 110, pp. 107-115.

Morrell, S., Shi, F., Tondo, L., 1997. Modelling and scale-up of high pressure grinding rolls. Paper presented at XX International Mineral Processing Congress - Aachen, Germany.

Morrell, S., 2004. Predicting the specific energy of autogenous and semi-autogenous mills from small diameter drill core samples. Minerals Engineering 17 (3), pp. 447-451.

Morrell, S., 2009. Using the SMC test® to predict comminution circuit performance. [cited 6th May, 2011]. Available from: http://www.smctesting.com/documents/Using_the_SMC_Test.pdf.

Morrell, S., 2010. Predicting the specific energy required for size reduction of relatively coarse feeds. Minerals Engineering 23 (2), pp. 151-153.

Morrell, S., 2011. About the SMC test®. [cited 6th May, 2011]. Available from: http://www.smctesting.com/about.

Mukherjee, A. N., 1940. Briquetting of coal. VI - No.3.

Muro, T., O'Brien, J., 2004. Terramechanics - land locomotion mechanics. Netherlands: A. A. Balkema Publishers.

Mütze, T., Klaus, H., 2008. Compressive stress: Effect of stress velocity on confined particle bed comminution. Chemical Engineering Research and Design 86, pp. 379-383.

Nakao, T., Fityus, S., Tamate, S., 2008. Direct shear testing of a marginal material using a large shear box. Geotechnical Testing Journal Vol. 31 No. 5.

Ntsele, C., Sauermann, G., 2007. The HPGR technology - the heart and future of the diamond liberation process. The Journal of the Southern African Institute of Mining and Metallurgy.

Oettel, W., Nguyen, A., Husemann, K., Bernhardt, C., 2001. Comminution in confined particle beds by single compressive load. International Journal of Mineral Processing 63, pp. 1-16.

Oettel, W., Husemann, K., 2004. The effect of a grinding aid on comminution of fine limestone particle beds with single compressive load. International Journal of Mineral Processing 74, pp. 239-248.

Onafeko, O., Reece, A. R., 1967 Soil stresses and deformations beneath rigid wheels. Journal of Terramechanics Vol. 4, No. l, pp. 59-80.

Onafeko, O., 1969. Analysis of the rolling resistance losses of wheels operating on deformable terrain. Journal of Agricultural Engineering Research 14 (2), pp. 176-182.

Reid, K. J., 1965. A solution to the batch grinding equation. Chemical Engineering Science 20, pp. 953-963.

Rule, C. M., Smit, I., Cope, A. J., Humphries, G. A., 2008. Commissioning of the Polycom 2.2/1.6 5.6 MW HPGR at Anglo Platinum's new Mogalakwena North Concentrator. Comminution 2008, Falmouth, Cornwall, UK.

Schneider, C. L., Marques, M., Alves, V. K., 2008. A scale up model for HPGR hard rock grinding. 2nd International Symposium on Iron Ore, São Luís City, Maranhão State, Brazil.

Schneider, C. L., Alves, V. K., Austin, L. G., 2009. Modelling the contribution of specific grinding pressure for the calculation of HPGR product size distribution. Minerals Engineering 22 (7-8), pp. 642-649.

Schönert, K., 1979. Aspects of the physics of breakage relevant to comminution. Fourth Tewksburg Symposium, Melbourne, Australia.

Schönert, K. 1979. Verfahren zur fein- und feinstzerkleinerung von Materialien Spröden Stoffverhaltens. Patent DE 27 08 053 C3, filed 1979, and issued 19th July, 1979.

Schönert, K., 1985. Sizing of high pressure roller mills. Zement Kalk Gips International.

Schönert, K., 1988. A first survey of grinding with high-compression roller mills. International Journal of Mineral Processing 22, pp. 401-412.

Schönert, K., 1991. The characteristics of comminution with high pressure roller mills. KONA Powder and Particle Journal 9, pp. 149.

Schönert, K., Lubjuhn, U., 1992. Kompressionswinkel und Durchsatz der Gutbett-walzenmühle. Zement-Kalk- Gips.

Schönert, K., 1996. The influence of particle bed configurations and confinements on particle breakage. International Journal of Mineral Processing 44-45 (3), pp. 1-16.

Schönert, K., Sander, U., 2002. Shear stresses and material slip in high pressure roller mills. Powder Technology 136, pp. 136-144.

Seebach, M. von, Knobloch, O. R., 1987. High pressure grinding rolls in industrial application. Society of Mining Engineers, Denver, Colorado.

Shi, F., Kojovic, T., Larbi-Bram, S., Manlapig E., 2009 Development of a rapid particle breakage characterisation device – The JKRBT. Minerals Engineering 22, pp. 602-612.

Shibuya, S., Mitachi, T., Tamate, S., 1997. Interpretation of direct shear box testing of sands as quasi-simple shear. Géotechnique Vol. 47 No. 4, pp. 769 – 790.

Simoni, A., Houlsby, G. T., 2006. The direct shear strength and dilatancy of sand-gravel mixtures. Geotechnical and Geological Engineering Vol. 24, No. l, pp. 523-549.

Thyssenkrupp, 2007. POLYCOM® high-pressure grinding roll for the minerals industry. Brochure.

Torres, M., Casali, A., 2009. A novel approach for the modelling of high-pressure grinding rolls. Minerals Engineering 22 (13) (10), pp. 1137-1146.

Unland, G., Wang, U., 1998. Model of high pressure roller mills - a phenomenological-mathematical approach (part 1). Zement Kalk Gips International 7.

Unland, G., Wang, U., 1998. Model of high pressure roller mills - a phenomenological-mathematical approach (part 2). Zement Kalk Gips International 11, pp. 600

Wong, J. Y. 1993. Theory of ground vehicles. Second ed. USA: John Wiley & Sons, Inc.

Appendix A: HPGR Testing Error

HPGR testing error

Quantification of the error associated with the HPGR testing procedure are outlined in this section.

Splitting of feed sub-samples

As discussed previously, feed sub-samples were taken from bulk lots of material to determine the size distribution, bulk density as well as provide sample for laboratory scale test development. A rotary splitter used for this purpose, separated a 200 litre volume of material into eight separate compartments. The content of one compartment was halved through the use of a riffle splitter and used for material analysis. The error in the splitting procedure was measured through carrying out size distributions for material contained in each compartment. The repeatability of size distributions is inescapably incorporated into the determined error value.

From the coefficient of variation found for the size distributions, shown in Figure A50, it can be seen that the greatest error was found at the coarsest sieve size of 32 mm.

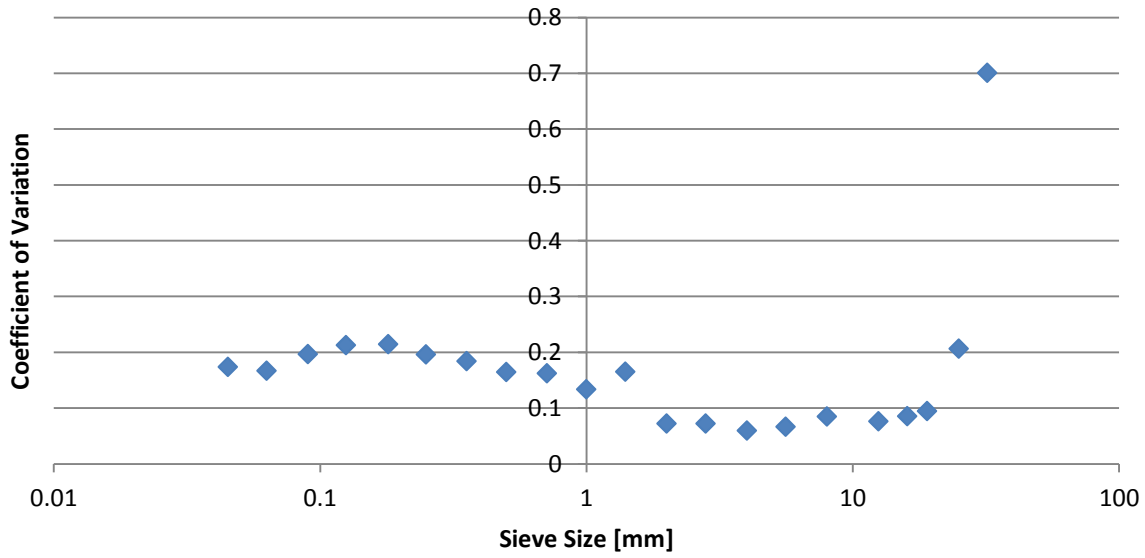

Figure A50 - Coefficient of variation per sieve size

Taking into account the small amount of +32 mm particles contained in the sample, the associated error is magnified by the scarcity and angularity of the coarse particles. A result which could be likened to the nugget effect encountered when sampling coarse gold bearing samples. Comparison of the coefficient of variation to the weight retained on each sieve showed that the lowest variation was recorded for sieve sizes containing a large proportion of the overall sample.

The coefficient of variation for the percentage of weight retained is shown in Figure A51.

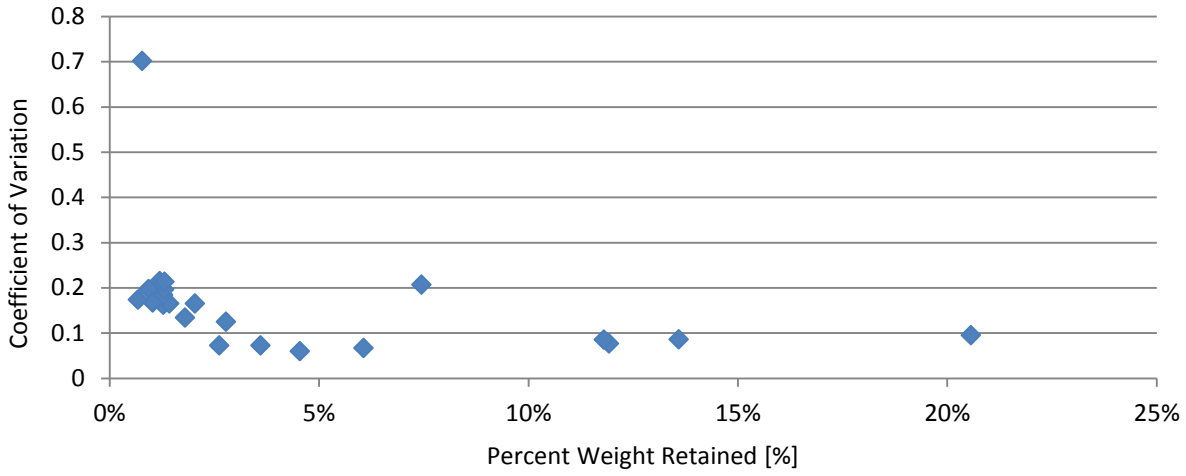

Figure A51 - Coefficient of variation versus percent weight retained

In order to explore the influence of sample particle sizes on HPGR parameters, size distributions were represented by single parameters which included the 80th and 50th percentage particle sizes and the Gaudin-Schuhmann slope parameter, m, for a top size of 32 mm. The Gaudin-Schuhmann equation was found to provide a better fit to HPGR feed size distribution data than other equations, such as the Rosin-Rammler equation. The size modulus of the Gaudin-Schuhmann equation was not varied as all samples had an equivalent top size. Variations in these parameters due to splitting error are shown in Table A20. It was found that the standard relative errors recorded for F80 and F50 percentage particle sizes and the Gaudin-Schuhmann m parameter were less than 3.5%. A significantly greater error was calculated for the finer F20 percentage particle size.

Table A20 - Variation due to sample splitting

Description	F80	F50	F20	Slope m
Units	[mm]	[mm]	[mm]	[-]
Mean	21.57	13.82	3.04	0.68
Standard Error	0.19	0.32	0.34	0.02
Standard Relative Error	0.9%	2.3%	11.2%	3.5%
Standard Deviation	0.55	0.91	0.96	0.07
Range	1.54	2.56	2.63	0.19
Number of Datapoints	8	8	8	8
Confidence Level (95 %)	0.46	0.76	0.80	0.06

Typical pilot HPGR feed was used for establishment of the error incorporated with splitting and sieving sample. The resulting quantification of error provides a valuable indication of the variation associated with the feed parameters.

Deviation from machine setpoint parameters

The deviation of machine parameters from PLC setpoints is measurable through analysis of instrumented data.

Specific pressing force

Fluctuations in hydraulic pressure during testing are inevitable due to the direct influence of gap oscillations on the displacement of hydraulic fluid. Nitrogen accumulators and relief valves work in line with the hydraulic cylinders to ensure that the hydraulic pressure is close to the setpoint value. Keeping the deviation to a minimum was important as the specific pressing force value was an important test parameter which was used in some cases to group sets of data. Table A21 shows the deviation of specific pressing force for tests used in this study.

Table A21 - Pilot HPGR pressing force deviation from setpoint

Description	**Units**	**Values**				
Setpoint FSP	[N/mm^2]	**2**	**2.5**	**3**	**4**	**5**
Datapoints (No. of Tests)	[No.]	5	11	8	28	12
Mean Test FSP	[N/mm^2]	1.98	2.47	2.93	3.94	4.96
Standard Deviation	[N/mm^2]	0.07	0.04	0.05	0.04	0.03
Minimum FSP	[N/mm^2]	1.92	2.42	2.85	3.78	4.91
Maximum FSP	[N/mm^2]	2.08	2.54	3.02	3.99	5.00
Coefficient of Variation	[-]	0.04	0.02	0.02	0.01	0.01
Relative Standard Error	[%]	1.61%	0.49%	0.64%	0.20%	0.19%

Roll speed

The roll speed of the pilot HPGR was controlled by a variable frequency drive (VFD) via the PLC interface. A sensor located on the drive-train served to measure the roll speed and allowed for a deviation to be quantified. A majority of the tests included in the test database were carried out at a peripheral roll speed of 0.75 ms^{-1}. At this speed setpoint, a relative standard error of less than 0.18% was observed for a total of 62 tests. For this reason, deviations in roll speed were not seen as a significant source of error.

HPGR test repeatability

An attempt at quantifying the error accounted to testing with the pilot HPGR was made through running four individual tests using equivalent feed and setpoint parameters. The variation in logged parameters is displayed in Table A22. Also included is the variation in parameters which are calculated from a combination of logged machine data and material feed weight. The highest relative standard error of 1.93%, was recorded for specific throughput constant $\dot{m}$. When considering this error it must be taken into account that the $\dot{m}$ value is calculated from recorded roll speed, feed weight and test time. Therefore it is dependent on the greatest amount of parameters which in turn have an associated error.

Table A22 - Variation in HPGR testing results

HPGR Repeatability Tests	Logged Parameters				Calculated Parameters		
	Gap	FSP	Power	Speed	kWh/t	tph	$\dot{m}$
Units	[mm]	[N/mm^2]	[kW]	[ms^{-1}]	[kWh/t]	[tph]	[ts/hm^3]
Mean	22.09	3.95	66.97	0.75	1.54	38.03	306.94
Standard Error	0.067	0.004	0.498	0.007	0.009	0.456	5.926
Standard Relative Error	0.30%	0.10%	0.74%	0.93%	0.58%	1.20%	1.93%
Standard Deviation	0.13	0.01	1.00	0.01	0.02	0.91	11.85
Range	0.32	0.02	2.03	0.03	0.04	1.91	24.18
Number of Datapoints	4	4	4	4	4	4	4
Confidence Level (95 %)	0.21	0.01	1.59	0.02	0.03	1.45	18.86
Dependence on no. of recorded parameters	-	-	-	-	2	2	3

The analysis of testing repeatability was also dependent on the accuracy of splitting equally representative sample into four individual feed drums. Any inaccuracy die to moisture or size segregation during sample splitting would have affected all of the seven HPGR parameters displayed in Table A22. Hence, the displayed errors unavoidably also include the effect of variation in feed preparation. Although the dataset used for variation analysis was comparatively small, the resulting variation in recorded and calculated results was deemed to confirm the suitability of the pilot testing procedure for the development of a reference database.

Appendix B: Direct Shear Box Test Error

Shear testing error

Three tests were repeated to gain an understanding of the repeatability of the test outcomes. The largest associated error was found to lie with cohesion and was deemed excessive for the purposes of this study. A type I characteristic curve was determined for all three test attempts, thus the curve type was identified as a potential qualitative outcome. The peak and critical state angles were deemed to be suitably accurate for the purposes of the study.

The fitted k parameter was found to vary with the magnitude of the normal load. For this reason the squared error for each of the five normal loads was weighted to diminish the bias of higher normal loads on the final fitted value of k.

Table A23 - Shear test repeatability

Item	Peak Angle	Critical State Angle	Cohesion	k Peak	k – Critical State
Units	[deg.]	[deg.]	[N/m^2]	[mm]	[mm]
Mean	36.5	34.0	1117	0.554	0.380
Standard Error	0.519	0.215	584.4	0.023	0.026
Standard Relative Error	1.42%	0.63%	52.32%	4.20%	6.80%
Standard Deviation	0.898	0.372	1012.2	0.040	0.045
Range	1.797	0.676	1974	0.081	0.088
Number of Datapoints	3	3	3	3	3

Appendix C: Shear Test Results

Test Summary	
Test Description:	Direct Shear Box Test
Approximate Shear Rate:	1 mm/min
Sample Description:	Copper - Nickel
Top Size (mm):	4
Moisture (%):	0
Determined k Value (mm):	0.94
Determined Peak Angle (degrees):	36.3
Determined Critical State Angle (degrees):	32.9
Determined Soil Type:	Type II

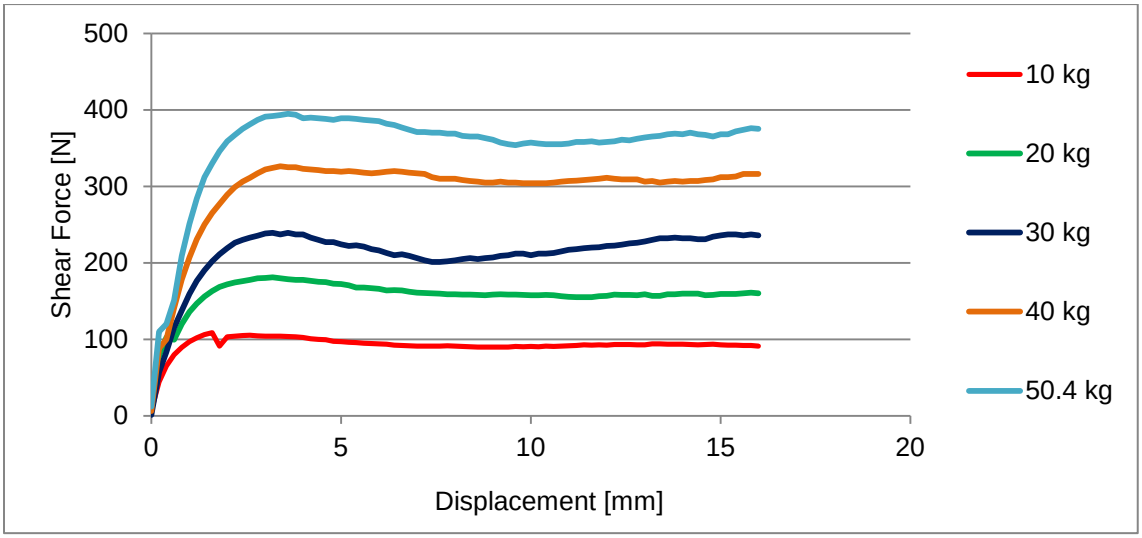

Figure A52 - Shear force and displacement

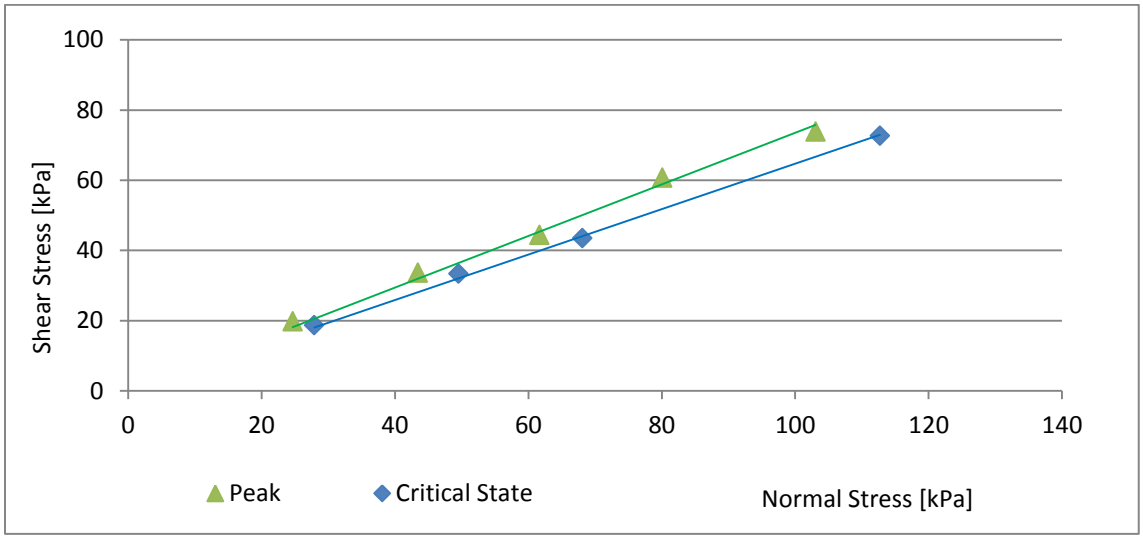

Figure A53 – Shear stress and normal stress

Test Summary	
Test Description:	Direct Shear Box Test
Approximate Shear Rate:	1 mm/min
Sample Description:	Copper - Nickel
Top Size (mm):	-4
Moisture (%):	2.5
Determined k Value (mm):	0.50
Determined Peak Angle (degrees):	NA
Determined Critical State Angle (degrees):	35.7
Determined Soil Type:	Type I

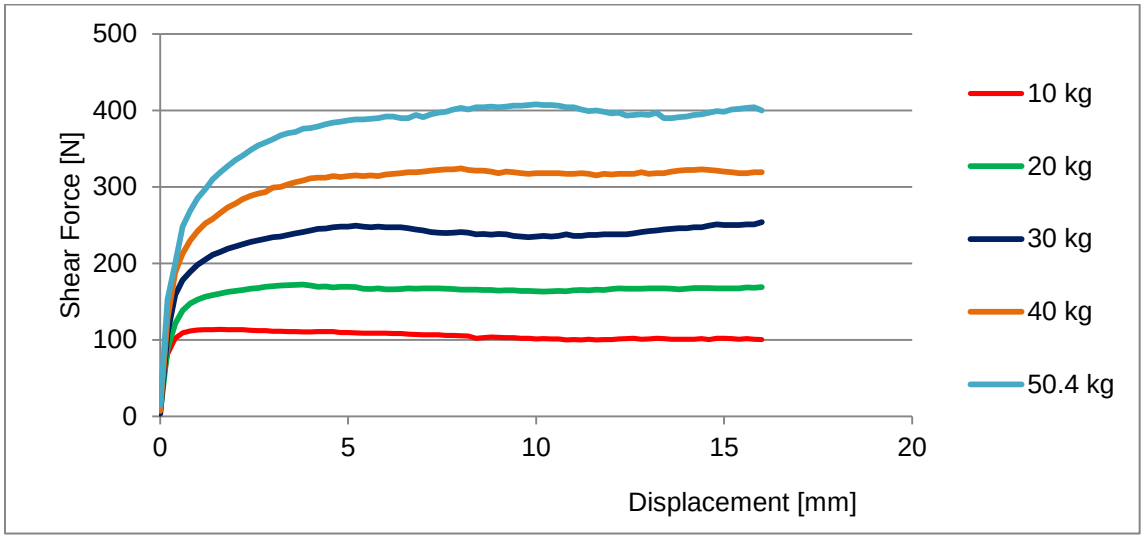

Figure A54 - Shear force and displacement

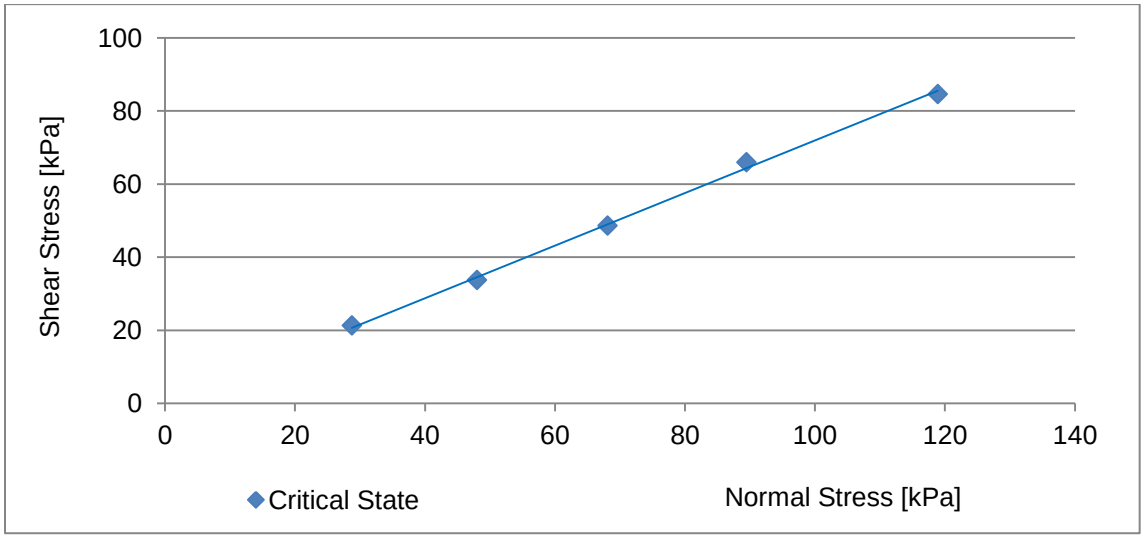

Figure A55 – Shear stress and normal stress

Test Summary	
Test Description:	Direct Shear Box Test
Approximate Shear Rate:	1 mm/min
Sample Description:	Copper - Nickel
Top Size (mm):	-4
Moisture (%):	5
Determined k Value (mm):	1.16
Determined Peak Angle (degrees):	NA
Determined Critical State Angle (degrees):	38.7
Determined Soil Type:	Type I

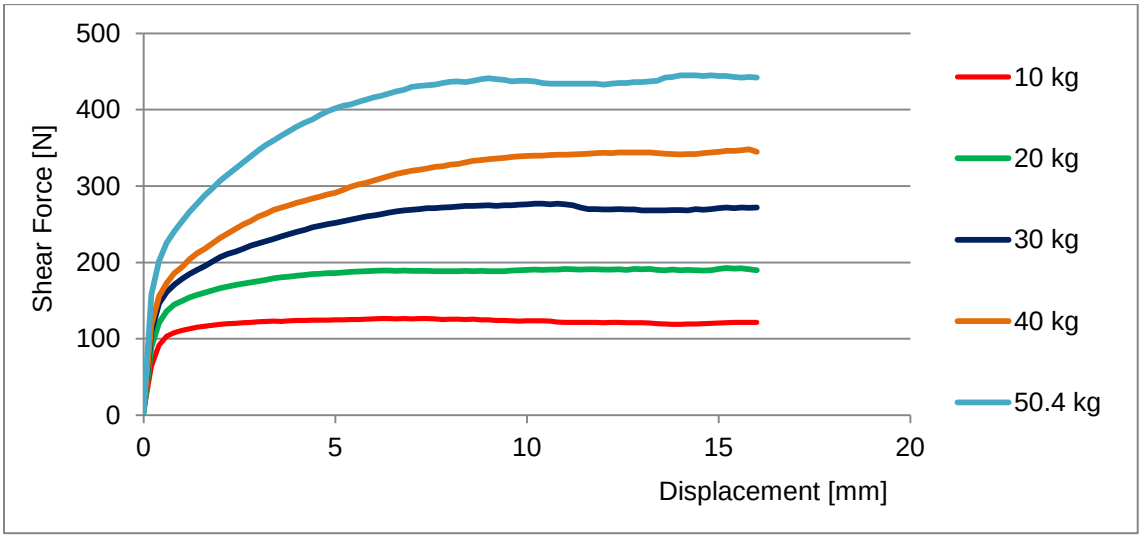

Figure A56 - Shear force and displacement

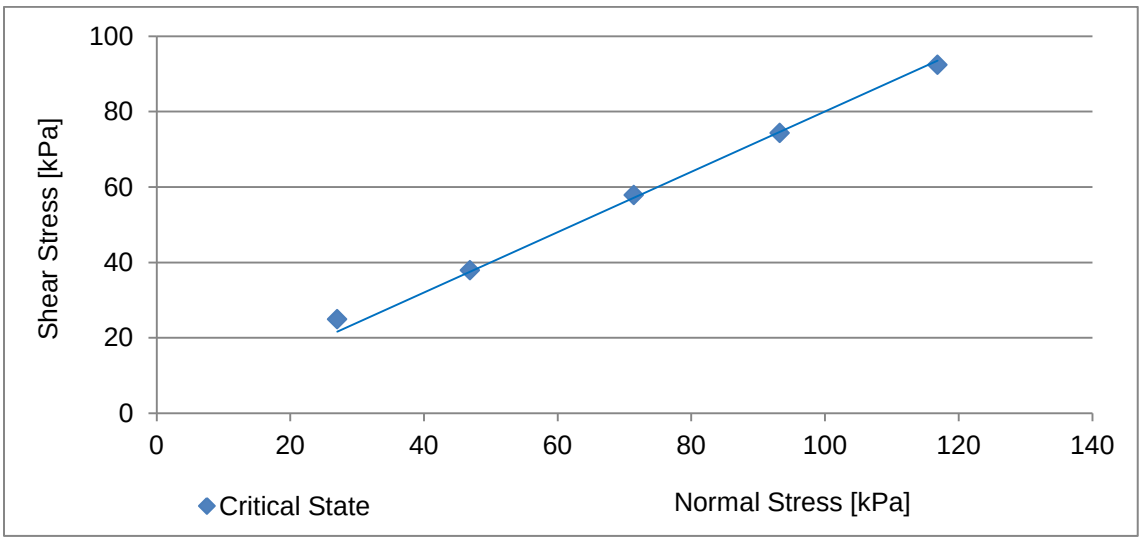

Figure A57 – Shear stress and normal stress

Test Summary	
Test Description:	Direct Shear Box Test
Approximate Shear Rate:	1 mm/min
Sample Description:	Copper Porphyry #1
Top Size (mm):	-4
Moisture (%):	0
Determined k Value (mm):	1.14
Determined Peak Angle (degrees):	39.9
Determined Critical State Angle (degrees):	35.9
Determined Soil Type:	Type II

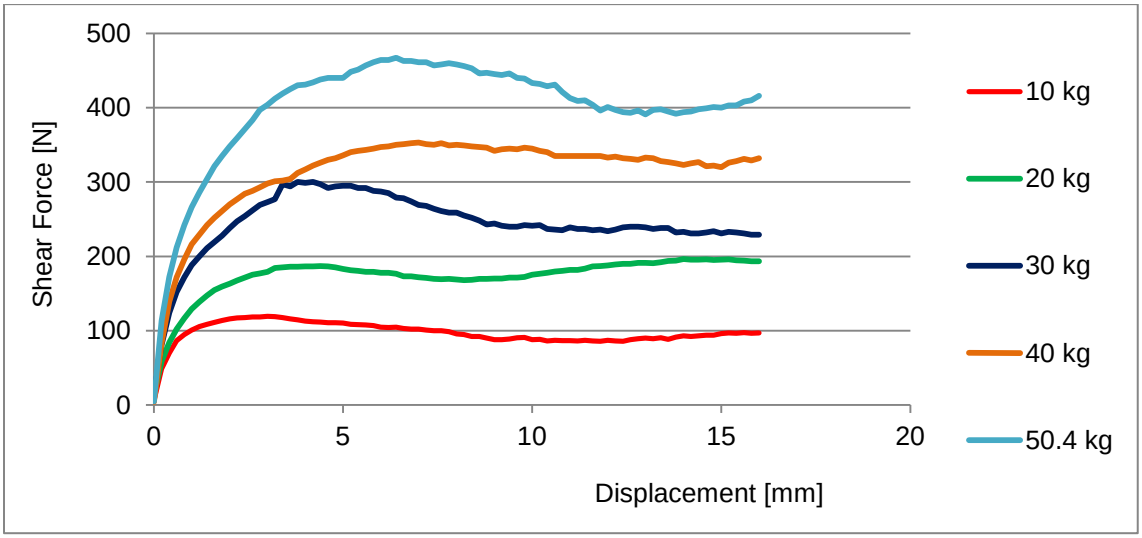

Figure A58 - Shear force and displacement

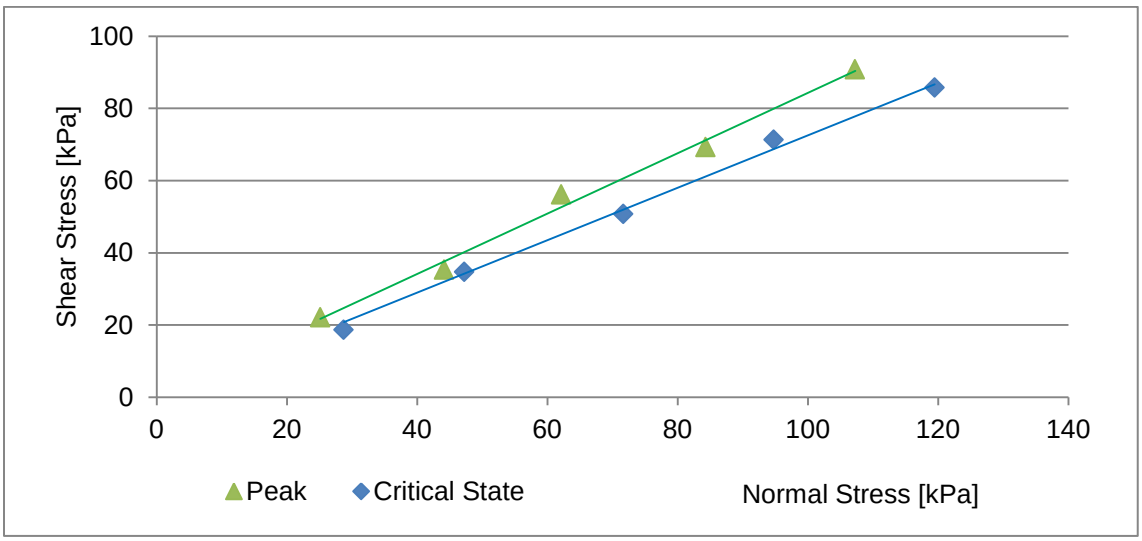

Figure A59 – Shear stress and normal stress

Test Summary	
Test Description:	Direct Shear Box Test
Approximate Shear Rate:	1 mm/min
Sample Description:	Copper Porphyry #1
Top Size (mm):	-4
Moisture (%):	2.5
Determined k Value (mm):	1.01
Determined Peak Angle (degrees):	NA
Determined Critical State Angle (degrees):	39.7
Determined Soil Type:	Type I

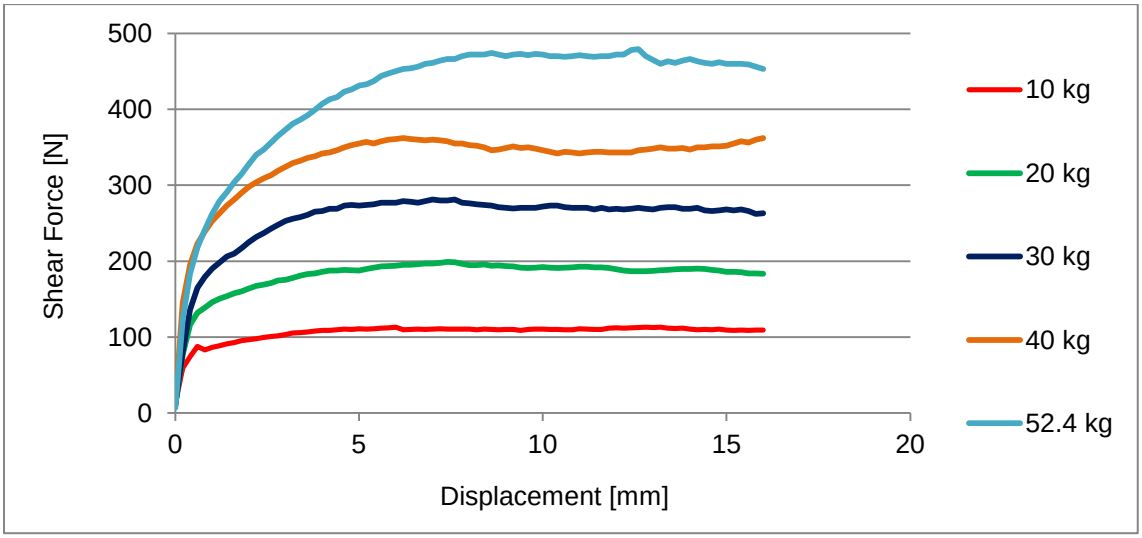

Figure A60 - Shear force and displacement

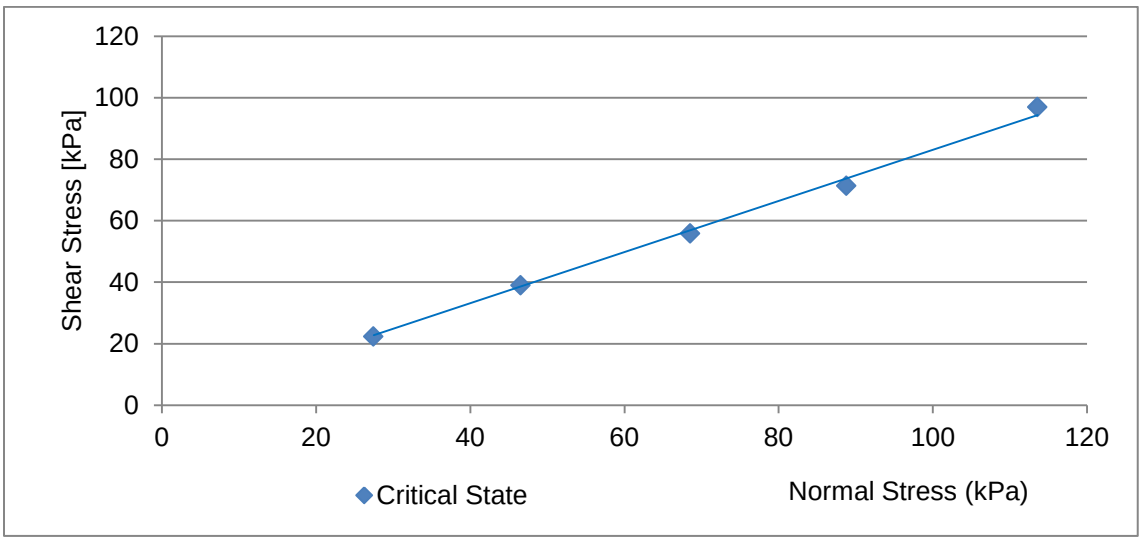

Figure A61 – Shear stress and normal stress

Test Summary	
Test Description:	Direct Shear Box Test
Approximate Shear Rate:	1 mm/min
Sample Description:	Copper Porphyry #1
Top Size (mm):	-4
Moisture (%):	4.5
Determined k Value (mm):	1.15
Determined Peak Angle (degrees):	NA
Determined Critical State Angle (degrees):	39.8
Determined Soil Type:	Type I

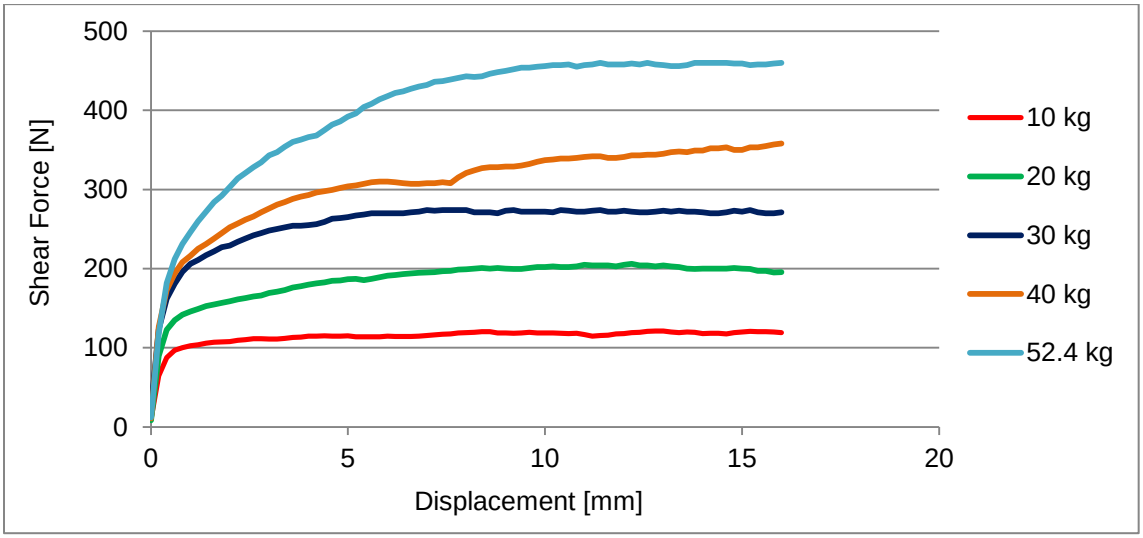

Figure A62 - Shear force and displacement

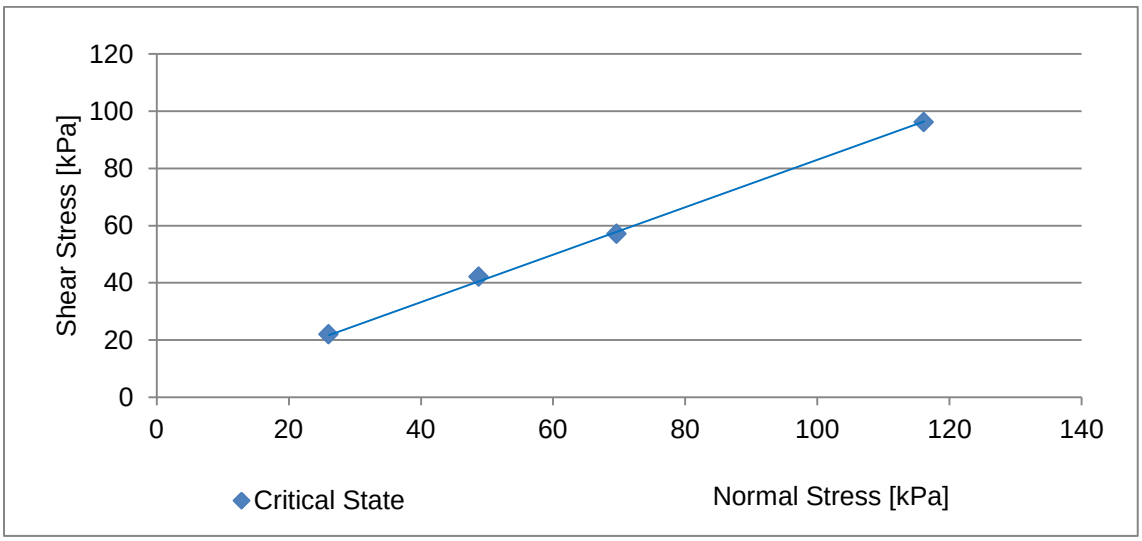

Figure A63 – Shear stress and normal stress

Test Summary	
Test Description:	Direct Shear Box Test
Approximate Shear Rate:	1 mm/min
Sample Description:	Ultra-Mafic / Mafic
Top Size (mm):	-4
Moisture (%):	0
Determined k Value (mm):	0.44
Determined Peak Angle (degrees):	41.1
Determined Critical State Angle (degrees):	36.1
Determined Soil Type:	Type II

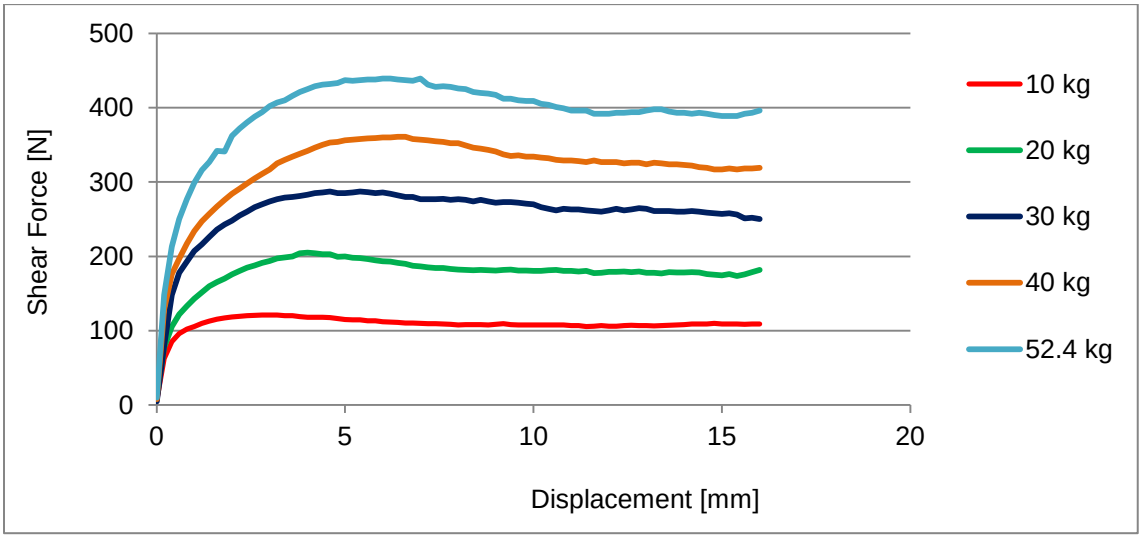

Figure A64 - Shear force and displacement

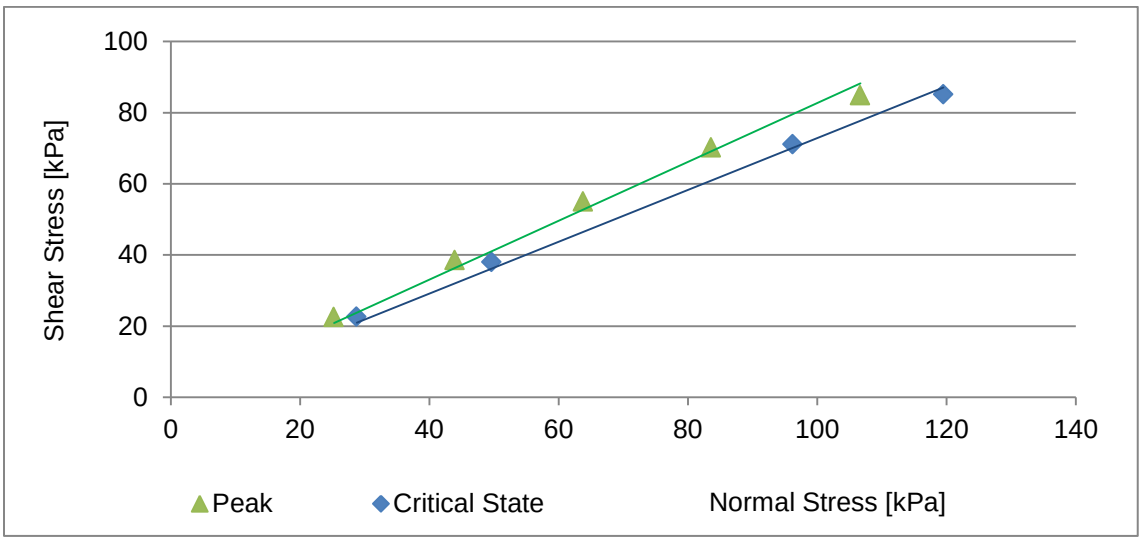

Figure A65 – Shear stress and normal stress

Test Summary	
Test Description:	Direct Shear Box Test
Approximate Shear Rate:	1 mm/min
Sample Description:	Ultra-Mafic / Mafic
Top Size (mm):	-4
Moisture (%):	5
Determined k Value (mm):	1.73
Determined Peak Angle (degrees):	NA
Determined Critical State Angle (degrees):	41.2
Determined Soil Type:	Type I

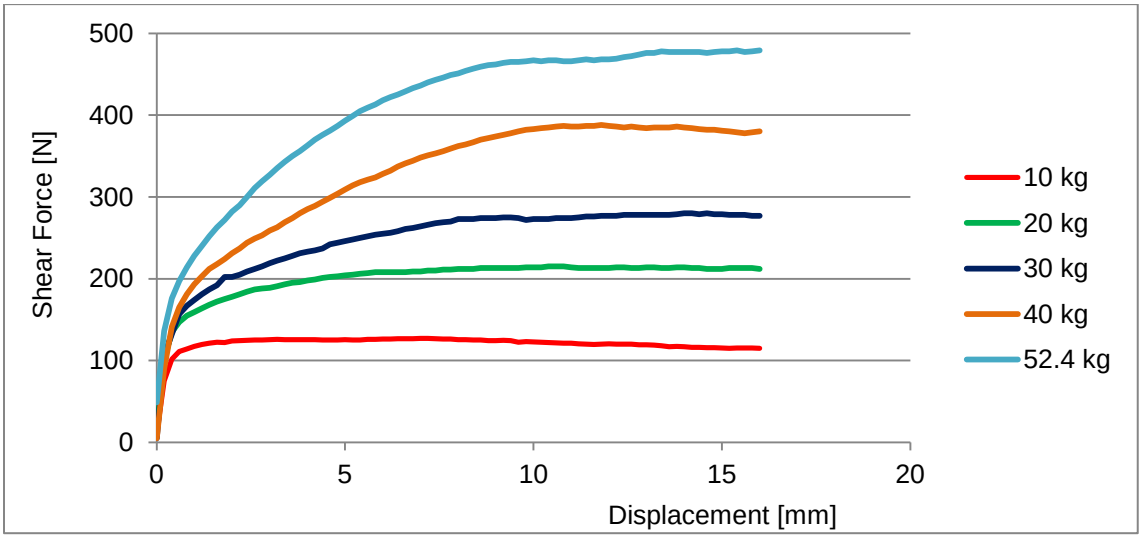

Figure A66 - Shear force and displacement

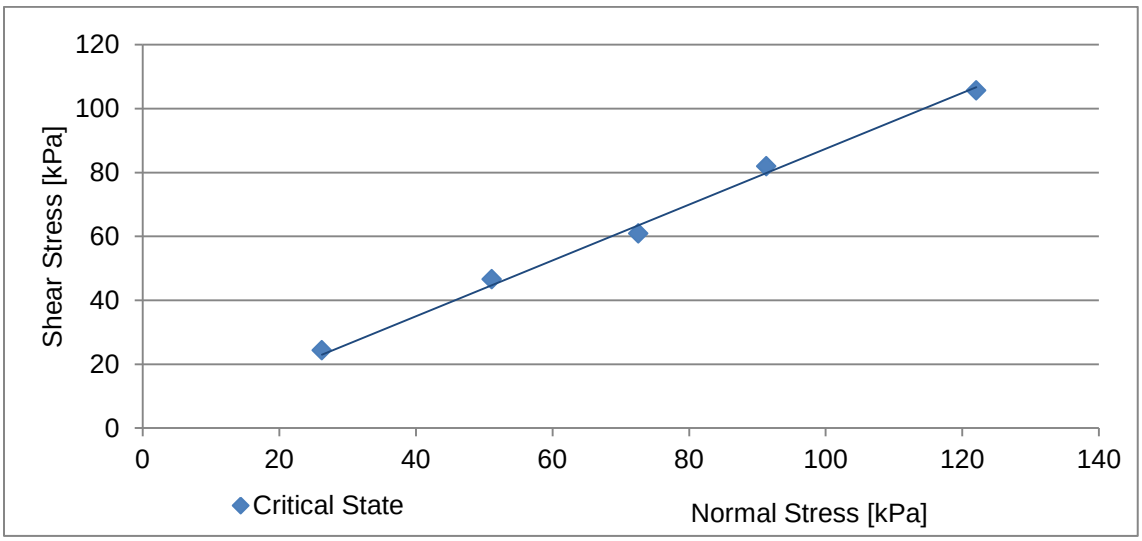

Figure A67 – Shear stress and normal stress

Test Summary	
Test Description:	Direct Shear Box Test
Approximate Shear Rate:	1 mm/min
Sample Description:	Ultra-Mafic / Mafic
Top Size (mm):	-4
Moisture (%):	3.3
Determined k Value (mm):	0.63
Determined Peak Angle (degrees):	42.5
Determined Critical State Angle (degrees):	39.1
Determined Soil Type:	Type II

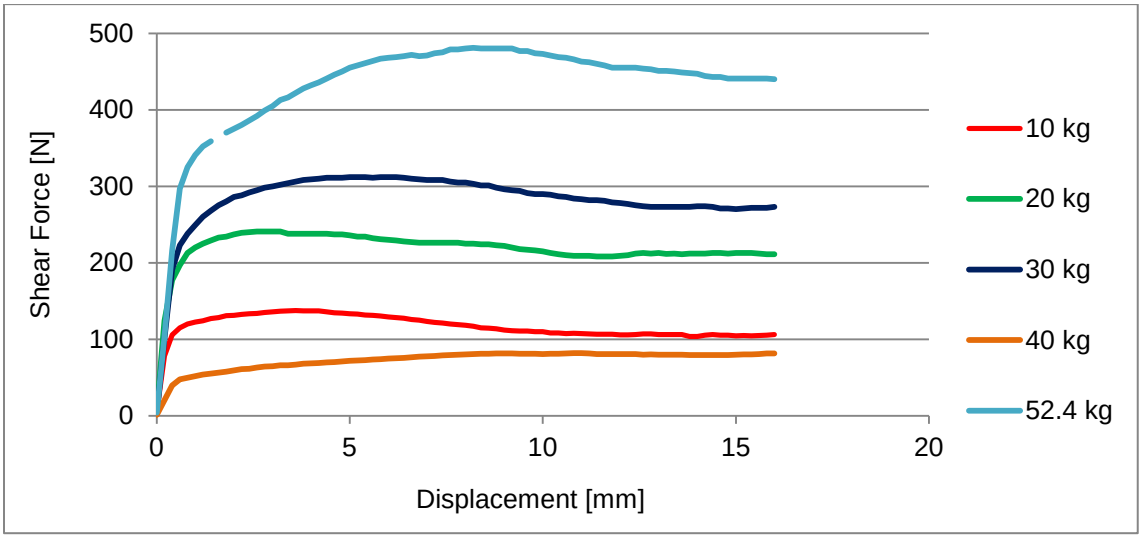

Figure A68 - Shear force and displacement

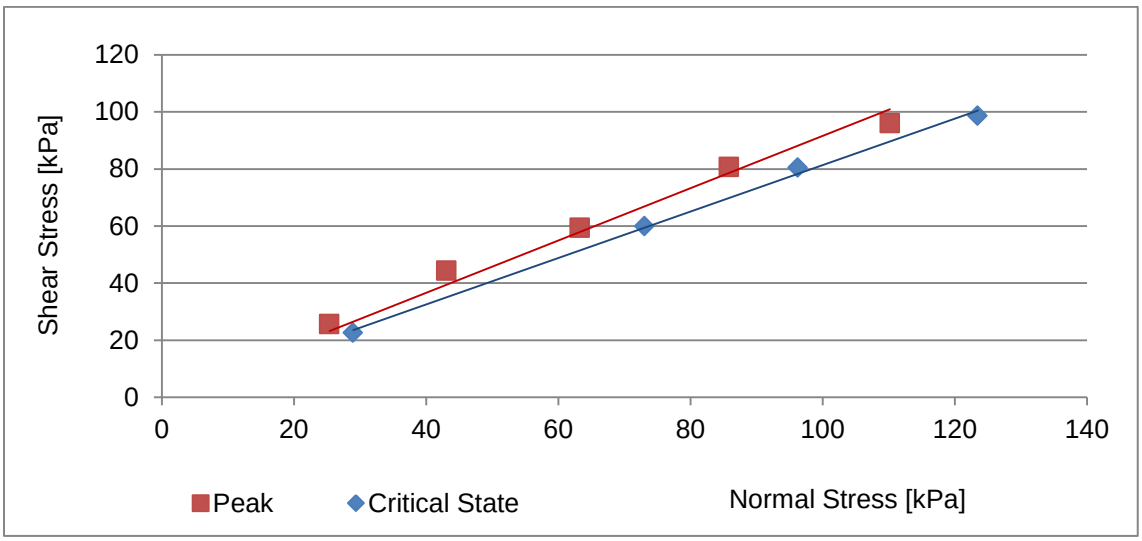

Figure A69 – Shear stress and normal stress

Test Summary	
Test Description:	Direct Shear Box Test
Approximate Shear Rate:	1 mm/min
Sample Description:	Copper Porphyry #2
Top Size (mm):	-4
Moisture (%):	0
Determined k Value (mm):	1.29
Determined Peak Angle (degrees):	40.9
Determined Critical State Angle (degrees):	38.2
Determined Soil Type:	Type II

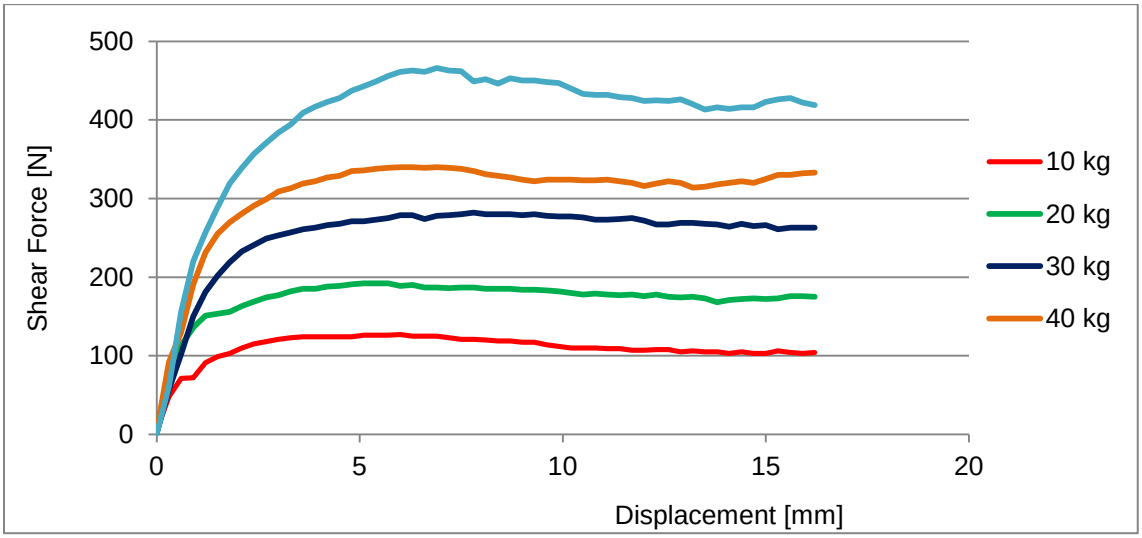

Figure A70 - Shear force and displacement

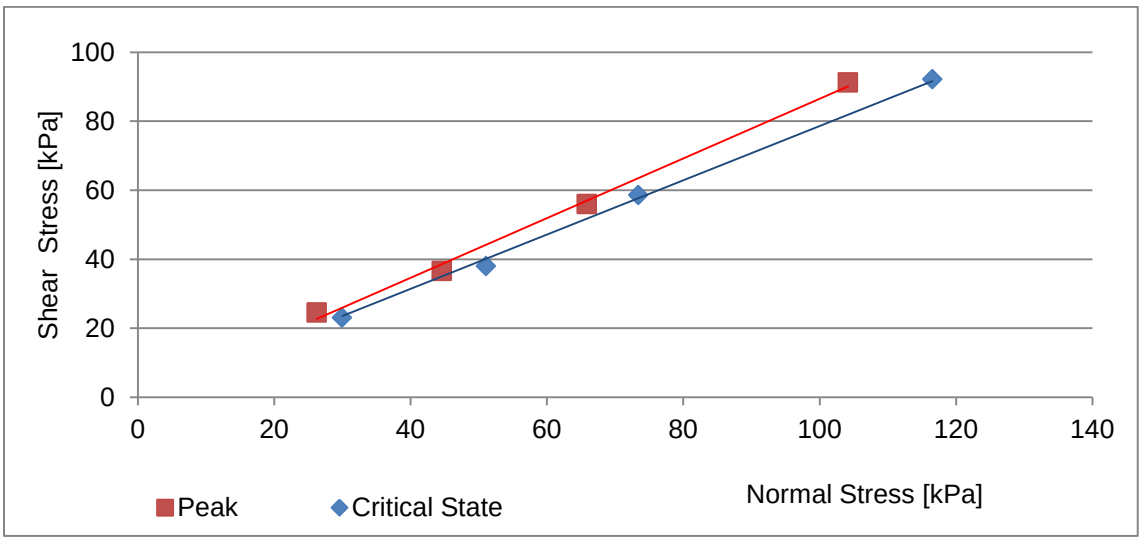

Figure A71 – Shear stress and normal stress

Test Summary	
Test Description:	Direct Shear Box Test
Approximate Shear Rate:	1 mm/min
Sample Description:	Copper Porphyry #2
Top Size (mm):	-4
Moisture (%):	2.5
Determined k Value (mm):	1.25
Determined Peak Angle (degrees):	NA
Determined Critical State Angle (degrees):	38.2
Determined Soil Type:	Type I

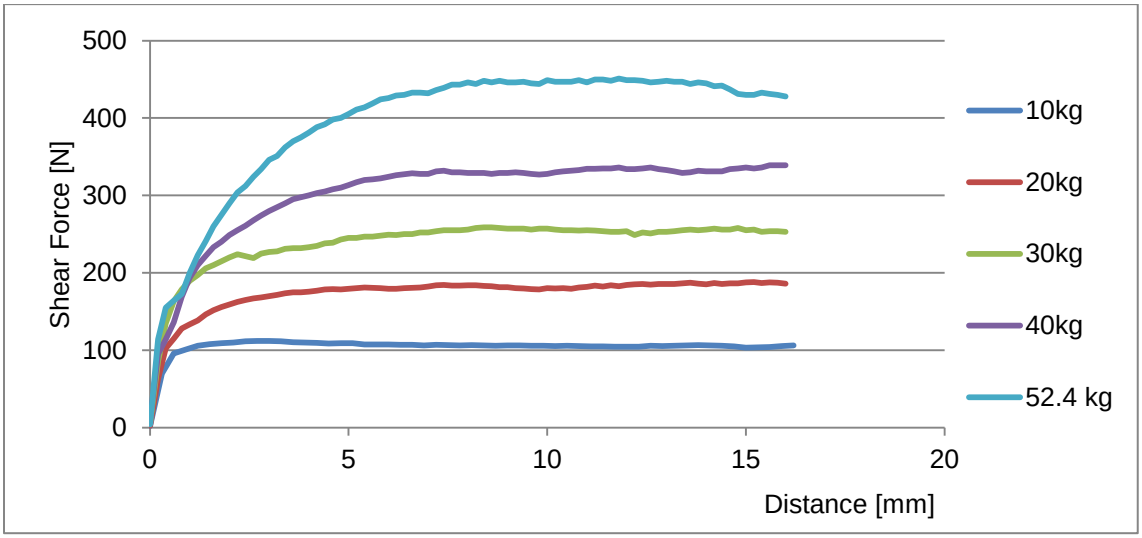

Figure A72 - Shear force and displacement

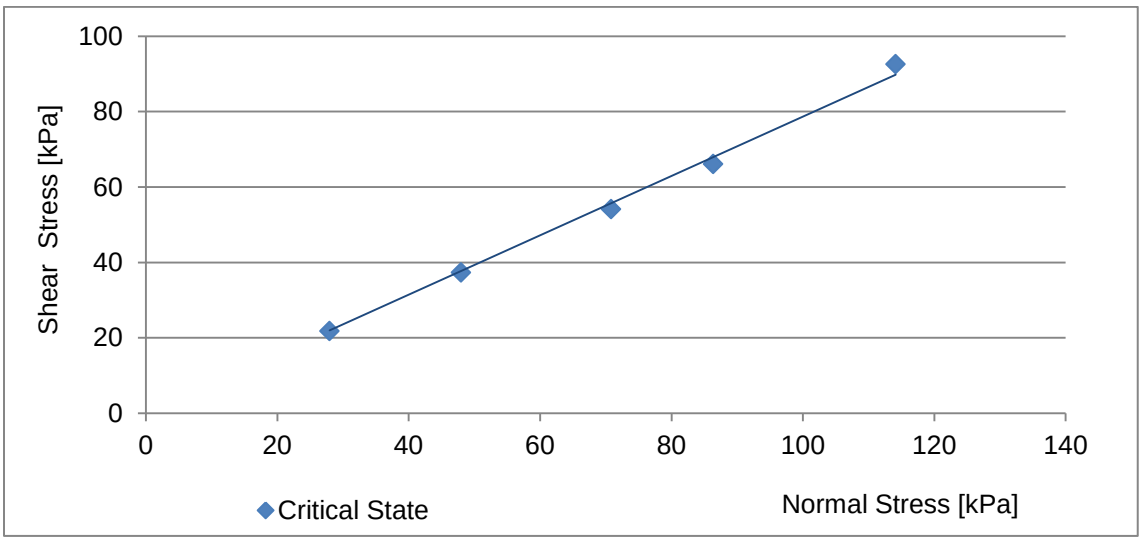

Figure A73 – Shear stress and normal stress

Test Summary	
Test Description:	Direct Shear Box Test
Approximate Shear Rate:	1 mm/min
Sample Description:	Copper Porphyry #2
Top Size (mm):	-4
Moisture (%):	5
Determined k Value (mm):	1.41
Determined Peak Angle (degrees):	NA
Determined Critical State Angle (degrees):	37.5
Determined Soil Type:	Type I

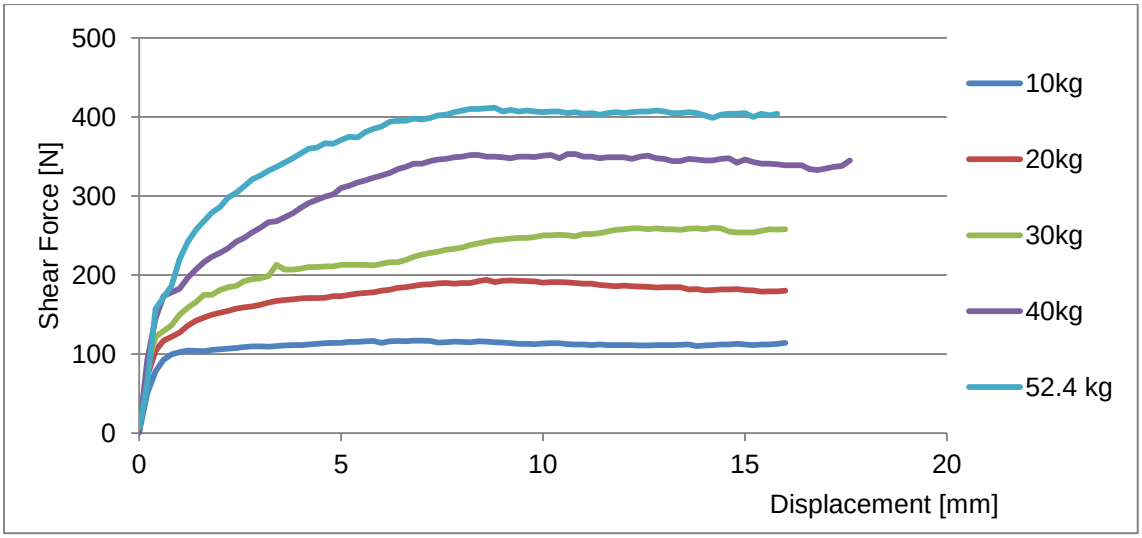

Figure A74 - Shear force and displacement

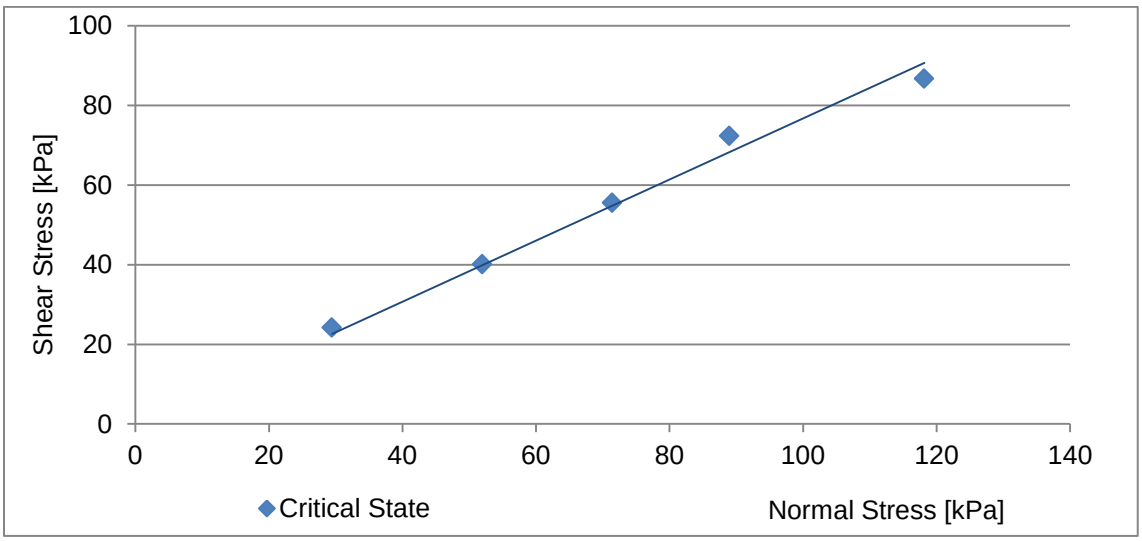

Figure A75 – Shear stress and normal stress

Test Summary	
Test Description:	Direct Shear Box Test
Approximate Shear Rate:	1 mm/min
Sample Description:	Dolomite
Top Size (mm):	-4
Moisture (%):	0
Determined k Value (mm):	0.51
Determined Peak Angle (degrees):	33.7
Determined Critical State Angle (degrees):	31.1
Determined Soil Type:	Type II

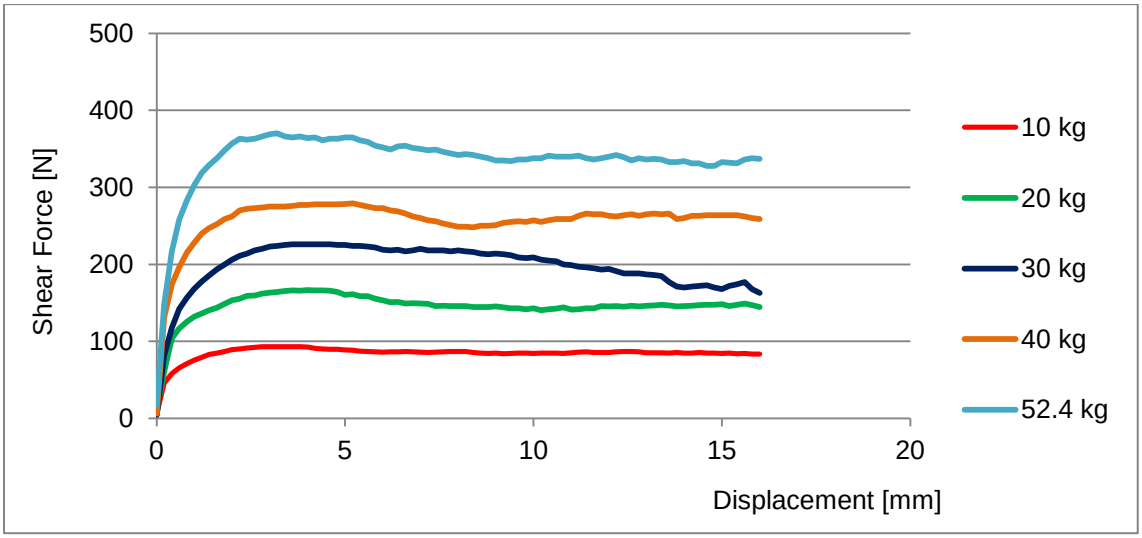

Figure A76 - Shear force and displacement

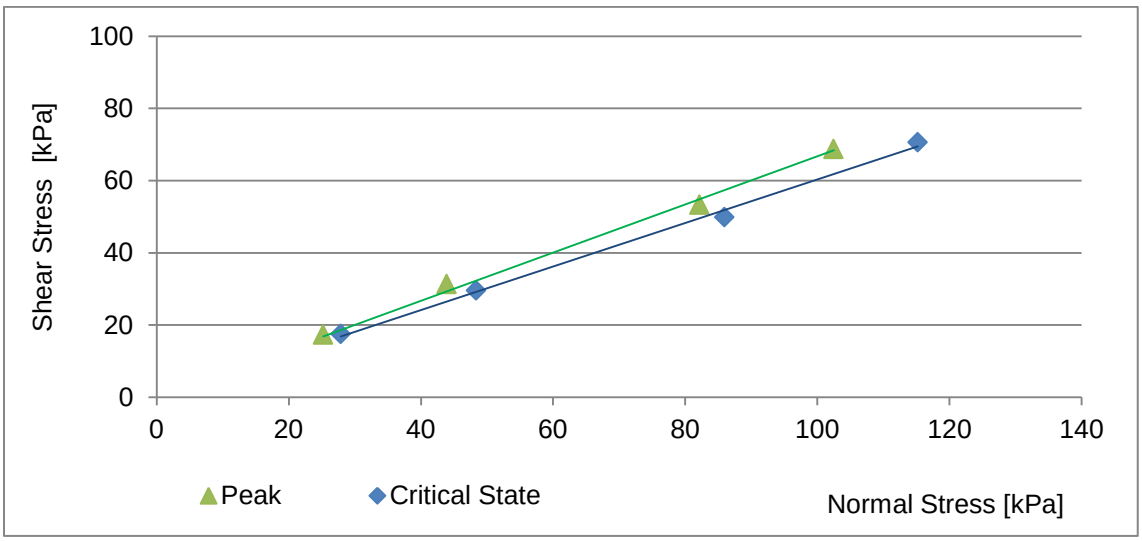

Figure A77 – Shear stress and normal stress

Test Summary	
Test Description:	Direct Shear Box Test
Approximate Shear Rate:	1 mm/min
Sample Description:	Dolomite
Top Size (mm):	-4
Moisture (%):	3.6
Determined k Value (mm):	0.55
Determined Peak Angle (degrees):	NA
Determined Critical State Angle (degrees):	32.3
Determined Soil Type:	Type I

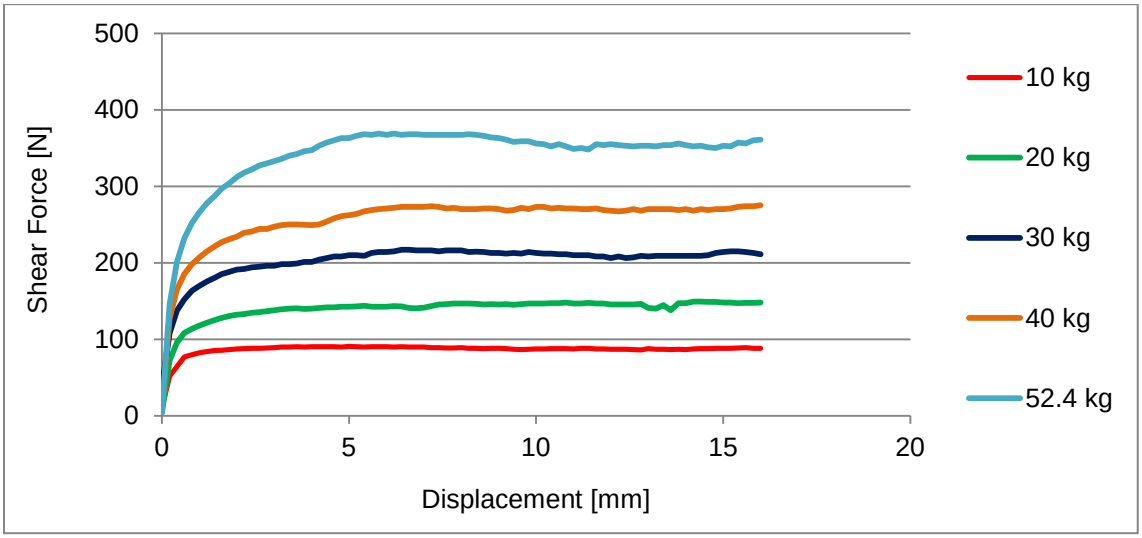

Figure A78 - Shear force and displacement

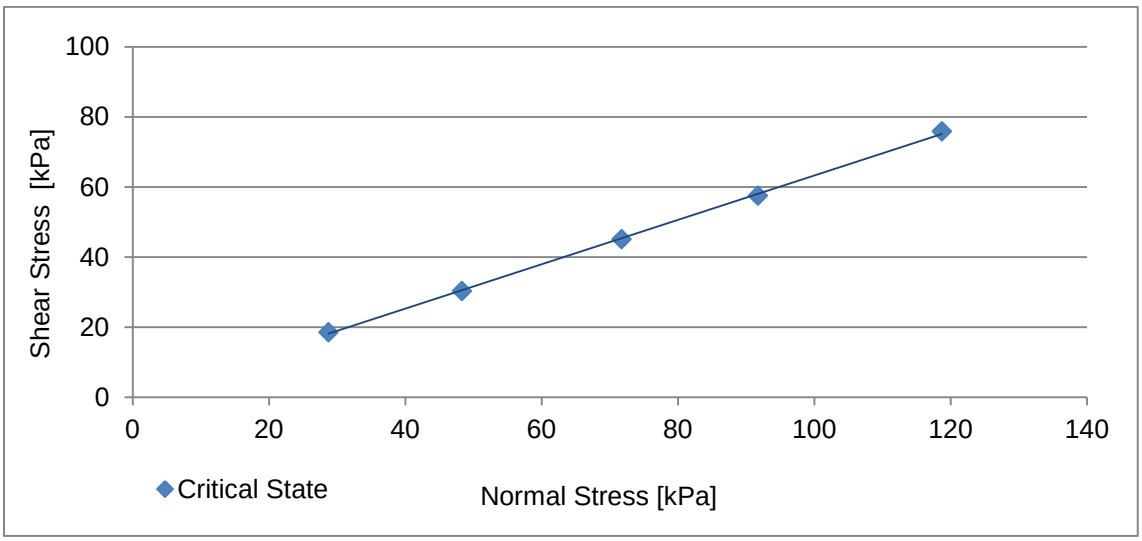

Figure A79 – Shear stress and normal stress

Test Summary	
Test Description:	Direct Shear Box Test
Approximate Shear Rate:	1 mm/min
Sample Description:	Taconite
Top Size (mm):	-4
Moisture (%):	2
Determined k Value (mm):	0.89
Determined Peak Angle (degrees):	43.9
Determined Critical State Angle (degrees):	40.3
Determined Soil Type:	Type IIA

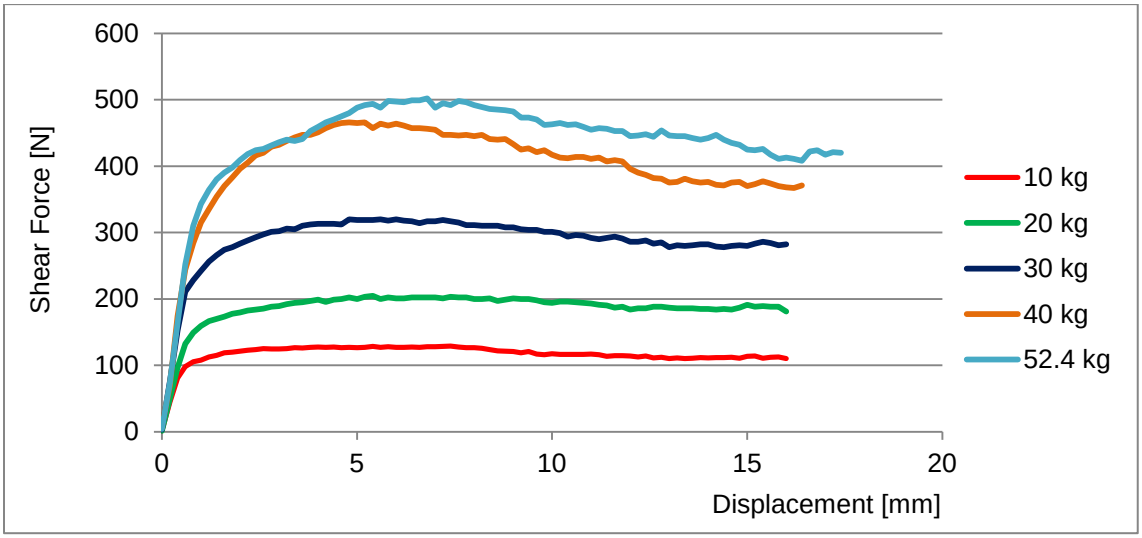

Figure A80 - Shear force and displacement

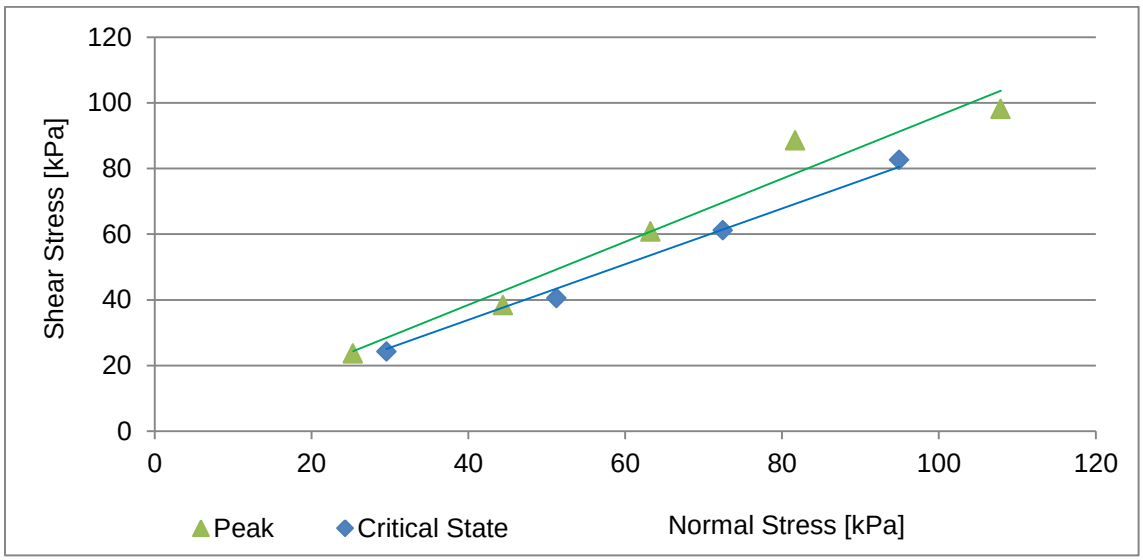

Figure A81 – Shear stress and normal stress

Test Summary	
Test Description:	Direct Shear Box Test
Approximate Shear Rate:	1 mm/min
Sample Description:	Taconite
Top Size (mm):	-4
Moisture (%):	0
Determined k Value (mm):	0.73
Determined Peak Angle (degrees):	40.0
Determined Critical State Angle (degrees):	37.3
Determined Soil Type:	Type II

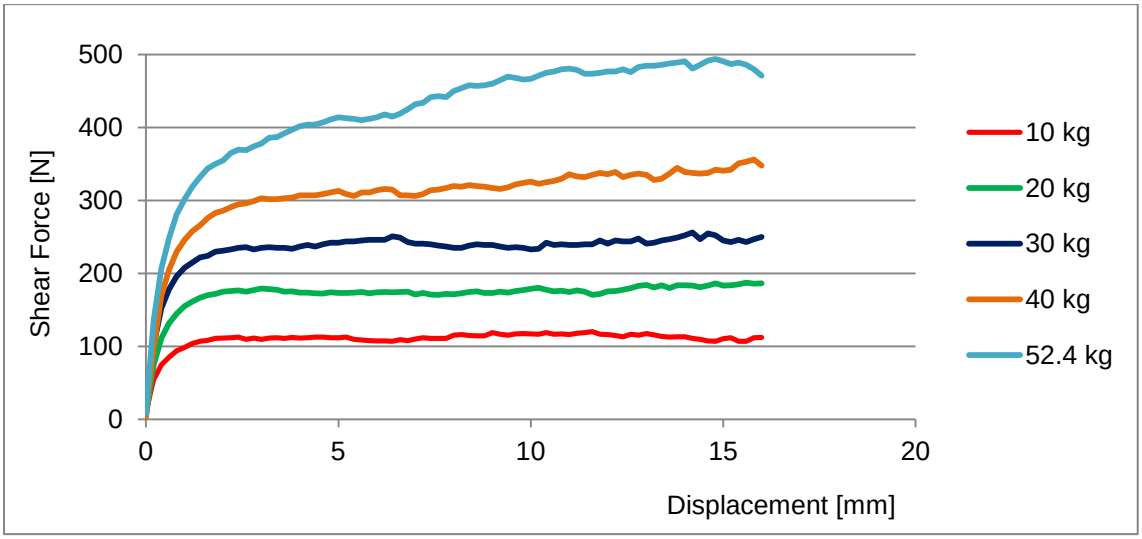

Figure A82 - Shear force and displacement

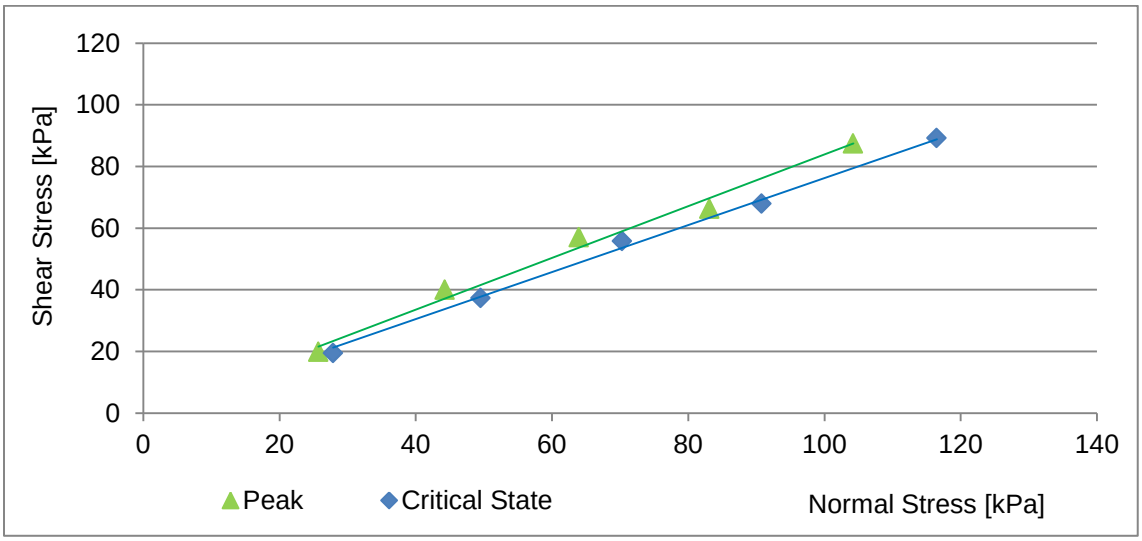

Figure A83 – Shear stress and normal stress

Test Summary	
Test Description:	Direct Shear Box Test
Approximate Shear Rate:	1 mm/min
Sample Description:	Taconite
Top Size (mm):	-4
Moisture (%):	5
Determined k Value (mm):	0.47
Determined Peak Angle (degrees):	NA
Determined Critical State Angle (degrees):	36.1
Determined Soil Type:	Type I

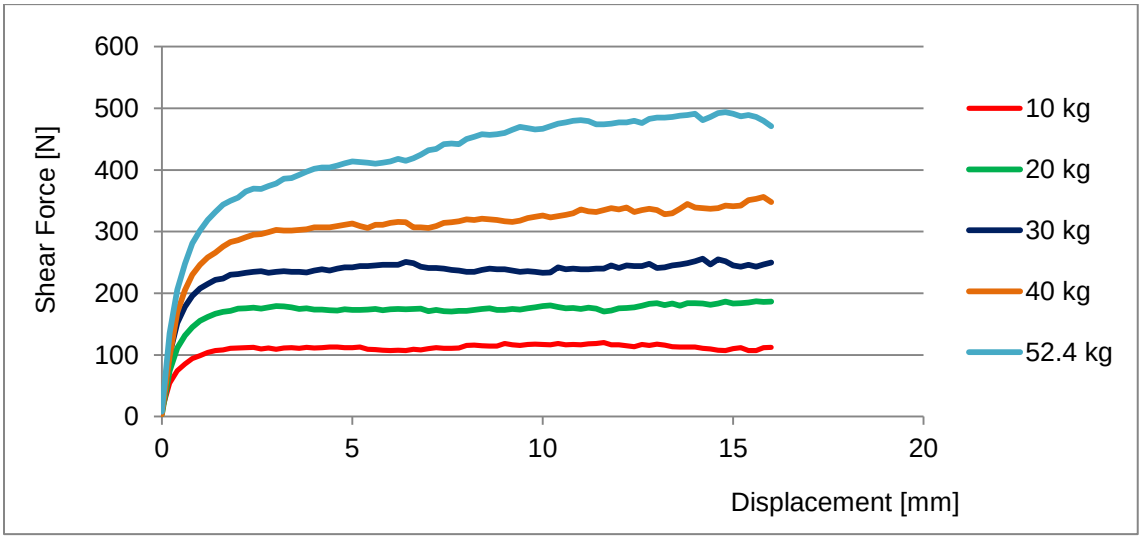

Figure A84 - Shear force and displacement

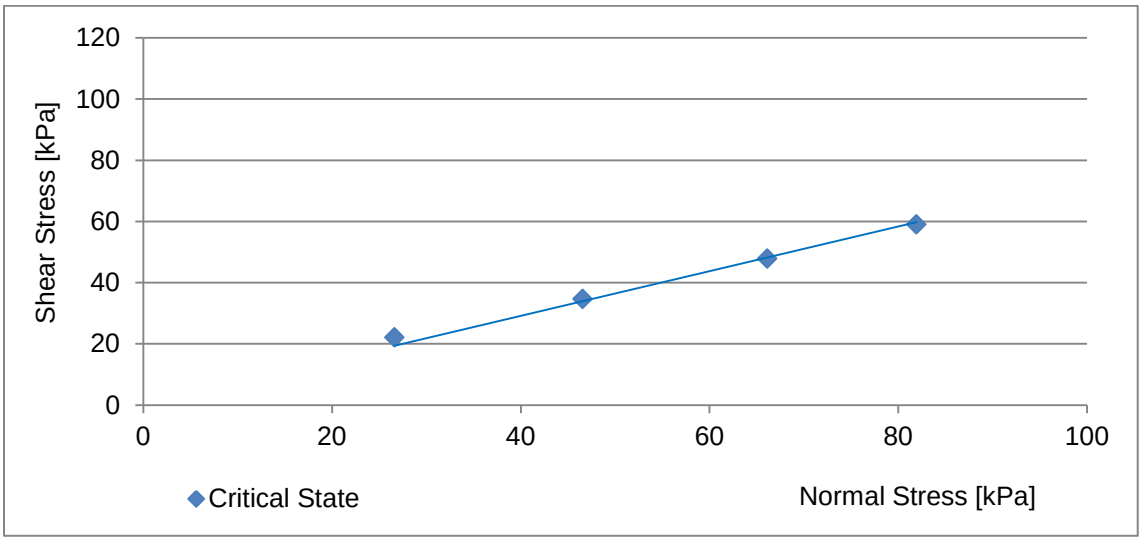

Figure A85 – Shear stress and normal stress

Test Summary	
Test Description:	Direct Shear Box Test
Approximate Shear Rate:	1 mm/min
Sample Description:	Steel Balls
Top Size (mm):	-4
Moisture (%):	0
Determined k Value (mm):	0.43
Determined Peak Angle (degrees):	35.8
Determined Critical State Angle (degrees):	NA
Determined Soil Type:	Type IIA

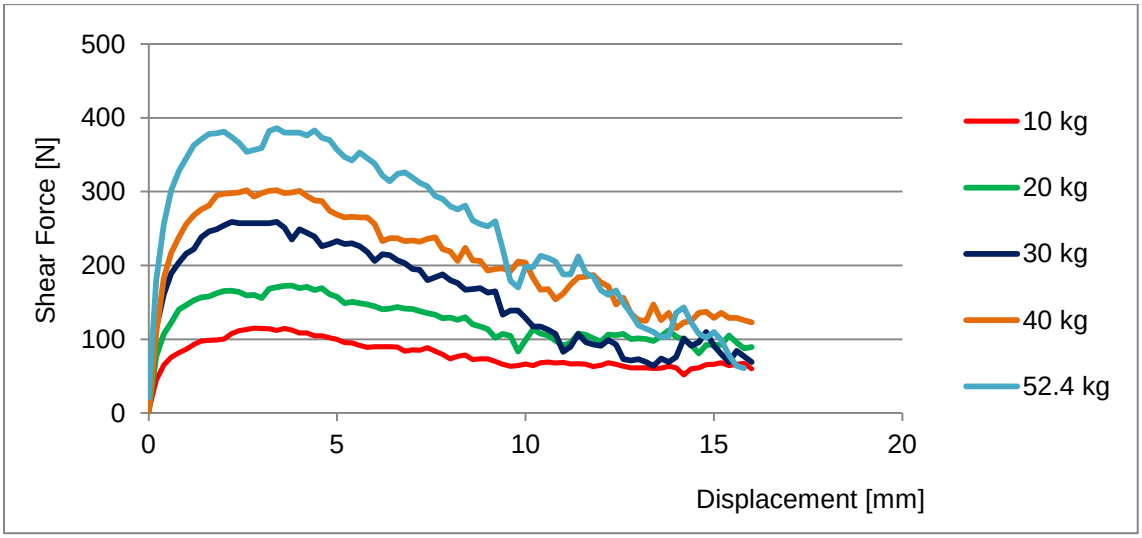

Figure A86 - Shear force and displacement

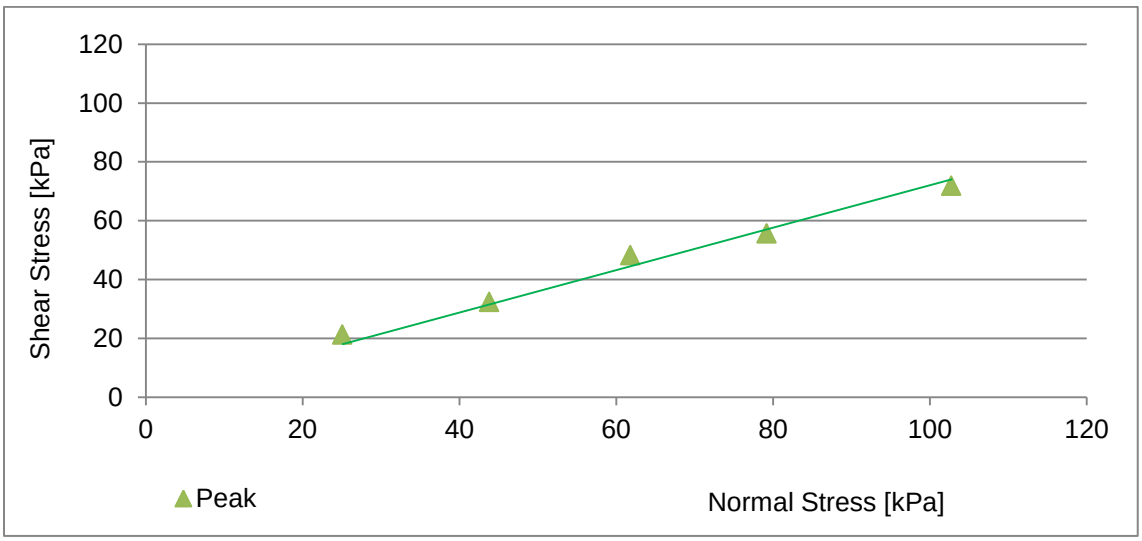

Figure A87 – Shear stress and normal stress

Test Summary	
Test Description:	Direct Shear Box Test
Approximate Shear Rate:	1 mm/min
Sample Description:	Limestone
Top Size (mm):	-4
Moisture (%):	0
Determined k Value (mm):	0.46
Determined Peak Angle (degrees):	NA
Determined Critical State Angle (degrees):	36.2
Determined Soil Type:	Type I

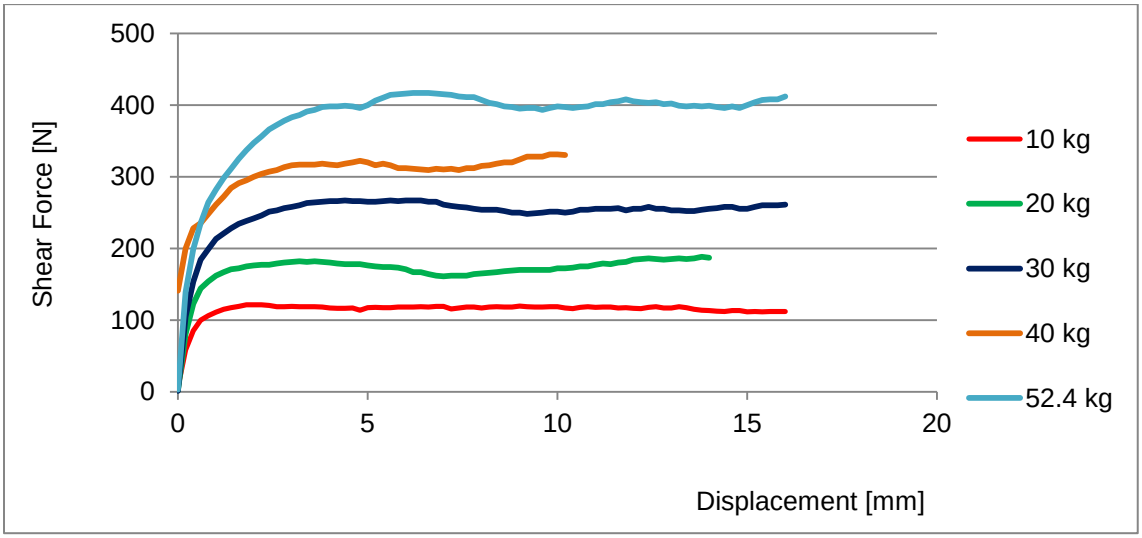

Figure A88 - Shear force and displacement

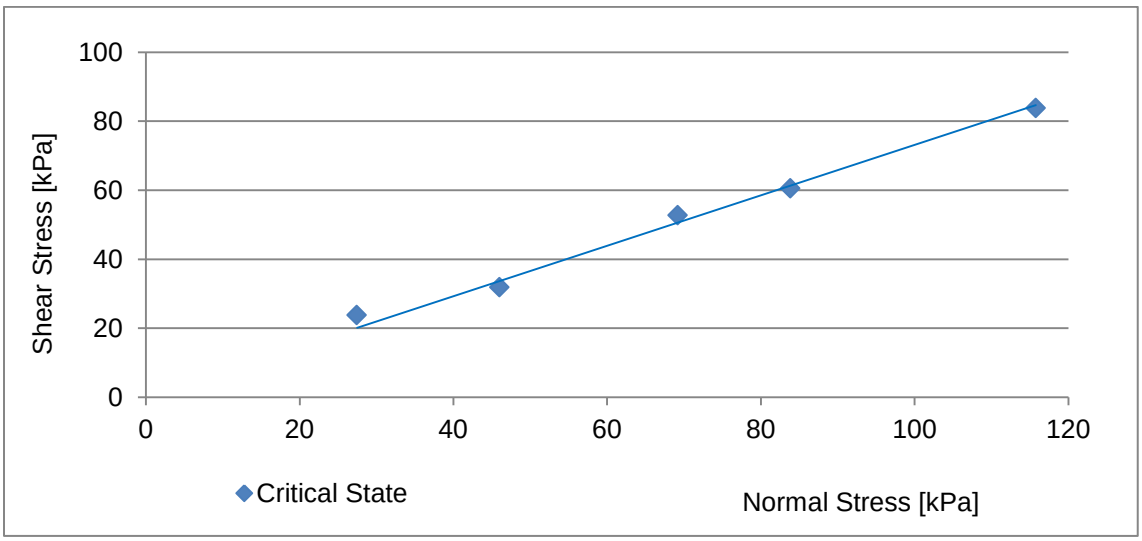

Figure A89 – Shear stress and normal stress

Test Summary	
Test Description:	Direct Shear Box Test
Approximate Shear Rate:	1 mm/min
Sample Description:	Limestone
Top Size (mm):	-4
Moisture (%):	5
Determined k Value (mm):	1.77
Determined Peak Angle (degrees):	NA
Determined Critical State Angle (degrees):	42.3
Determined Soil Type:	I

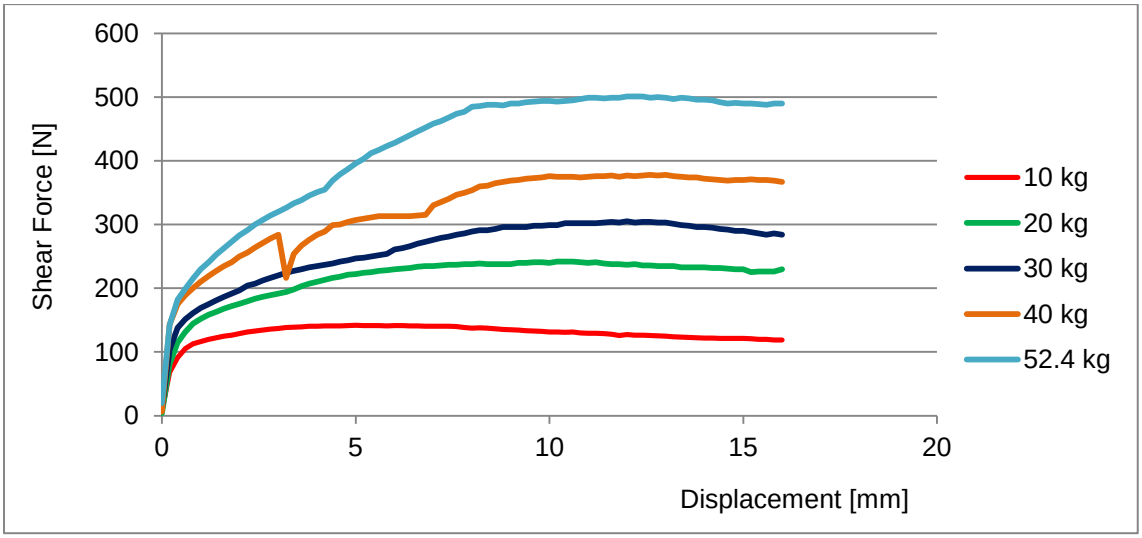

Figure A90 - Shear force and displacement

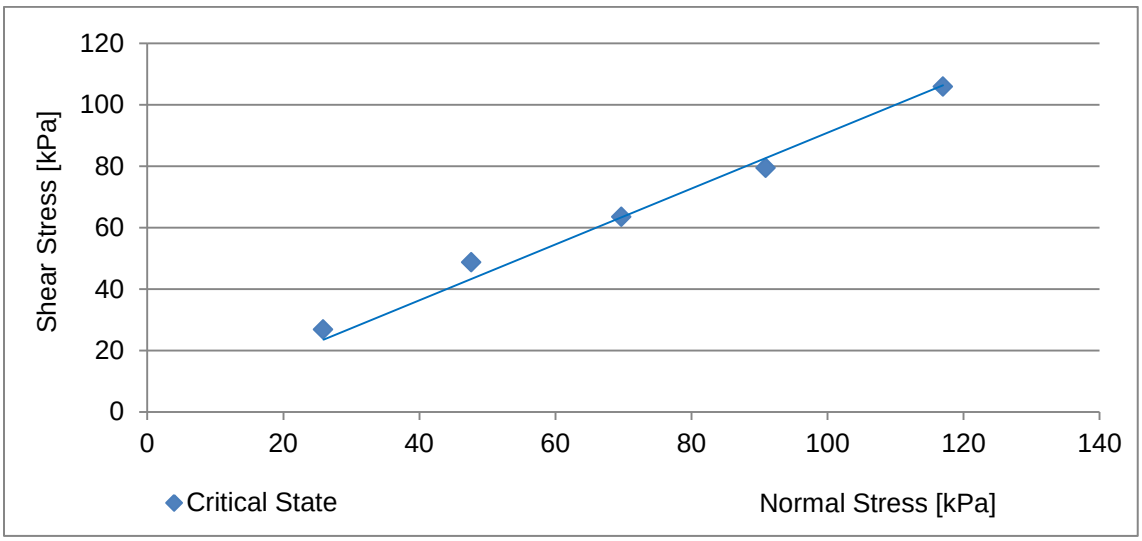

Figure A91 – Shear stress and normal stress

Test Description:	Direct Shear Box Test
Approximate Shear Rate:	1 mm/min
Sample Description:	Limestone
Top Size (mm):	-4
Moisture (%):	10
Determined k Value (mm):	0.72
Determined Peak Angle (degrees):	43.9
Determined Critical State Angle (degrees):	38.6
Determined Soil Type:	I & II

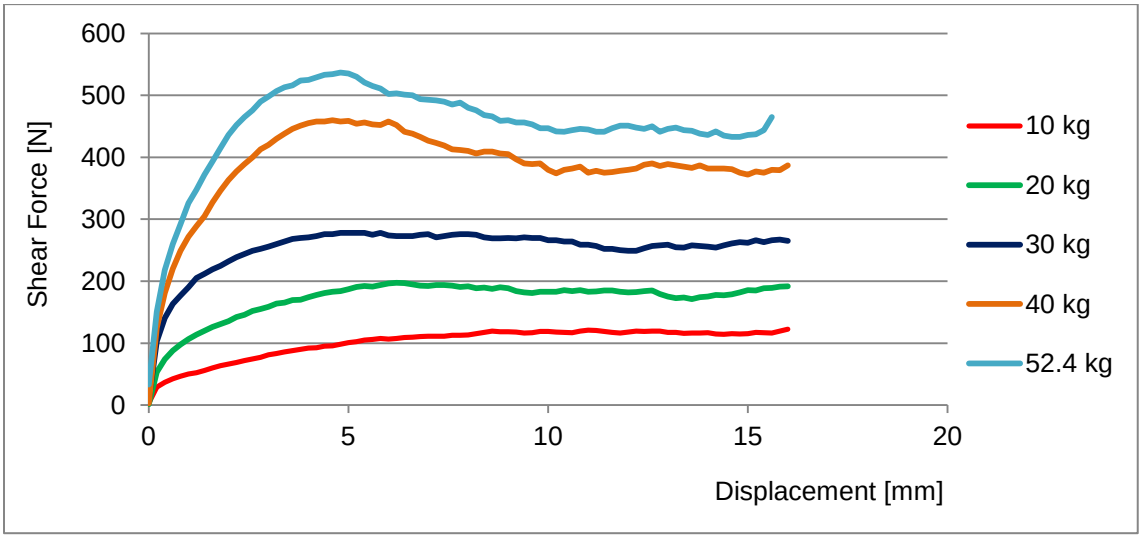

Figure A92 - Shear force and displacement

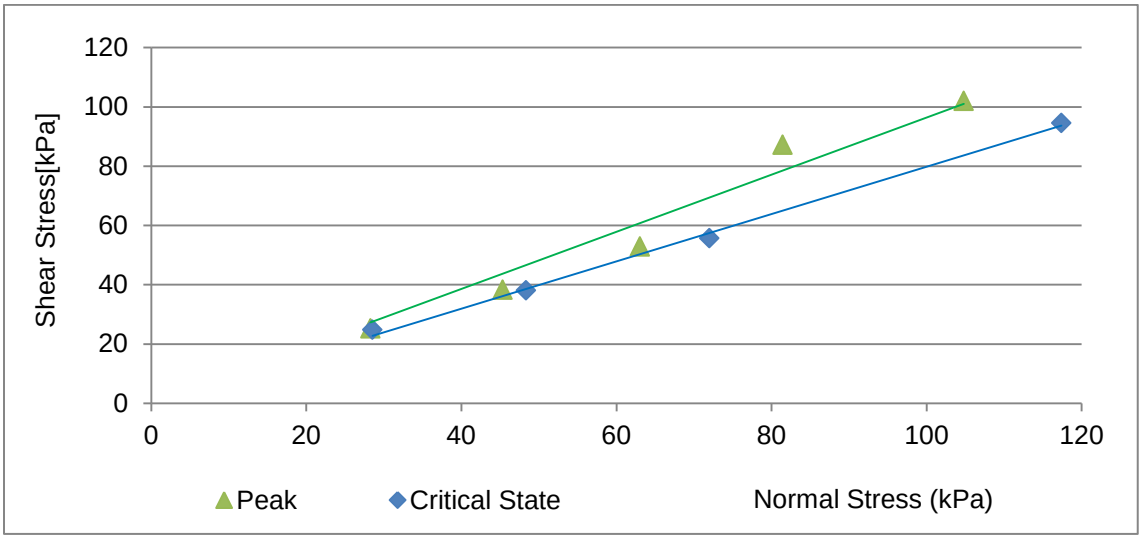

Figure A93 – Shear stress and normal stress

Test Description:	Direct Shear Box Test
Approximate Shear Rate:	1 mm/min
Sample Description:	Volcanogenic Gold
Top Size (mm):	-4
Moisture (%):	2.5
Determined k Value (mm):	0.53
Determined Peak Angle (degrees):	NA
Determined Critical State Angle (degrees):	35.8
Determined Soil Type:	I

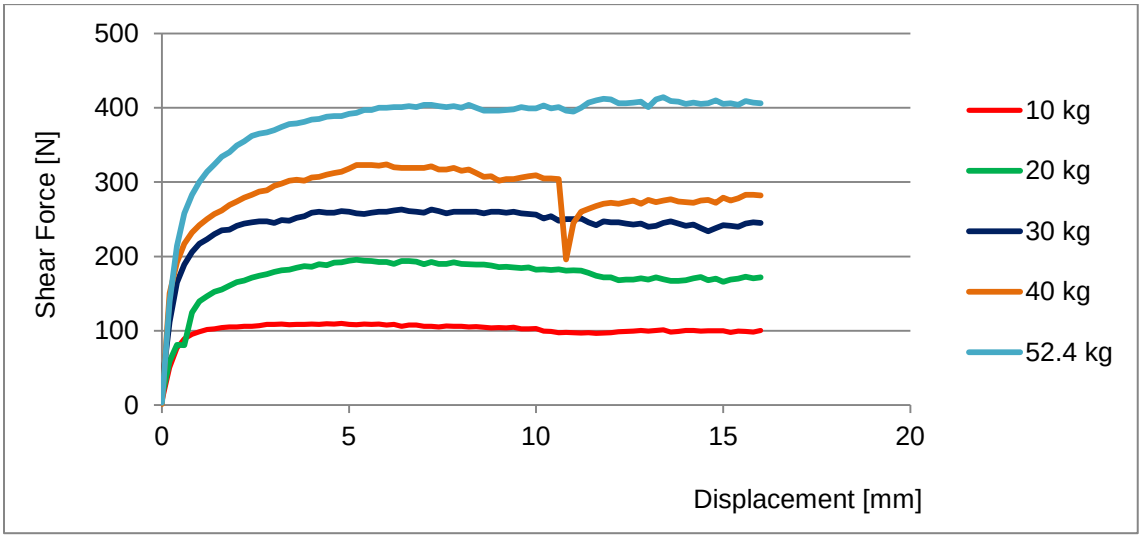

Figure A94 - Shear force and displacement

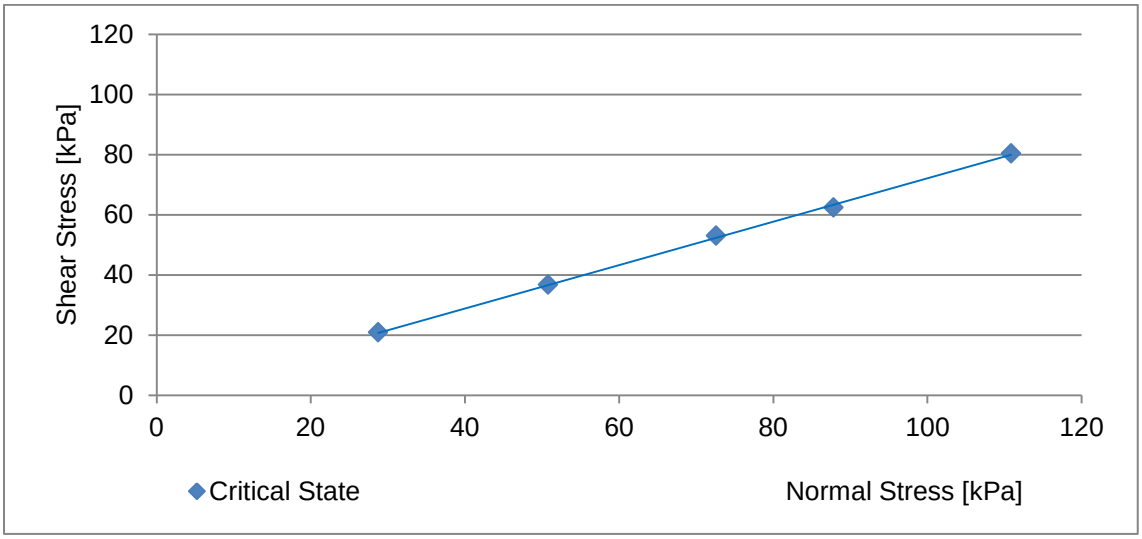

Figure A95 – Shear stress and normal stress

Test Description:	Direct Shear Box Test
Approximate Shear Rate:	1 mm/min
Sample Description:	Copper Porphyry #3
Top Size (mm):	-4
Moisture (%):	2.5
Determined k Value (mm):	0.99
Determined Peak Angle (degrees):	NA
Determined Critical State Angle (degrees):	40.0
Determined Soil Type:	I

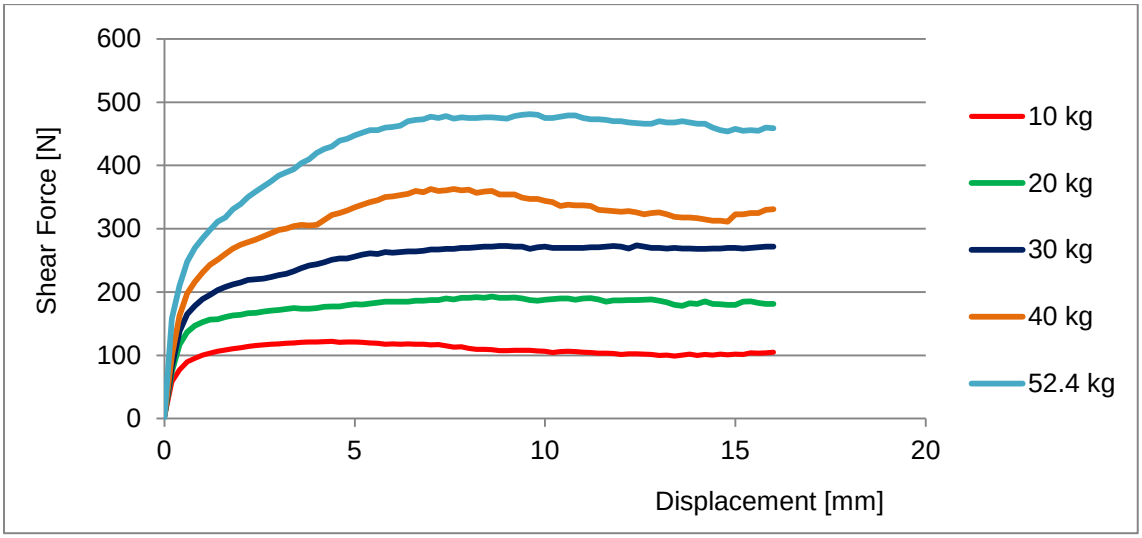

Figure A96 - Shear force and displacement

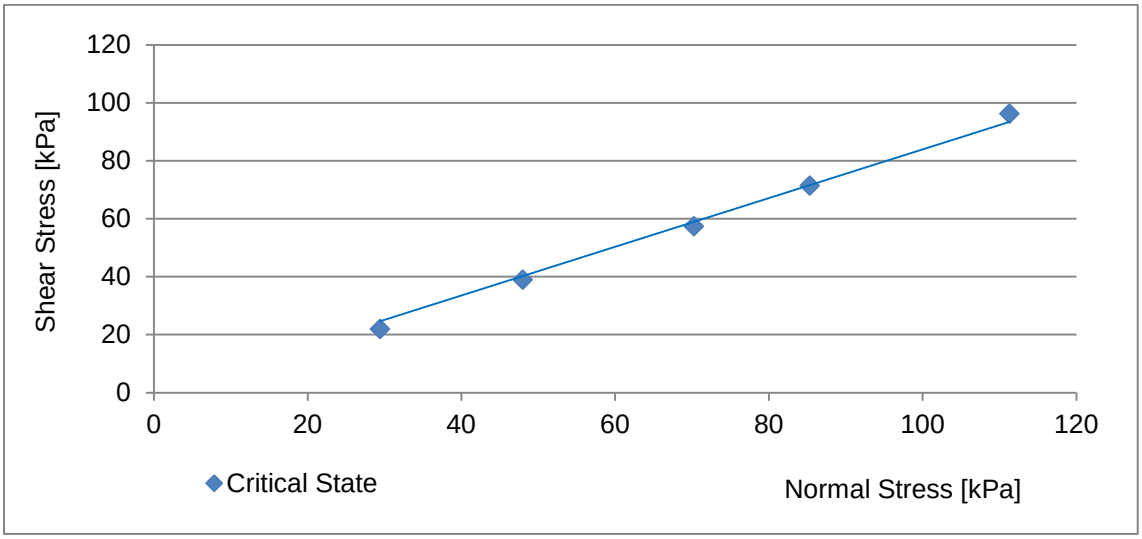

Figure A97 – Shear stress and normal stress

Test Description:	Direct Shear Box Test
Approximate Shear Rate:	1 mm/min
Sample Description:	Quartz
Top Size (mm):	-4
Moisture (%):	2.3
Determined k Value (mm):	0.27
Determined Peak Angle (degrees):	33.3
Determined Critical State Angle (degrees):	31.3
Determined Soil Type:	II

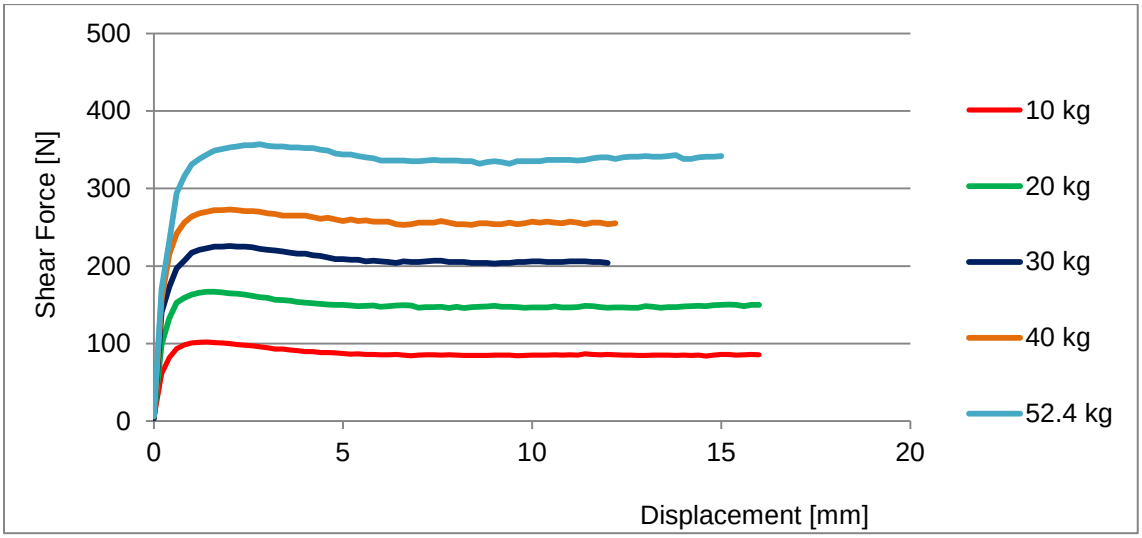

Figure A98 - Shear force and displacement

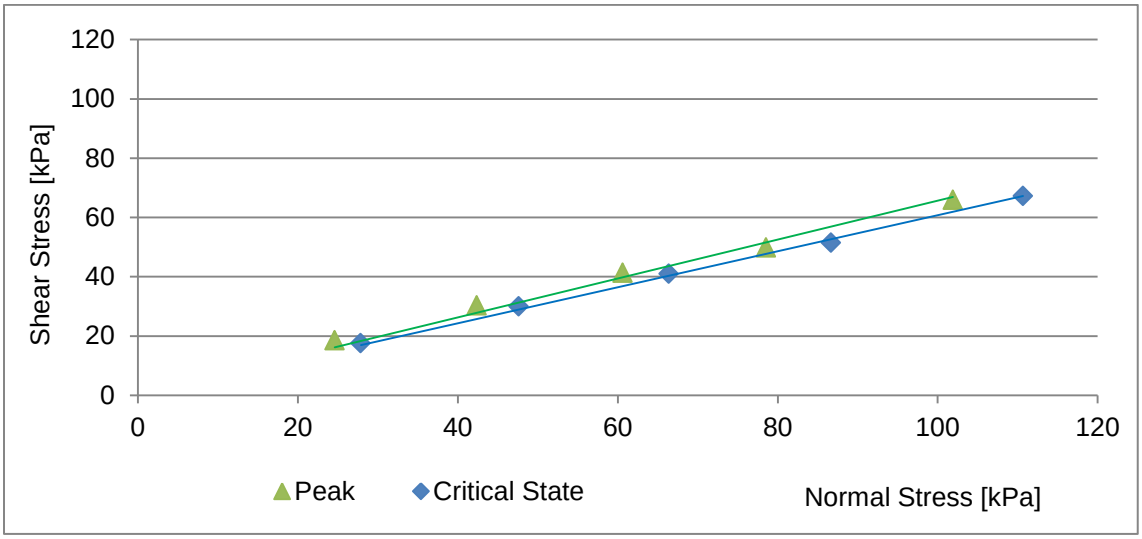

Figure A99 – Shear stress and normal stress

Test Description:	Direct Shear Box Test
Approximate Shear Rate:	1 mm/min
Sample Description:	Copper Porphyry #4
Top Size (mm):	-4
Moisture (%):	2.5
Determined k Value (mm):	1.08
Determined Peak Angle (degrees):	40.2
Determined Critical State Angle (degrees):	38.9
Determined Soil Type:	II

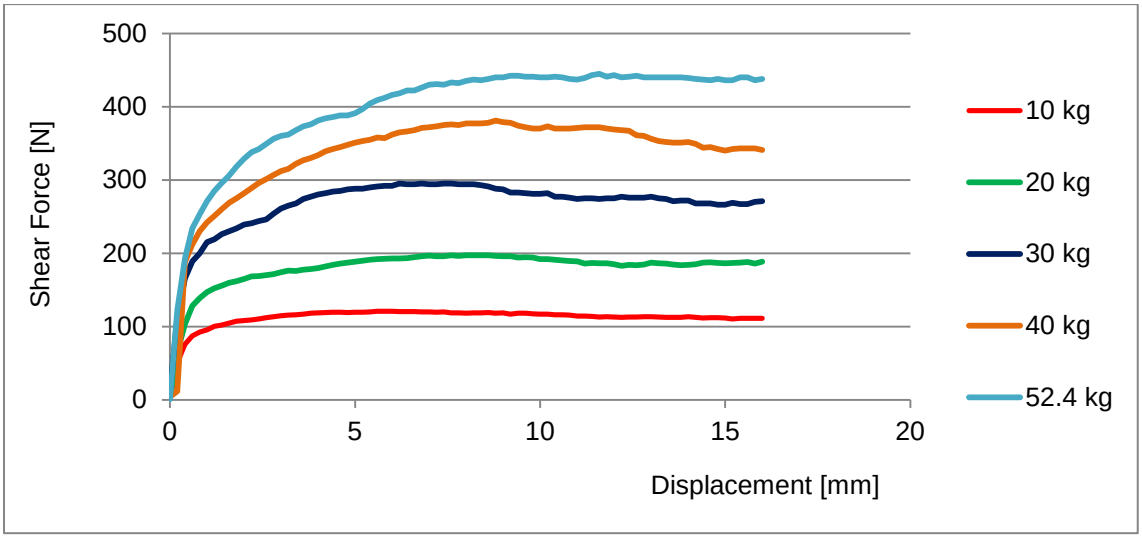

Figure A100 - Shear force and displacement

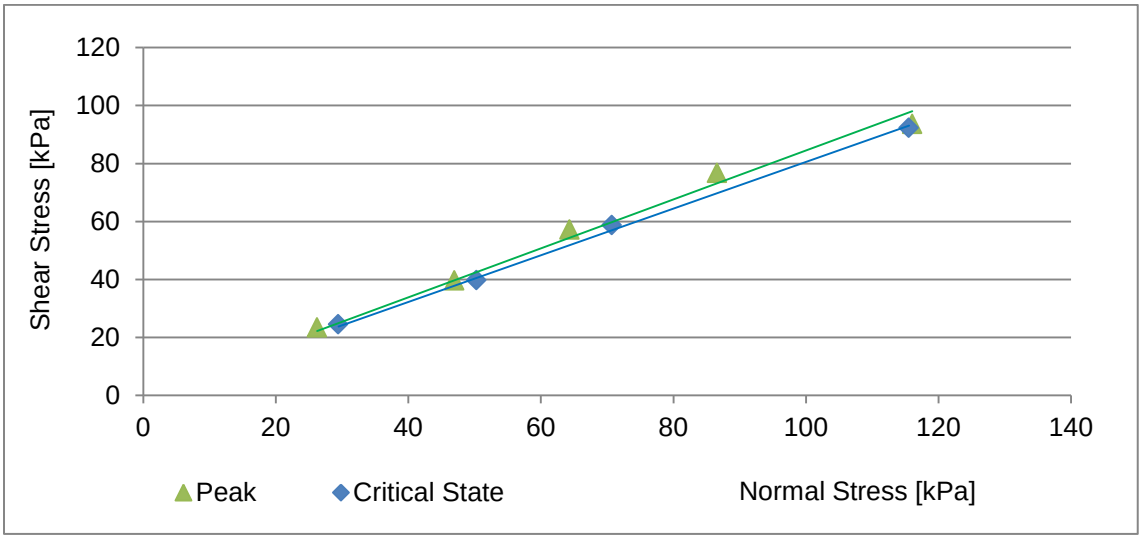

Figure A101 – Shear stress and normal stress

Test Description:	Direct Shear Box Test
Approximate Shear Rate:	1 mm/min
Sample Description:	Limestone & Dolomite
Top Size (mm):	-4
Moisture (%):	5
Determined k Value (mm):	0.44
Determined Peak Angle (degrees):	35.0
Determined Critical State Angle (degrees):	34.2
Determined Soil Type:	II

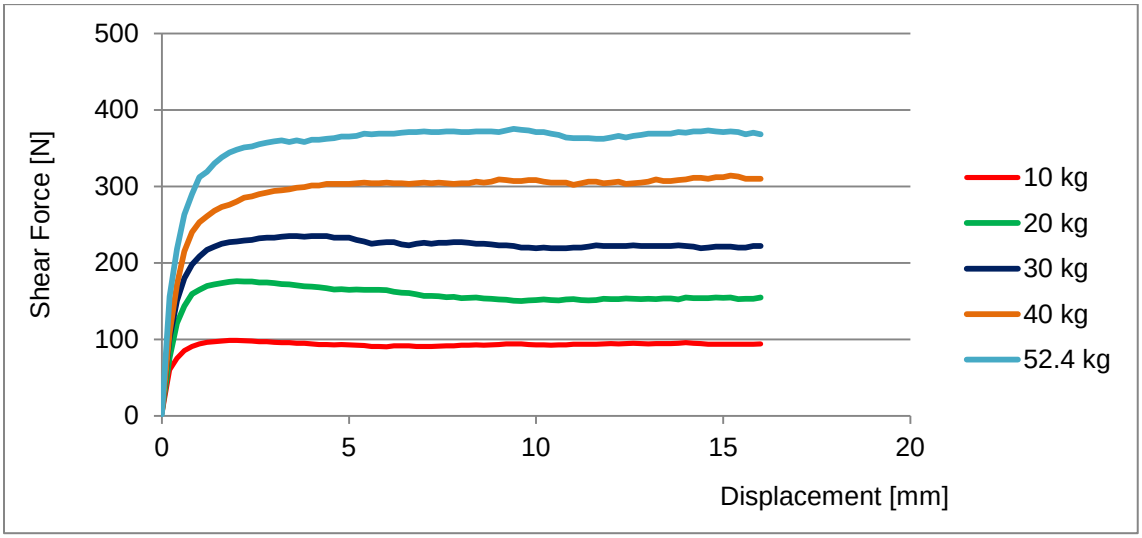

Figure A102 - Shear force and displacement

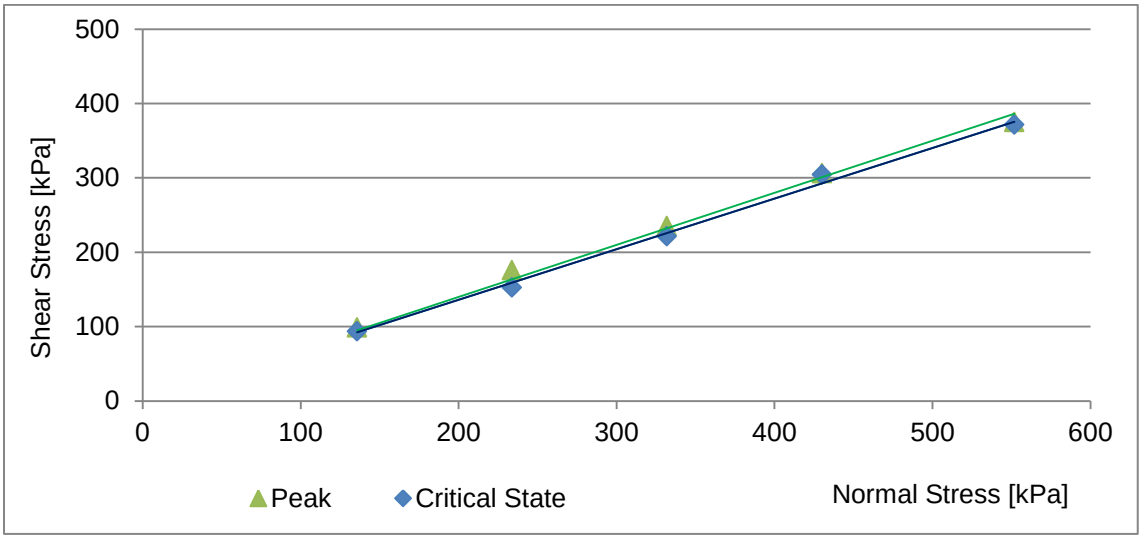

Figure A103 – Shear stress and normal stress

Test Description:	Direct Shear Box Test
Approximate Shear Rate:	1 mm/min
Sample Description:	Kimberlite #1
Top Size (mm):	-4
Moisture (%):	8
Determined k Value (mm):	1.08
Determined Peak Angle (degrees):	NA
Determined Critical State Angle (degrees):	40.4
Determined Soil Type:	Type I

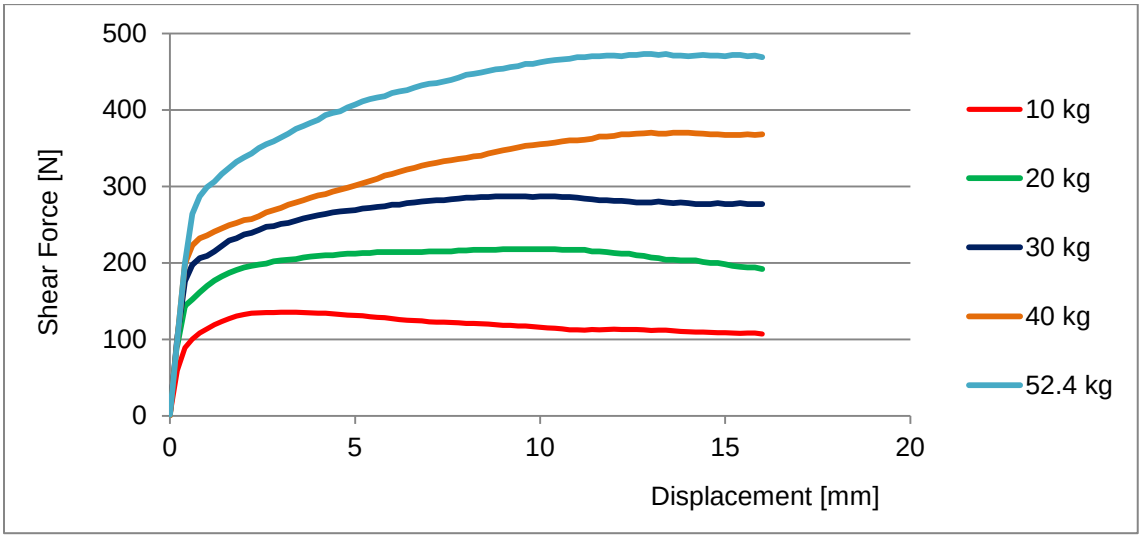

Figure A104 - Shear force and displacement

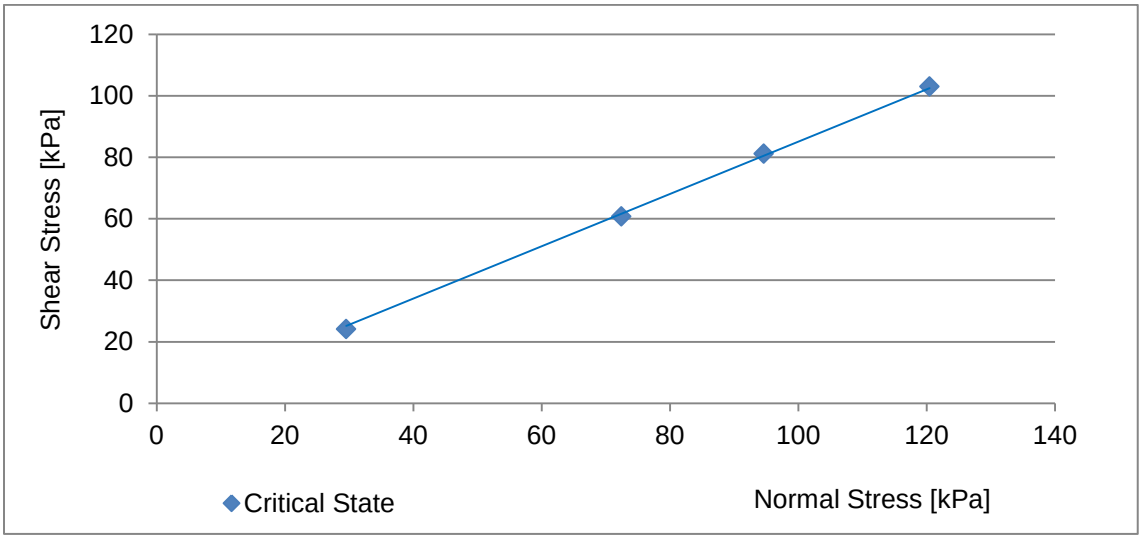

Figure A105 – Shear stress and normal stress

Test Description:	Direct Shear Box Test
Approximate Shear Rate:	1 mm/min
Sample Description:	Kimberlite #2
Top Size (mm):	-4
Moisture (%):	5
Determined k Value (mm):	0.53
Determined Peak Angle (degrees):	40.6
Determined Critical State Angle (degrees):	36.3
Determined Soil Type:	Type II

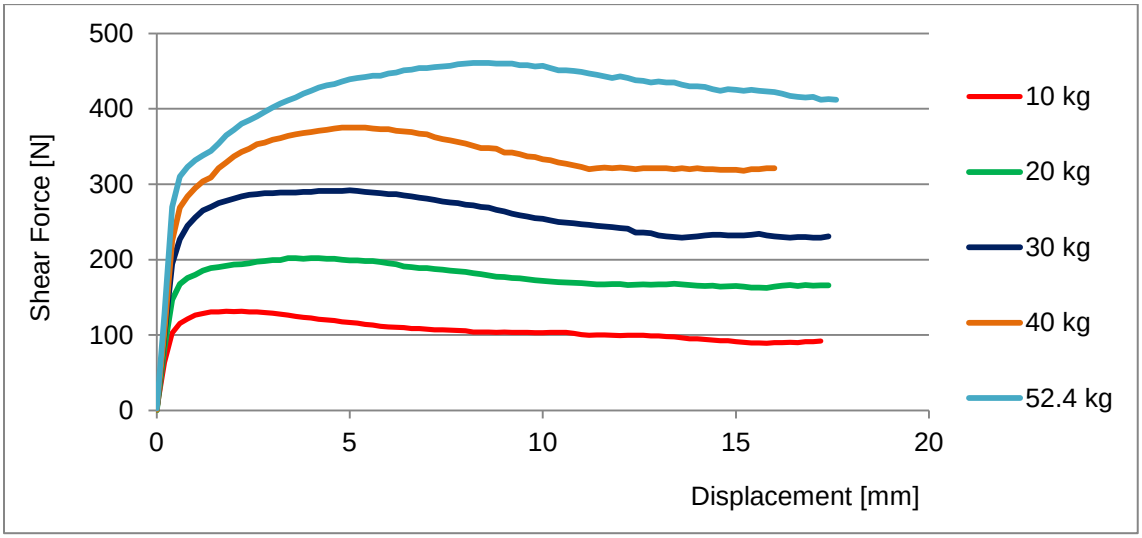

Figure A106 - Shear force and displacement

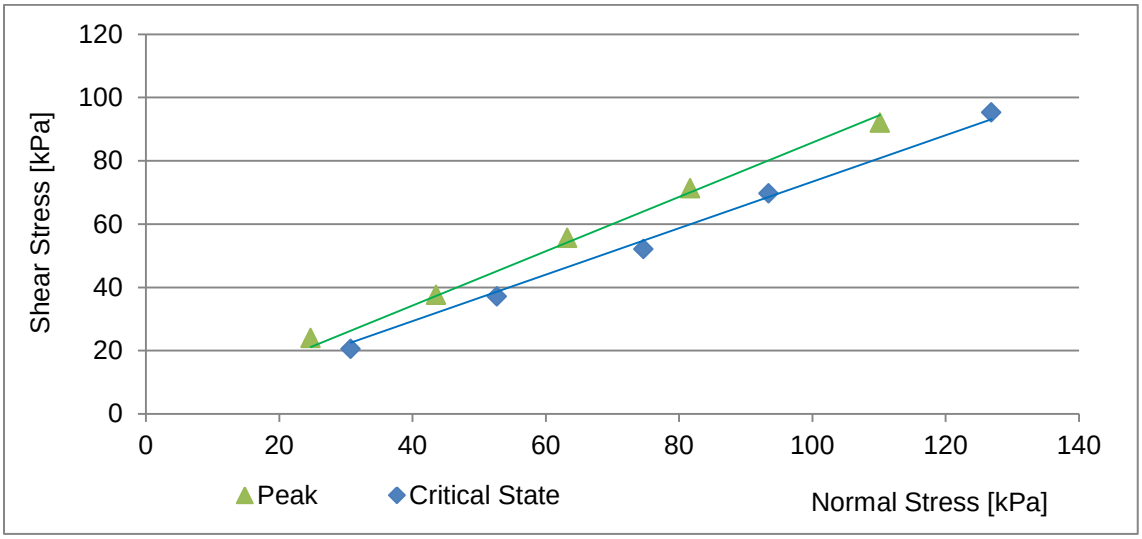

Figure A107 – Shear stress and normal stress

Test Summary	
Test Description:	Direct Shear Box Test
Approximate Shear Rate:	1 mm/min
Sample Description:	Copper Nickel
Top Size (mm):	-4 mm HPGR Product
Moisture (%):	0
Determined k Value (mm):	1.02
Determined Peak Angle (degrees):	NA
Determined Critical State Angle (degrees):	34.2
Determined Soil Type:	Type I

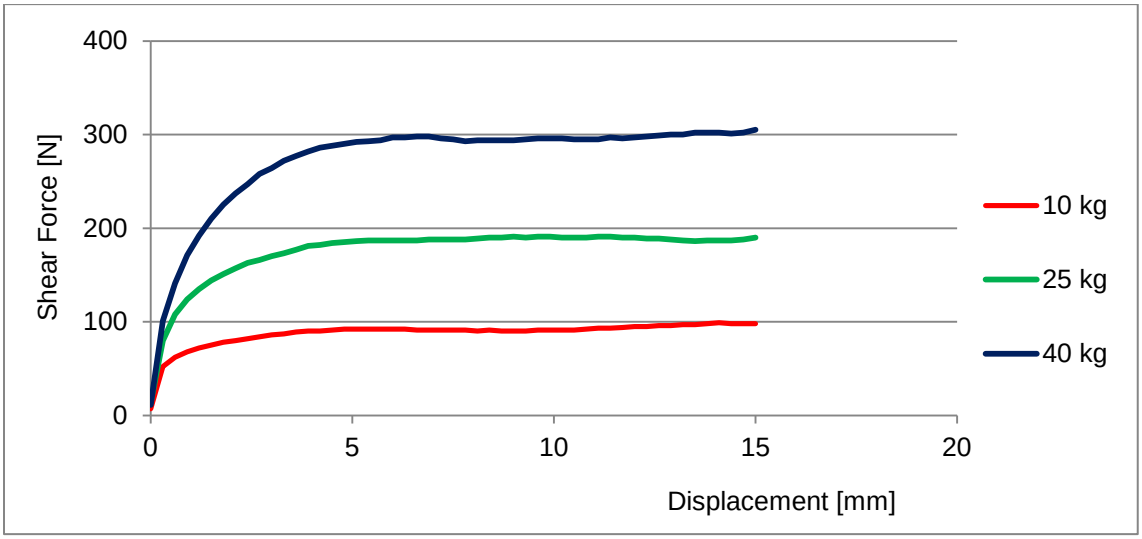

Figure A108 - Shear force and displacement

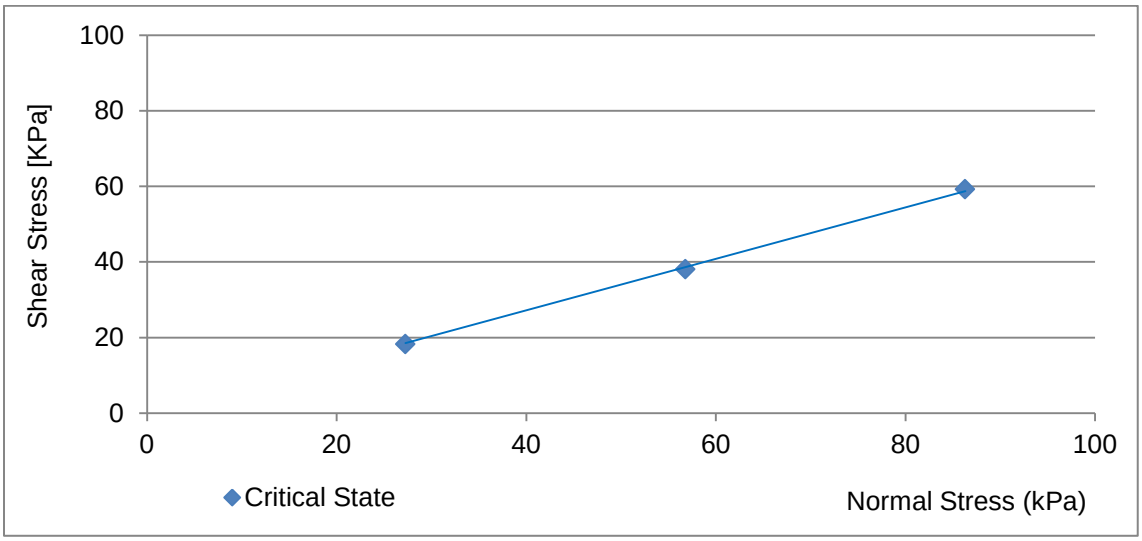

Figure A109 – Shear stress and normal stress

Test Summary	
Test Description:	Direct Shear Box Test
Approximate Shear Rate:	1 mm/min
Sample Description:	Copper Nickel
Top Size (mm):	-5.6 mm HPGR Product
Moisture (%):	0
Determined k Value (mm):	1.05
Determined Peak Angle (degrees):	NA
Determined Critical State Angle (degrees):	35.8
Determined Soil Type:	Type I

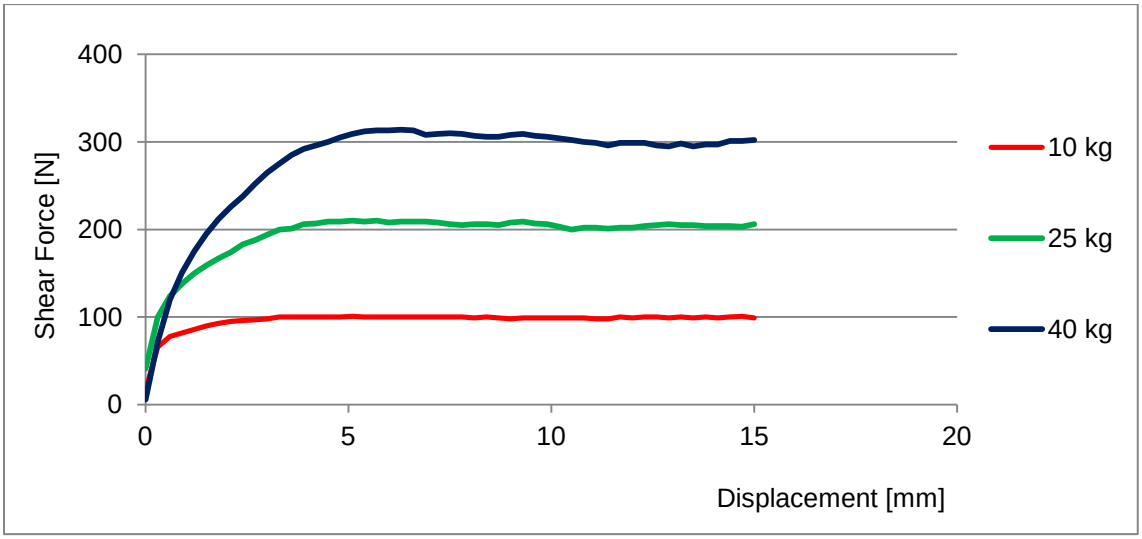

Figure A110 - Shear force and displacement

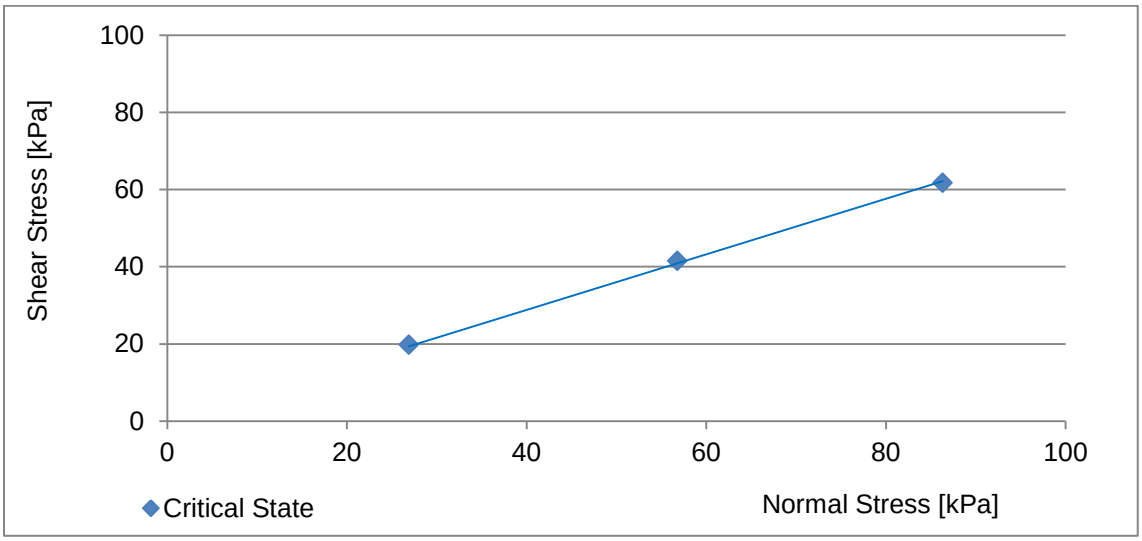

Figure A111 – Shear stress and normal stress

Test Summary	
Test Description:	Direct Shear Box Test
Approximate Shear Rate:	1 mm/min
Sample Description:	Copper Nickel
Top Size (mm):	-8 mm HPGR Product
Moisture (%):	0
Determined k Value (mm):	0.95
Determined Peak Angle (degrees):	NA
Determined Critical State Angle (degrees):	36.5
Determined Soil Type:	Type I

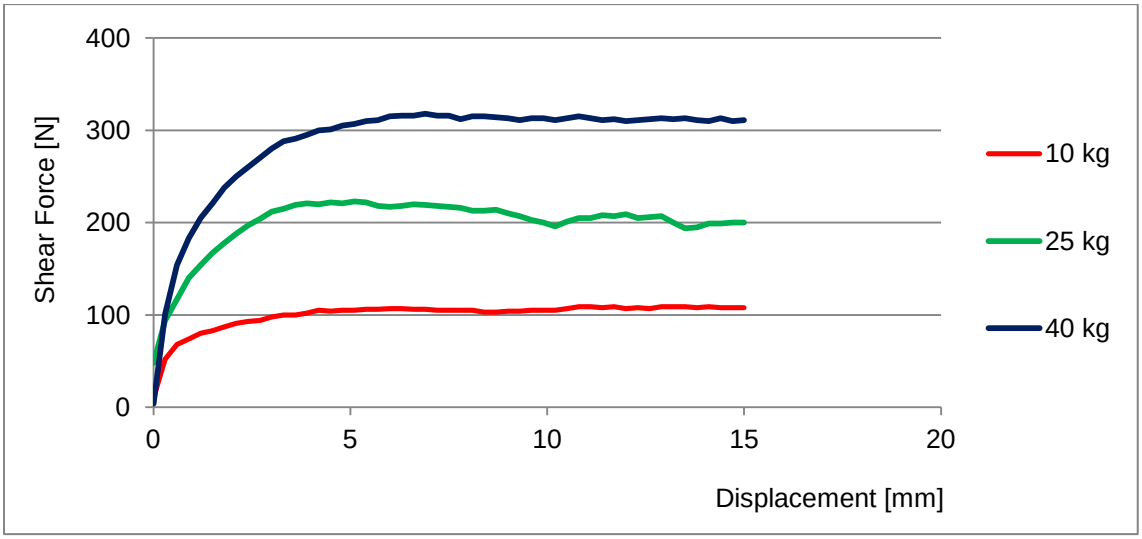

Figure A112 - Shear force and displacement

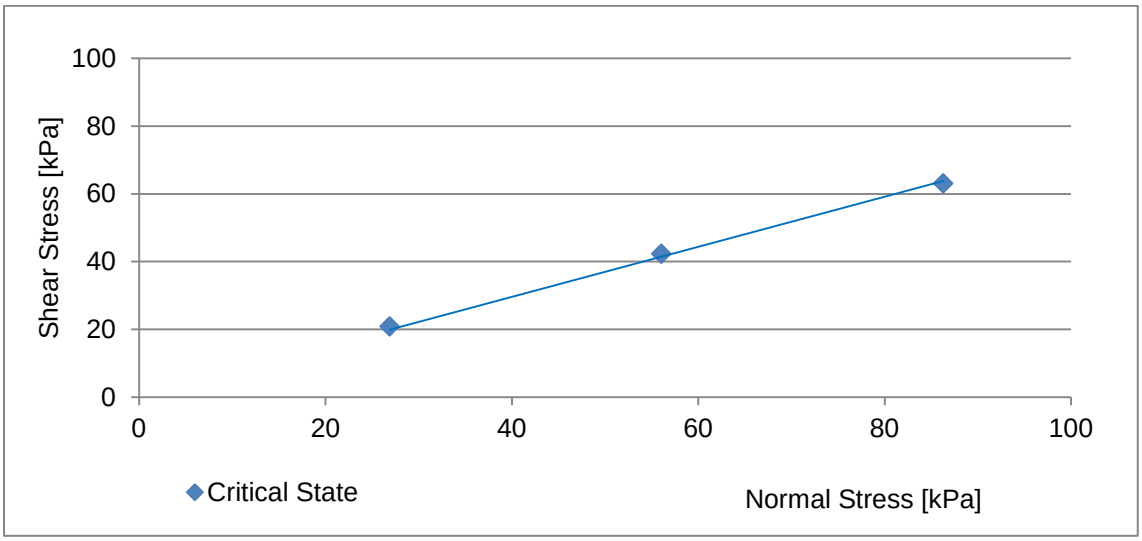

Figure A113 – Shear stress and normal stress

Appendix D: High Pressure Piston Press Results

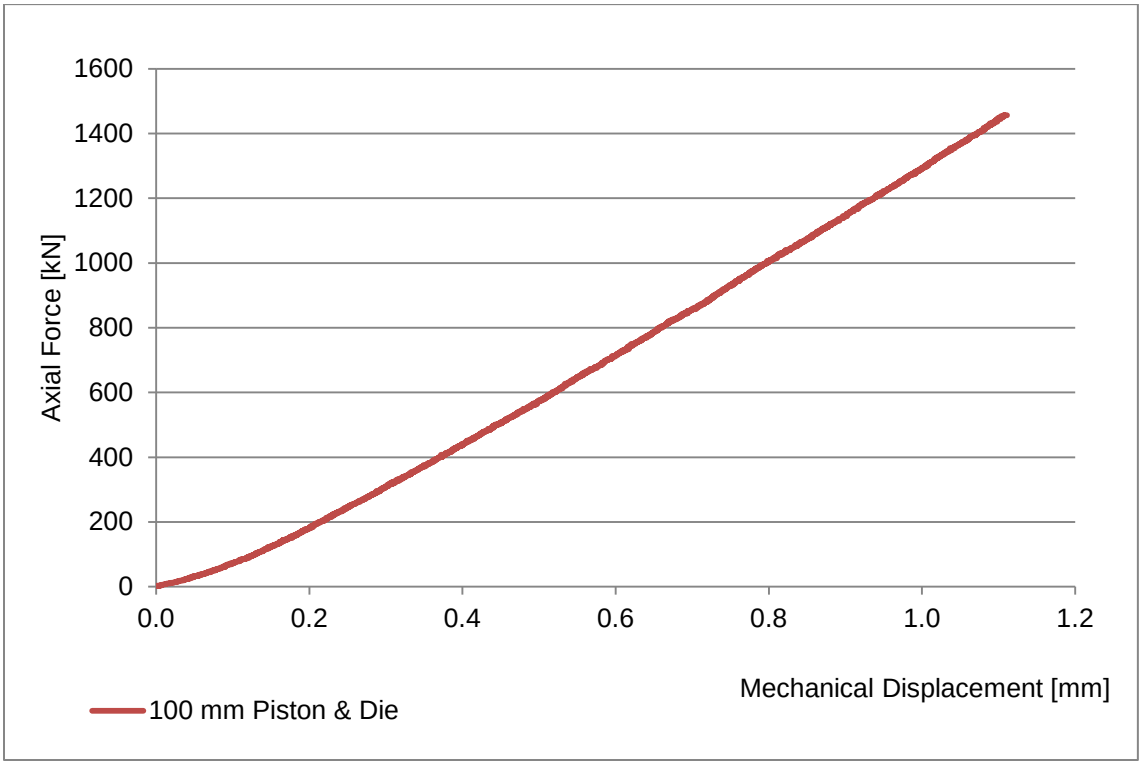

Figure A114 - Mechanical deflection of piston press equipment, 100 mm piston and die under load

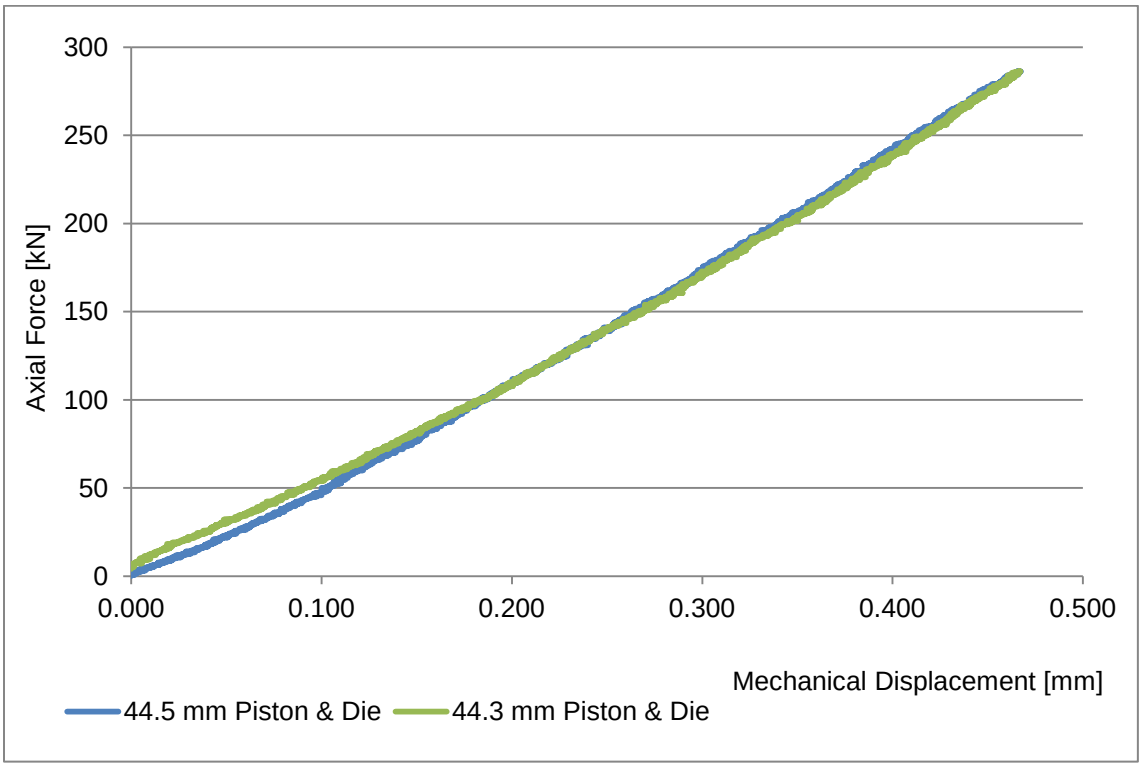

Figure A115 - Mechanical deflection of piston press equipment, 45 mm piston and die under load

Test Summary	
Test Description:	100 mm diameter piston tests
Approximate Test Time (min):	13
Sample Description:	Copper Porphyry #1
Top Size (mm):	-4
Moisture (%):	0 & 2.5

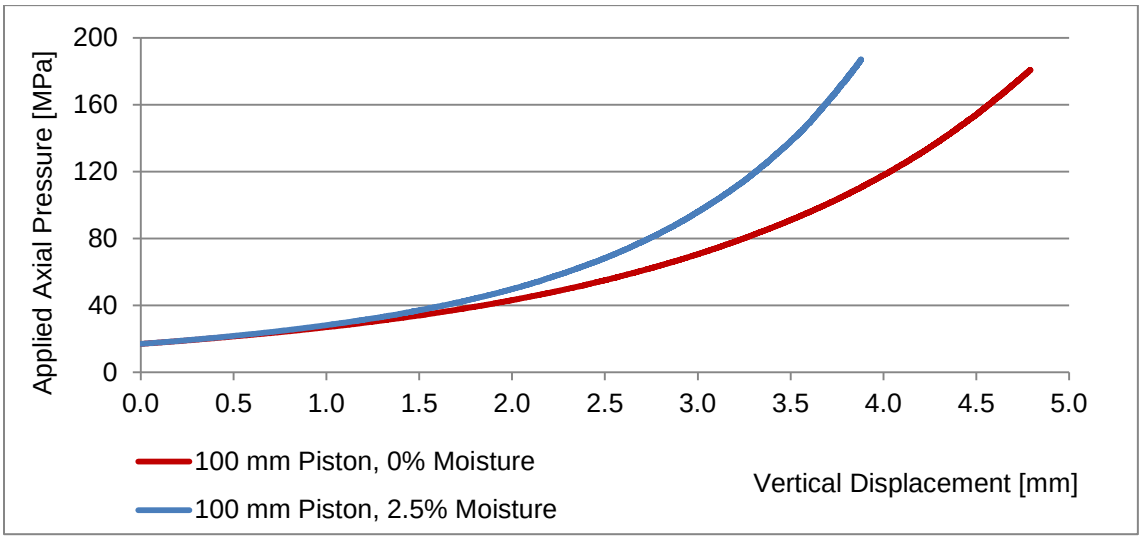

Figure A116 - Net displacement of sample under pressure in 100 mm piston & die

Test Summary	
Test Description:	45 & 100 mm diameter piston tests
Approximate Test Time (min):	13
Sample Description:	Dolomite and limestone
Top Size (mm):	-4
Moisture (%):	3.6

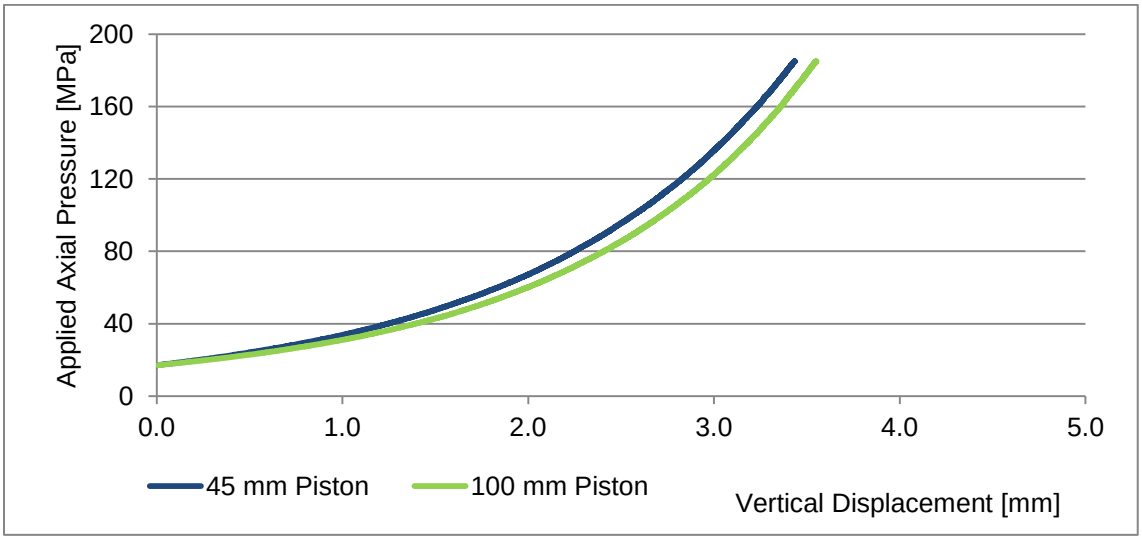

Figure A117 - Net displacement of sample under pressure

Test Summary	
Test Description:	45 & 100 mm diameter piston tests
Approximate Test Time (min):	13
Sample Description:	Dolomite
Top Size (mm):	-4
Moisture (%):	3.6

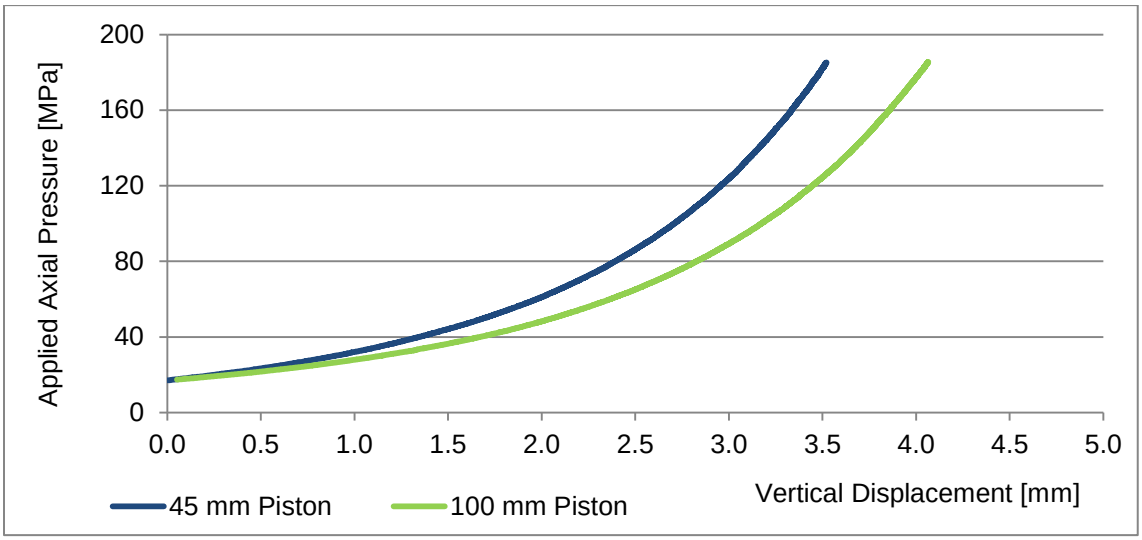

Figure A118 - Net displacement of sample under pressure

Test Summary	
Test Description:	45 & 100 mm diameter piston tests
Approximate Test Time (min):	13
Sample Description:	Quartz
Top Size (mm):	-4
Moisture (%):	2.3

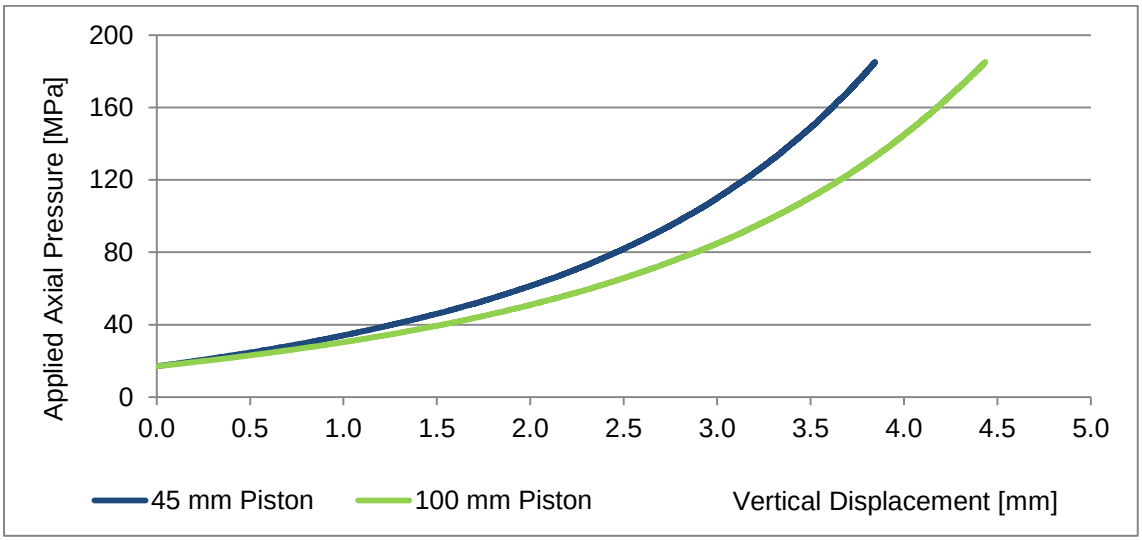

Figure A119 - Net displacement of sample under pressure

Test Summary	
Test Description:	45 & 100 mm diameter piston tests
Approximate Test Time (min):	13
Sample Description:	Copper Porphyry #2
Top Size (mm):	-4
Moisture (%):	5

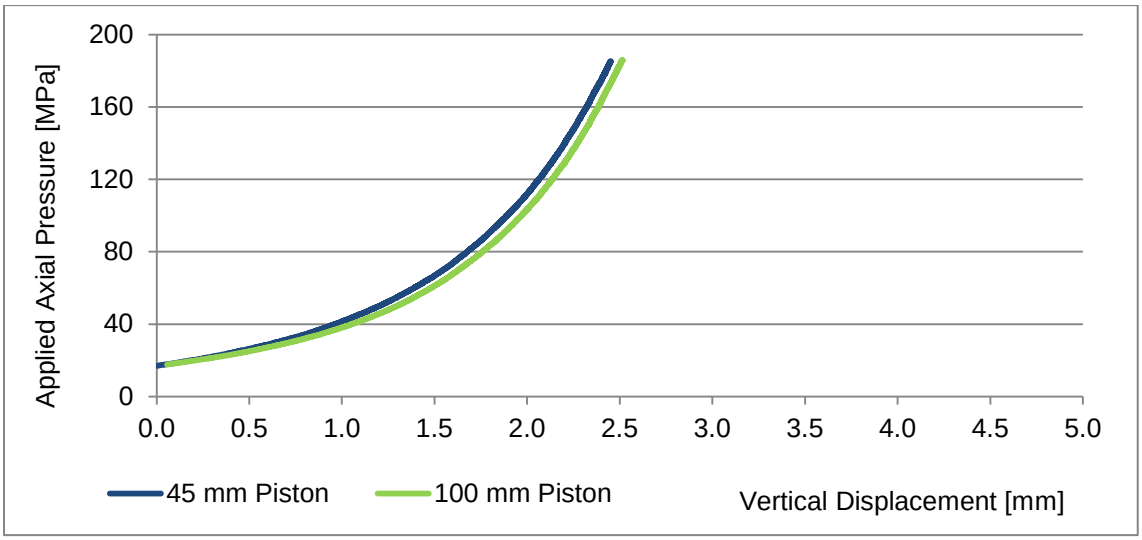

Figure A120 - Net displacement of sample under pressure

Test Summary	
Test Description:	45 & 100 mm diameter piston tests
Approximate Test Time (min):	13
Sample Description:	Copper Porphyry #2
Top Size (mm):	-4
Moisture (%):	2.5

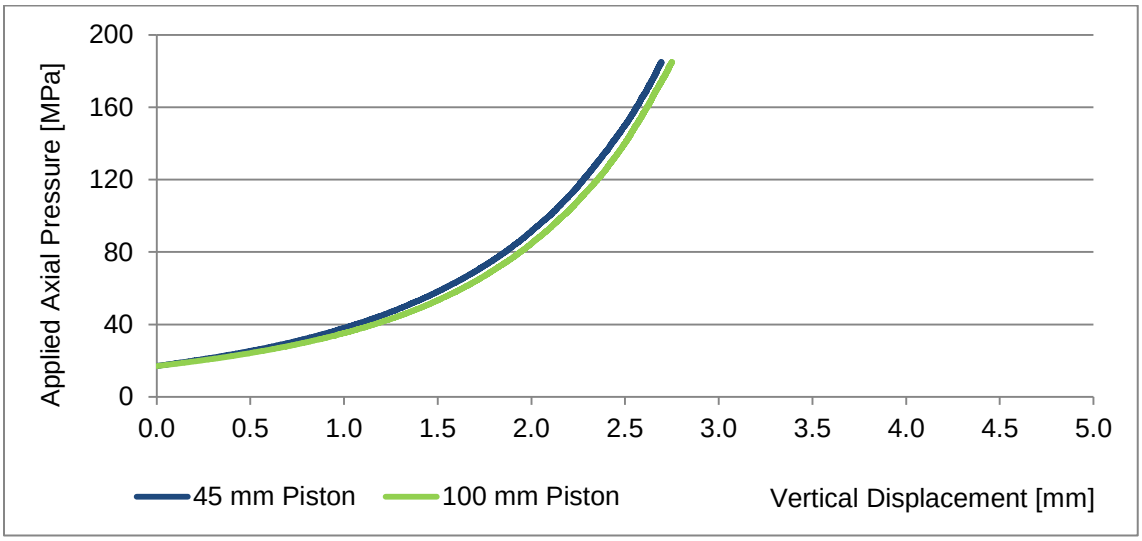

Figure A121 - Net displacement of sample under pressure

Test Summary

Test Description:	45 & 100 mm diameter piston tests
Approximate Test Time (min):	13
Sample Description:	Limestone
Top Size (mm):	-4
Moisture (%):	2.4

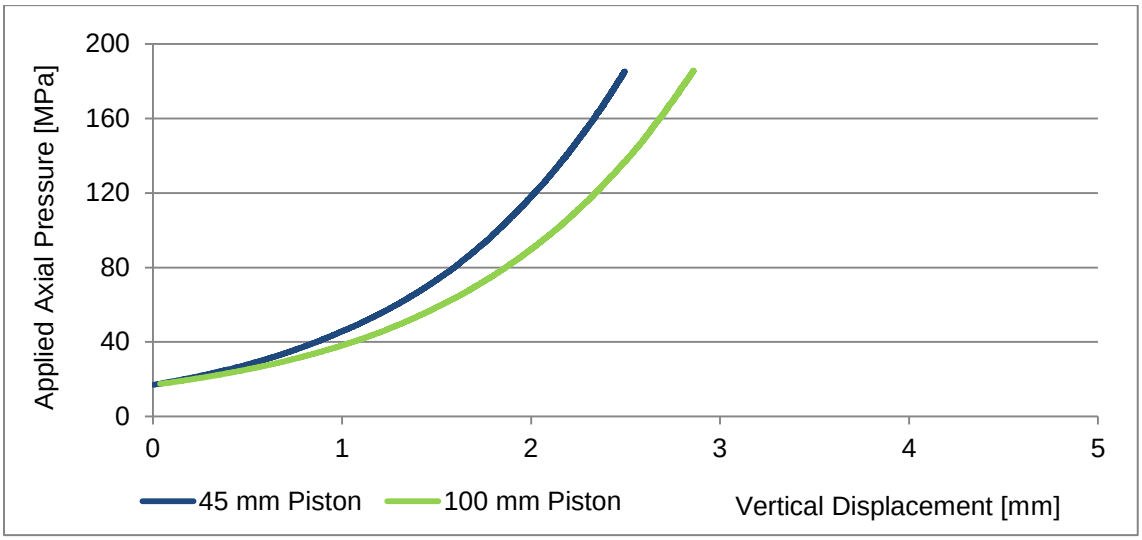

Figure A122 - Net displacement of sample under pressure

Test Summary

Test Description:	45 & 100 mm diameter piston tests
Approximate Test Time (min):	13
Sample Description:	Limestone
Top Size (mm):	-4
Moisture (%):	5

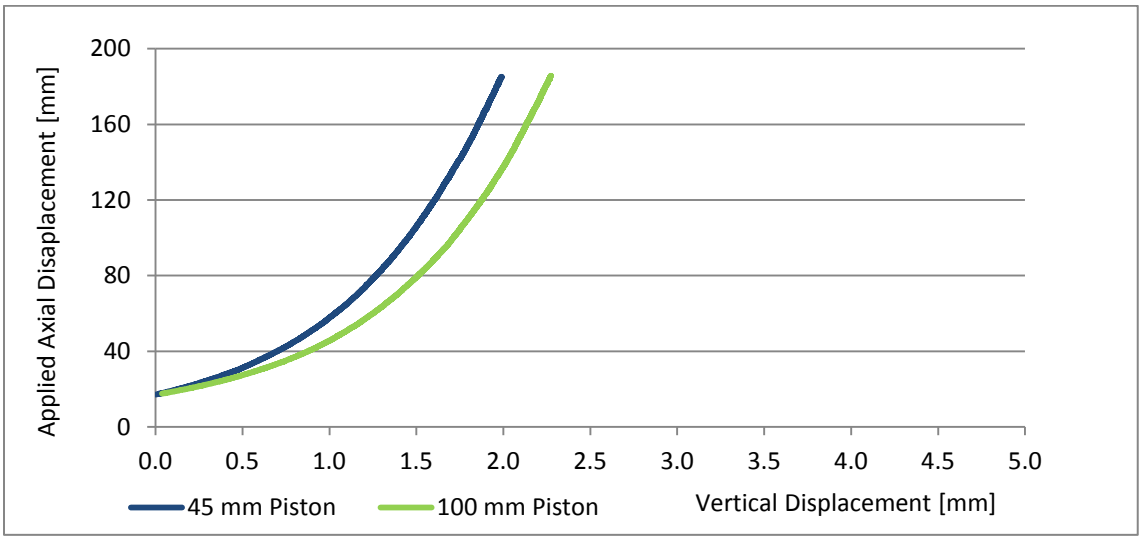

Figure A123 - Net displacement of sample under pressure

Test Summary	
Test Description:	45 & 100 mm diameter piston tests
Approximate Test Time (min):	13
Sample Description:	Limestone
Top Size (mm):	-4
Moisture (%):	10

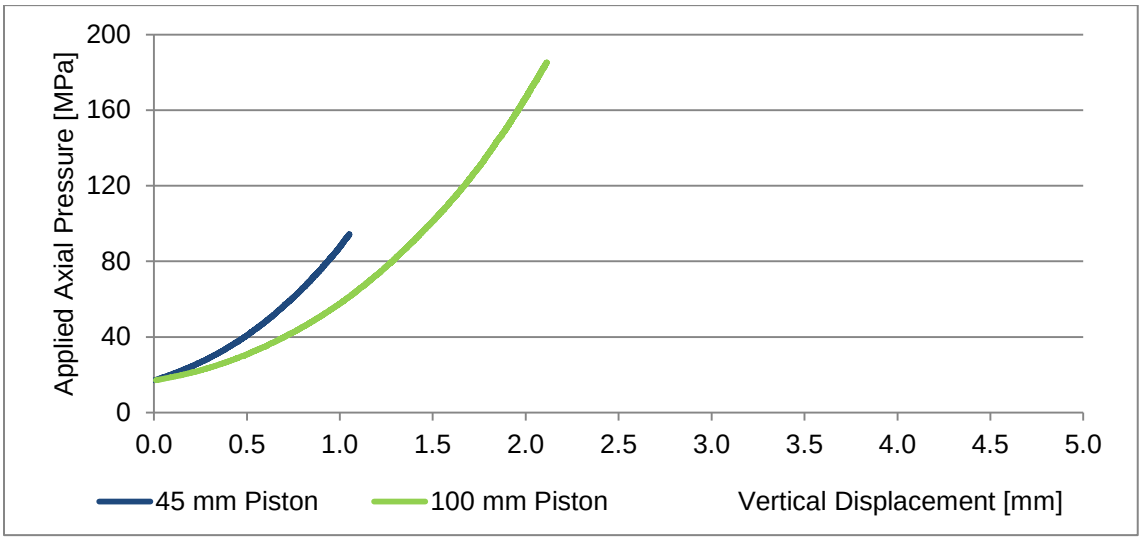

Figure A124 - Net displacement of sample under pressure

Test Summary	
Test Description:	45 & 100 mm diameter piston tests
Approximate Test Time (min):	13
Sample Description:	Taconite
Top Size (mm):	-4
Moisture (%):	0

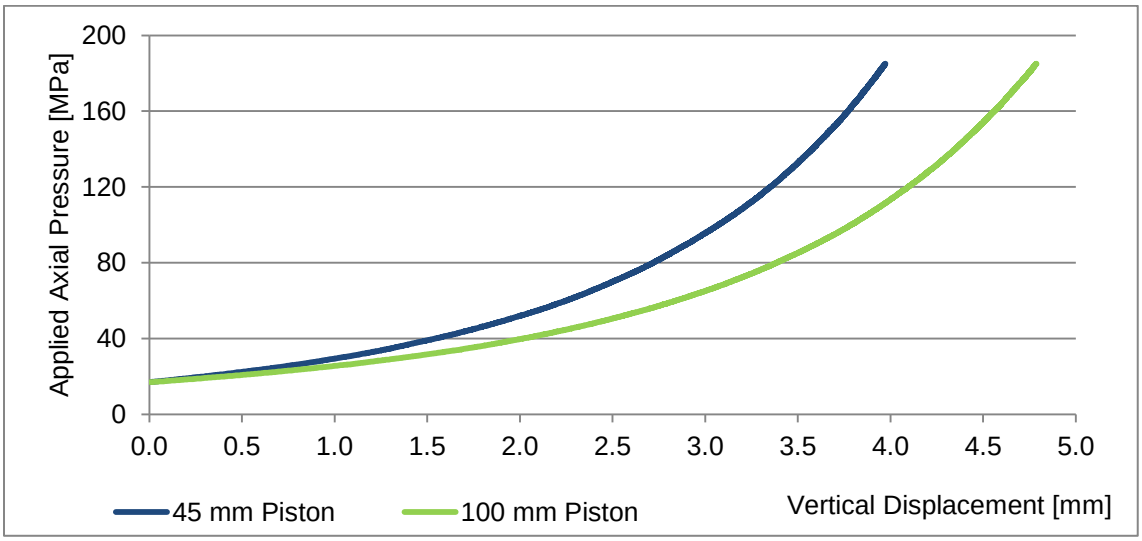

Figure A125 - Net displacement of sample under pressure

Test Summary	
Test Description:	45 & 100 mm diameter piston tests
Approximate Test Time (min):	13
Sample Description:	Taconite
Top Size (mm):	-4
Moisture (%):	2

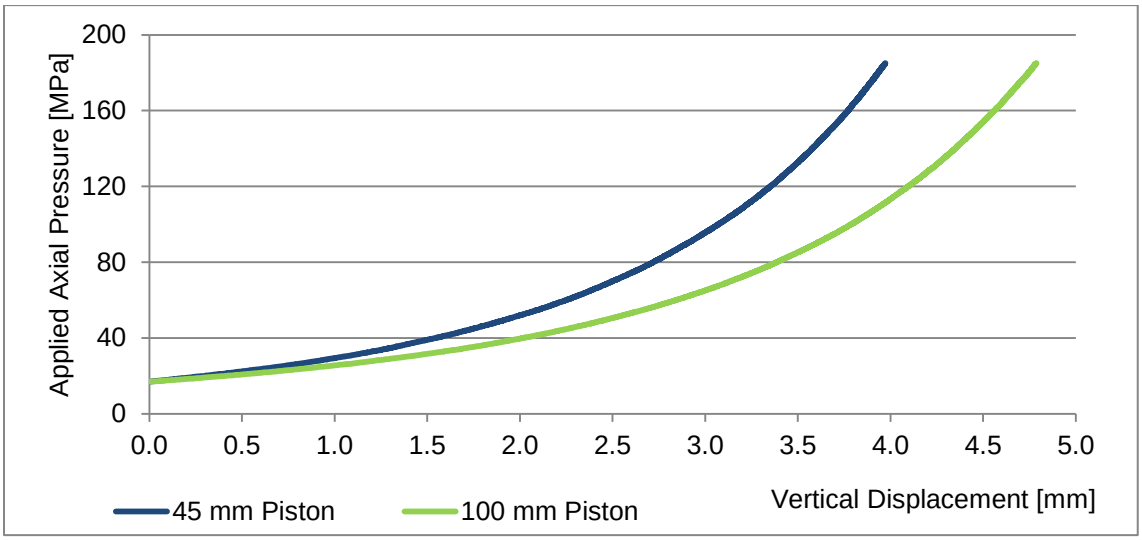

Figure A126 - Net displacement of sample under pressure

Test Summary	
Test Description:	45 & 100 mm diameter piston tests
Approximate Test Time (min):	13
Sample Description:	Copper Nickel
Top Size (mm):	-4
Moisture (%):	2.5

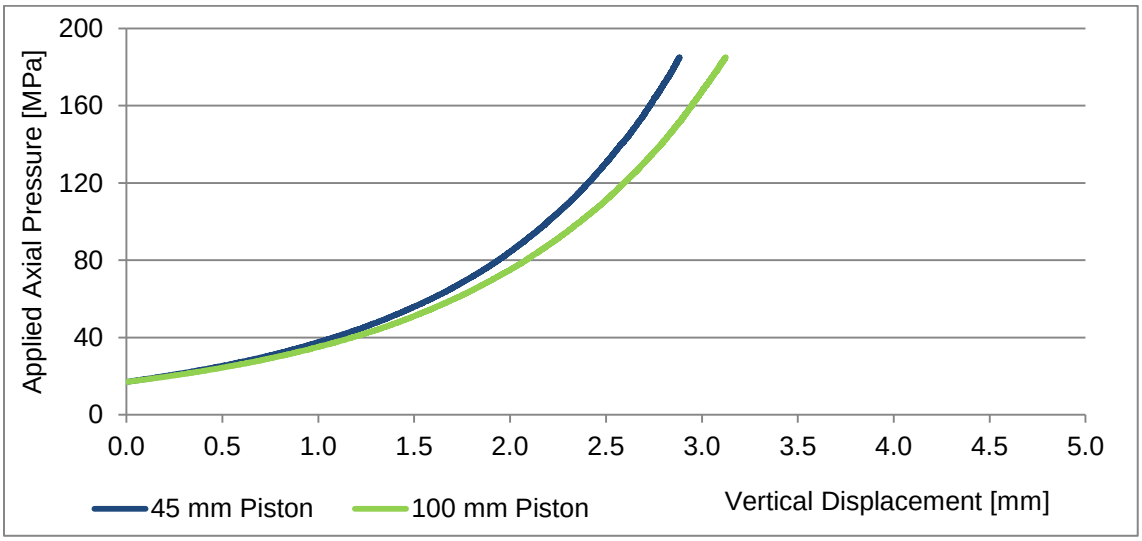

Figure A127 - Net displacement of sample under pressure

Test Summary

Test Description:	45 & 100 mm diameter piston tests
Approximate Test Time (min):	13
Sample Description:	Copper Nickel
Top Size (mm):	-4
Moisture (%):	5

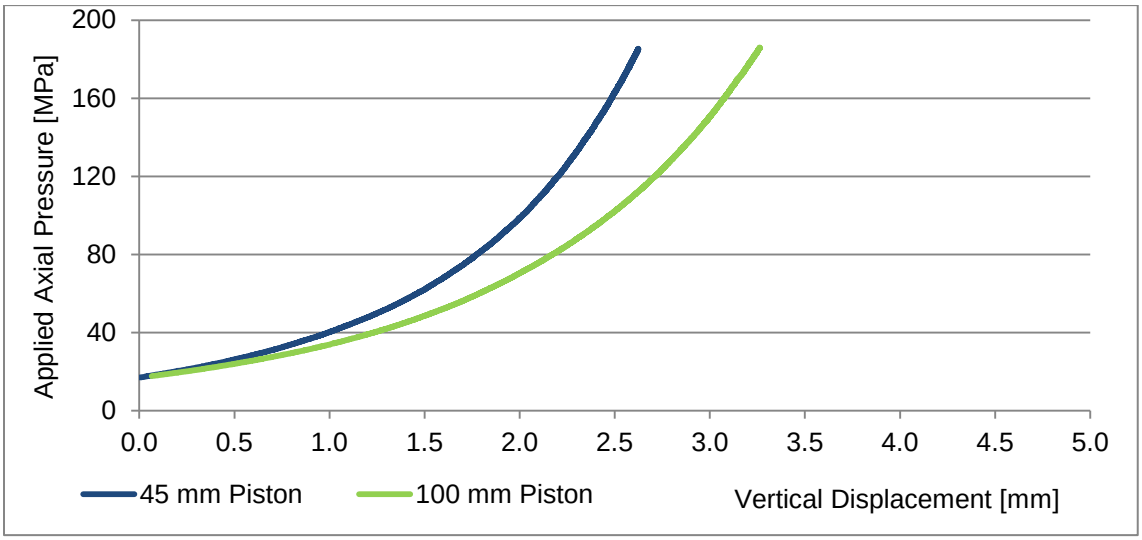

Figure A128 - Net displacement of sample under pressure

Test Summary

Test Description:	100 mm diameter piston test
Approximate Test Time (min):	13
Sample Description:	Mafic / Ultra-Mafic
Top Size (mm):	-4
Moisture (%):	3.5

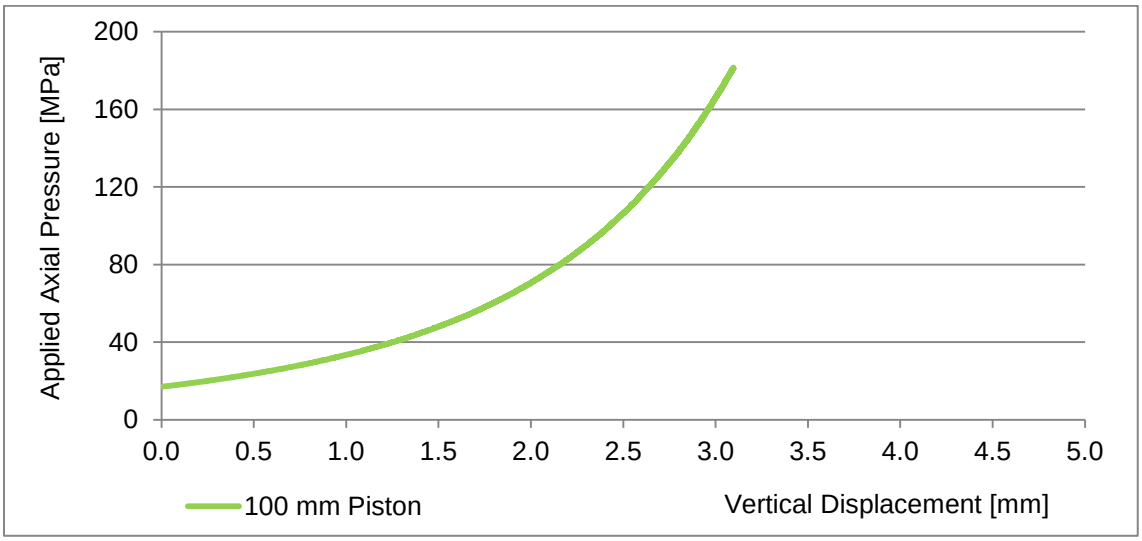

Figure A129 - Net displacement of sample under pressure

Test Summary	
Test Description:	45 & 100 mm diameter piston tests
Approximate Test Time (min):	13
Sample Description:	Steel Balls
Top Size (mm):	-4
Moisture (%):	0

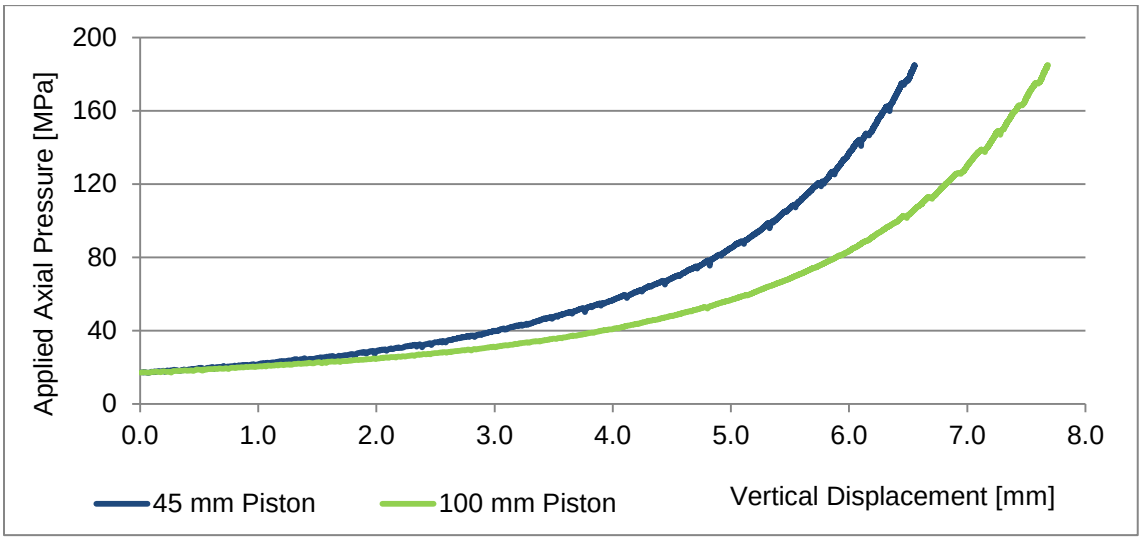

Figure A130 - Net displacement of sample under pressure

Test Summary	
Test Description:	45 & 100 mm diameter piston tests
Approximate Test Time (min):	13
Sample Description:	Copper Porphyry #3
Top Size (mm):	-4
Moisture (%):	2.5

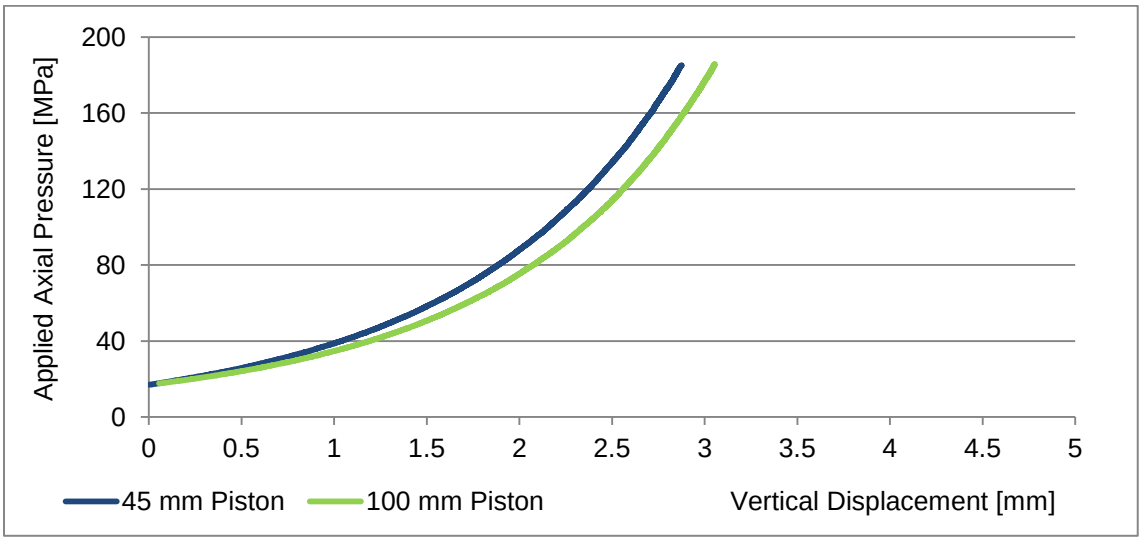

Figure A131 - Net displacement of sample under pressure

Test Summary

Test Description:	45 & 100 mm diameter piston tests
Approximate Test Time (min):	13
Sample Description:	Copper Porphyry #4
Top Size (mm):	-4
Moisture (%):	2.5

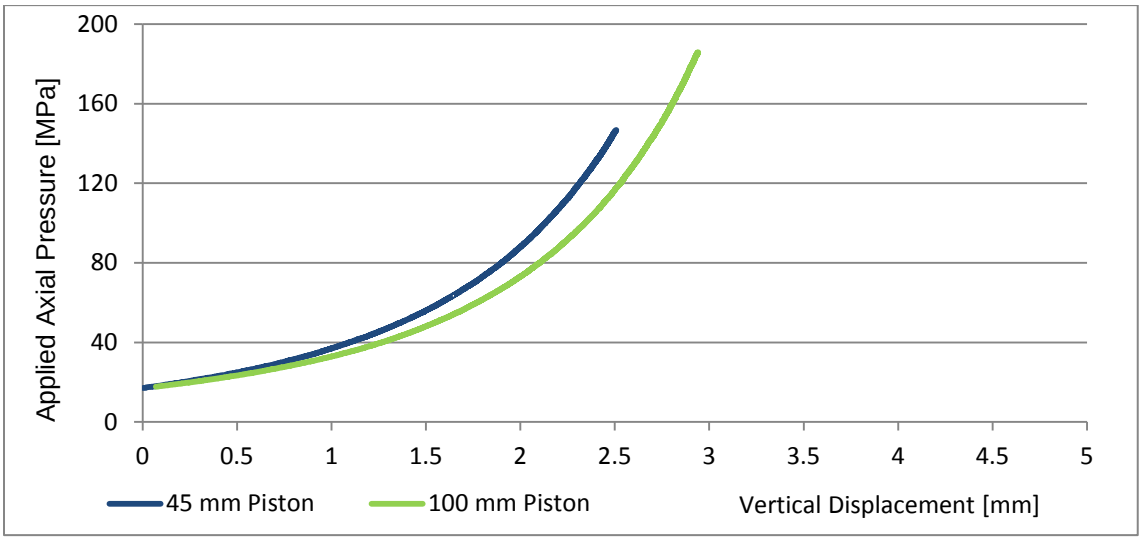

Figure A132 - Net displacement of sample under pressure

Test Summary

Test Description:	100 mm diameter piston test
Approximate Test Time (min):	13
Sample Description:	Kimberlite #1
Top Size (mm):	-4
Moisture (%):	8

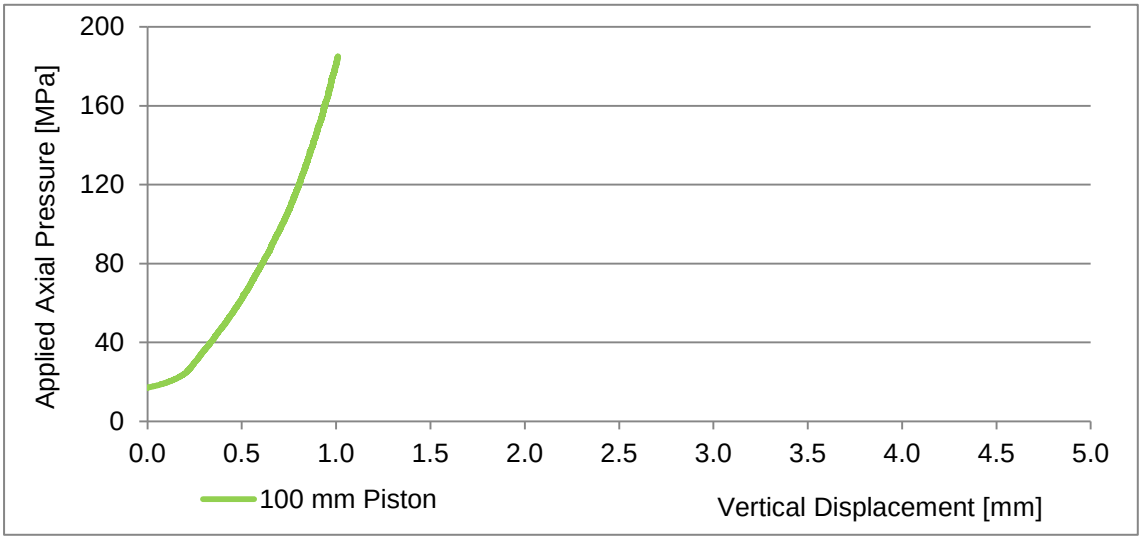

Figure A133 - Net displacement of sample under pressure

Test Summary

Test Description:	45 & 100 mm diameter piston tests
Approximate Test Time (min):	13
Sample Description:	Volcanogenic Gold
Top Size (mm):	-4
Moisture (%):	2.5

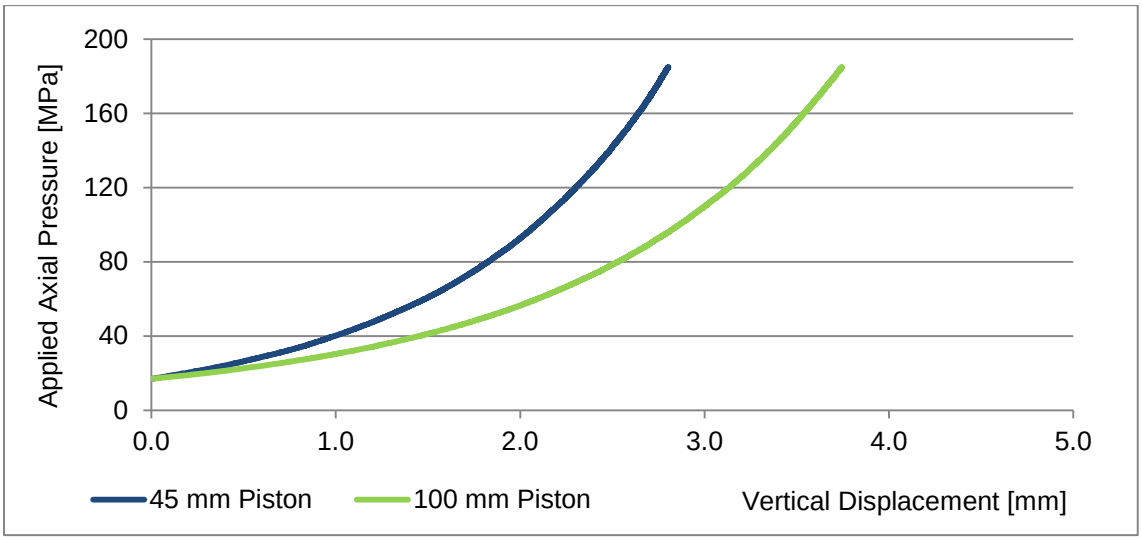

Figure A134 - Net displacement of sample under pressure

Appendix E: Low Pressure Piston Press Results

Test Summary	
Test Description:	100 mm diameter piston test
Displacement Rate (mm/min):	2
Sample Description:	Copper Porphyry #1
Top Size (mm):	-4
Moisture (%):	0.9

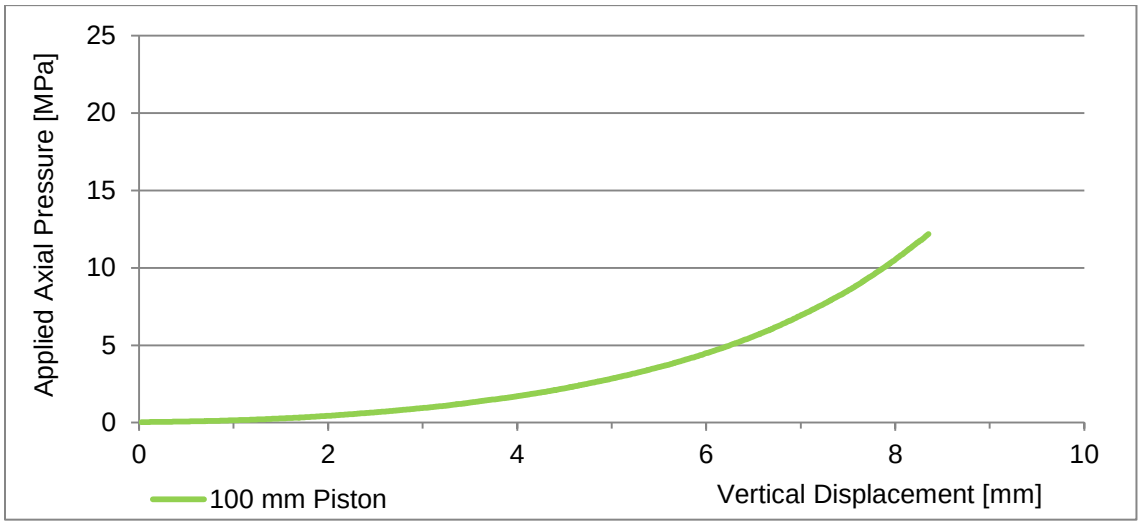

Figure A135 - Net displacement of sample under pressure

Test Summary	
Test Description:	100 mm diameter piston test
Displacement Rate (mm/min):	2
Sample Description:	Copper Porphyry #1
Top Size (mm):	-4
Moisture (%):	2.5

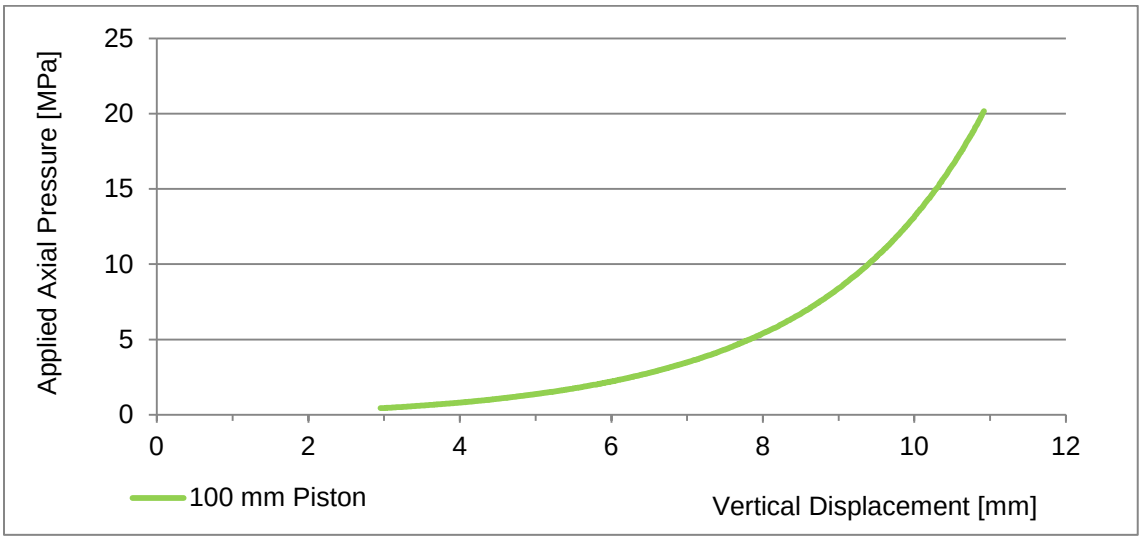

Figure A136 - Net displacement of sample under pressure

Test Summary

Test Description:	100 mm diameter piston test
Displacement Rate (mm/min):	2
Sample Description:	Dolomite
Top Size (mm):	-4
Moisture (%):	3.6

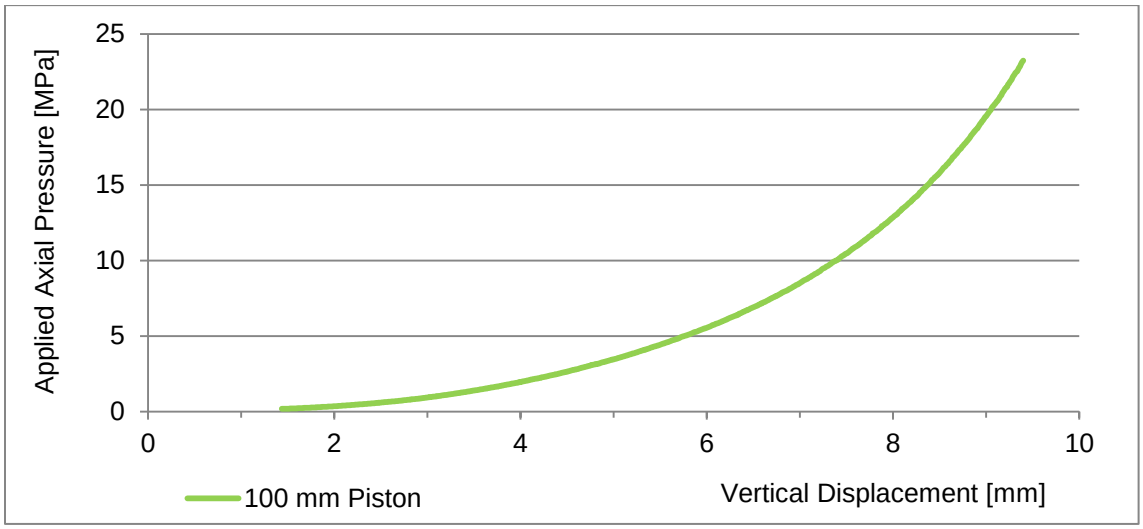

Figure A137 - Net displacement of sample under pressure

Test Summary

Test Description:	45 & 100 mm diameter piston tests
Displacement Rate (mm/min):	2
Sample Description:	Copper Porphyry #2
Top Size (mm):	-4
Moisture (%):	2.5

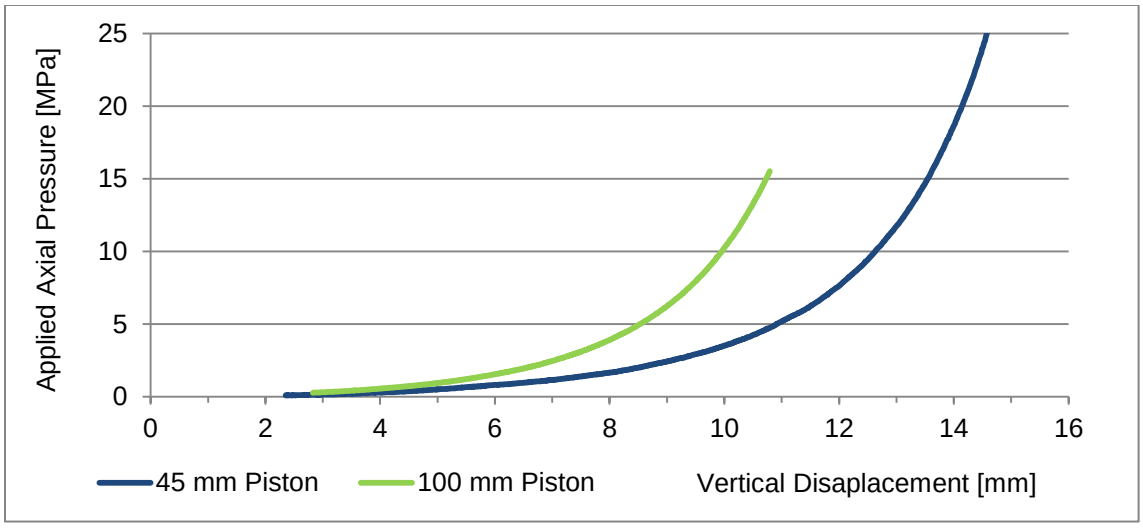

Figure A138 - Net displacement of sample under pressure

Test Summary	
Test Description:	45 & 100 mm diameter piston tests
Displacement Rate (mm/min):	2
Sample Description:	Copper Nickel
Top Size (mm):	-4
Moisture (%):	1

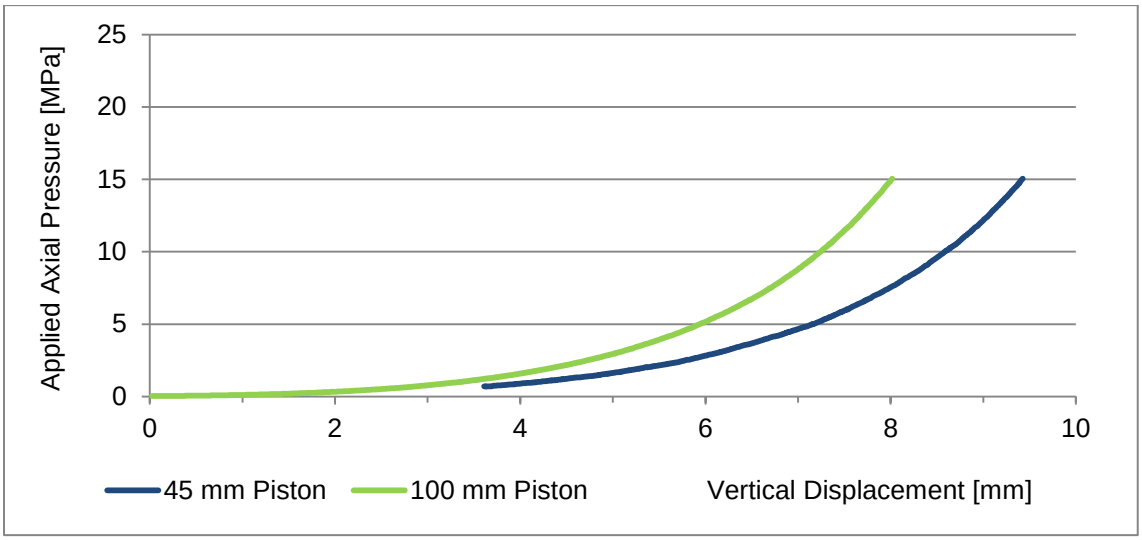

Figure A139 - Net displacement of sample under pressure

Test Summary	
Test Description:	45 & 100 mm diameter piston tests
Displacement Rate (mm/min):	2
Sample Description:	Copper Nickel
Top Size (mm):	-4
Moisture (%):	2.5

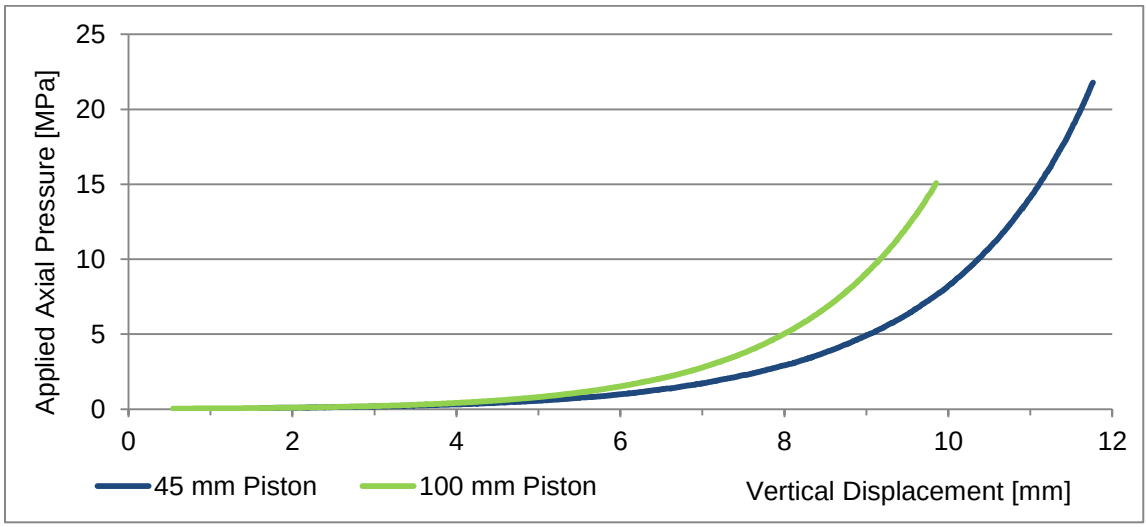

Figure A140 - Net displacement of sample under pressure

Test Summary

Test Description:	45 & 100 mm diameter piston tests
Displacement Rate (mm/min):	2
Sample Description:	Copper Nickel
Top Size (mm):	-4
Moisture (%):	5

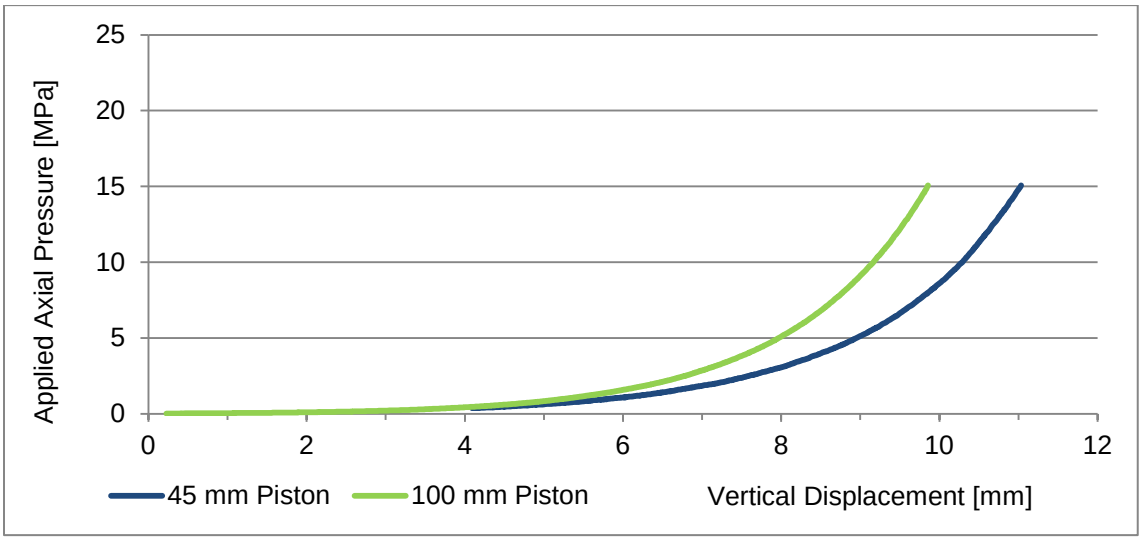

Figure A141 - Net displacement of sample under pressure

Test Summary

Test Description:	100 mm diameter piston test
Displacement Rate (mm/min):	2
Sample Description:	Taconite
Top Size (mm):	-4
Moisture (%):	2

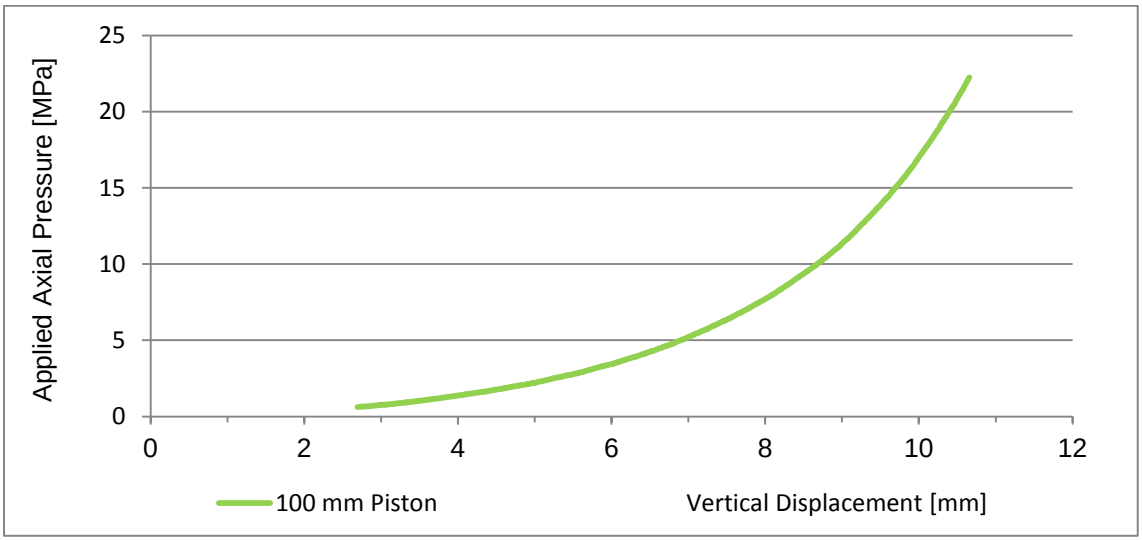

Figure A142 - Net displacement of sample under pressure

Test Summary	
Test Description:	100 mm diameter piston test
Displacement Rate (mm/min):	2
Sample Description:	Mafic /Ultra-Mafic
Top Size (mm):	-4
Moisture (%):	2.4

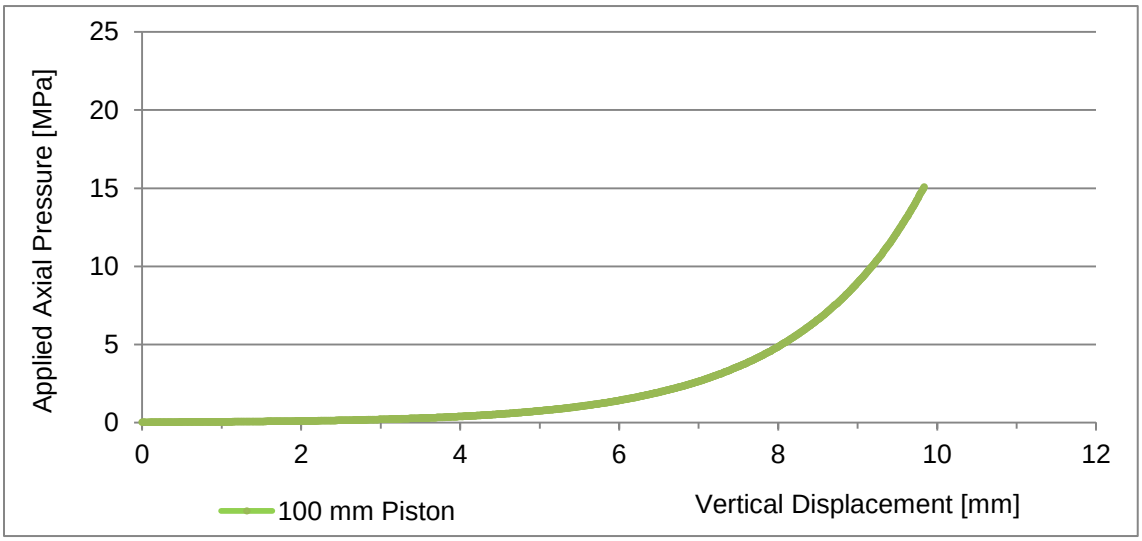

Figure A143 - Net displacement of sample under pressure

Test Summary

Test Description:	45 & 100 mm diameter piston tests
Displacement Rate (mm/min):	2
Sample Description:	Mafic /Ultra-Mafic
Top Size (mm):	-4
Moisture (%):	3.3

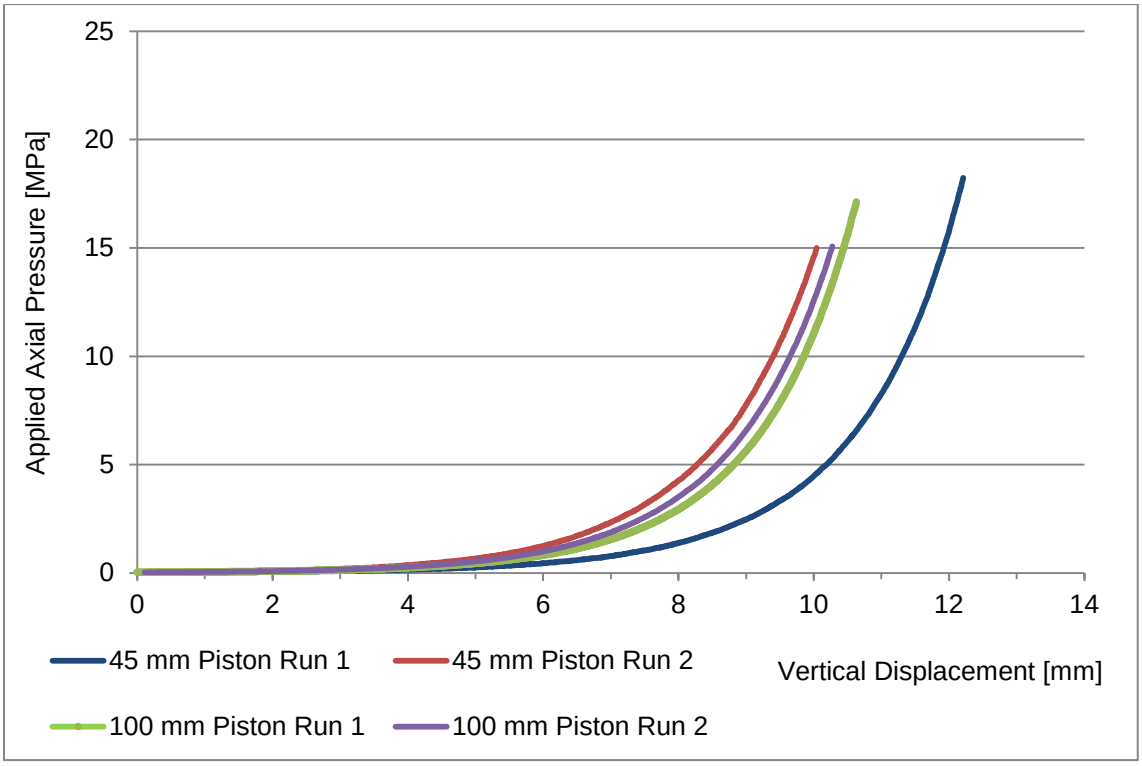

Figure A144 - Net displacement of sample under pressure

Test Summary

Test Description:	100 mm diameter piston test
Displacement Rate (mm/min):	2
Sample Description:	Mafic /Ultra-Mafic
Top Size (mm):	-4
Moisture (%):	5.2

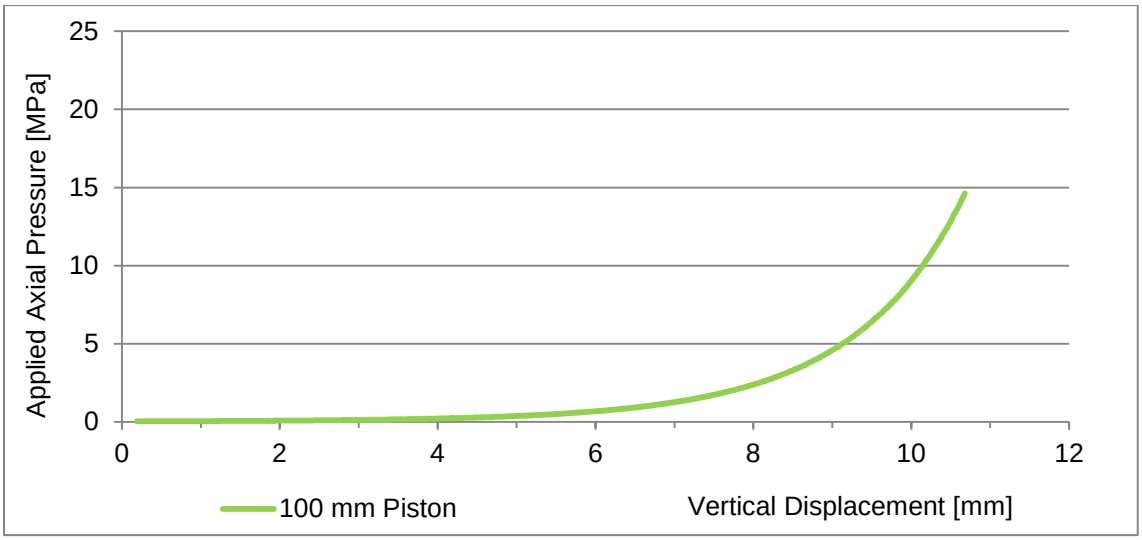

Figure A145 - Net displacement of sample under pressure

Test Summary

Test Description:	100 mm diameter piston test
Displacement Rate (mm/min):	2
Sample Description:	Steel Balls
Top Size (mm):	-4
Moisture (%):	0

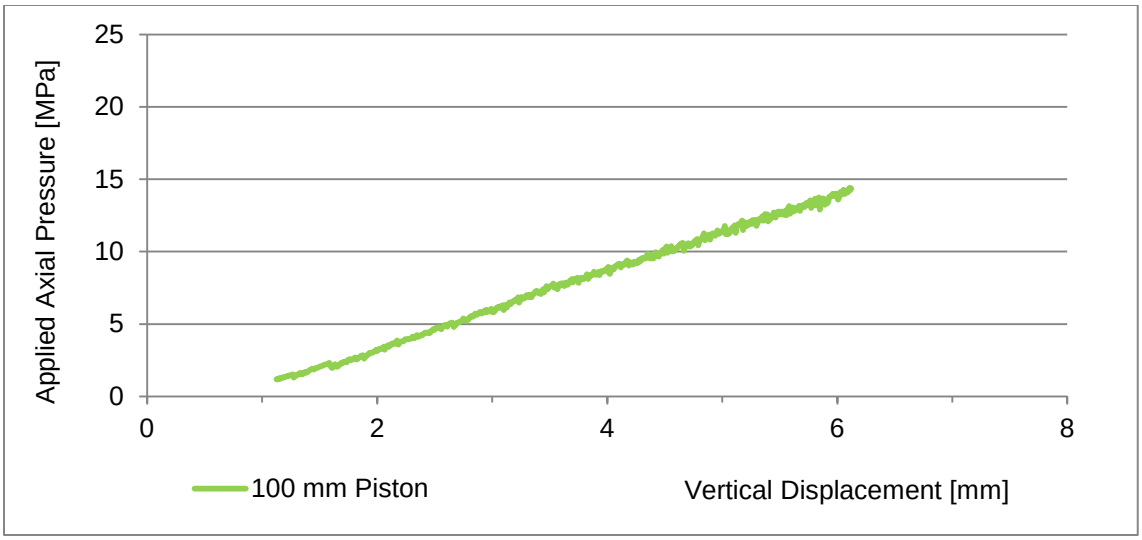

Figure A146 - Net displacement of sample under pressure

Test Summary	
Test Description:	45 & 100 mm diameter piston tests
Displacement Rate (mm/min):	2
Sample Description:	Quartz
Top Size (mm):	-4
Moisture (%):	2.3

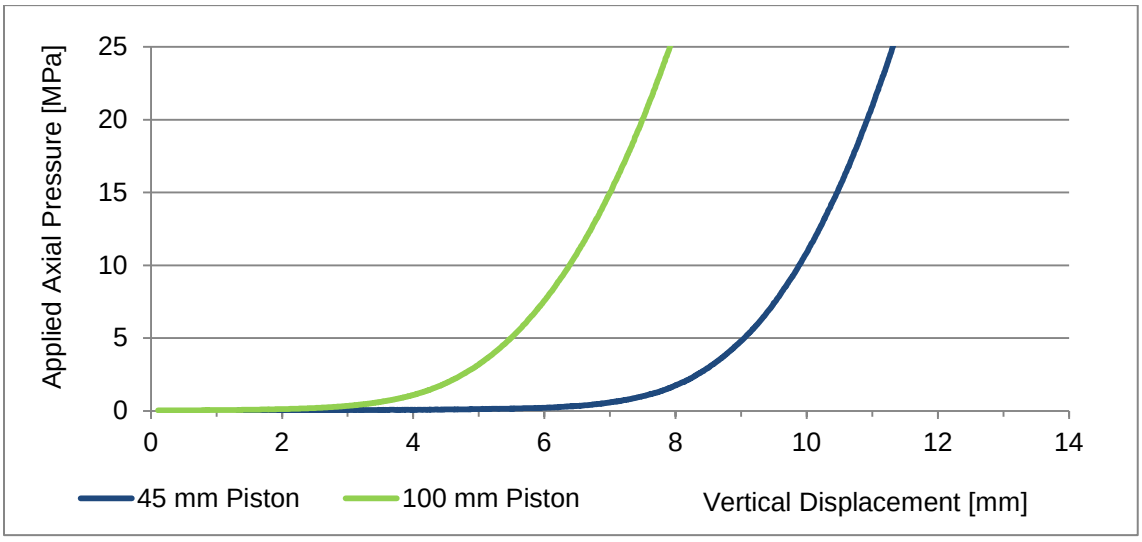

Figure A147 - Net displacement of sample under pressure

Test Summary	
Test Description:	100 mm diameter piston test
Displacement Rate (mm/min):	2
Sample Description:	Kimberlite #1
Top Size (mm):	-4
Moisture (%):	8

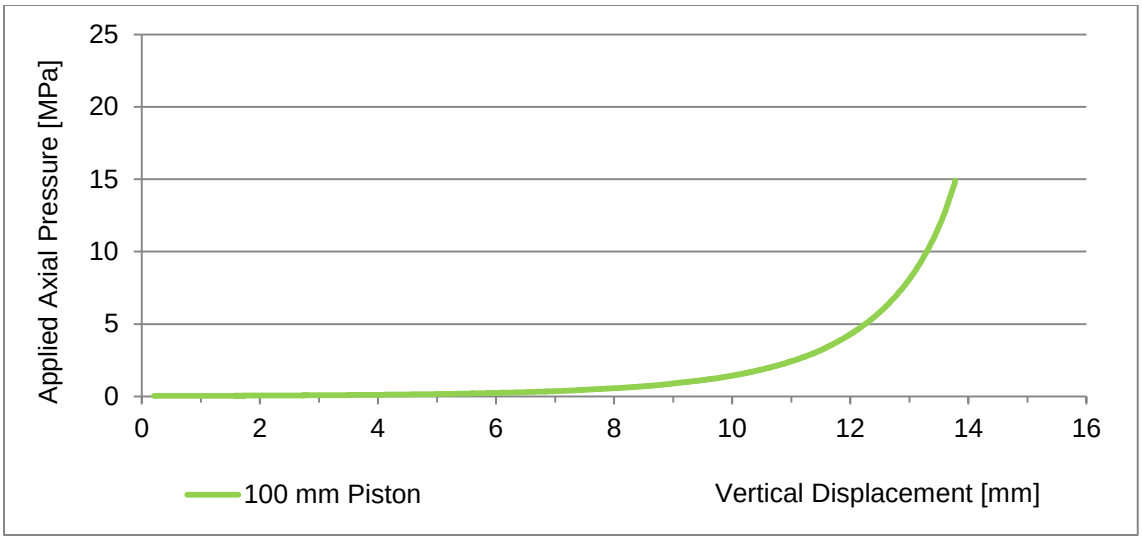

Figure A148 - Net displacement of sample under pressure

Test Summary	
Test Description:	100 mm diameter piston test
Displacement Rate (mm/min):	2
Sample Description:	Kimberlite #2
Top Size (mm):	-4
Moisture (%):	5

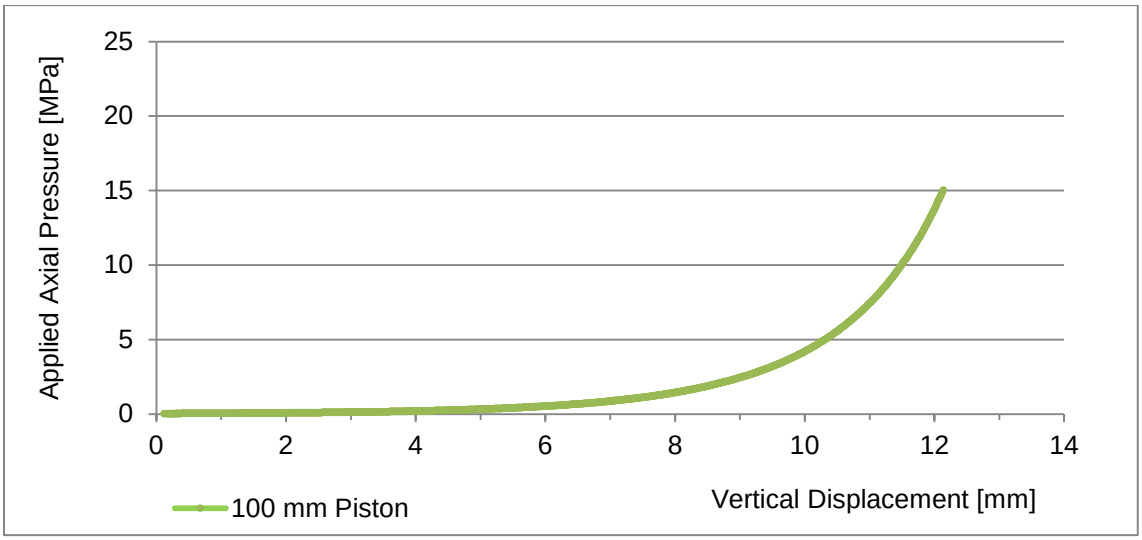

Figure A149 - Net displacement of sample under pressure

Test Summary	
Test Description:	45 & 100 mm diameter piston tests
Displacement Rate (mm/min):	2
Sample Description:	Volcanogenic Gold
Top Size (mm):	-4
Moisture (%):	2.5

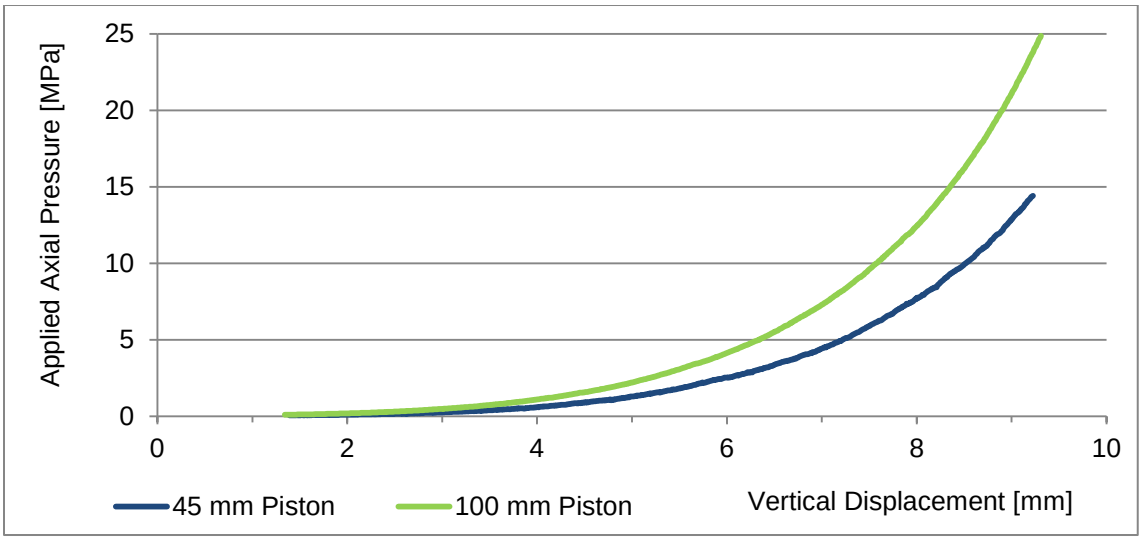

Figure A150 - Net displacement of sample under pressure